Nanorods&Nanowires&Nanosheets

1-Dimensional Nanostructures
P. Yang and Y. Xia
Adv. Mater. **2003**, 15, 353.

- Important for interconnects of nanoscale devices
- Nanoscale sensors
- Nanoscale electronic and optoelectronic devices

- Semiconductor nanowires
- Metal Nanowires
- Metal oxide nanowires

Shapes matter in nanocrystals

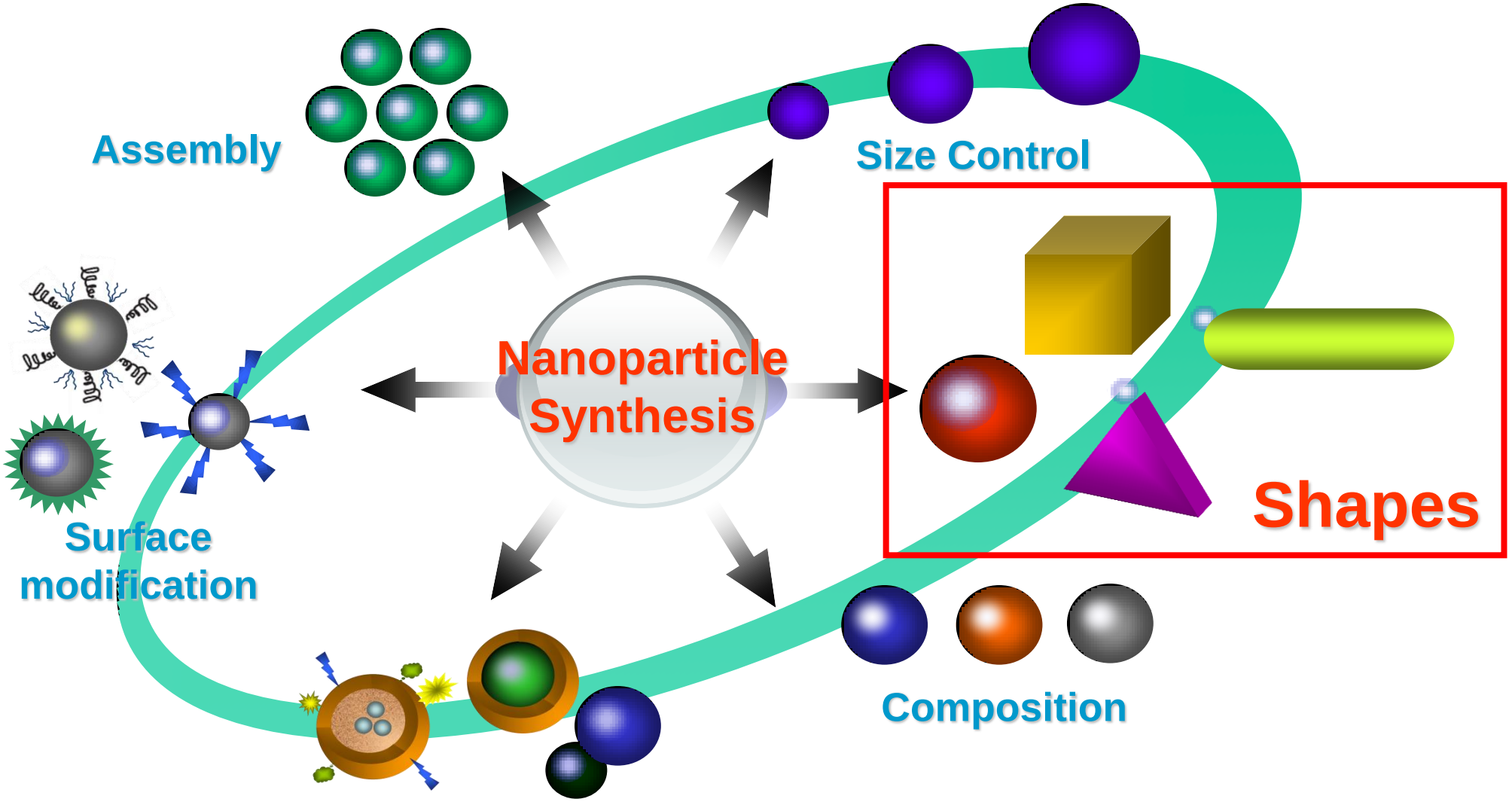

J. Park, et al. *Angew. Chem. Int. Ed.* **2007**, 46, 4630
S. Kwon & T. Hyeon *Acc. Chem. Res*. **2008**. 41, 1696.

Anisotropic nanocrystals including Nanorods and Nanowires are known to exhibit improved optical and magnetic characteristics compared to spherical counterparts.

Challenges

- **Quantum sized nanorods and nanowires (usually diameters < ~ 20 nm)**
- **Diameter control**
- **Large scale synthesis**

Nanocrystal shape vs. Quantum confinement

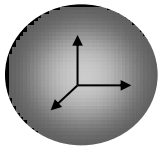

0-D structure
(Spheres or Cubes)
3-D confinement

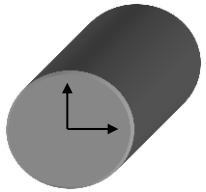

1-D structure
(Wire or Rod)
2-D confinement

2-D structure
(Ribbon or Plate)
1-D confinement

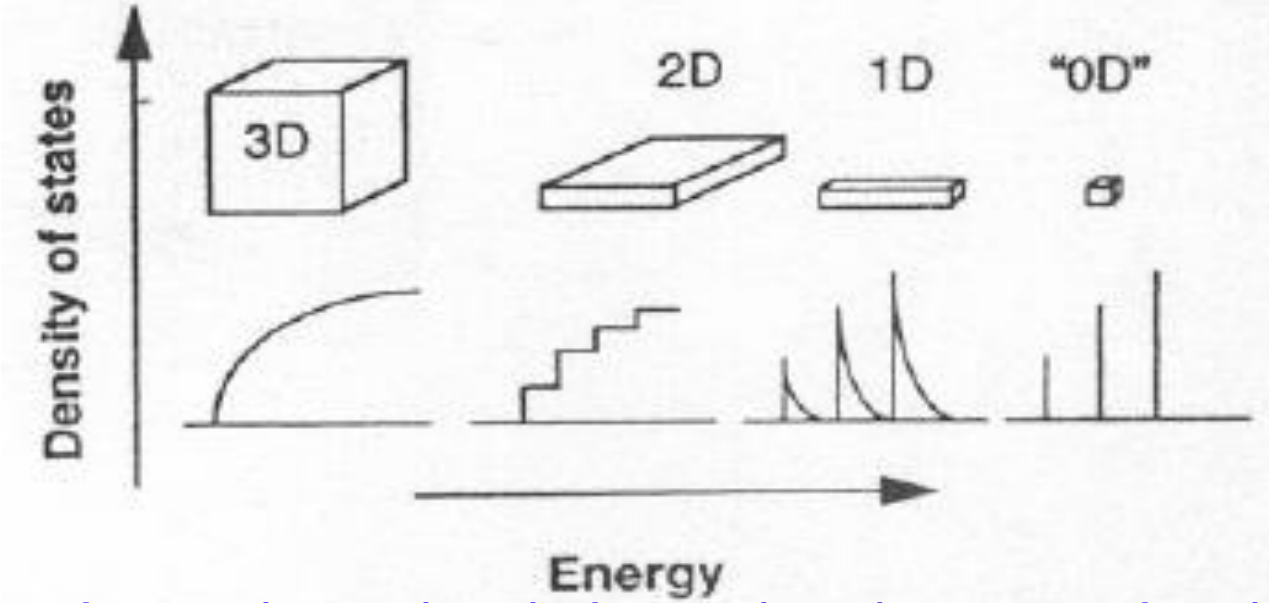

Density of states in one band of a semiconductor as a function of dimension

A. P. Alivisatos, Science, **1996**, *271*, 933.

Strategies to Synthesize 1-D Nanostructures

Intrinsic anisotropic Crystallographic structure

Using templates

Oriented attachment

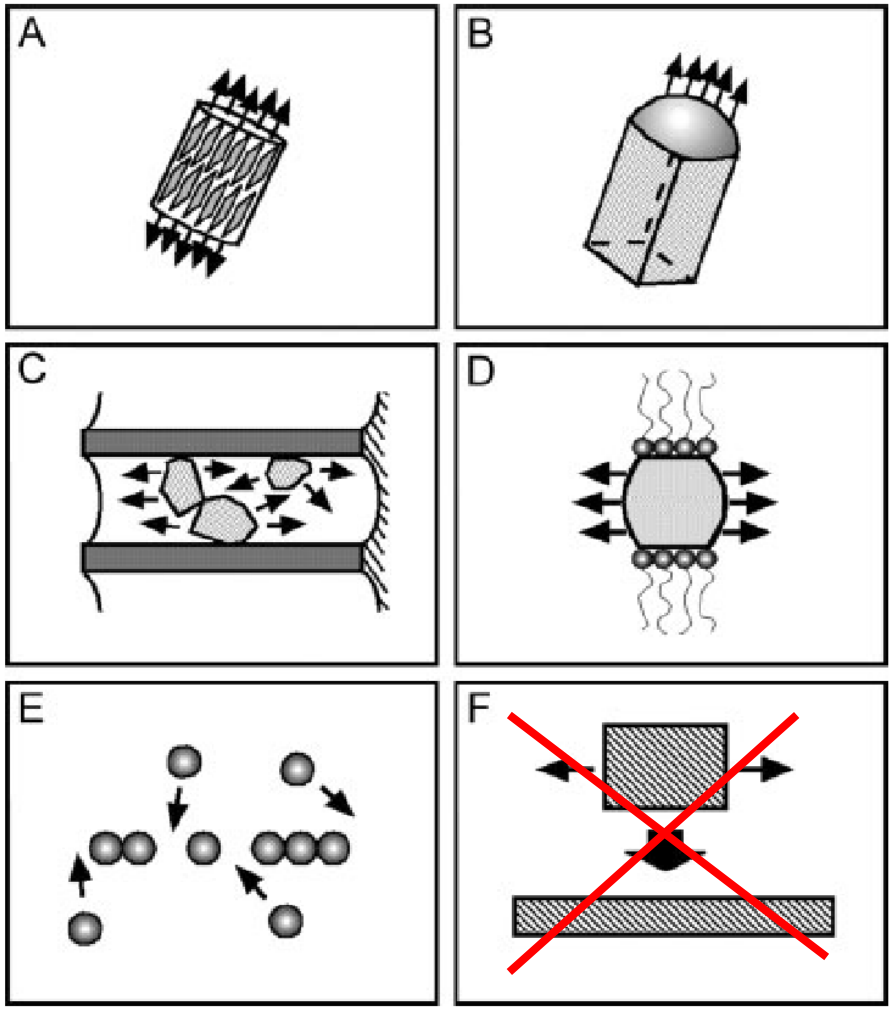

Vapor-(or Solution) Liquid-Solid process

Kinetic control by capping reagents

Size reduction from 1-D microstructure

P. Yang and Y. Xia *Adv. Mater.* **2003**, 15, 353.

1. Growth in templates

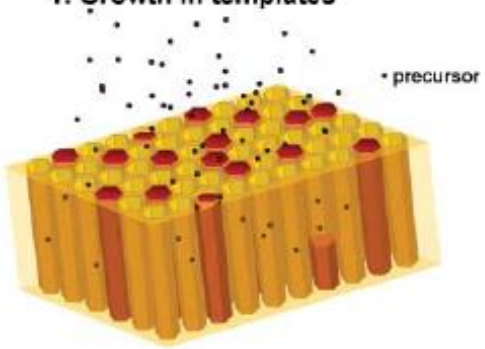

2. Growth promoted by a catalyst

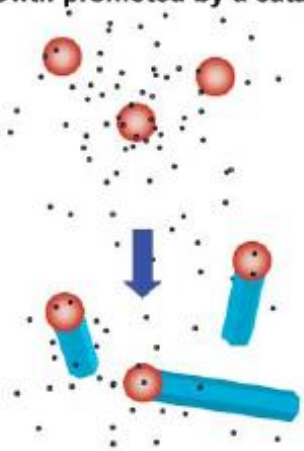

3. Oriented attachment

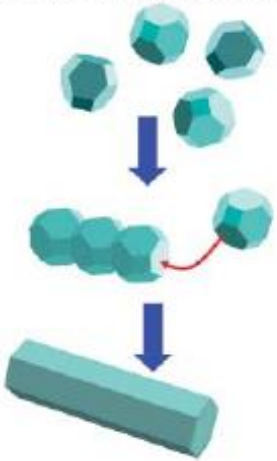

4. Growth by selective adhesion

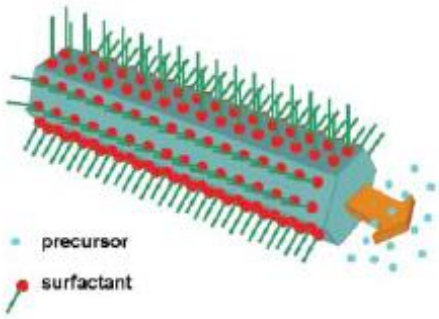

5. Growth in the presence of external fields

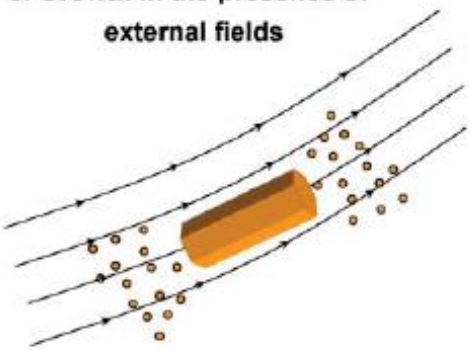

6. Seeded growth

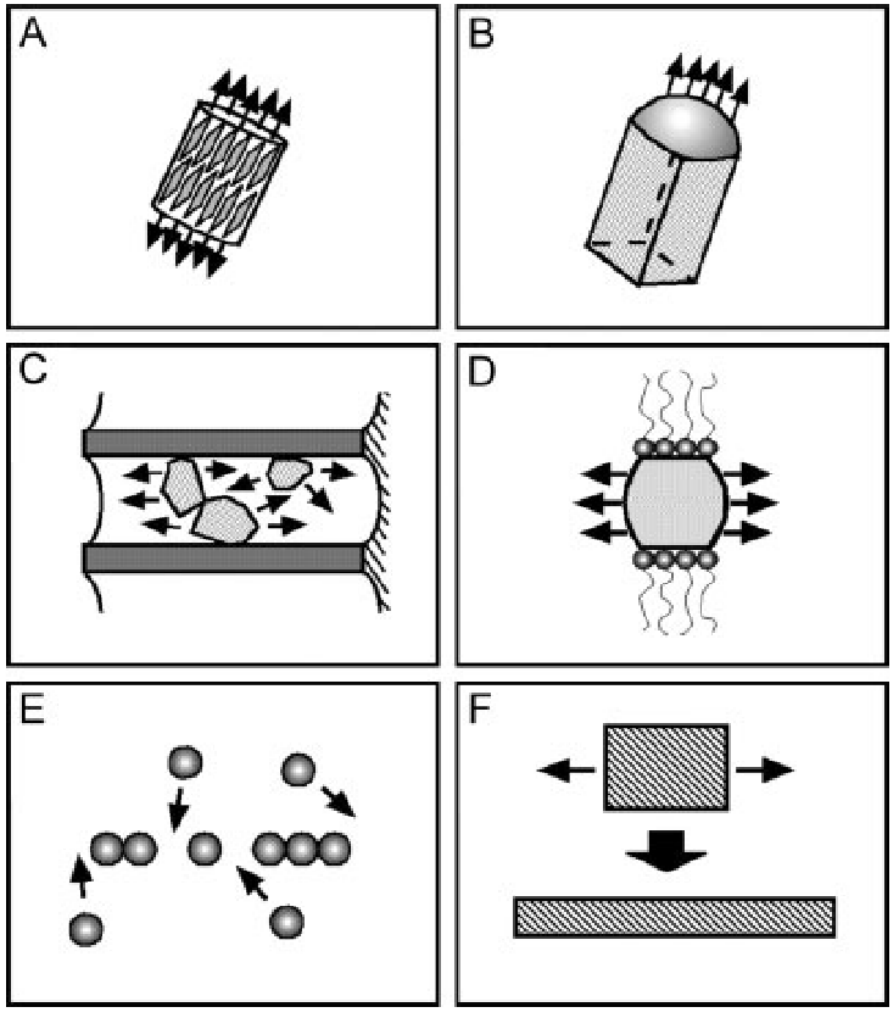

Part I.

Using Intrinsically Anisotropic Crystal Structures

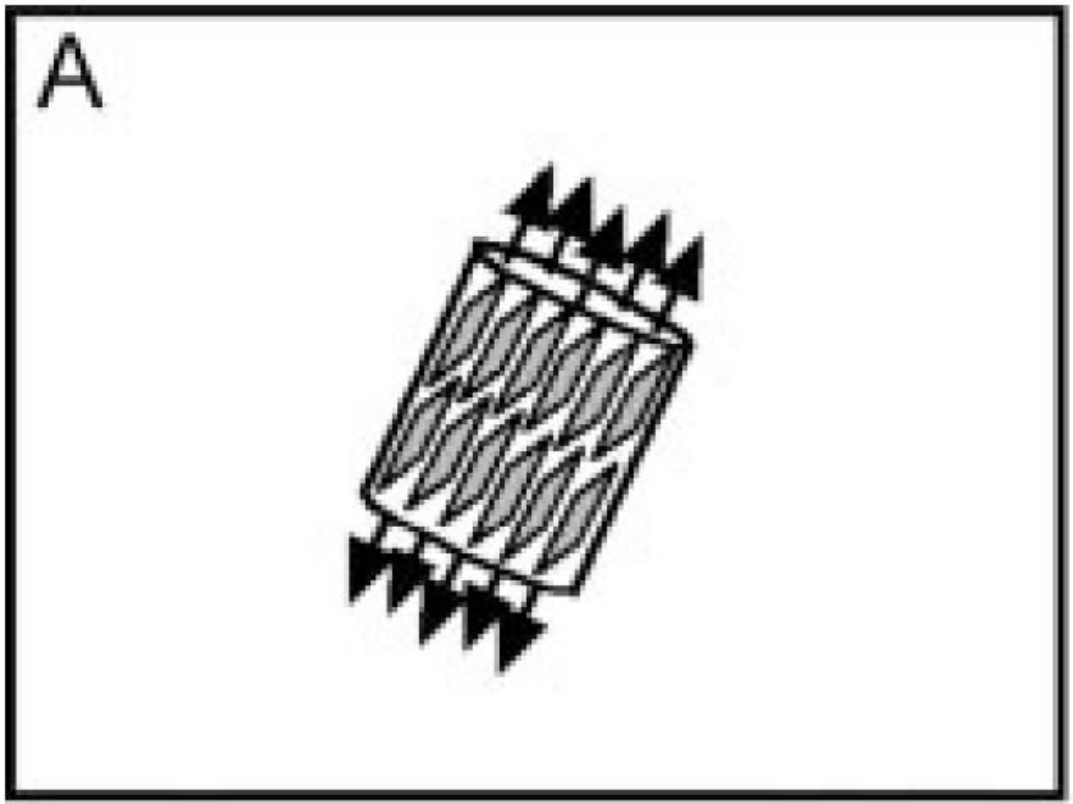

Various ZnO Nanowires

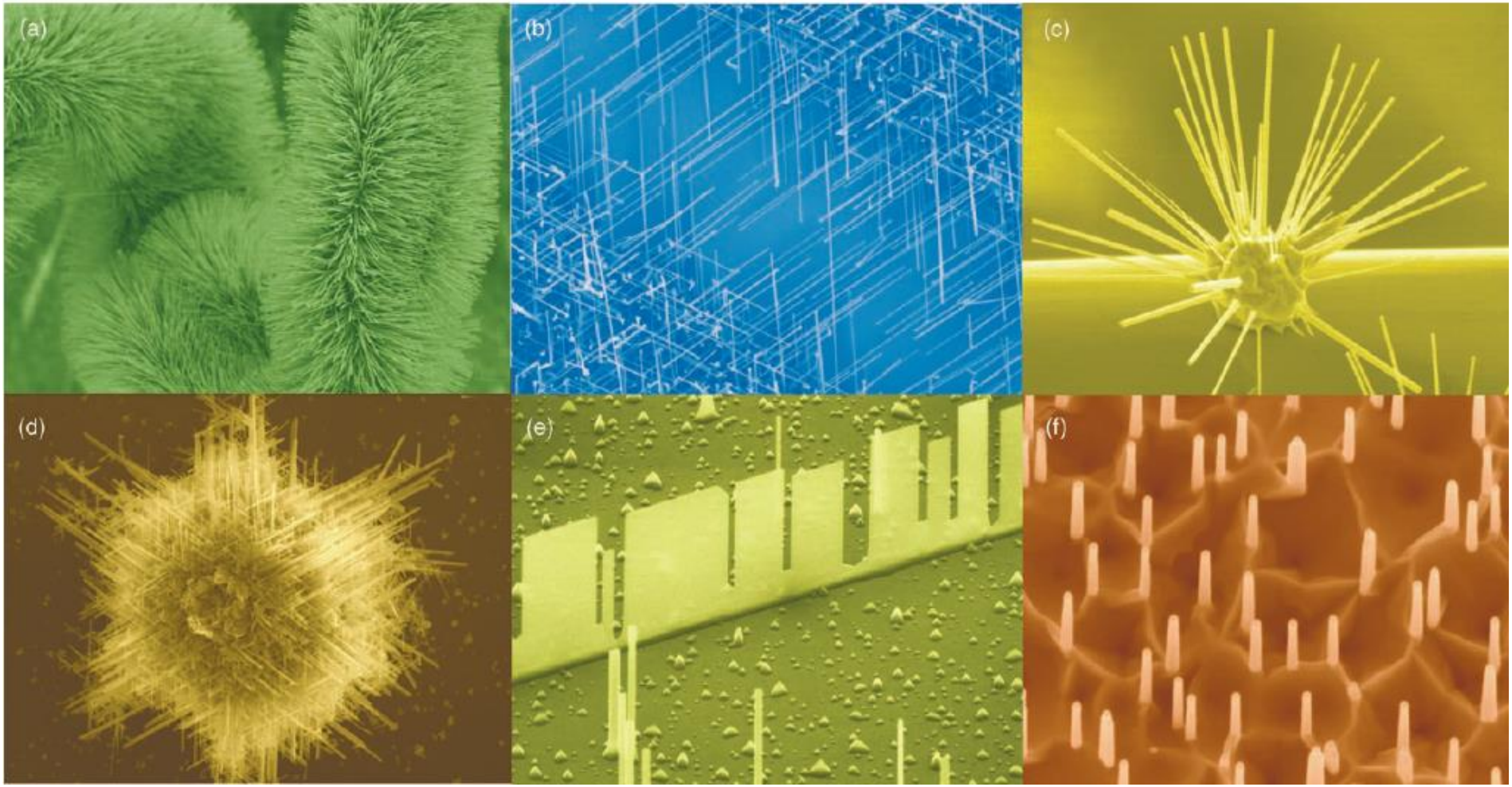

Hong Jin Fan, Peter Werner, and Margit Zacharias* *Small* **2006**, 2, 700.

Jinwoo Cheon (Yonsei University), *J. Phys. Chem. B* **2005,** *109,* 14795.

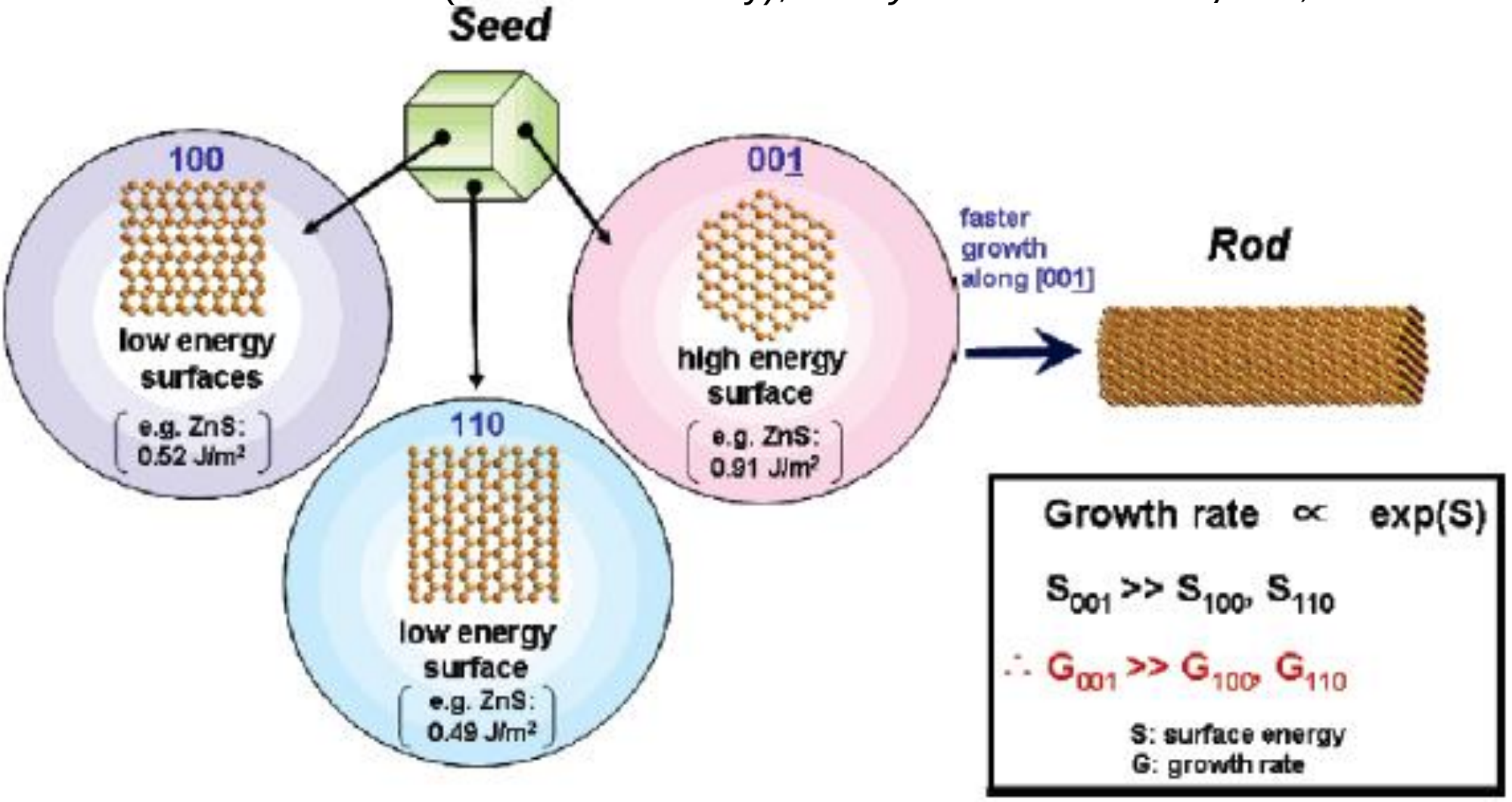

Surface energy initiated anisotropic growth of one-dimensional semiconductor nanorods with wurtzite structures.

• In general, the surface energy of {001} faces of the wurtzite structure is much larger than those of other faces due to the high packing density and a large number of under-coordinated atoms of the {001} faces.

• Such surface energy difference results in significant growth rate differences between different crystallographic directions, since the growth rate is exponentially proportional to the surface energy.

• The growth rate along the <001> directions is much faster compared to other directions, which finally results in progressive elongation along the <001> directions of the nanocrystals and formation of one-dimensional rod structures

Jinwoo Cheon (Yonsei University), *J. Phys. Chem. B* **2005,** *109,* 14795.

Selenium Nanowires

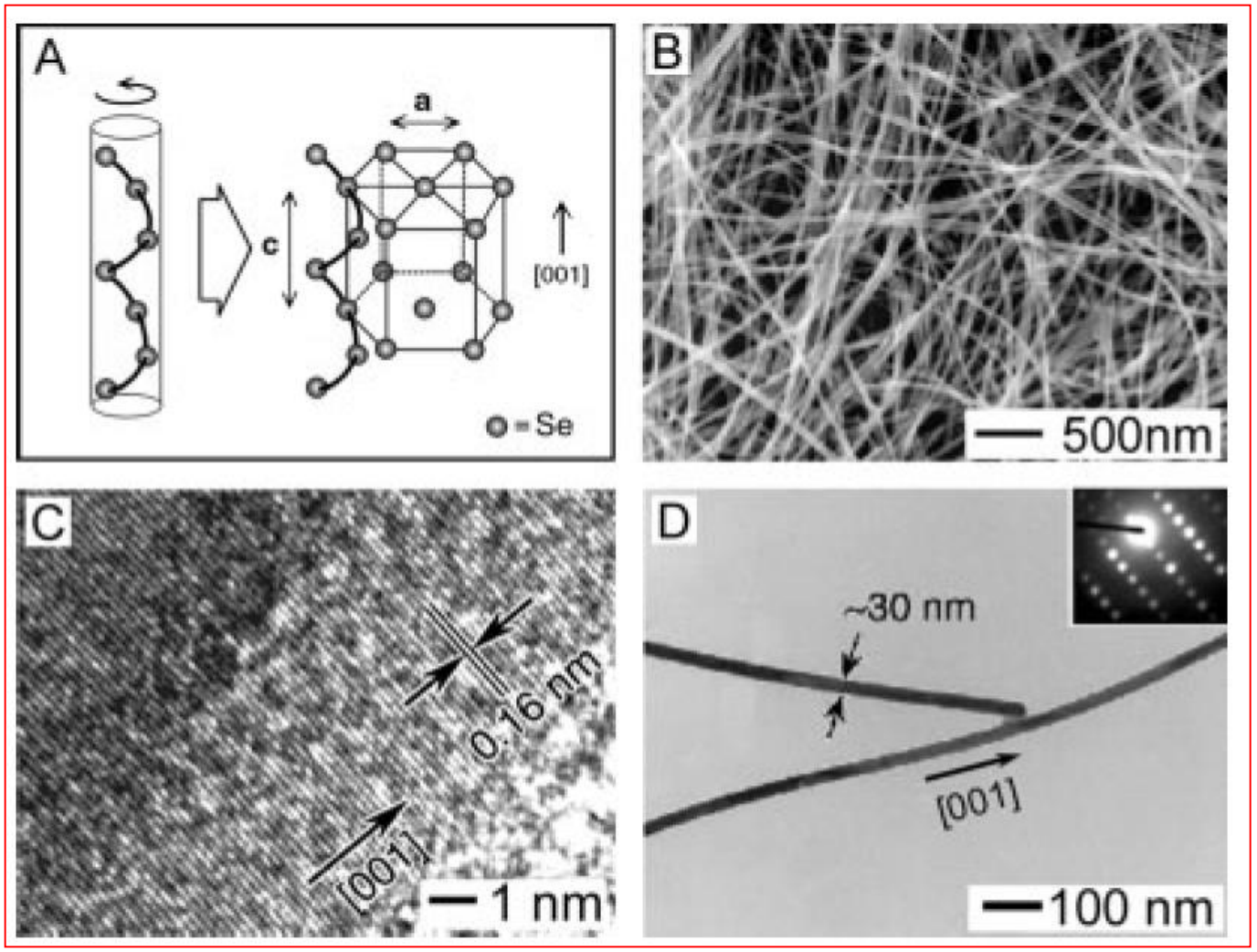

$$H_2SeO_3 + N_2H_4 \longrightarrow Se\,(\downarrow) + N_2\,(\uparrow) + 3H_2O$$

B. Gates, Y. Yin, Y. Xia, *J. Am. Chem. Soc.* **2000**, *122*, 12582.

Nanobelts of Semiconducting Oxides,

Zhong Lin Wang (Georogia Inst. Tech.)

Science **2001**, *291*, 1927

• Ultralong beltlike (or ribbonlike) nanostructures (so-called nanobelts) were successfully synthesized for semiconducting oxides of zinc, tin, indium, cadmium, and gallium by simply evaporating the desired commercial metal oxide powders at high temperatures.

Review: Novel Nanostructures of Functional Oxides Synthesized by Thermal Evaporation, Z. L. Wang, *Adv. Func. Mater*. **2003**, 9.
Hong Jin Fan, Peter Werner, and Margit Zacharias* *Small* **2006**, 2, 700.

Thermal Evaporation Apparatus

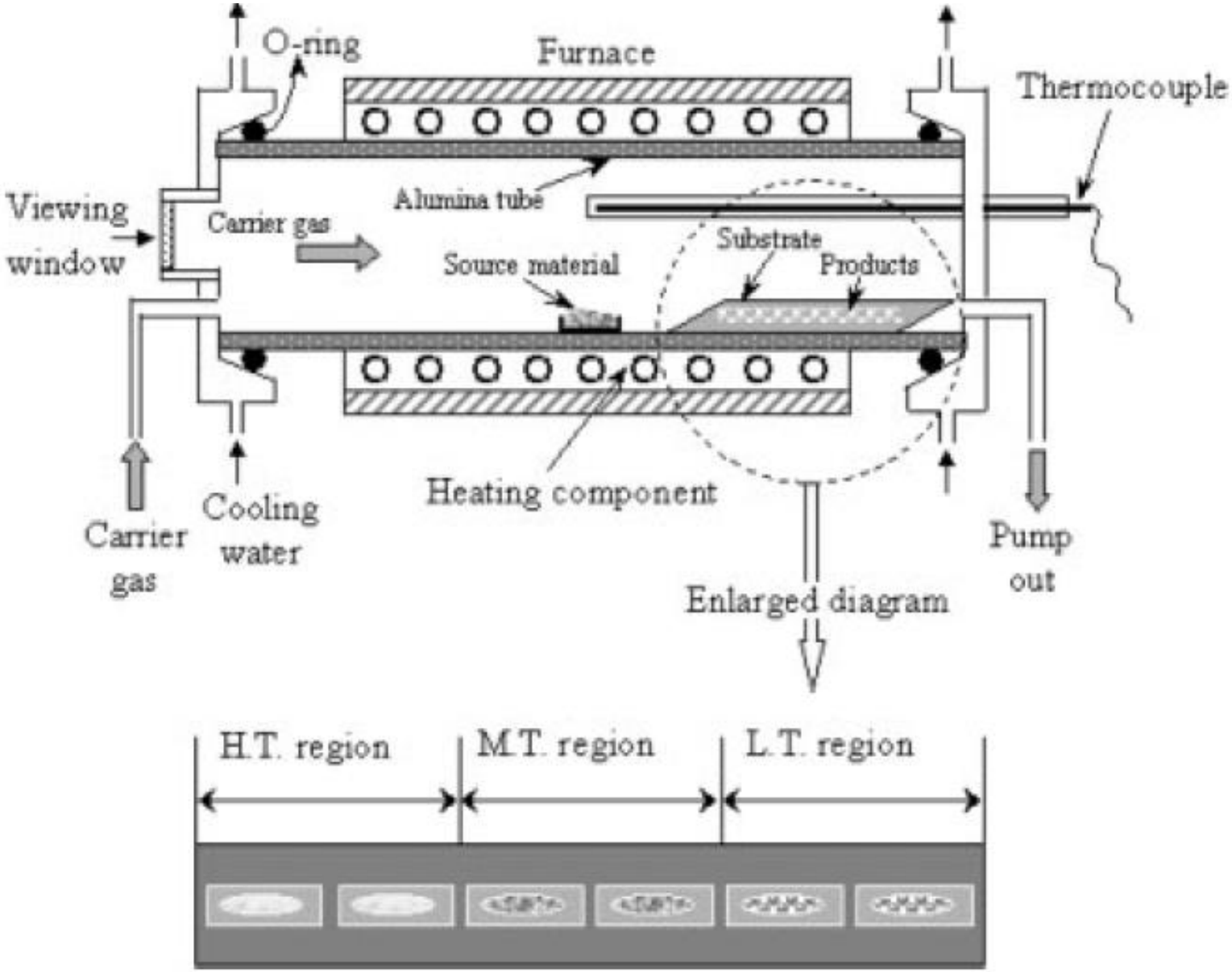

Z. L. Wang, *Adv. Func. Mater*. **2003**, 9.

SnO_2

PbO_2

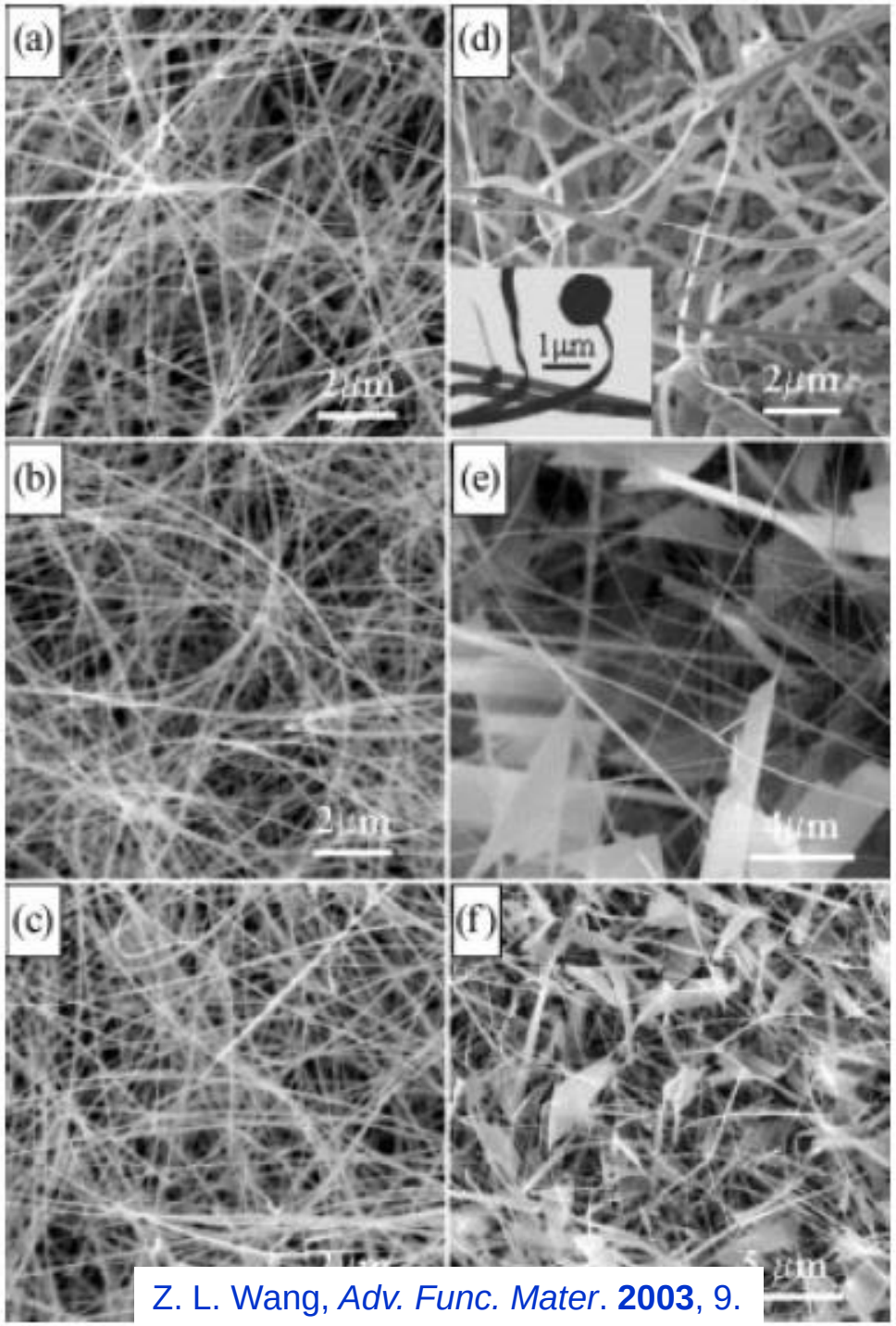

ZnO

CdO

In_2O_3

Ga_2O_3

Z. L. Wang, *Adv. Func. Mater*. **2003**, 9.

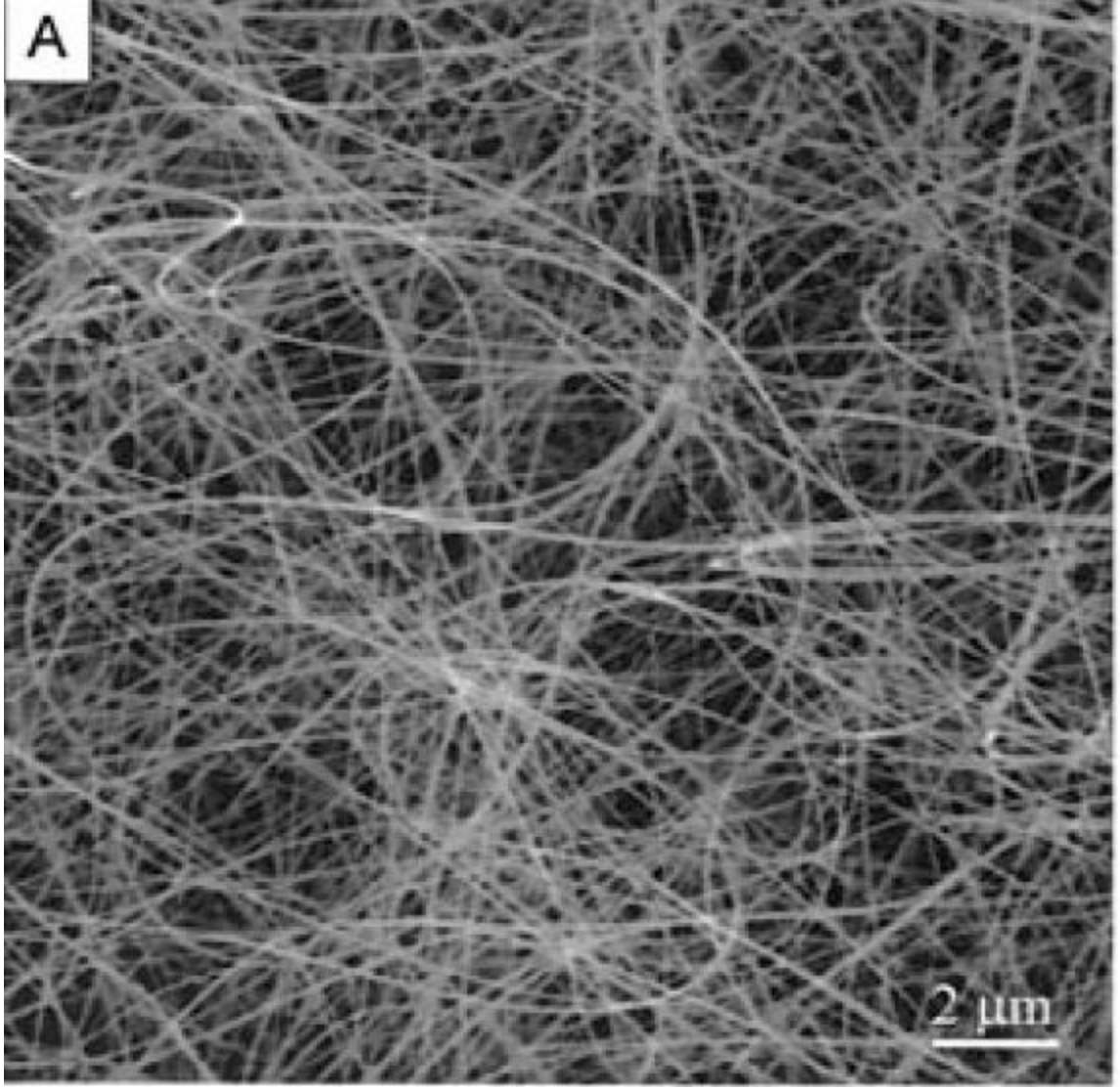

They have a rectangle-like cross section with typical widths of 30 to 300 nanometers, width-to-thickness ratios of 5 to 10, and lengths of up to a few millimeters.

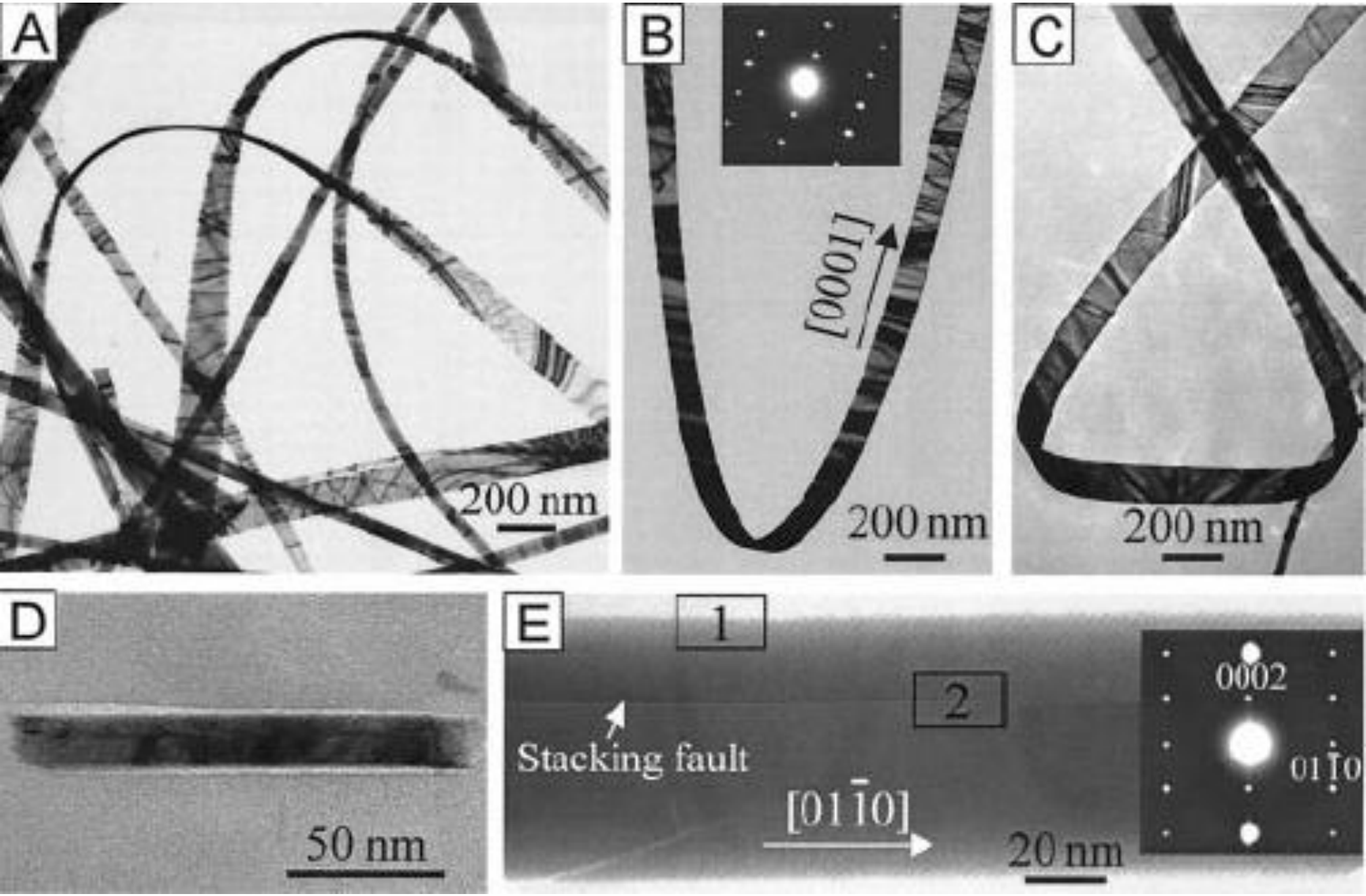
A
200 nm
B
[0001]
200 nm
C
200 nm
D
50 nm
E
1
2
Stacking fault
[01$\bar{1}$0]
20 nm
0002
01$\bar{1}$0

Part II.

Introduction of Liquid-Solid Interface To Reduce Symmetry of a Seed (Vapor-Liquid-Solid Process)

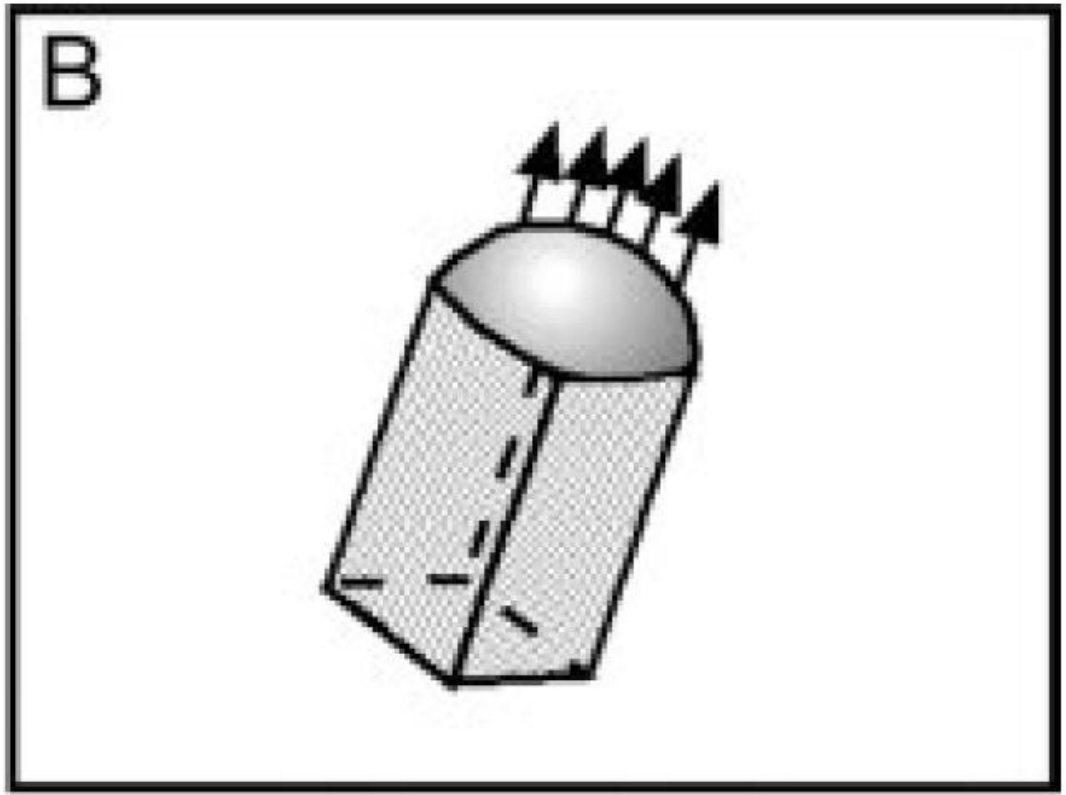

A Laser Ablation Method for the Synthesis of Crystalline Semiconductor Nanowires

C. M. Lieber in Harvard University

Science **1998**, 279, 208; cited **3,214** times.

- Laser ablation: formation of catalyst clusters
- Vapor-liquid-solid growth of nanowires
- Single-crystal silicon (6 ~ 20 nm) and germanium nanowires (3 ~ 9 nm)
- Length of 1 ~ 30 micrometer

Similar to Catalytic Chemical Vapor Deposition Growth of Carbon Nanotubes using Fe, Co, Ni nanoparticles as Catalysts

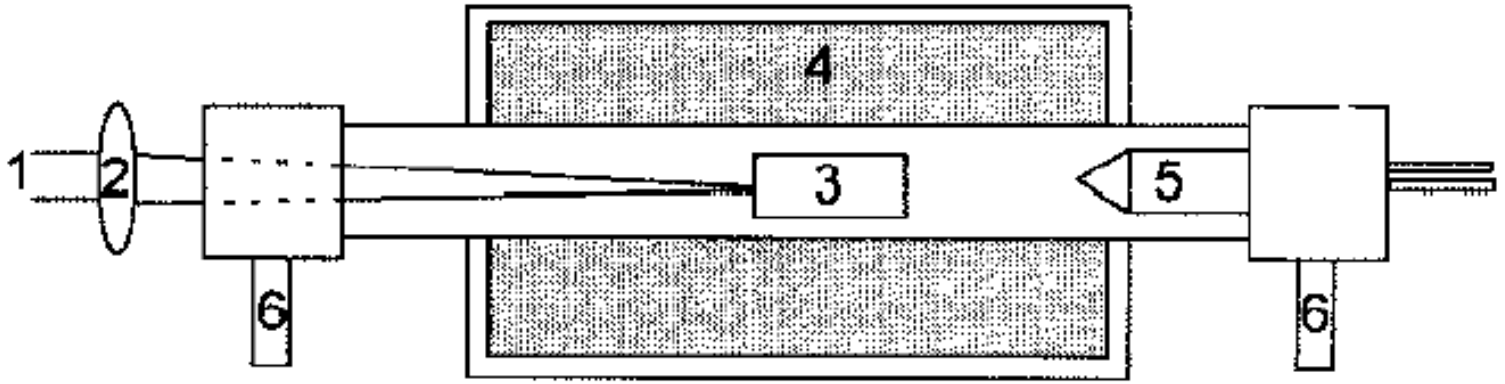

Fig. 1. Schematic of the nanowire growth apparatus. The output from a pulsed laser (1) is focused (2) onto a target (3) located within a quartz tube; the reaction temperature is controlled by a tube furnace (4). A cold finger (5) is used to collect the product as it is carried in the gas flow that is introduced (6, left) through a flow controller and exits (6, right) into a pumping system.

TEM images of Si Nanowires

Si0.9Fe0.1 as catalyst target

7.8 nm core with total 17 nm including Amorphous oxide sheath

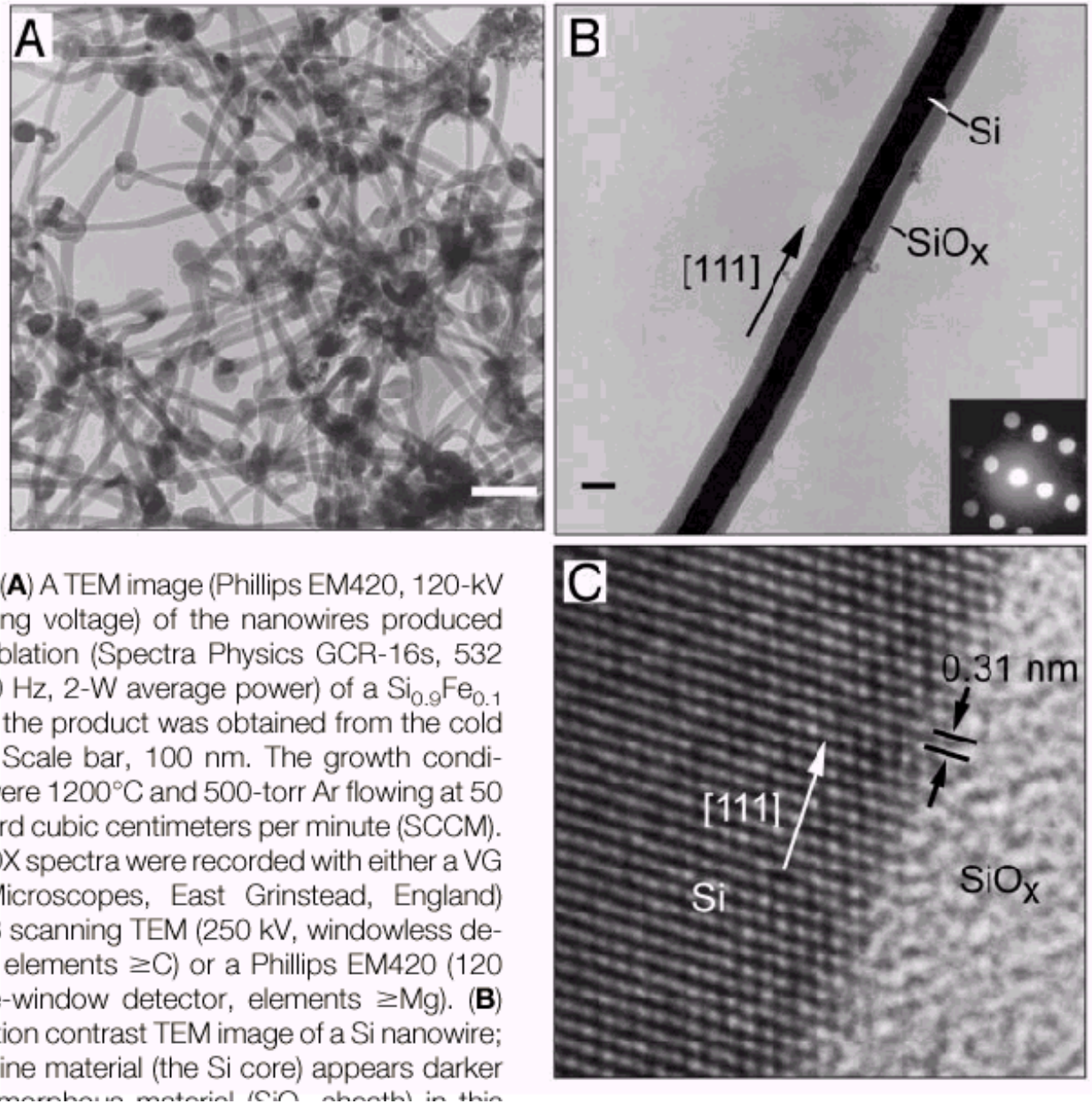

Fig. 2. (**A**) A TEM image (Phillips EM420, 120-kV operating voltage) of the nanowires produced after ablation (Spectra Physics GCR-16s, 532 nm, 10 Hz, 2-W average power) of a $Si_{0.9}Fe_{0.1}$ target; the product was obtained from the cold finger. Scale bar, 100 nm. The growth conditions were 1200°C and 500-torr Ar flowing at 50 standard cubic centimeters per minute (SCCM). The EDX spectra were recorded with either a VG (VG Microscopes, East Grinstead, England) HB603 scanning TEM (250 kV, windowless detector, elements ≥C) or a Phillips EM420 (120 kV, Be-window detector, elements ≥Mg). (**B**) Diffraction contrast TEM image of a Si nanowire; crystalline material (the Si core) appears darker

TEM images of Ge Nanowires

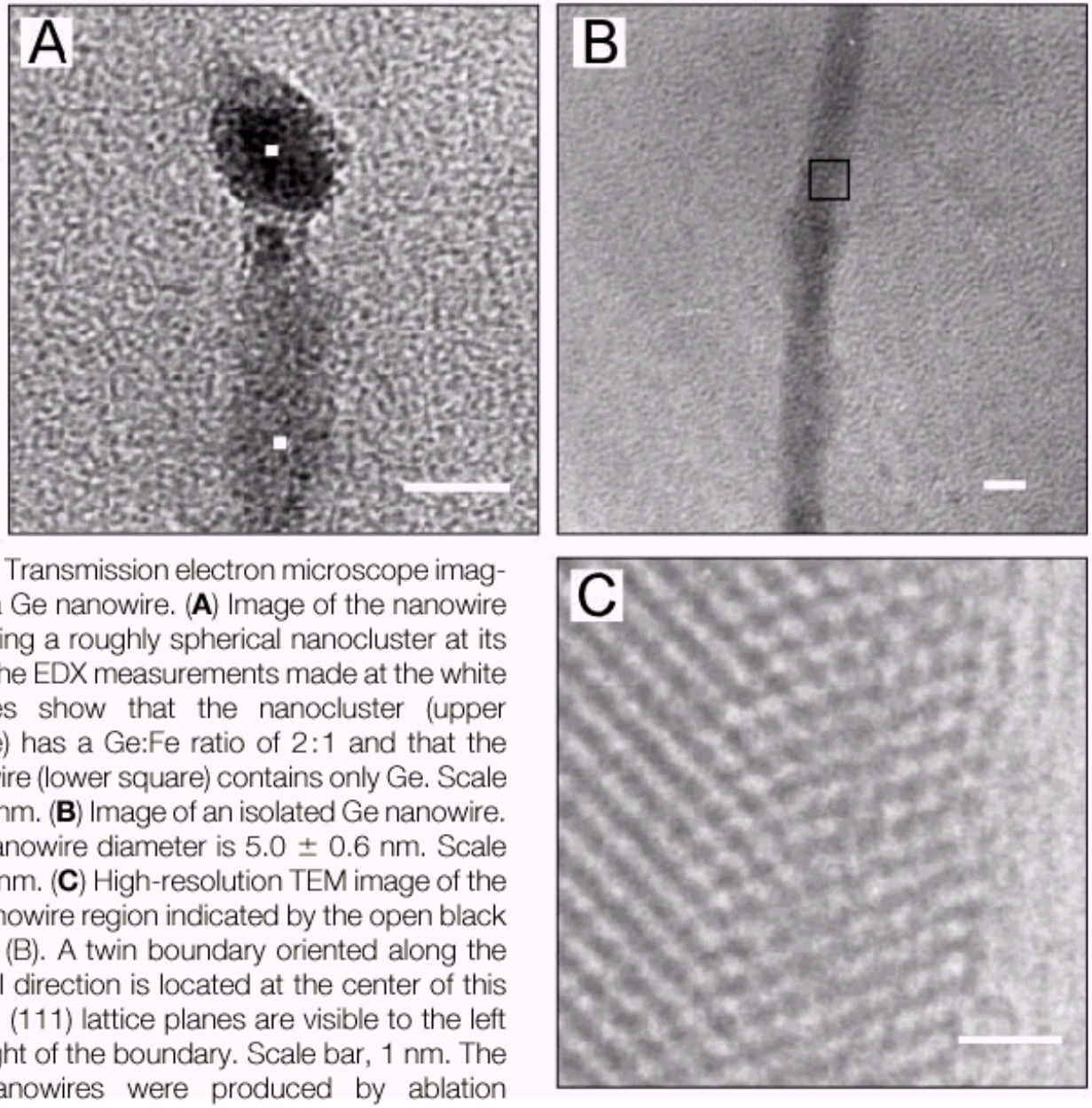

Fig. 4. Transmission electron microscope images of a Ge nanowire. (**A**) Image of the nanowire exhibiting a roughly spherical nanocluster at its end. The EDX measurements made at the white squares show that the nanocluster (upper square) has a Ge:Fe ratio of 2:1 and that the nanowire (lower square) contains only Ge. Scale bar, 9 nm. (**B**) Image of an isolated Ge nanowire. The nanowire diameter is 5.0 ± 0.6 nm. Scale bar, 5 nm. (**C**) High-resolution TEM image of the Ge nanowire region indicated by the open black box in (B). A twin boundary oriented along the vertical direction is located at the center of this image; (111) lattice planes are visible to the left and right of the boundary. Scale bar, 1 nm. The Ge nanowires were produced by ablation

Growth Mechanism

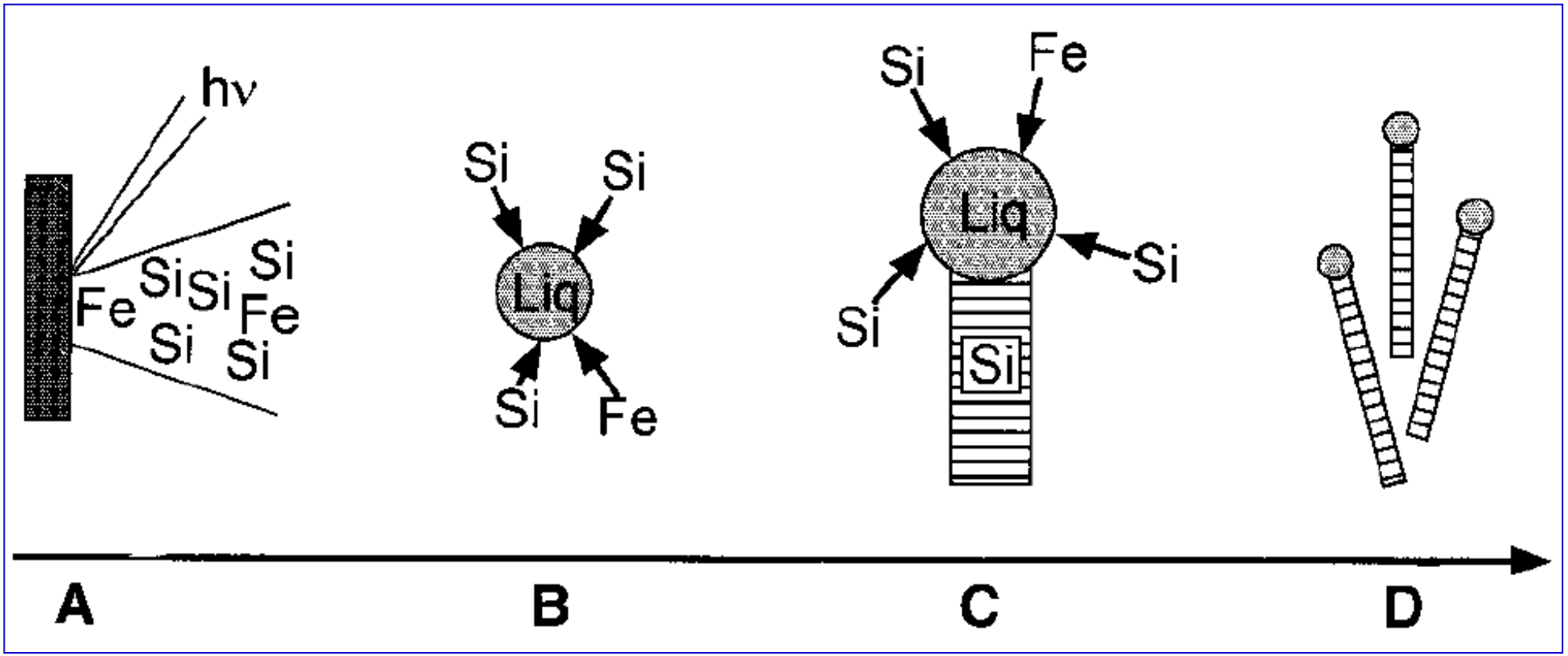

1. Formation of FeSi2 in the end-clusters
2. NW grow after liquid supersaturated

No growth of nanowires below 1207 ^{o}C (no liquid Si cluster formation)

Growth of 1-D Nanowires

- **Use of metal alloy**
- **phase diagrams for alloys**

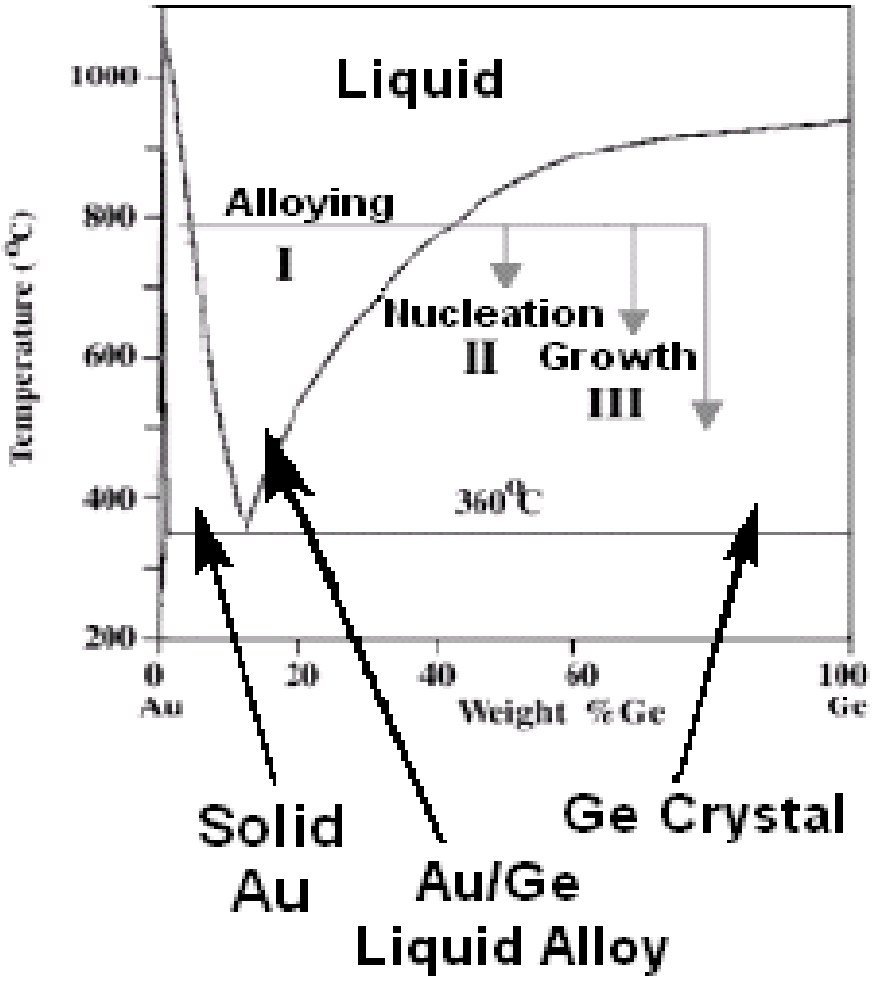

Wu, Y.; Yang, P. *J. Am. Chem. Soc.* **2001**, 123, 3165-3166.

Growth of 1-D Nanowires via Vapor-Liquid-Solid mechanism

✓ **Phase diagram**

Appl. Phys. Lett., 4 , 1964 , 889, Acc. Chem. Res., 32, 435

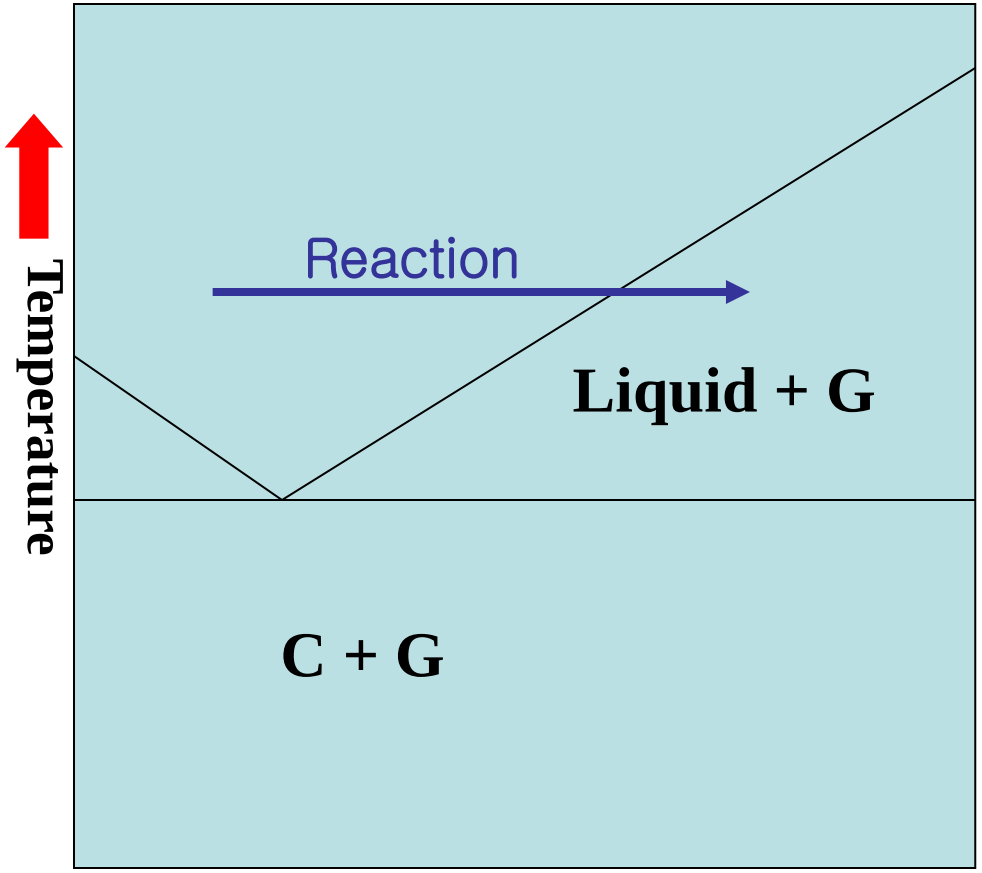

Catalyst solvent at high temperature

↓

Liquid droplet solution

↓

Saturation

↓

Nanowire growth

Laser-assisted growth of GaN nanowires

JACS **2000**, 122, 188 by Lieber

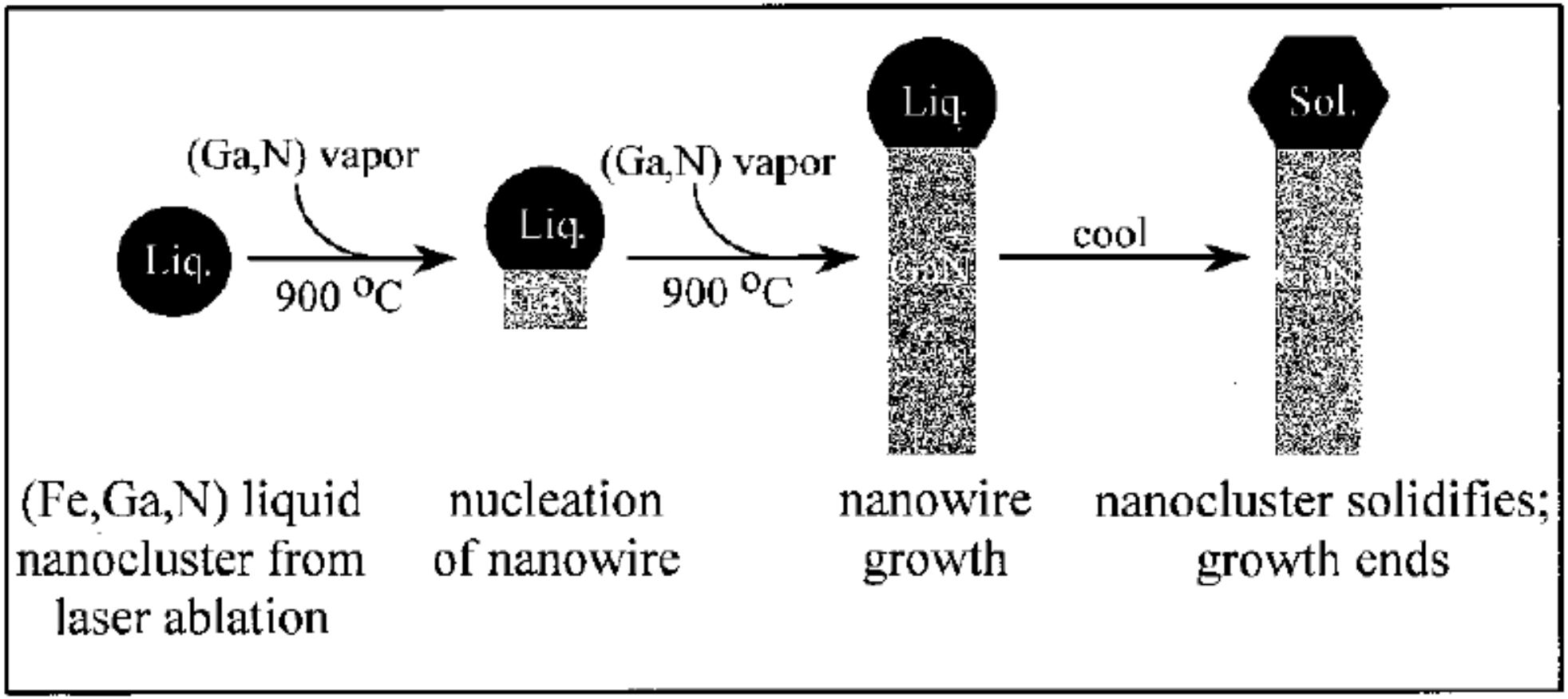

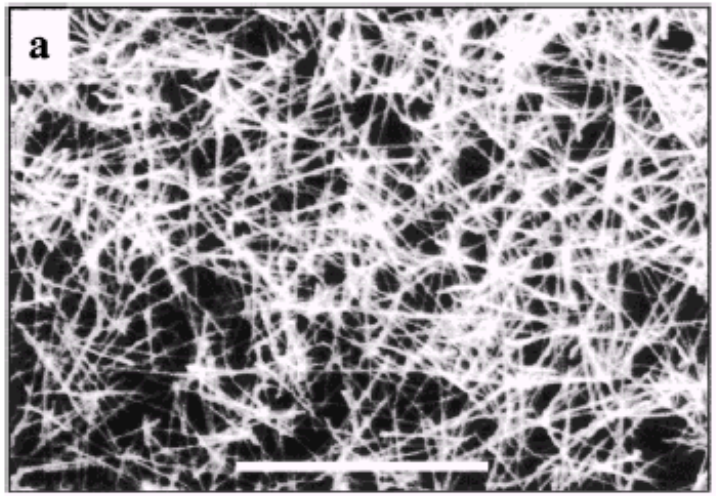
a

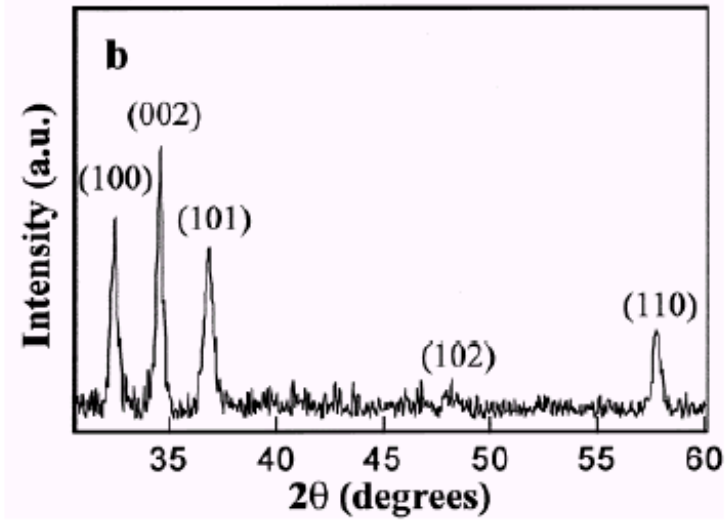
b
(002)
(100)
(101)
(110)
(10$\bar{2}$)
Intensity (a.u.)
35
40
45
50
55
60
2θ (degrees)

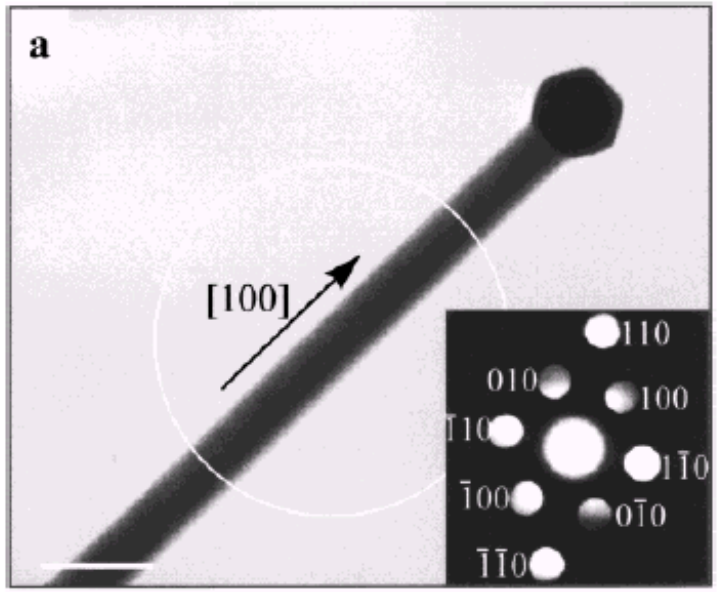
a
[100]
110
010
100
$\bar{1}$10
1$\bar{1}$0
$\bar{1}$00
0$\bar{1}$0
$\bar{1}\bar{1}$0

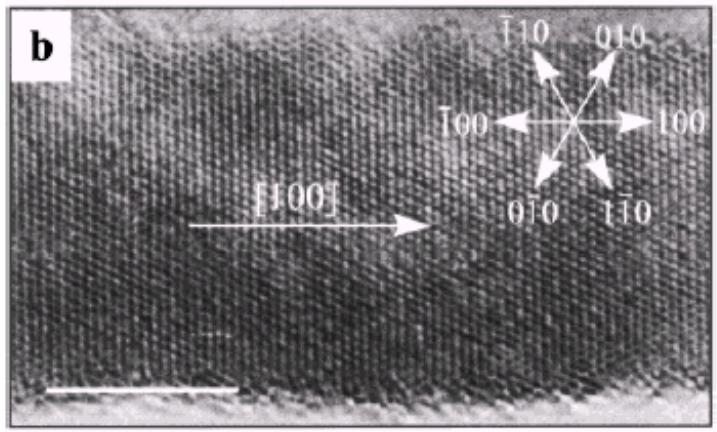
b
$\bar{1}$10
010
$\bar{1}$00
100
[100]
0$\bar{1}$0
1$\bar{1}$0

Diameter-Selective Synthesis of Semiconductor Nanowires

JACS **2000**, 122, 8801 by Lieber

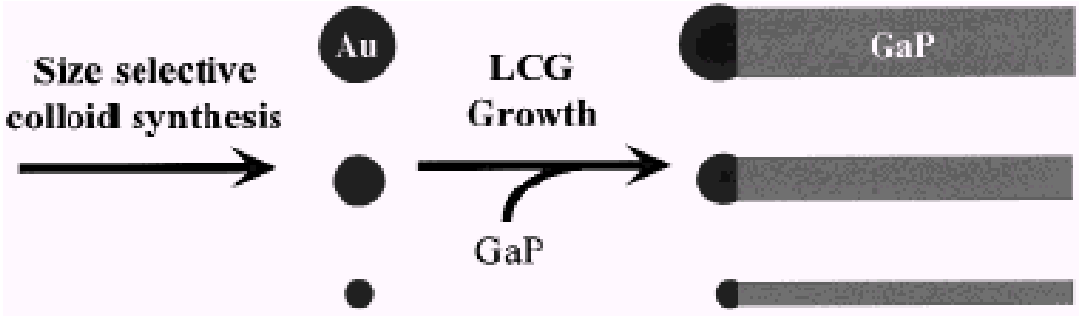

Figure 1. Schematic depicting the use of monodisperse gold colloids as catalysts for the growth of well-defined GaP semiconductor nanowires.

Using 9, 20, 30 nm sized Au nanoparticles
Deposited on SiO2 support as catalysts
Laser lablation of Ga and P target
To generate Diameter-controlled GaP nanowires

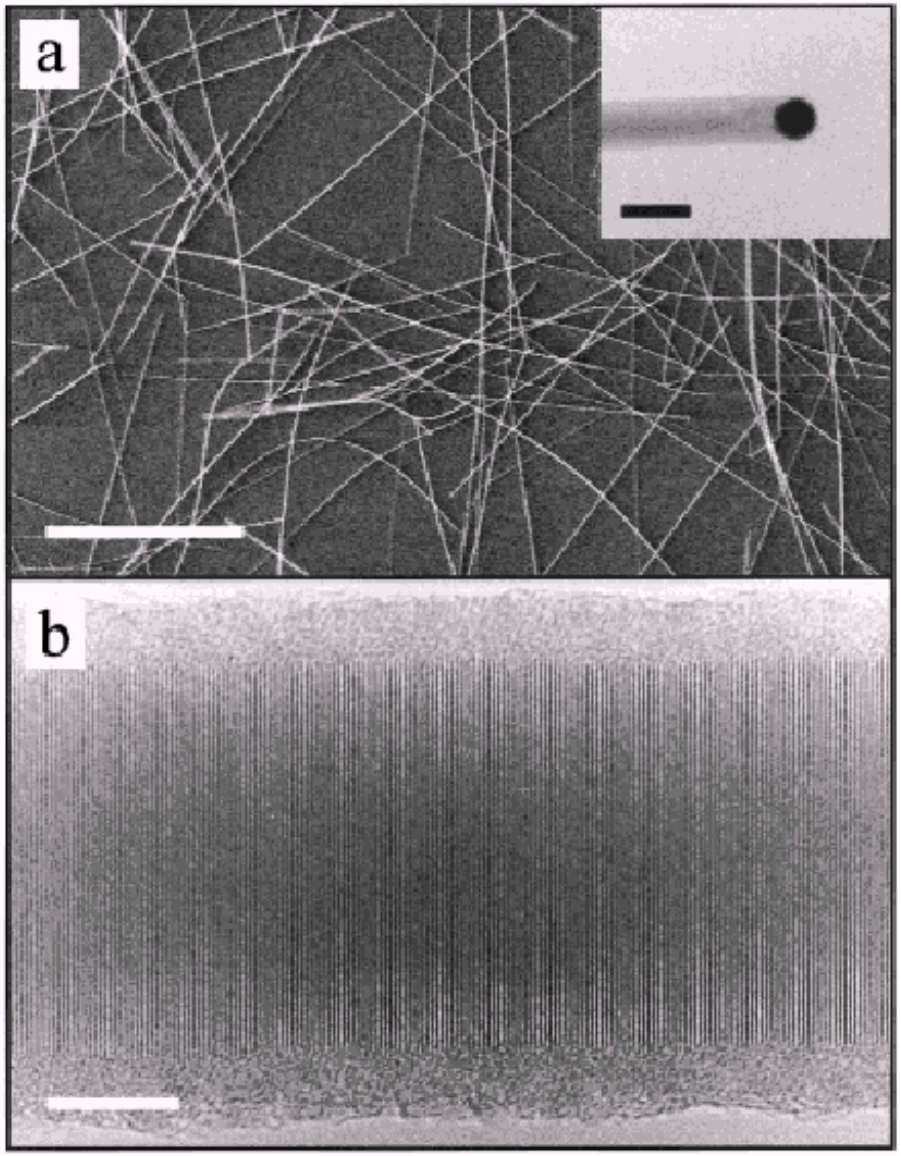

28 nm
Au nanoparticles
As catalysts

(111) Direction growth

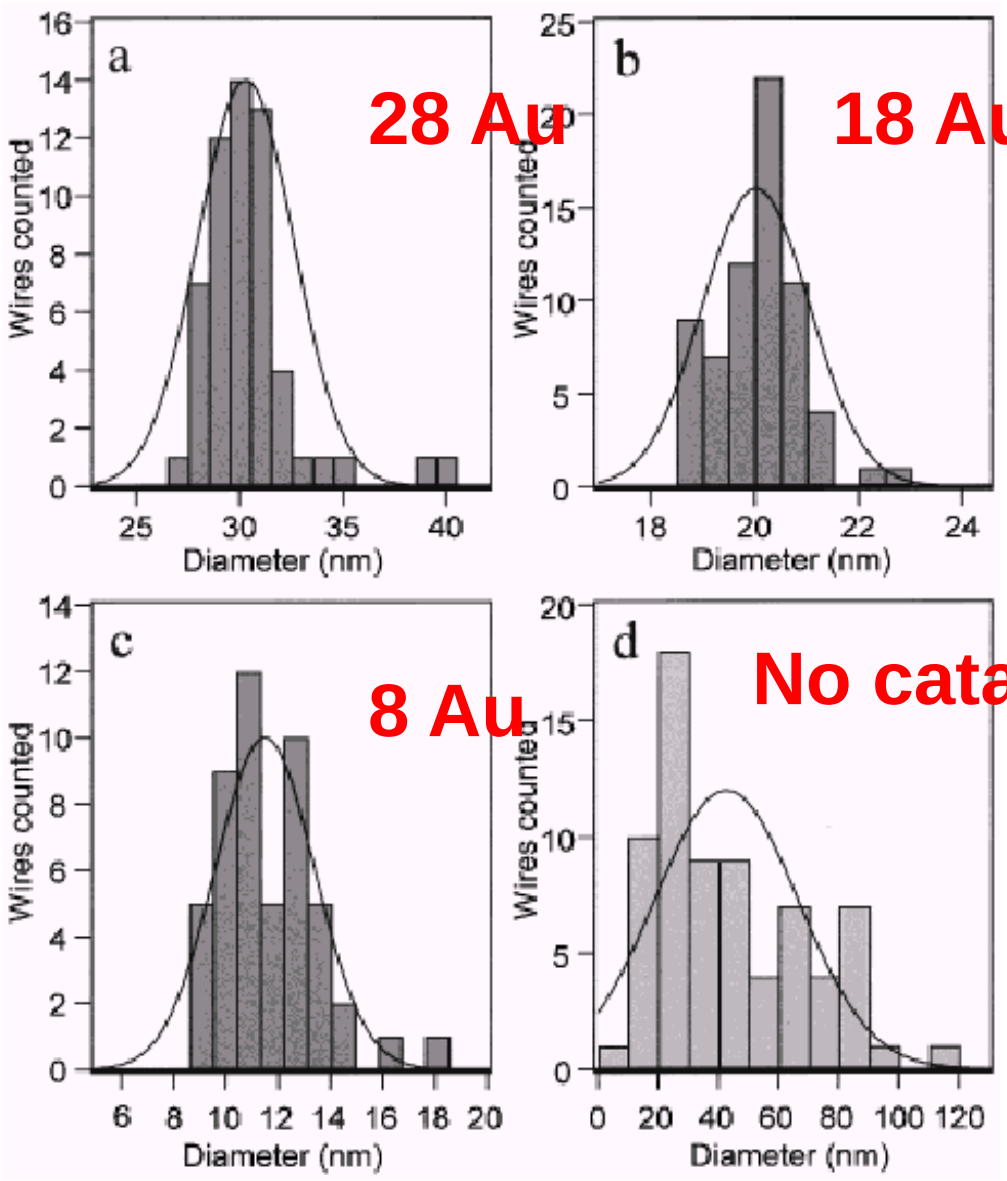
a
28 Au
b
18 Au
30
20
c
8 Au
d
No catalyst
11
Wires counted
Diameter (nm)

General Synthesis of Compound Semiconductor Nanowires

Adv. Mater. 2000, 12, 298

By Lieber.

Laser-assisted catalytic growth

III-V (GaAs, GaP, InAs, and InP

II-VI (ZnS, ZnSe, CdSe, CdS)

Ternary III-V (GaAs/P, InAs/P)

SiGe alloys

Diameters from 3 –10th of nm

Lengths of 10th of micrometer

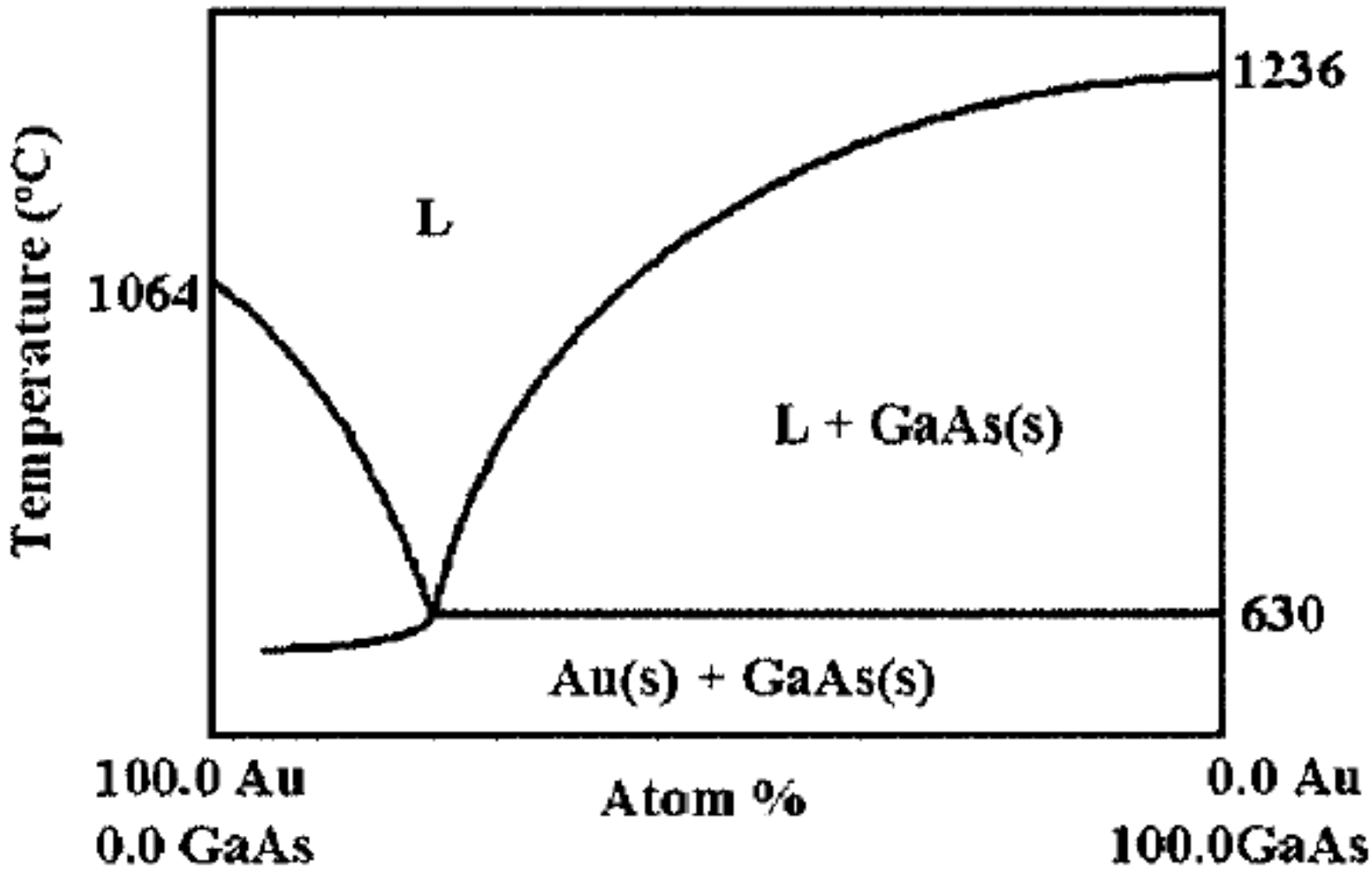

udobinary phase diagram for Au and GaAs. The liquid Au–Ga–As

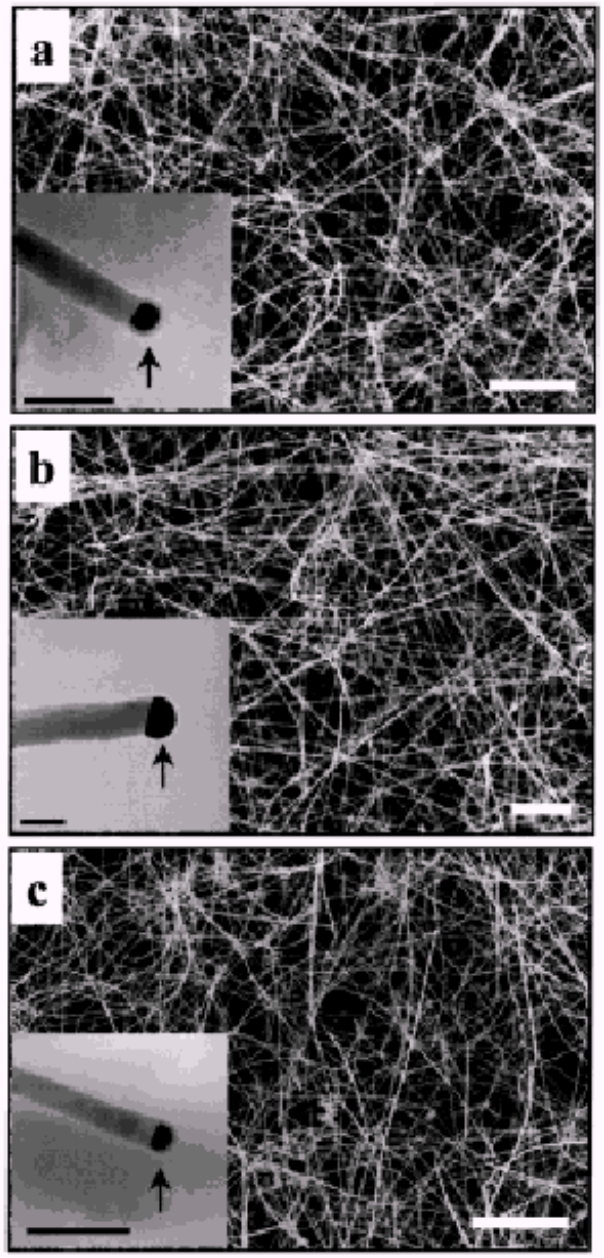

Fig. 2. FE-SEM images of a) GaAs, b) GaP, and c) $GaAs_{0.6}P_{0.4}$

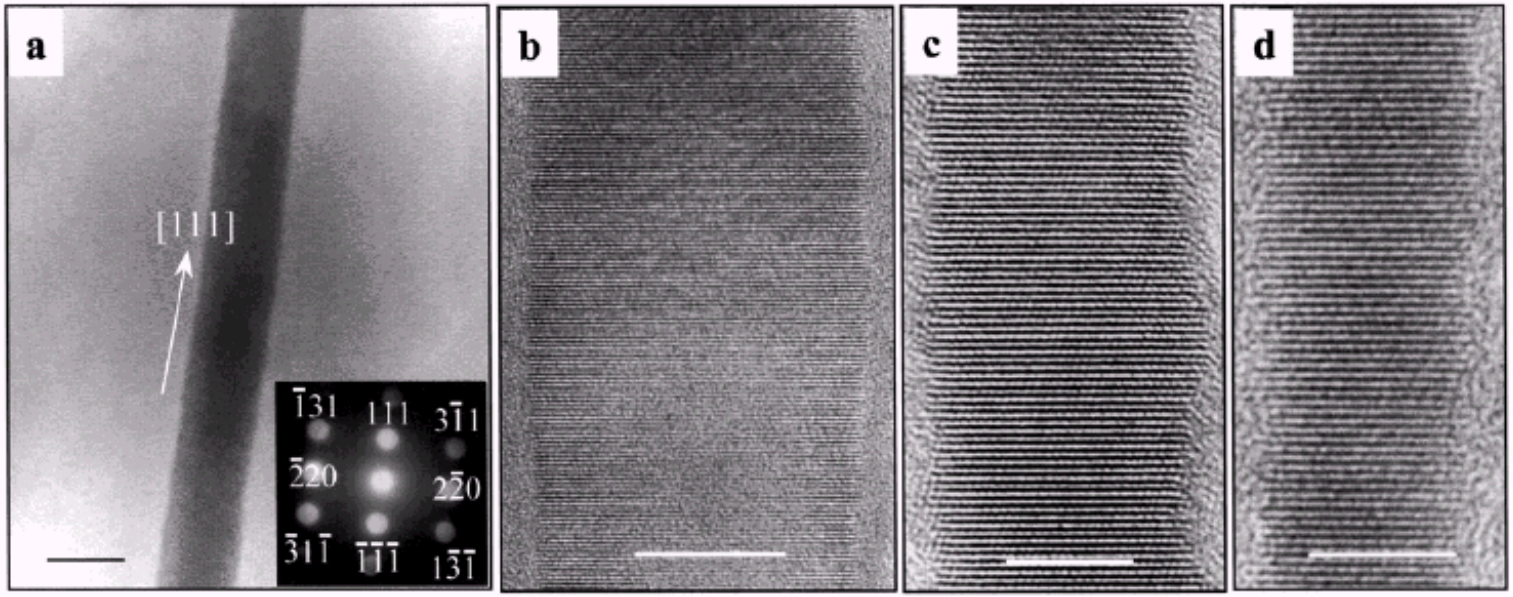

Fig. 3. a) Diffraction contrast TEM image of a ca. 20 nm diameter GaAs nanowire. The inset shows a convergent beam electron diffraction pattern (ED) recorded along the (112) zone axis. The (111) direction of the ED pattern is parallel to the wire axis, and thus shows that growth occurs along the (111) direction. The scale bar corresponds to 20 nm. b) High-resolution TEM image of a ca. 20 nm diameter GaAs nanowire. The lattice spacing perpendicular to the nanowire axis, 0.32 ± 0.01 nm, is in good agreement with the 0.326 nm spacing of (111) planes in bulk GaAs. The scale bar corresponds to

Structure characterization by HRTEM, EDX, ED.

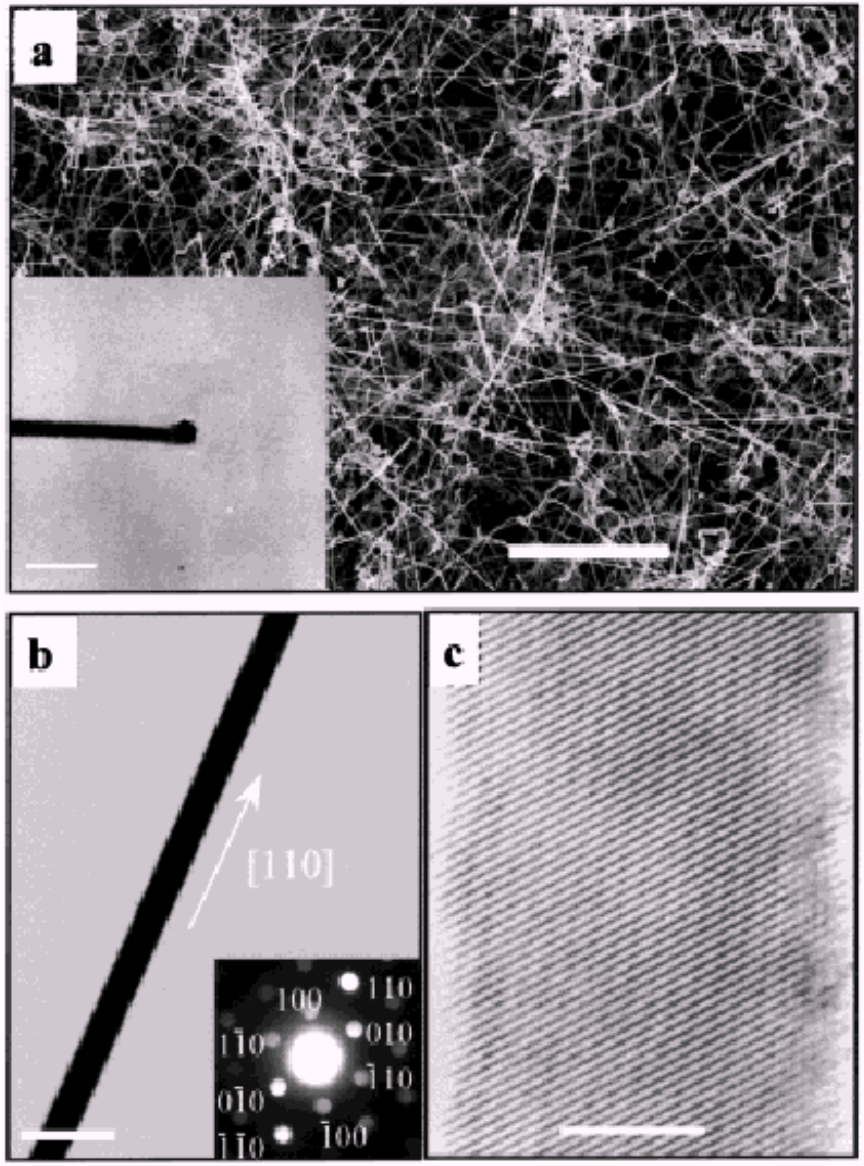

Fig. 4. a) FE-SEM image of CdSe nanowires prepared by LCG. The bar corresponds to 2 μm. The inset is the TEM image of an individual

Summary of single-crystal nanowires

Material	Growth Temperature [°C]	Minimum Diameter [nm]	Average Diameter [nm]	Structure	Growth Direction	Ratio of Components
GaAs	800–1030	3	19	ZB	<111>	1.00 : 0.97
GaP	870–900	3–5	26	ZB	<111>	1.00 : 0.98
$GaAs_{0.6}P_{0.4}$	800–900	4	18	ZB	<111>	1.00 : 0.58 : 0.41
InP	790–830	3–5	25	ZB	<111>	1.00 : 0.98
InAs	700–800	3–5	11	ZB	<111>	1.00 : 1.19
$InAs_{0.5}P_{0.5}$	780–900	3–5	20	ZB	<111>	1.00 : 0.51 : 0.51
ZnS	990–1050	4–6	30	ZB	<111>	1.00 : 1.08
ZnSe	900–950	3–5	19	ZB	<111>	1.00 : 1.01
CdS	790–870	3–5	20	W	<100>, <002>	1.00 : 1.04
CdSe	680–1000	3–5	16	W	<110>	1.00 : 0.99
$Si_{1-x}Ge_x$	820–1150	3–5	18	D	<111>	$Si_{1-x}Ge_x$

Direct observation of Vapor-Liquid-Solid Nanowire Growth

JACS **2001**, 123, 3165, Yang at UC Berkeley

In-situ High temperature TEM studies

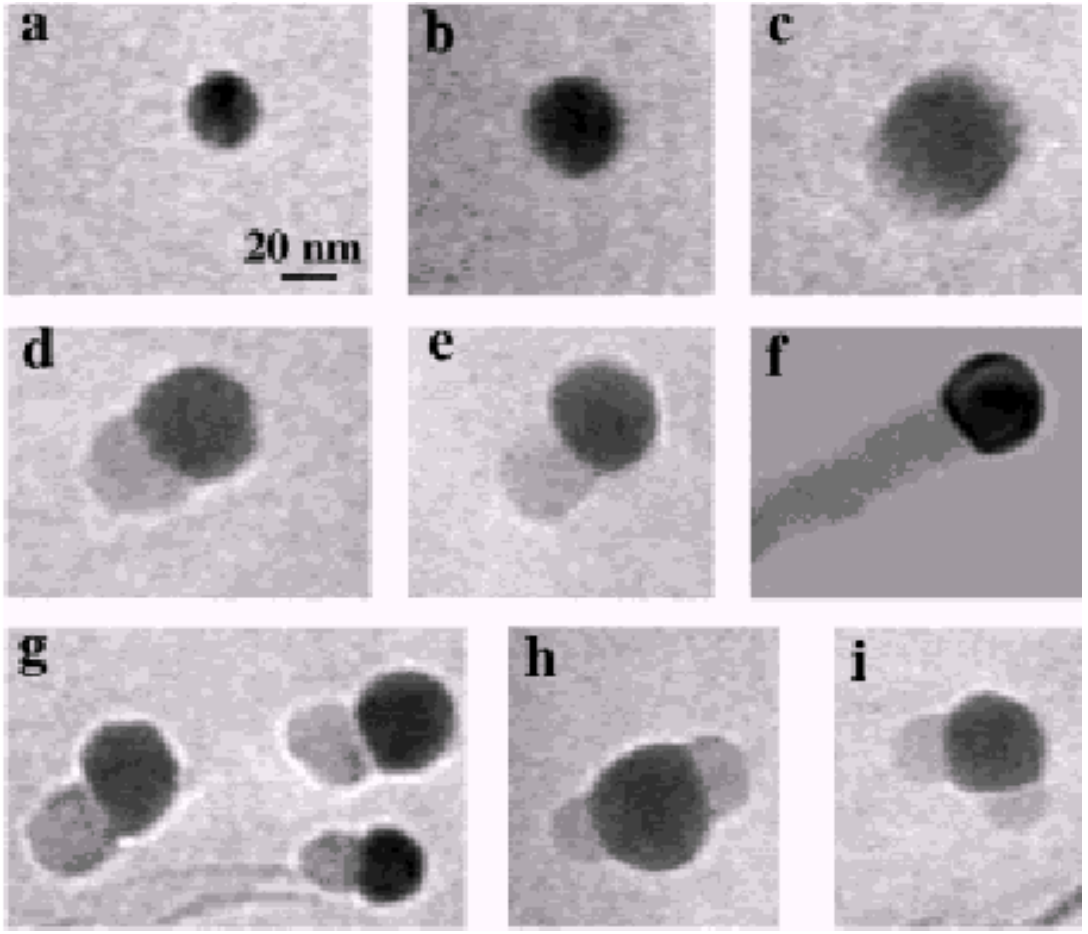

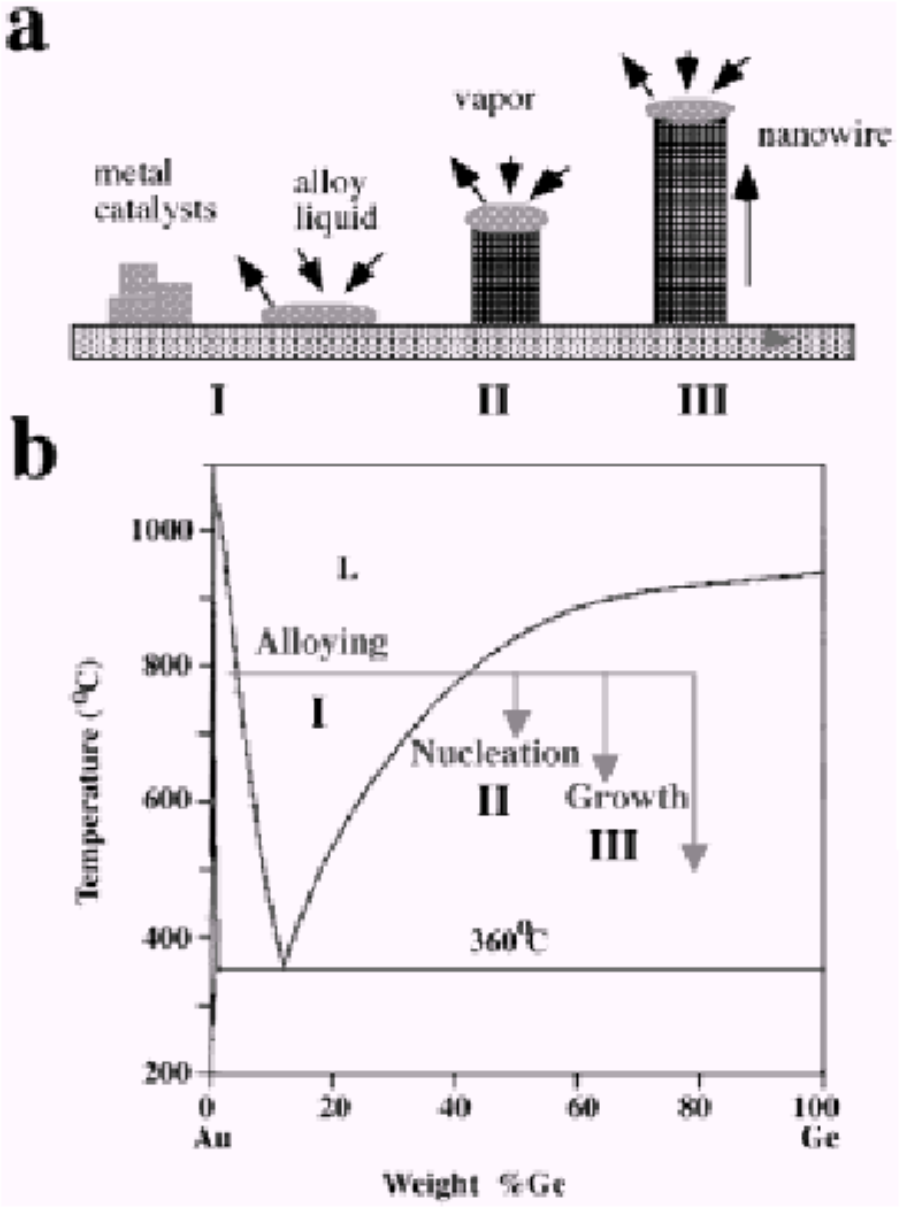

Diameter controlled synthesis of Si Nanowires

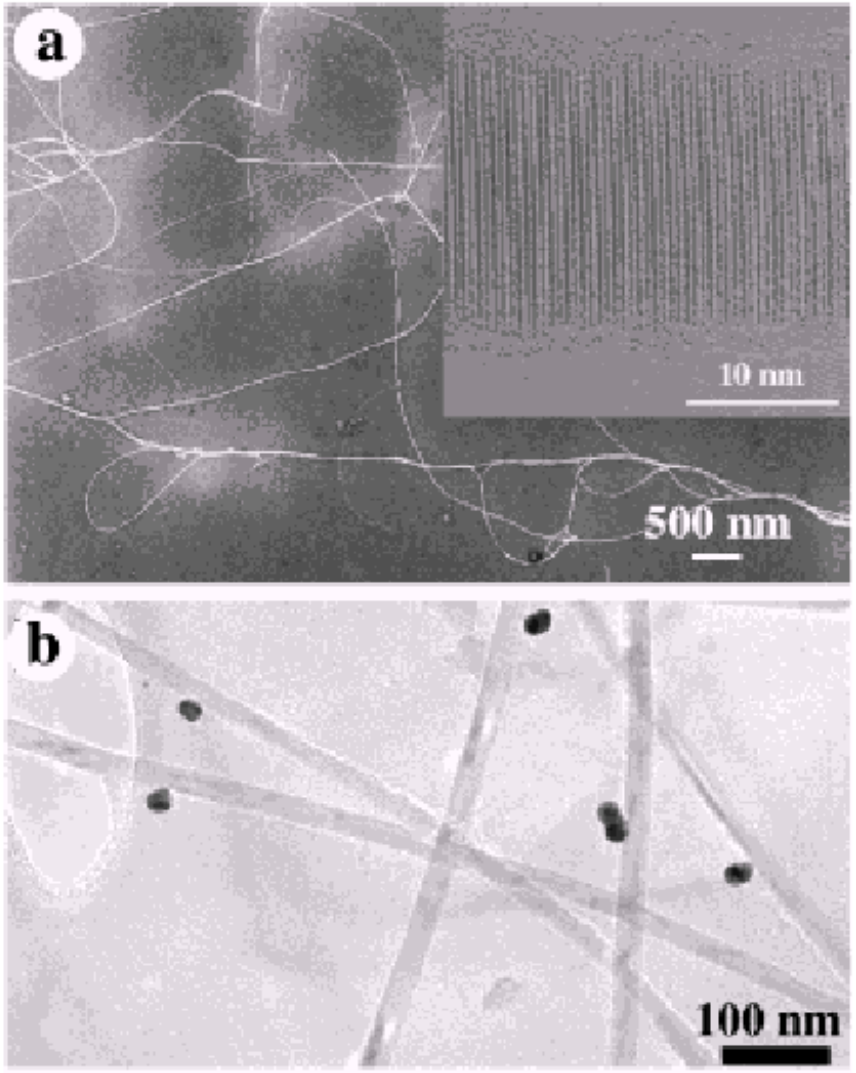

Figure 3. (a) FESEM image of Si nanowires grown on Au clusters embedded mesoporous silica thin film. Inset shows high-resolution TEM image of individual Si nanowire with the [111] lattice fringe. (b) TEM

Control of Thickness and Orientation of Solution-Grown Silicon Nanowires,

Brian A. Korgel (U. Texas), *Science* **2000**, *287*, 1471.

• Bulk quantities of defect-free silicon (Si) nanowires with nearly **uniform diameters ranging from 40 to 50 angstroms** were grown to a length of several micrometers with a supercritical fluid solution-phase approach.

• Alkanethiol coated gold nanocrystals (25 angstroms in diameter) were used as uniform seeds to direct one-dimensional Si crystallization in a solvent heated and pressurized above its critical point.

Solution-liquid-solid (SLS) Growth Process

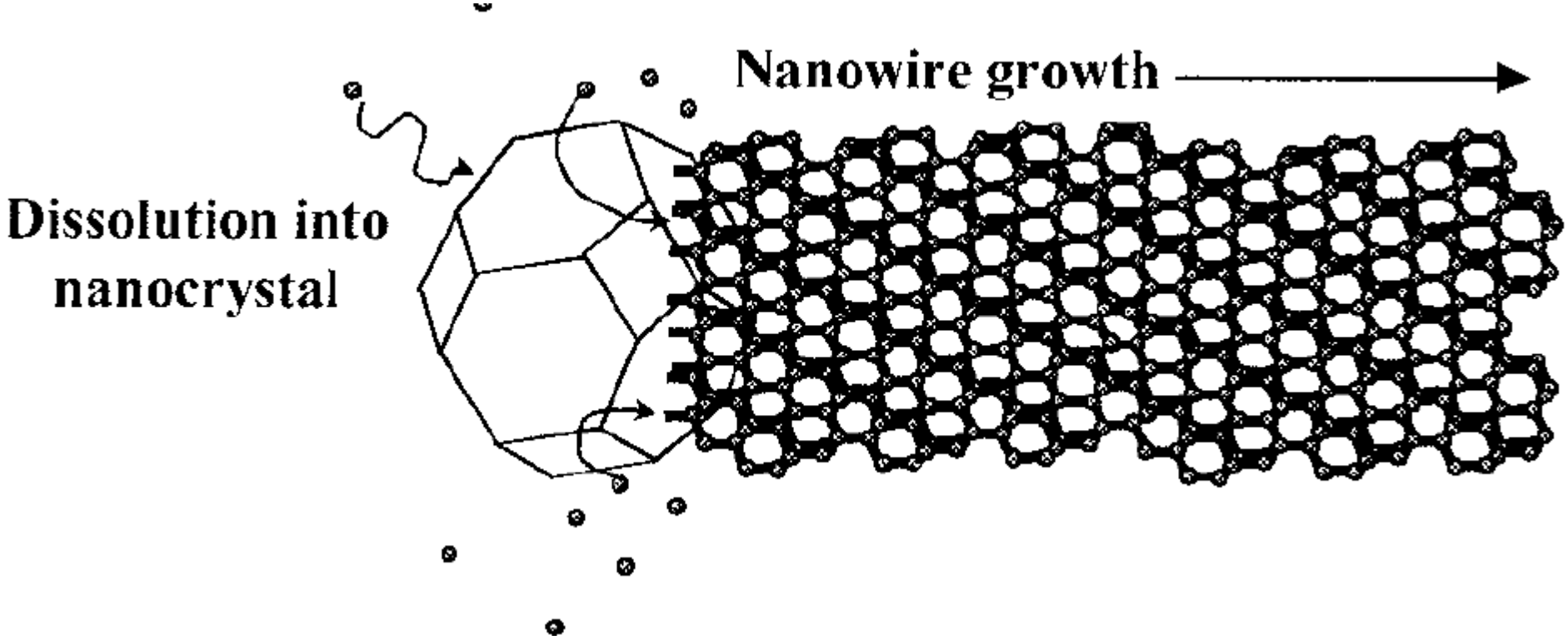

The orientation of the Si nanowires could be controlled with reaction pressure.

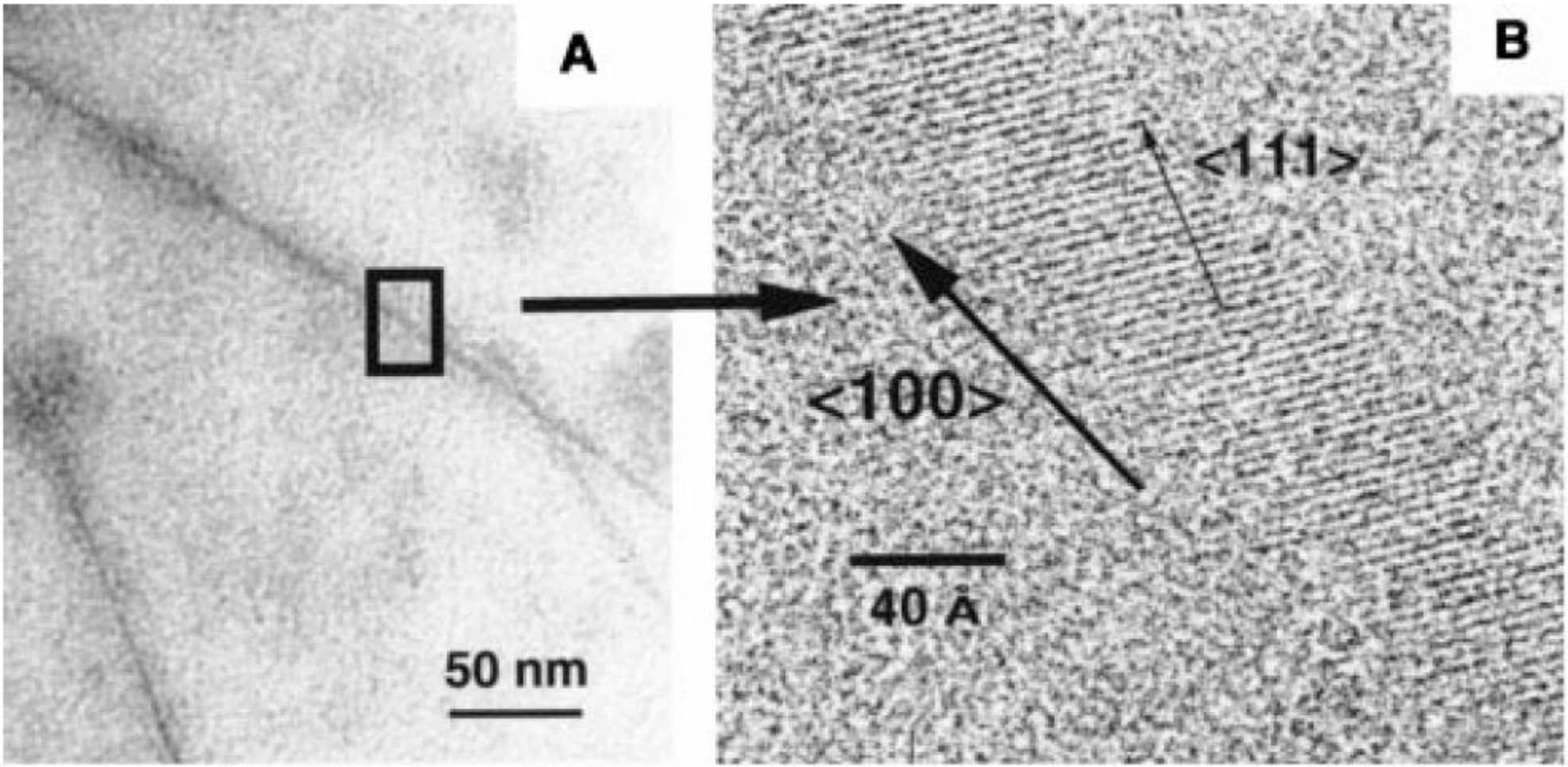

TEM images of Si nanowires synthesized at 500 ^{o}C in hexane at pressures of **200 bar (A and B)** and 270 bar (**C** and **D**).

The orientation of the Si nanowires could be controlled with reaction pressure.

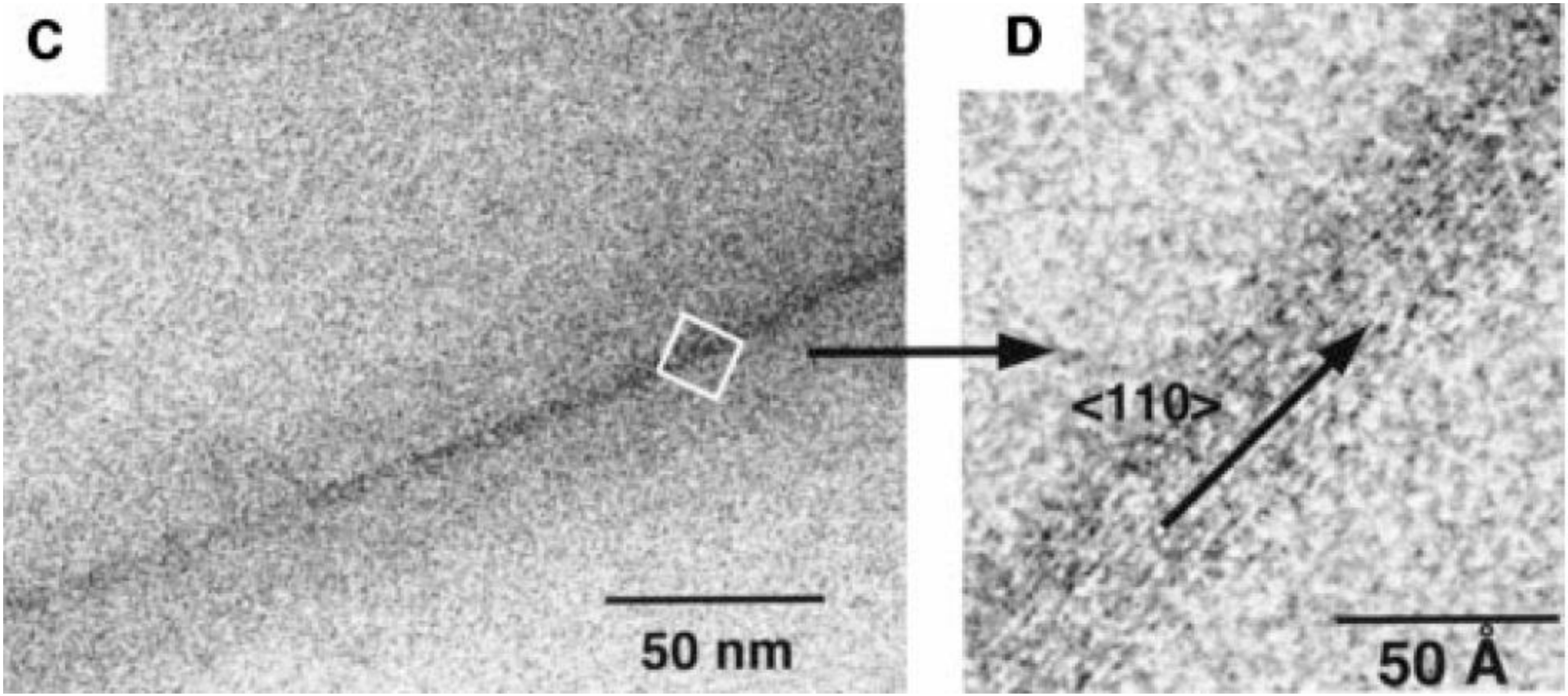

TEM images of Si nanowires synthesized at 500 ^{o}C in hexane at pressures of 200 bar (**A** and **B**) and **270 bar (C and D).**

Visible photoluminescence due to quantum confinement effects was observed, as were discrete optical transitions in the ultraviolet-visible absorbance spectra.

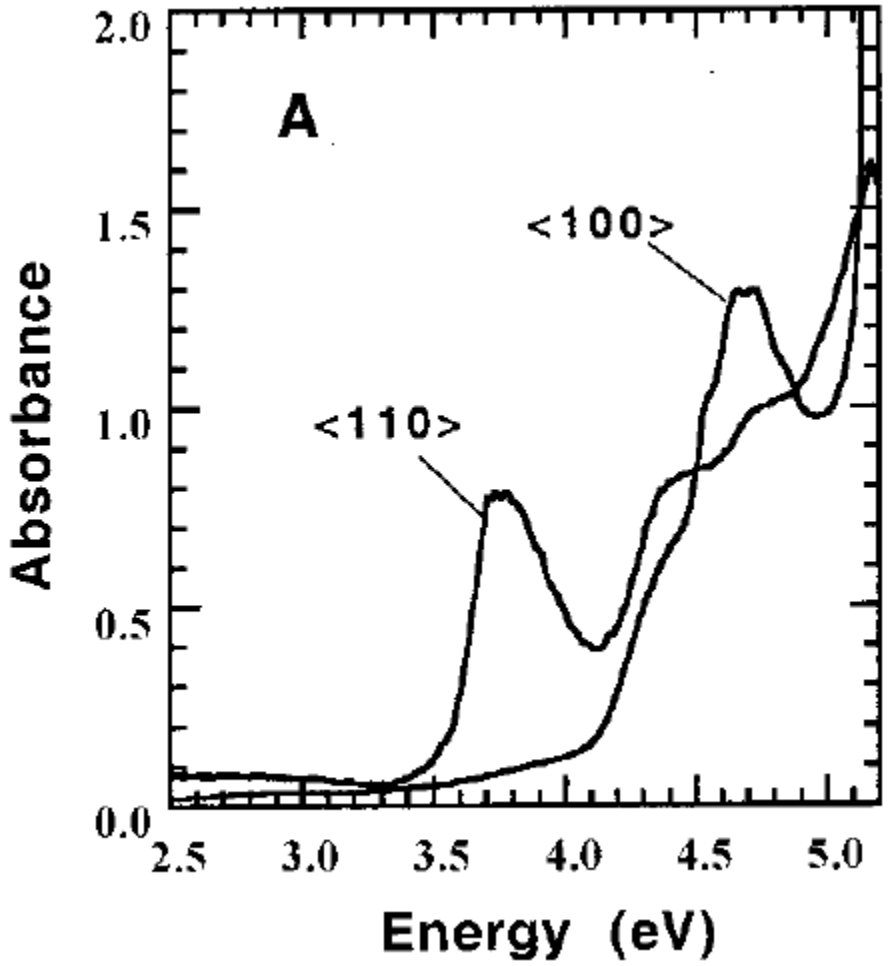

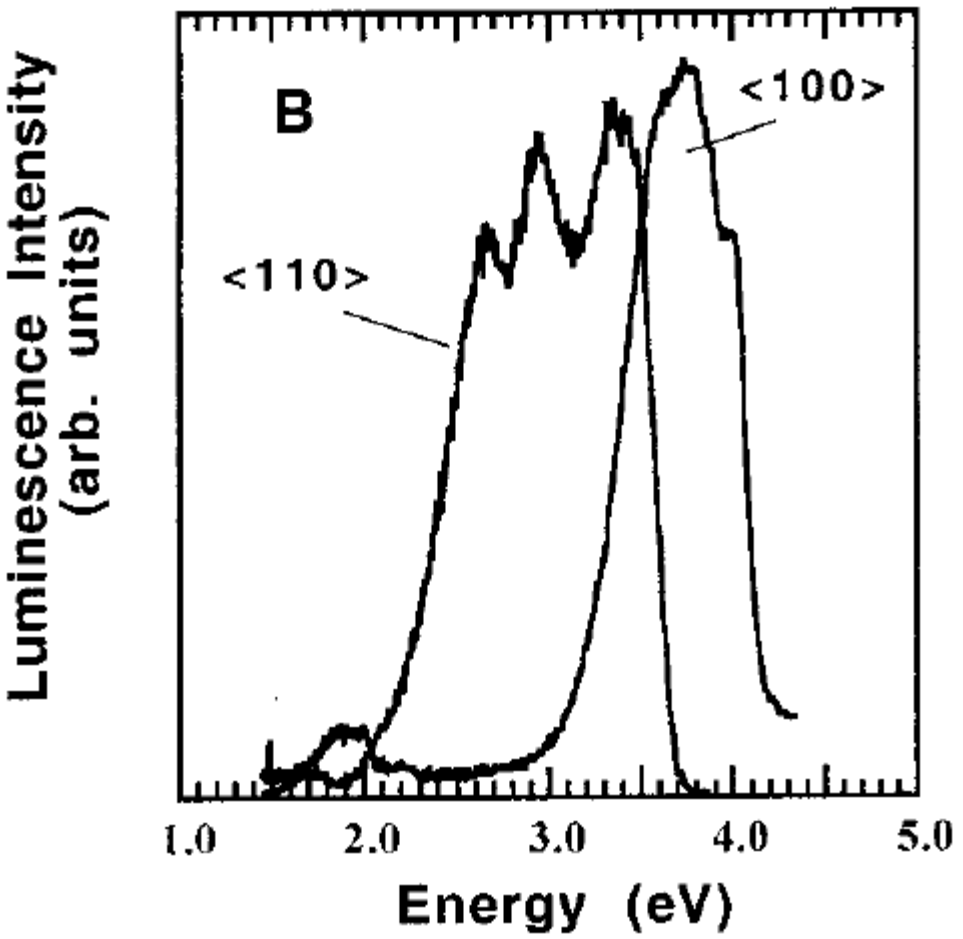

Ge Nanowires using Au Nanoparticles as Catalysts

JACS 2002, 124, by Korgel at U.Texas/ChemE

- Ge nanowires ranging from 10 ~ 150 nm in diameter and several micrometer in length in supercritical cyclohexane
- Alkanethiol-protected Au nanocrystals (2.5 nm or 6.5 nm)
- Solution-liquid-solid (SLS) growth mechanism

Solution-liquid-solid mechanism

Scheme 1. Binary Phase Diagram for the Au:Ge (Adapted from Ref 22)[a]

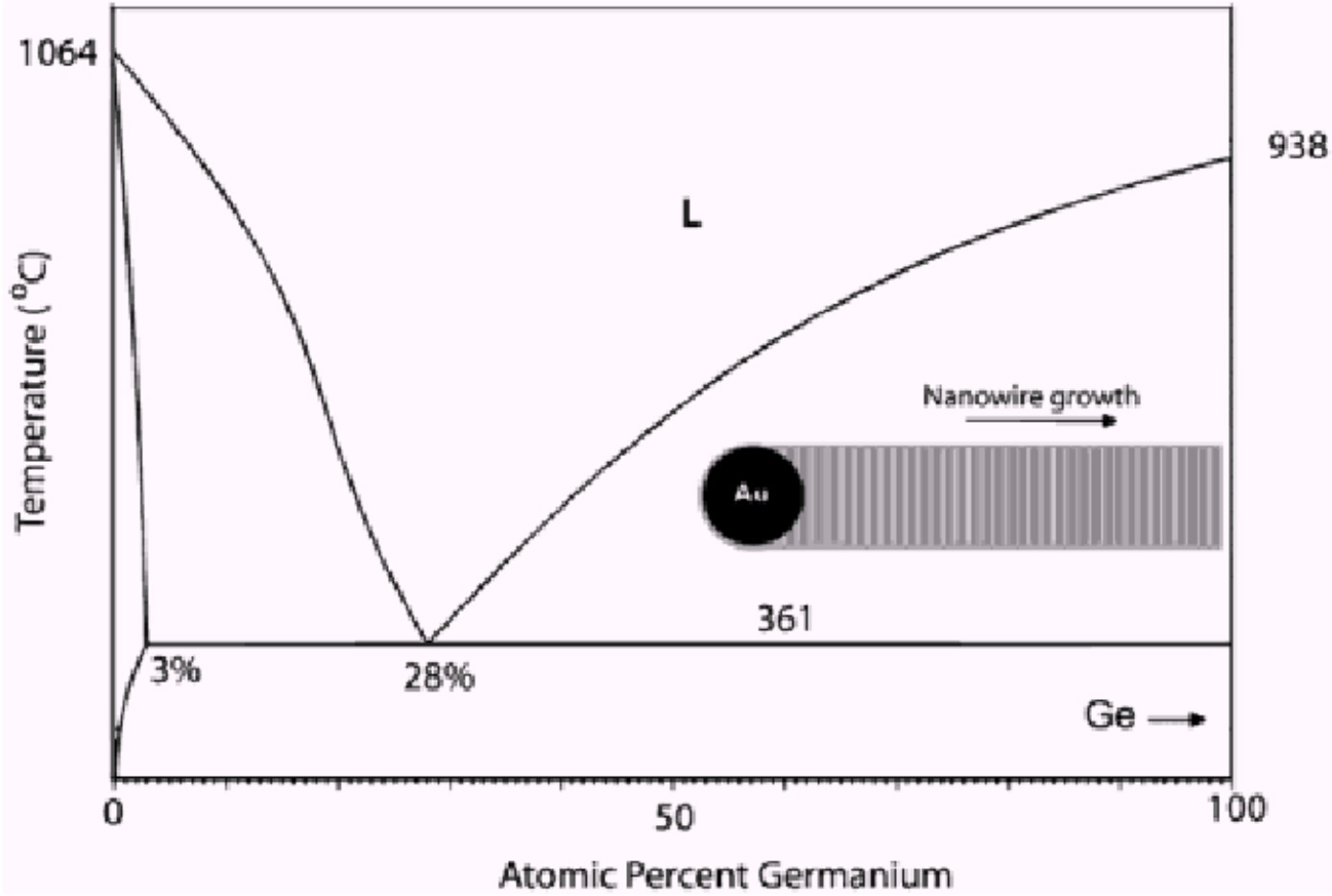

Tetraethylgermanium and biphenylgermanium as Ge Precursors

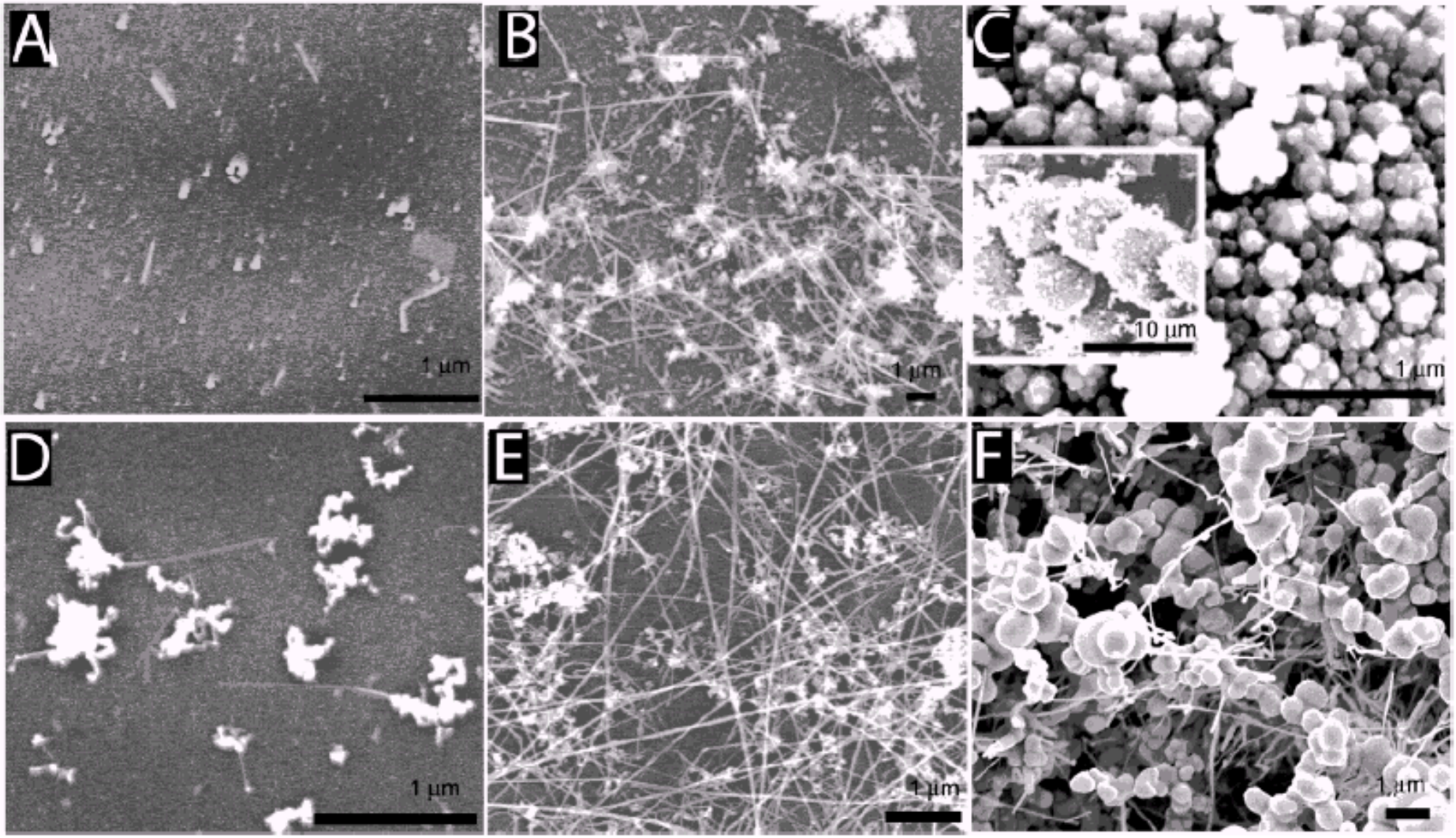

Figure 2. HRSEM images of Ge nanowires grown at 38 MPa for 20 min using TEG at (A) 300, (B) 400, (C) 500 °C. Ge nanowires grown at 38 M
8 min using DPG at (D) 300, (E) 400, and (F) 500 °C. The micrometer-sized particles in (C) and (F) are Ge particles, as confirmed by nanometer-sca
mapping. The morphology of wires produced from DPG with 20-min reaction time was similar to the those shown in (D)−(F). The inset in (C) s
low-magnification image of micrometer spheres formed at 500 °C.

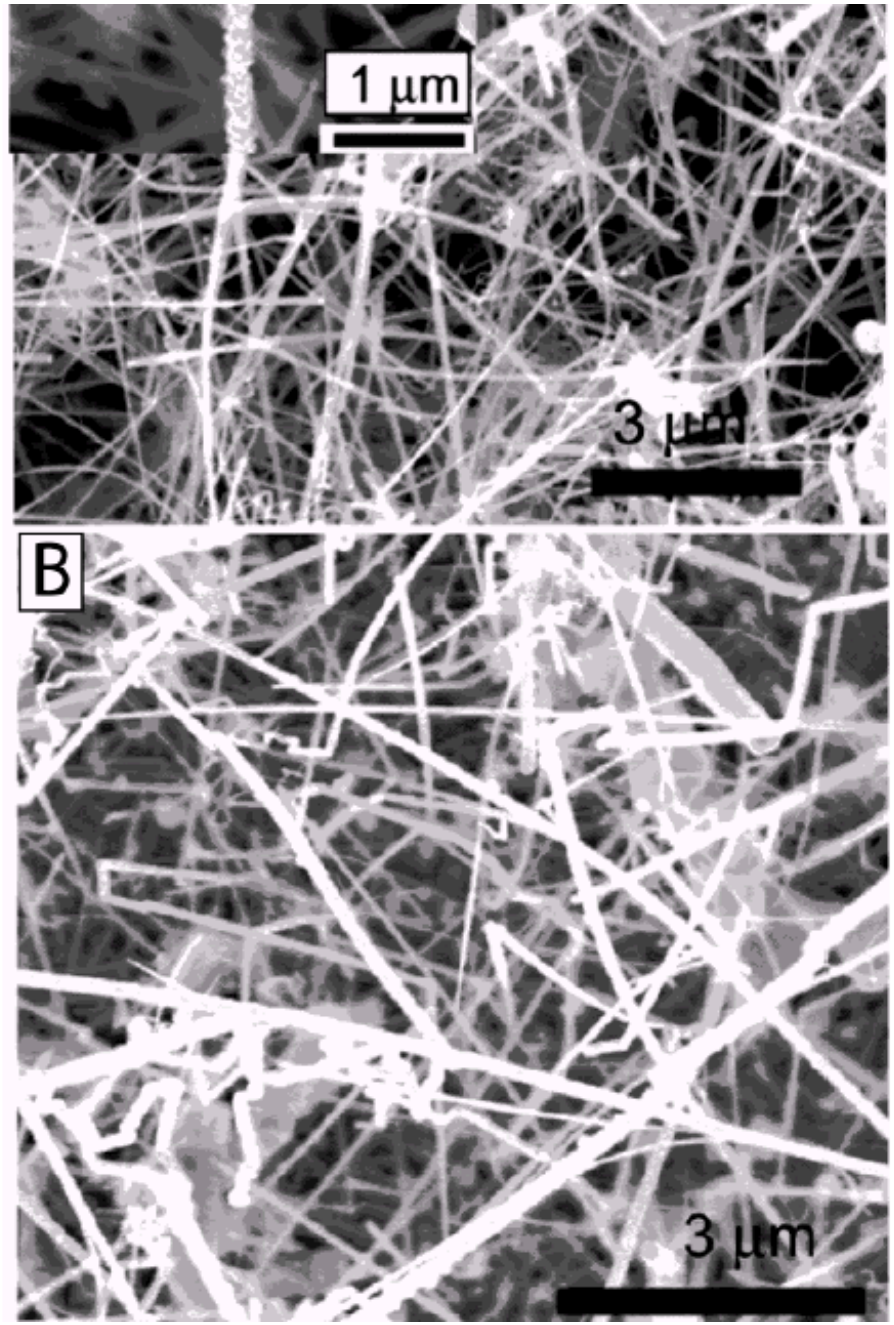
1 µm
3 µm
B
3 µm

Figure 4. HRTEM and XRD of Ge nanowires (A) synthesized from DPG at 350 °C and 38 MPa, exhibiting the 110 growth direction, and (B) synthesized from TEG at 400 °C and 38 MPa, growing in the 111 direction. (C) XRD pattern of a nanowire sample obtained from DPG at 400 °C and 38 MPa. The inset shows the corresponding SAED pattern recorded along the [111] axis.

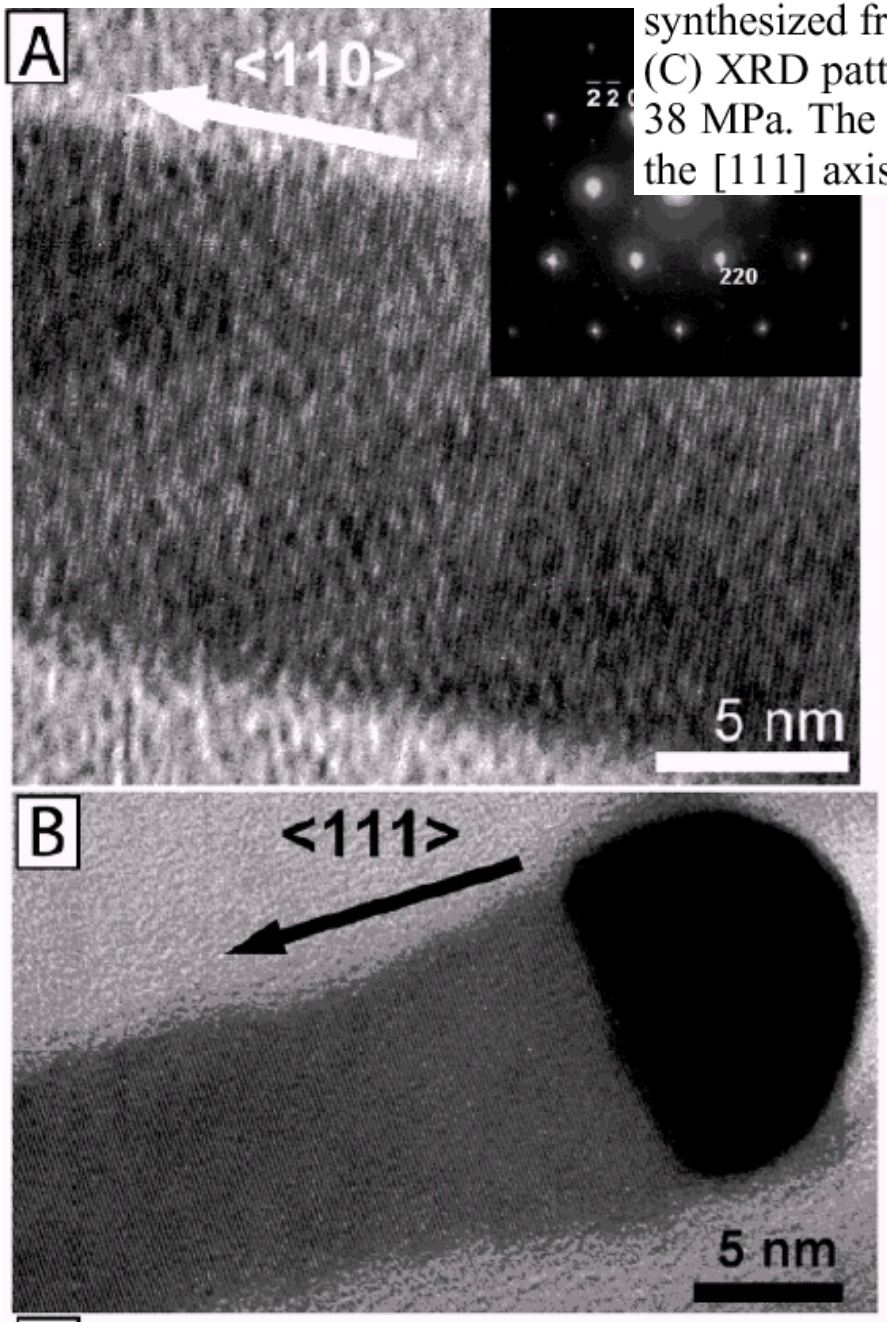

Different Ge precursor produces Nanowires with different Growth direction

Solution-Liquid-Solid (SLS) Growth of Silicon Nanowires, Brian A. Korgel, *J. Am. Chem. Soc.* **2008**, 130, 5436.

- Si nanowire growth by the SLS mechanism at atmospheric pressure using trisilane (Si3H8) as a reactant in octacosane (C28H58, bp = 430 C) or squalane (C30H62, bp = 423) and either gold (Au) or bismuth (Bi) nanocrystals as seeds.
- Au forms a eutectic with Si at 363 °C, and Bi forms a eutectic with Si at 264 °C.

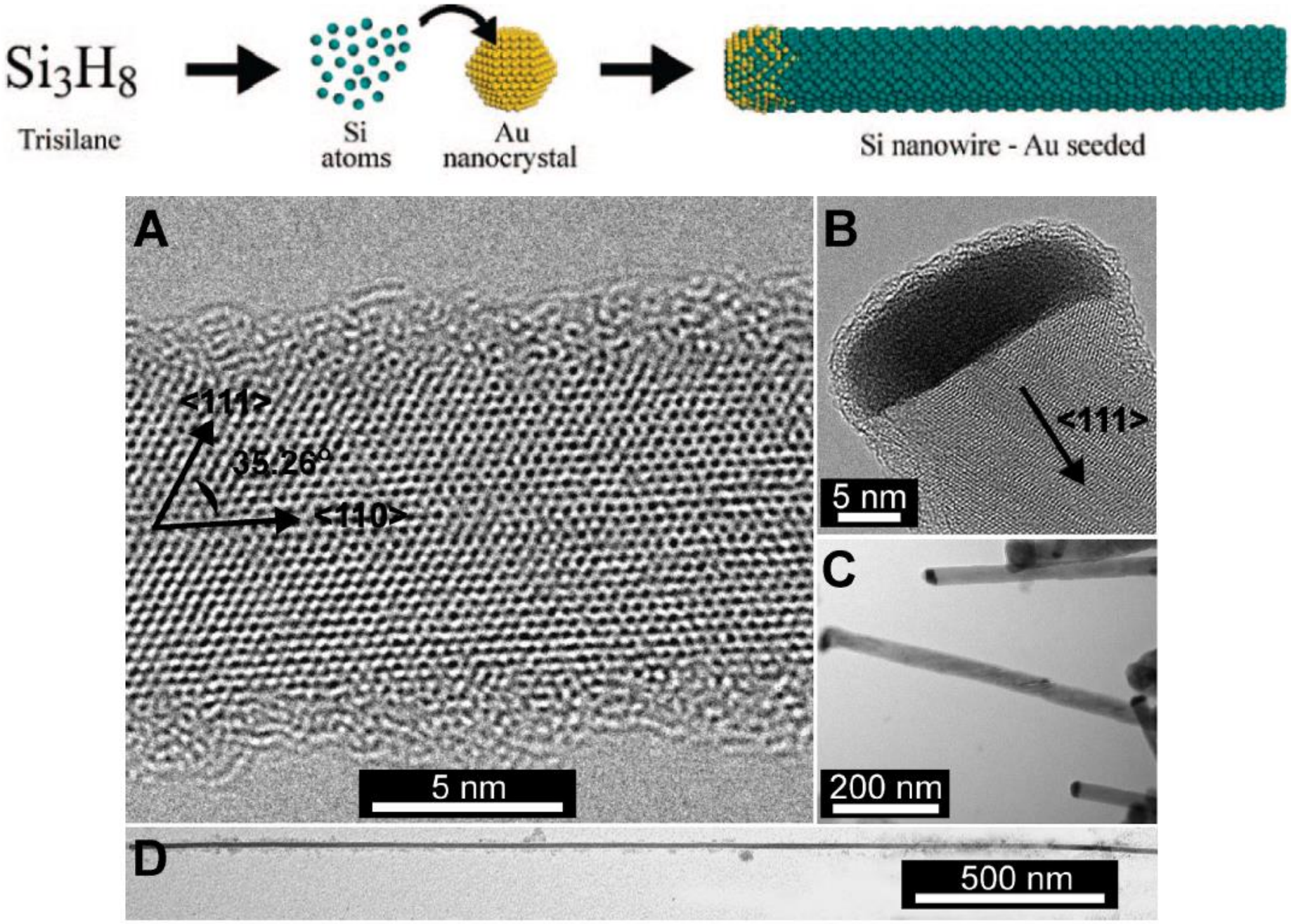
Si_3H_8
Trisilane
Si atoms
Au nanocrystal
Si nanowire - Au seeded
A
<111>
35.26°
<110>
5 nm
B
<111>
5 nm
C
200 nm
D
500 nm

Large scale synthesis of 4 mg (?) of Si nanowires

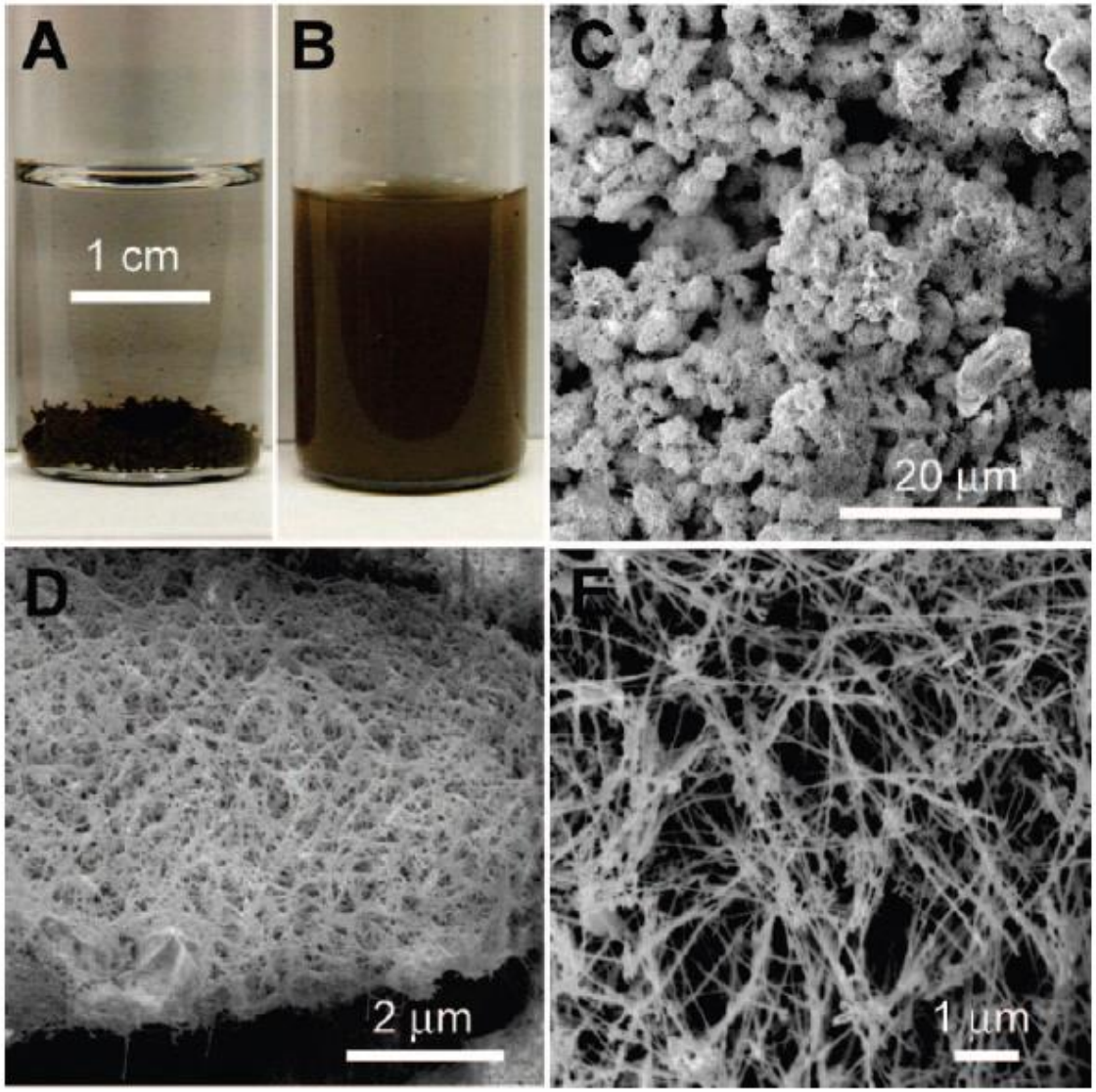

26 nm X 2.0 μm,

Kinetics of Individual Nucleation Events Observed in Nanoscale Vapor-Liquid-Solid Growth, F. M. Ross (IBM)

Science **2008**, 322, 1070.

- Nucleation and growth kinetics of solid silicon (Si) from liquid gold-silicon (AuSi) catalyst particles as the Si supersaturation increased.
- Nucleation is heterogeneous, occurring consistently at the edge of the AuSi droplet.

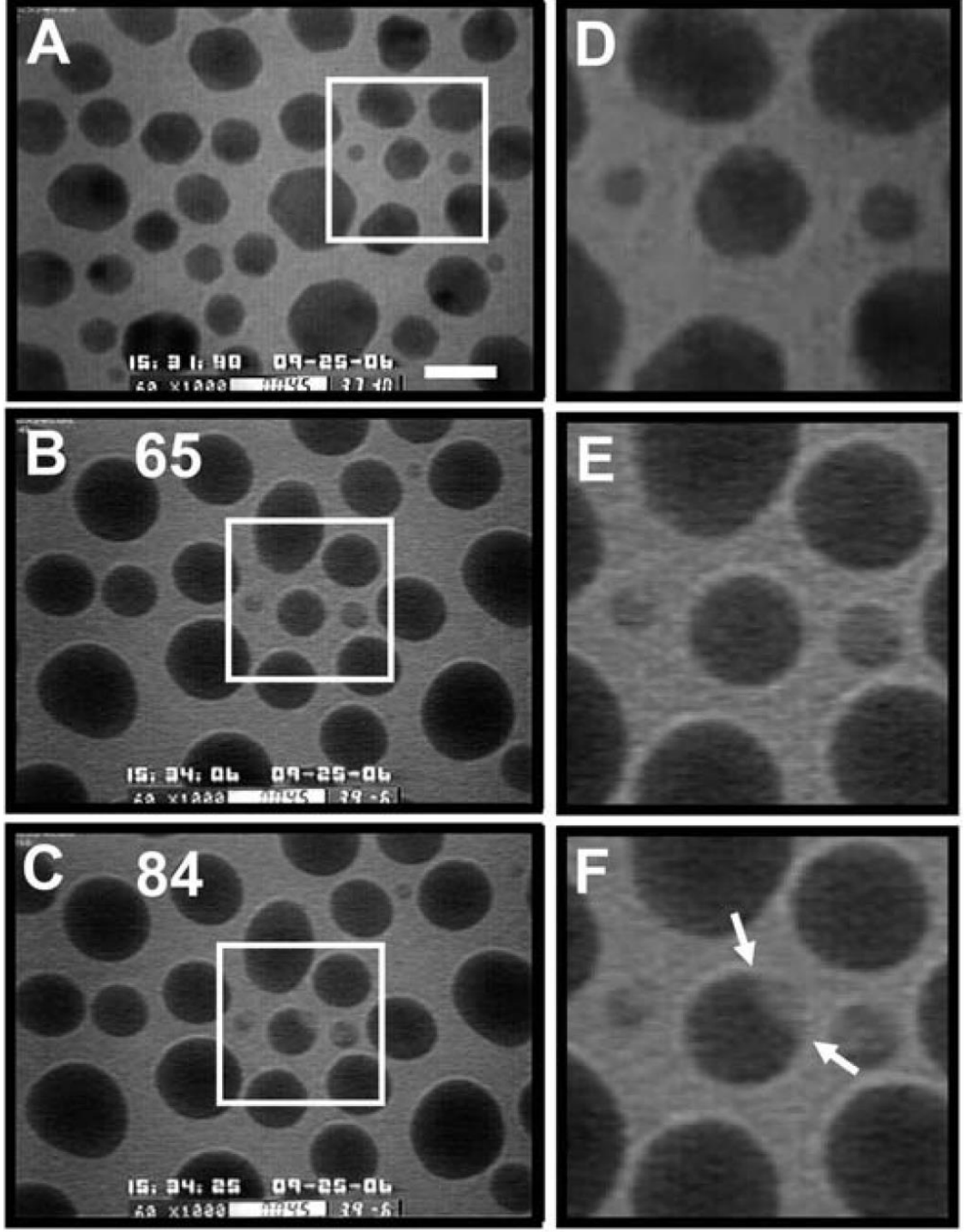
A
D
B
65
E
C
84
F

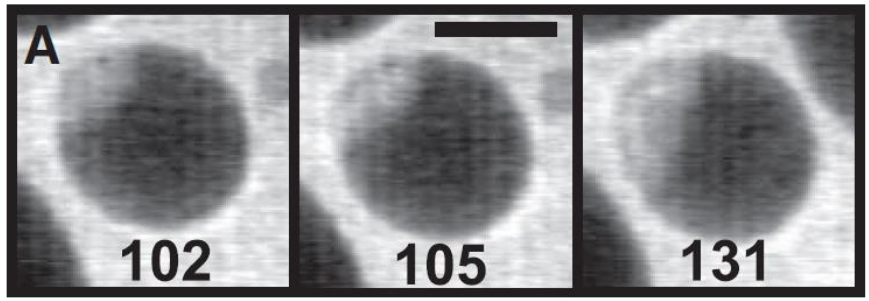
A
102
105
131

Formation of Compositionally Abrupt Axial Heterojunctions in Silicon-Germanium Nanowires, F. M. Ross (IBM)

Science **2009**, 326, 1247.

- Fabrication of compositionally abrupt interfaces in Si-Ge and Si-SiGe heterostructure nanowires by using solid Al-Au alloy catalyst rather than the conventional liquid semiconductor–metal eutectic droplets.
- Real-time imaging of growth kinetics reveals that a low solubility of Si and Ge in the solid particle accounts for the interfacial abruptness.

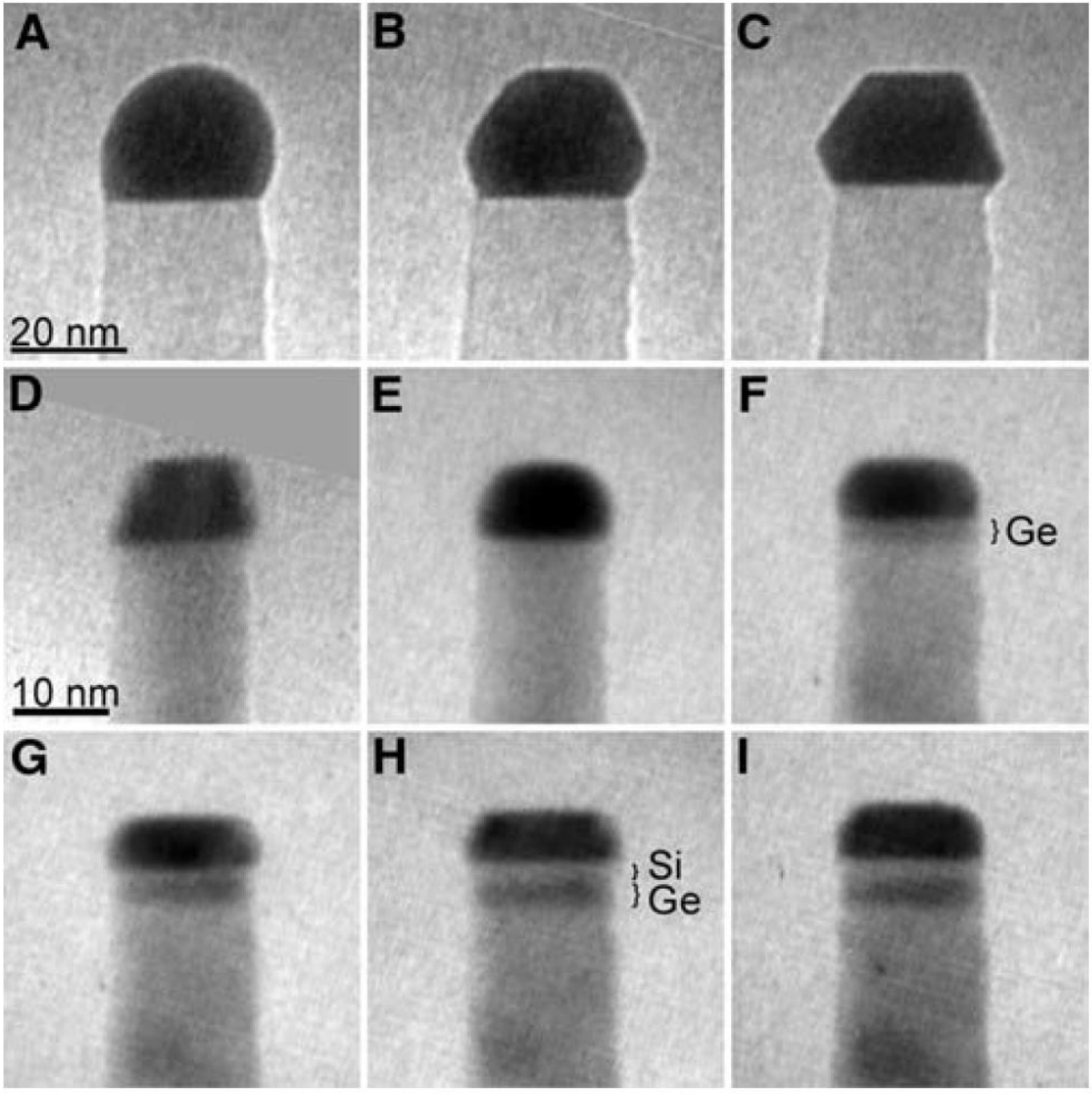
A
B
C
20 nm
D
E
F
Ge
10 nm
G
H
I
Si
Ge

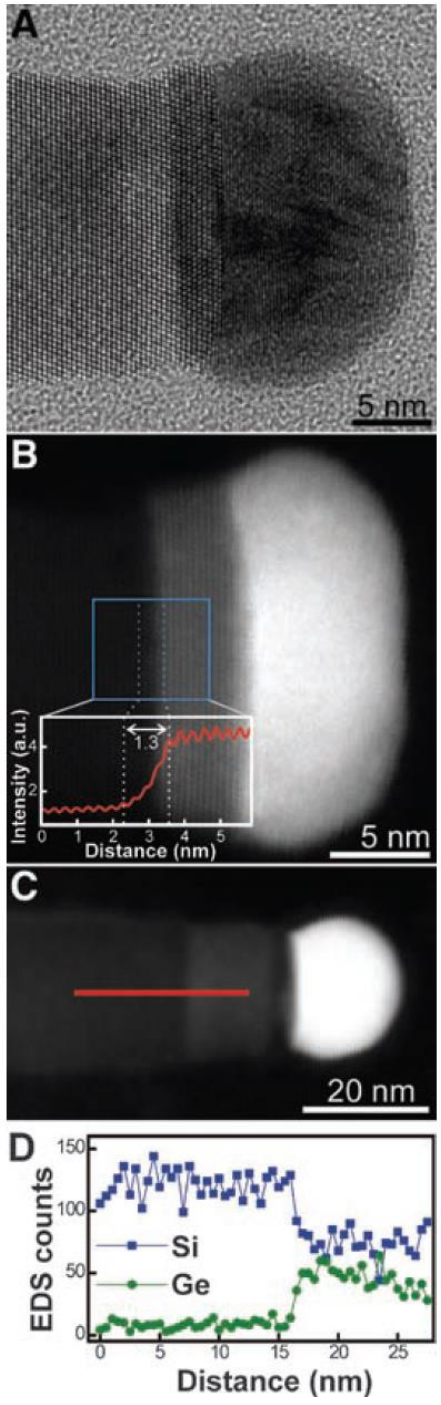
A
5 nm
B
Intensity (a.u.)
1.3
Distance (nm)
5 nm
C
20 nm
D
EDS counts
Si
Ge
Distance (nm)

Small-Diameter Silicon Nanowire Surfaces

S. T. Lee (Univ. Hong Kong), Science 2003, 299, 1874.

- SiNWs were prepared by an oxide-assisted growth method, in which SiO powders were heated to 1200°C in an alumina tube under a flowing gas of 4% H2 mixed in Ar.
- The wires had diameters in the range of a few to tens of nanometers and were composed primarily of a single crystalline Si core and an oxide sheath about one-third of the diameter.
- HF treatment removed oxide coating to get H-terminated Si Nanowires.

STM images of Si nanowires

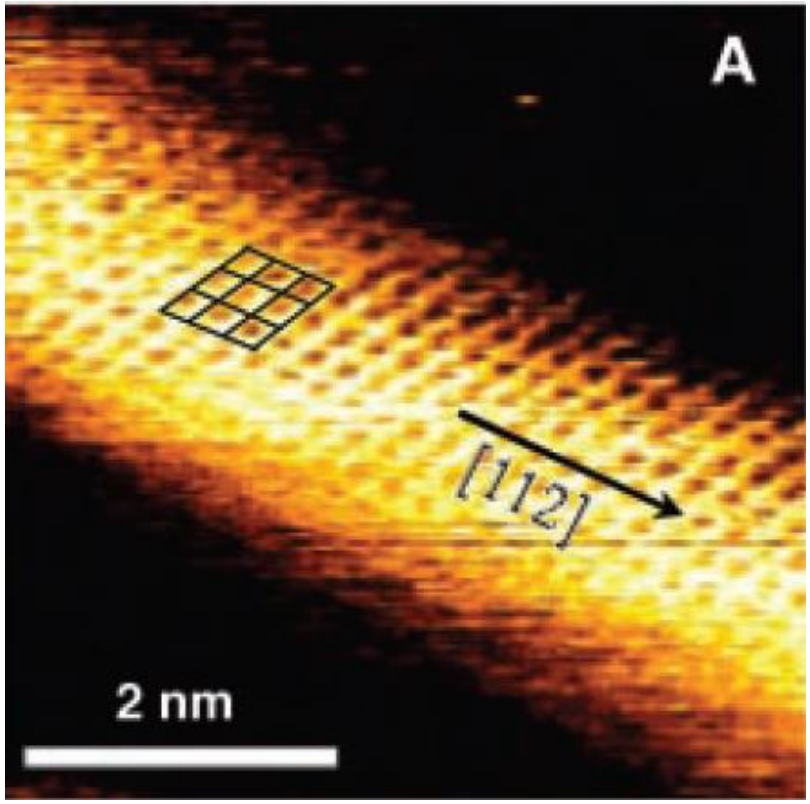

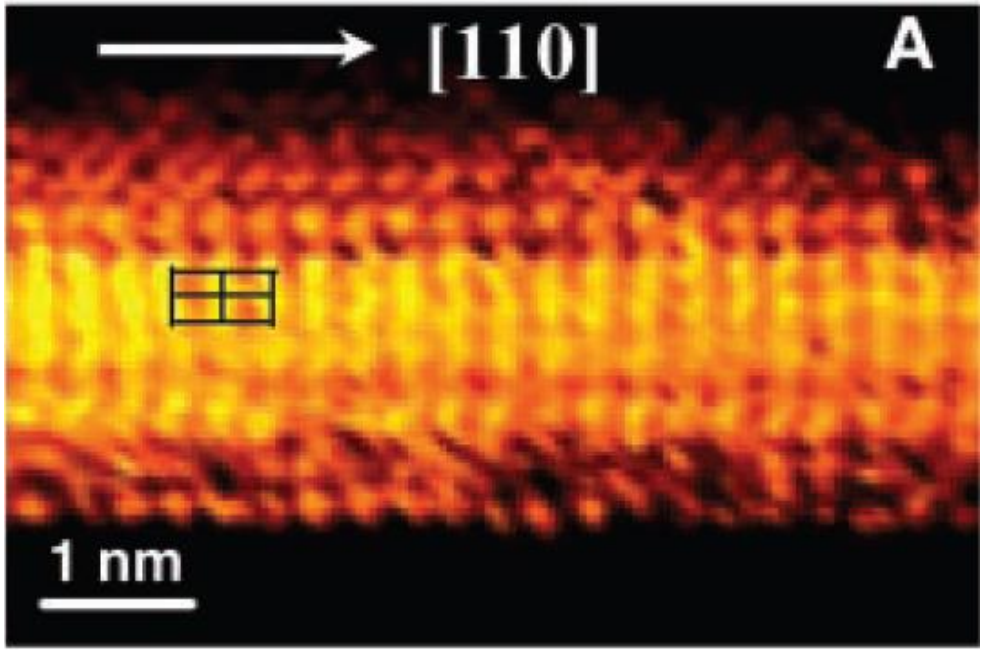

Two- versus three-dimensional quantum confinement in indium phosphide wires and dots

William E. Buhro (Washington University, St. Louis)

Nature Mater. **2003**, *2*, 517.

- Indium phosphide (InP) quantum wires

having diameters in the strong-confinement regime.

- Theoretical evidence to establish that the quantum

confinement observed in the InP wires is weakened

to the expected extent, relative to that in InP dots,

by the loss of one confinement dimension.

• **Monodisperse metallic (In) nanoparticles with controlled diameters by heterogeneous seeded growth.**

(Buhro,W. E.Heterogeneous seeded growth: a potentially general synthesis of monodisperse metallic nanoparticles. *J.Am. Chem. Soc.* **123,** 9198–9199 (2001)).

• SLS growth of InP quantum wires was conducted in solution at 203 °C by thermal decomposition of [Me2InP(SiMe3)2]2 in the presence of In-nanoparticles.

• Quantum wires were several micrometres in length, and possessed diameters that depended on the size of the catalyst nanoparticles used in their growth

Predictions of simple particle-in-a-box models for the size dependences of the kinetic confinement energies of electrons and holes in corresponding quantum wells, wires and dots.

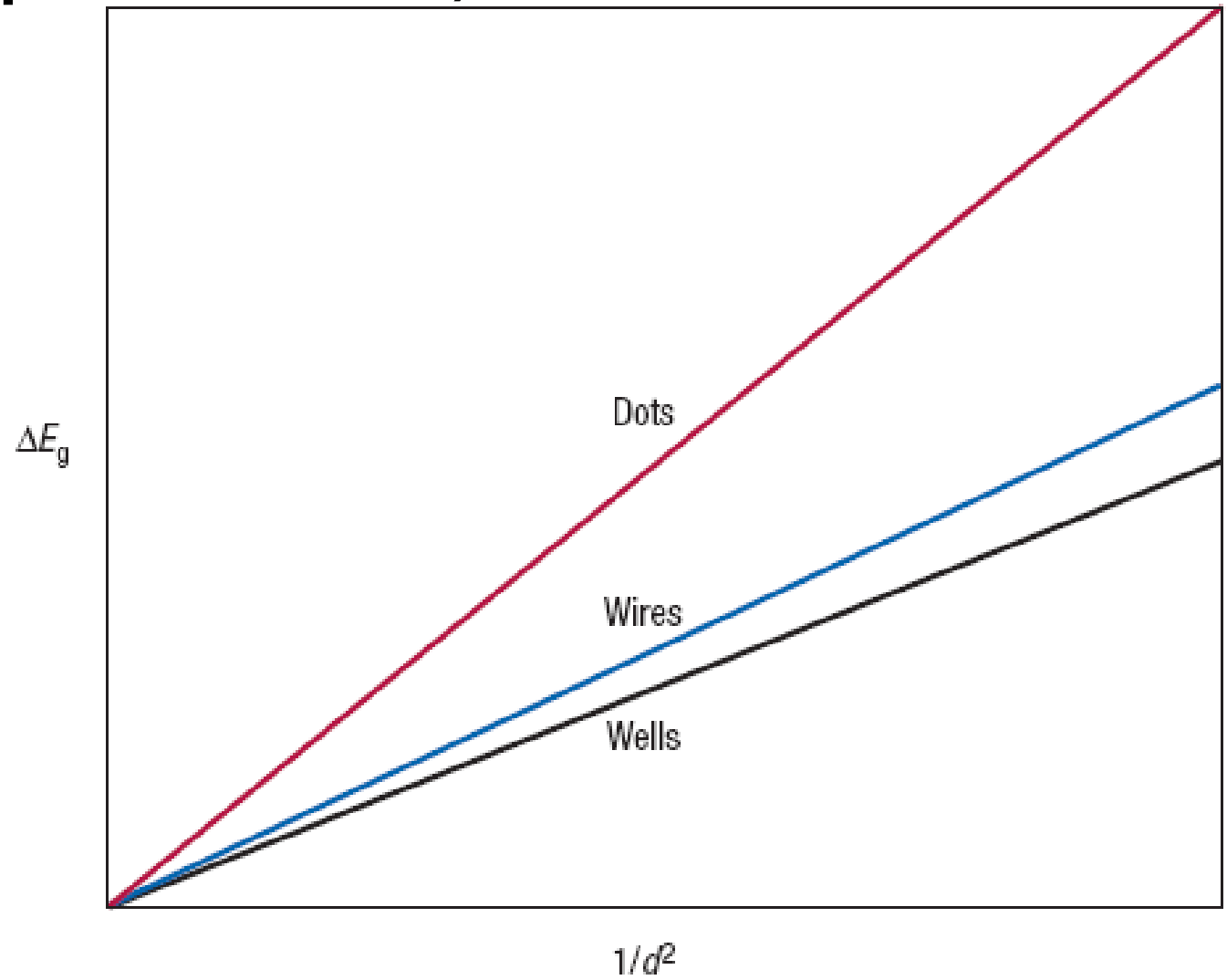

Electron diffraction established that the wires were crystalline with the [111] direction of the zinc-blende structure oriented parallel to their long axes.

Standard deviations of diameters: 13–21% of mean diameter.

The relationship between the diameters of the quantum wires (*d*wire) and the initial diameter of catalyst nanoparticles (*d*cat)

$$d_{\text{wire}}\,(\text{nm}) = (0.46 \pm 0.09) \cdot d_{\text{cat}}\,(\text{nm}) + (0.17 \pm 1.05)$$

Table 1 Size data for In-catalyst nanoparticles, InP quantum wires grown from them, and spectrocopic data for the quantum wires.

In nanoparticle diameter (nm)	InP quantum wire diameter (nm)	Exciton λ (nm)	E_g (eV)	ΔE_g (eV)
4.5*	3.49 ± 0.61 (± 17%)	711 ± 1	1.75 ± 0.01	0.40 ± 0.01
4.5*	3.53 ± 0.65 (± 18%)	720 ± 2	1.73 ± 0.01	0.38 ± 0.01
9.88 ± 0.795 (± 8.0%)	4.49 ± 0.75 (± 17%)	773 ± 1	1.61 ± 0.01	0.26 ± 0.01
9.88 ± 0.795 (± 8.0%)	4.86 ± 0.65 (± 13%)	784 ± 1	1.58 ± 0.01	0.24 ± 0.01
12.5*	5.55 ± 0.85 (± 15%)	798 ± 1	1.56 ± 0.01	0.21 ± 0.01
13.95 ± 1.35 (± 9.7%)	6.61 ± 1.03 (± 16%)	818 ± 1	1.52 ± 0.01	0.17 ± 0.01
20.57 ± 1.98 (± 9.6%)	8.84 ± 1.81 (± 20%)	842 ± 2	1.48 ± 0.01	0.13 ± 0.01
21.23 ± 2.05 (± 9.7%)	11.01 ± 2.29 (± 21%)	–	–	–

SLS growth of InP quantum wires was conducted in solution at 203 °C by thermal decomposition of $[Me_2InP(SiMe_3)_2]_2$ in the presence of In-nanoparticle catalysts.

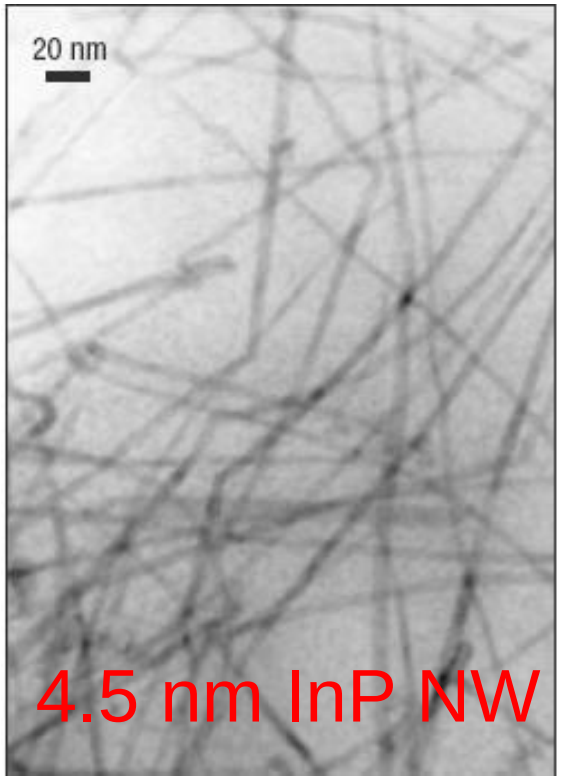

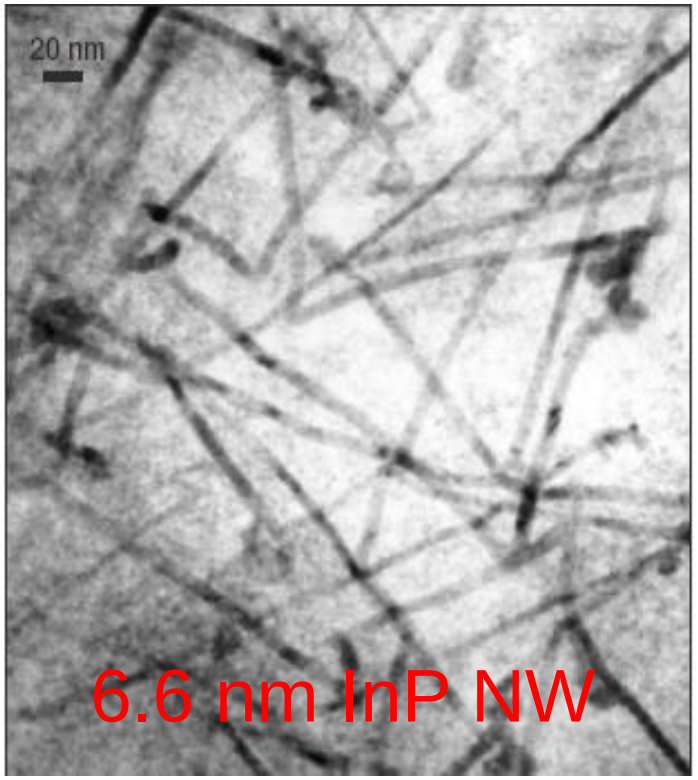

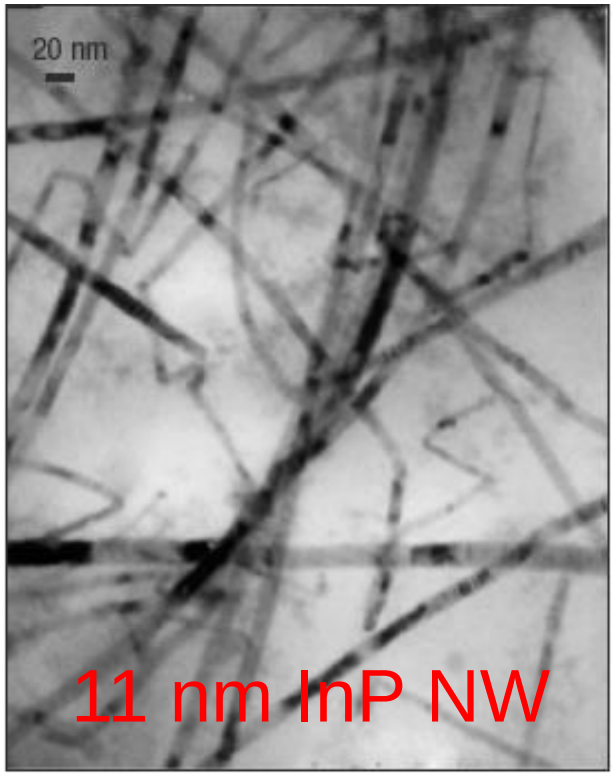

Poly(1-hexadecene0.67-*co*-vinylpyrrolidinone0.33) to stabilize both the catalyst nanoparticles and the product nanowires.

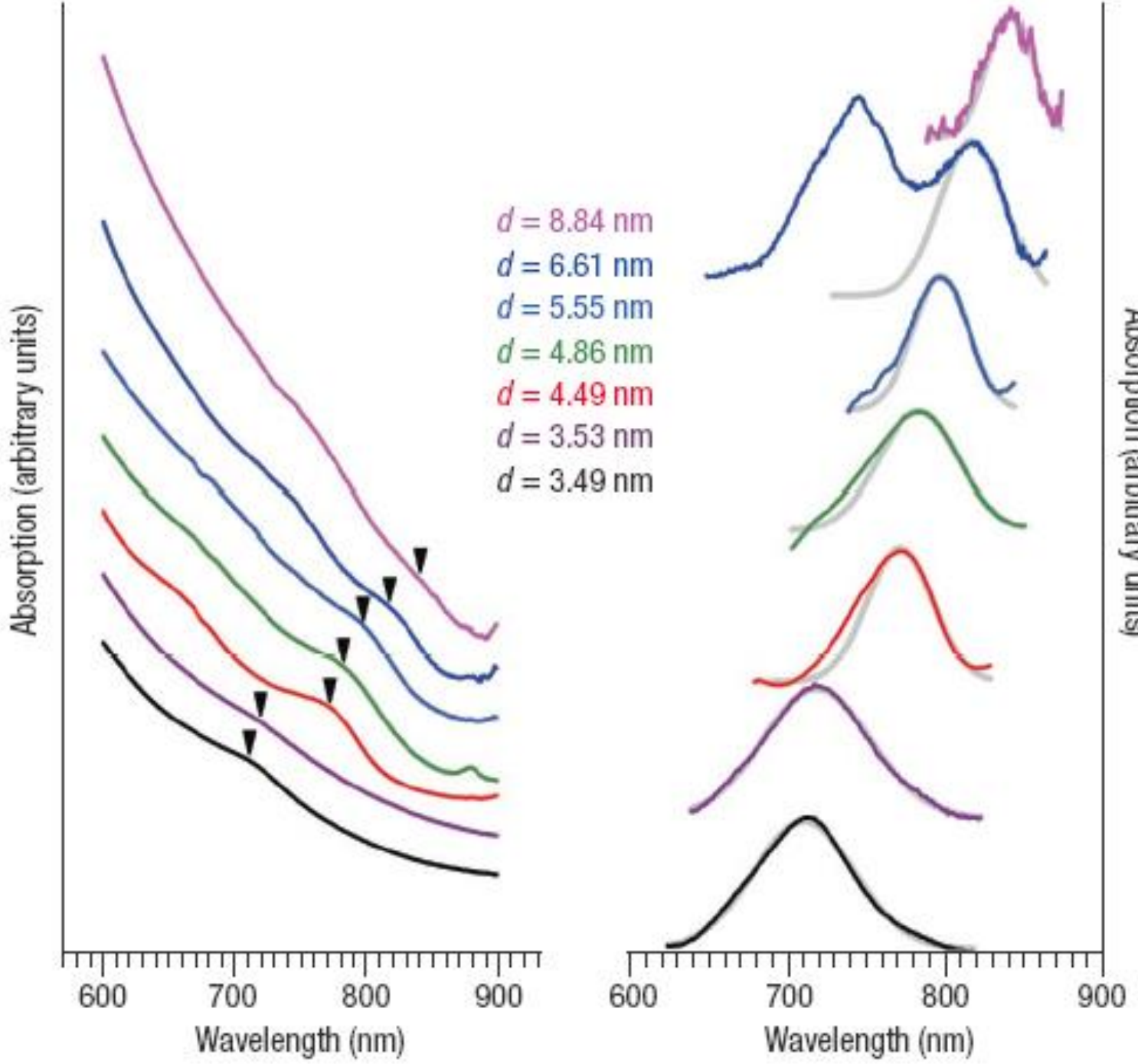
d = 8.84 nm
d = 6.61 nm
d = 5.55 nm
d = 4.86 nm
d = 4.49 nm
d = 3.53 nm
d = 3.49 nm
Absorption (arbitrary units)
600
700
800
900
Wavelength (nm)
Absorption (arbitrary units)
600
700
800
900
Wavelength (nm)

Figure 4 Experimental InP quantum-dot (red squares)[4–6] and quantum-wire (blue squares) data plotted as ΔE_g versus $1/d^2$. The lines are least-squares fits to the

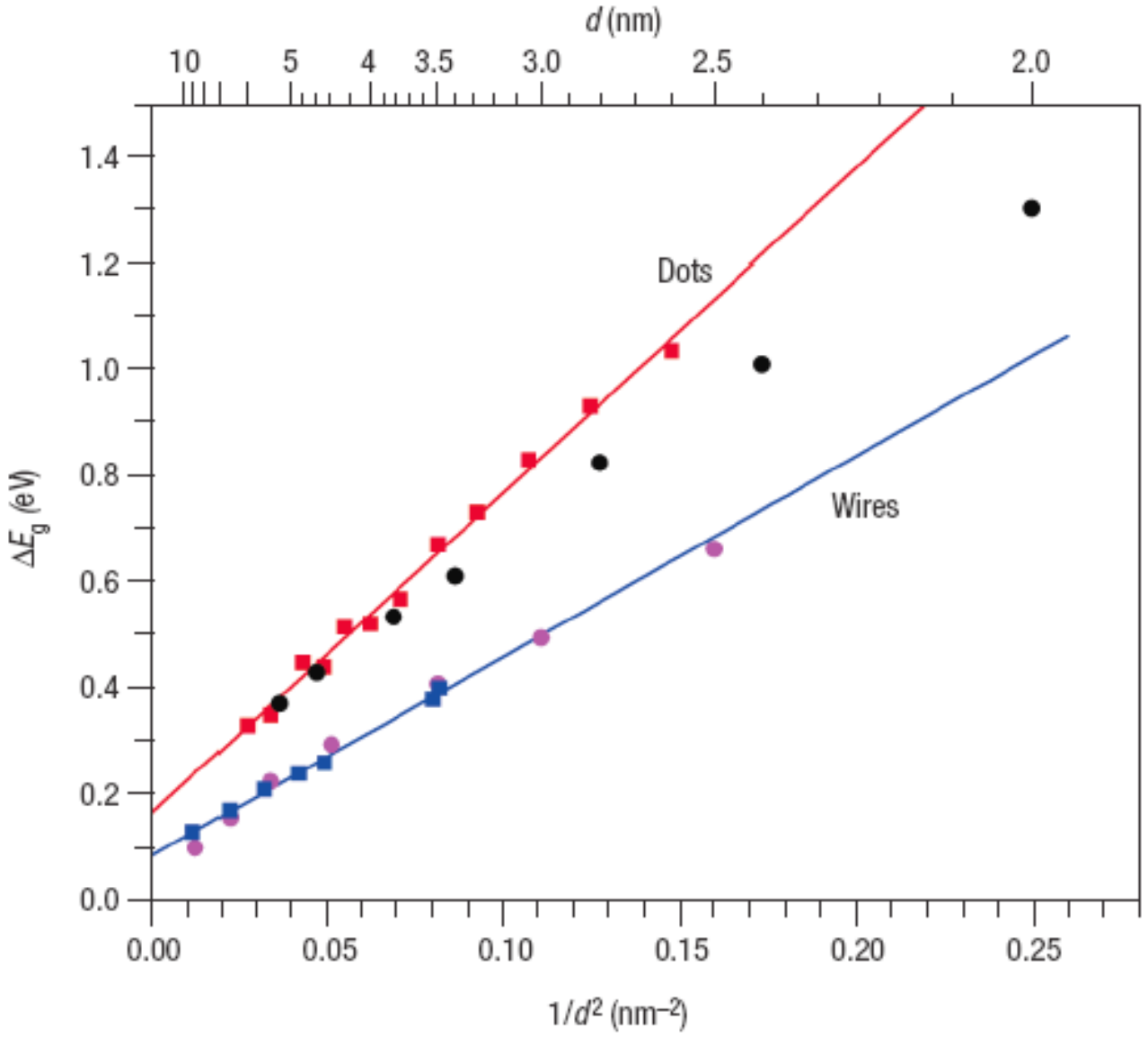

Figure 5 Theoretical and experimental InP quantum-dot and quantum-wire data plotted as ΔE_g versus $1/d^n$, for $n = 1.35$ (dot) and 1.45 (wire). The dotted lines are least-

$$\Delta E_g = B_{\text{dot}}/d^{1.35}$$

$$\Delta E_g = C_{\text{wire}}/d^{1.45}$$

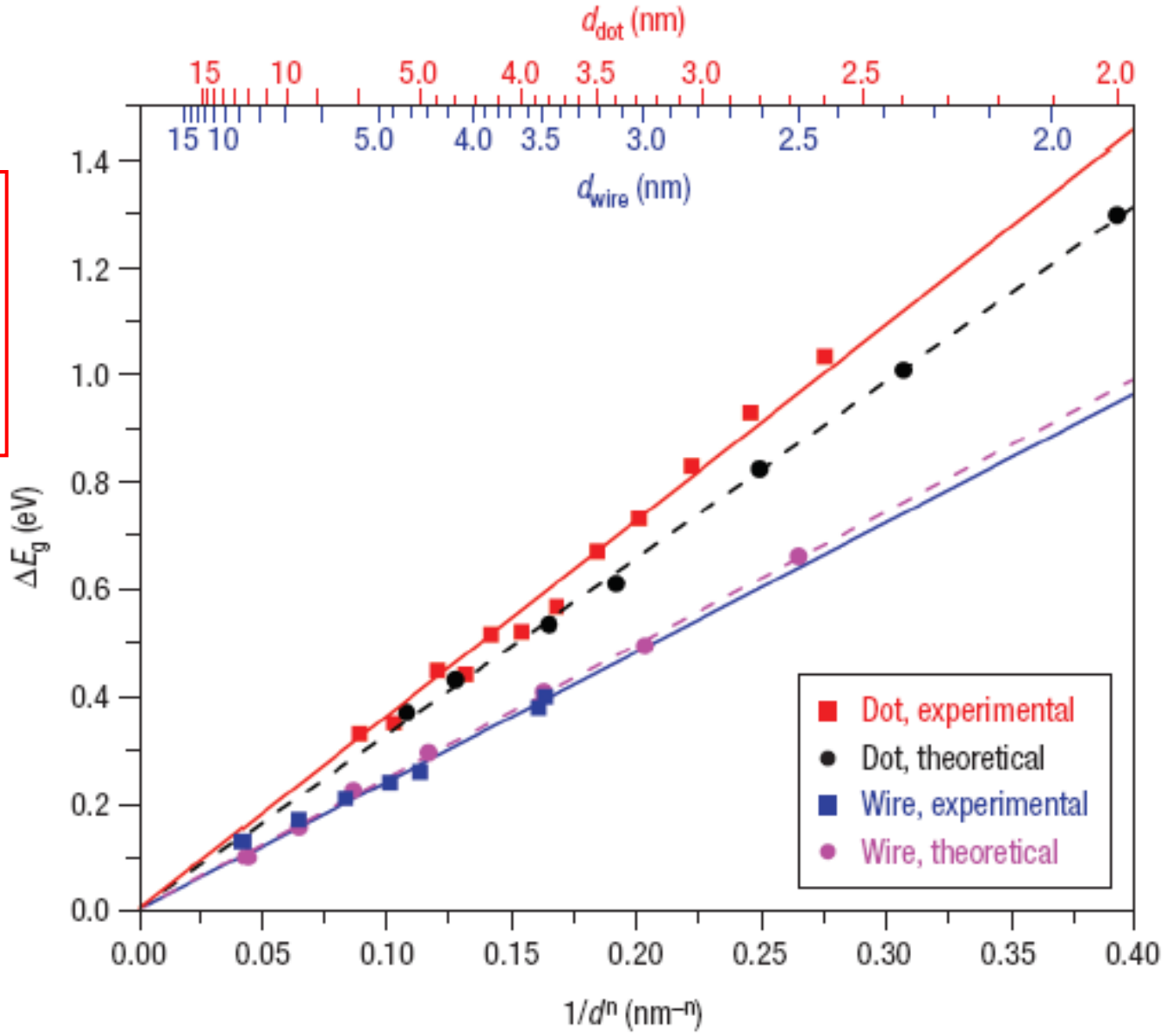

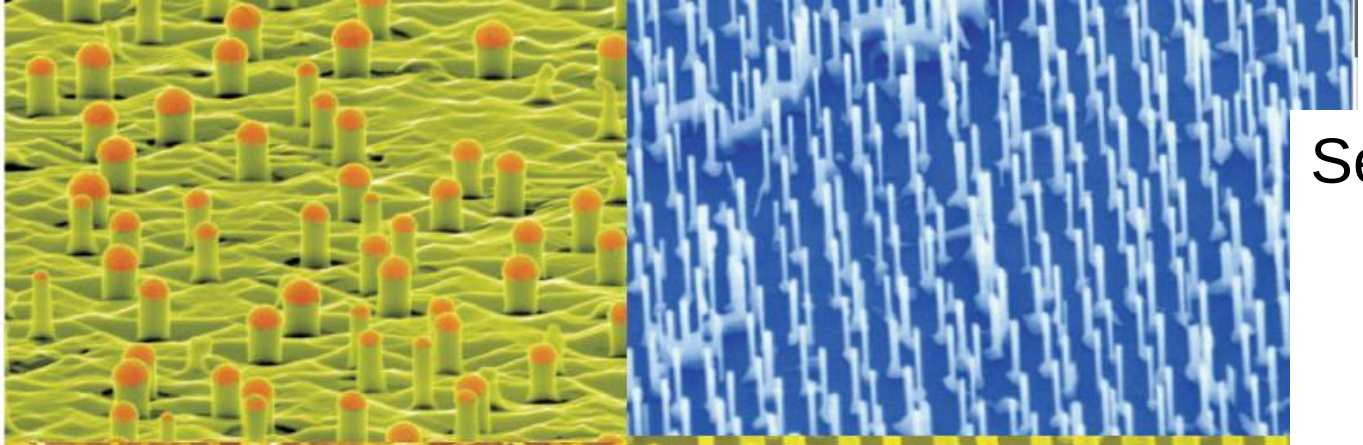

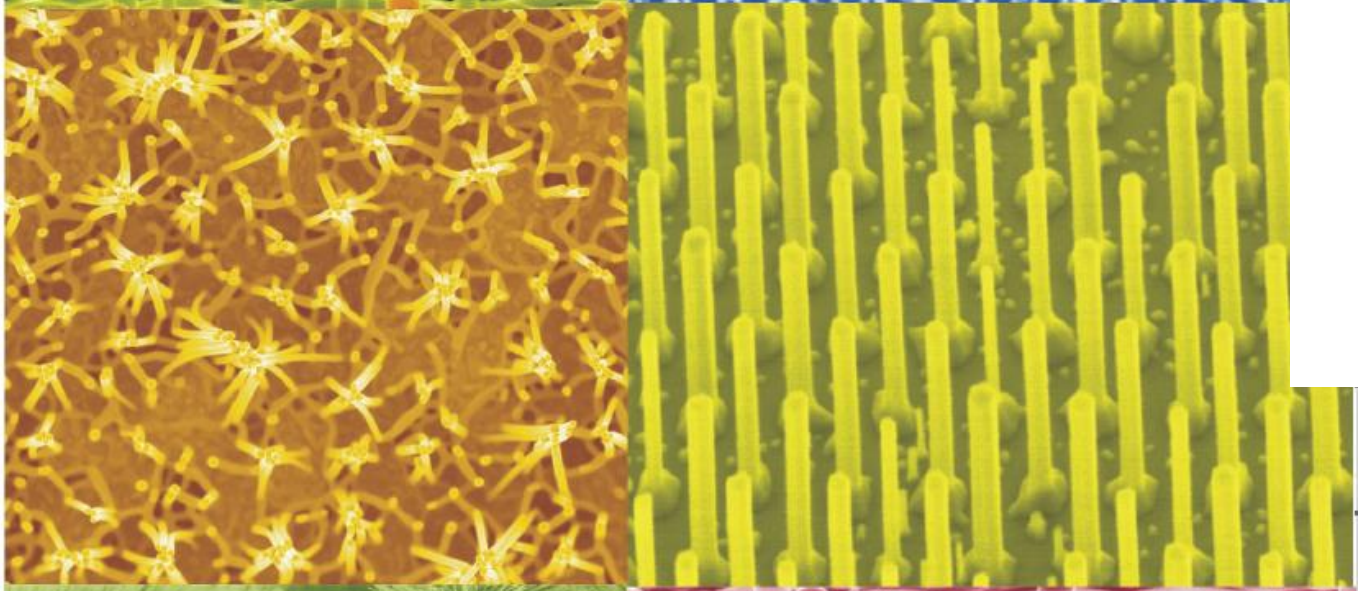

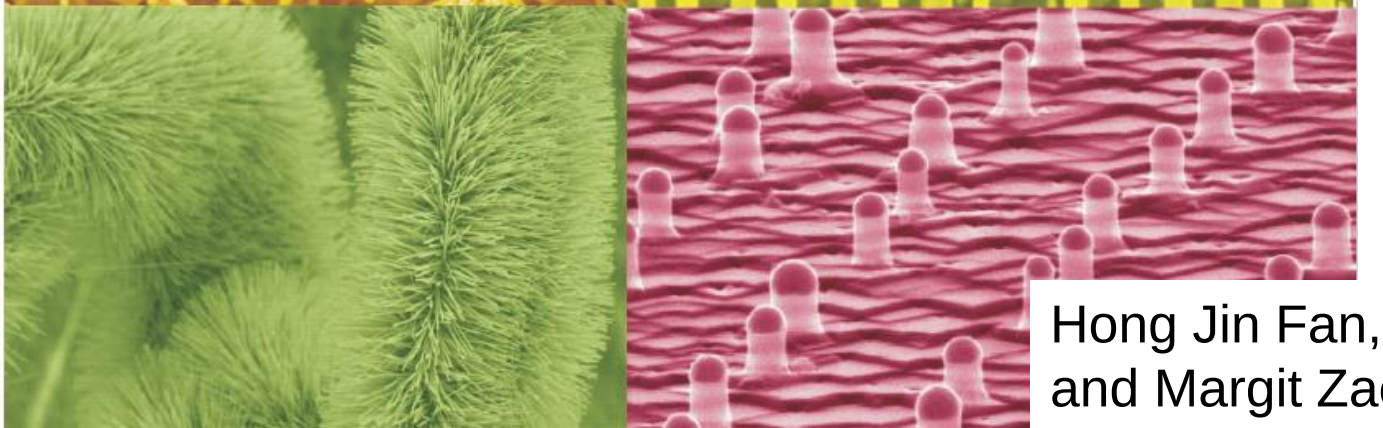

Semiconductor Nanowires: From Self-Organization To Patterned Growth

Patterned Nanowire Arrays using Nanoparticle Array As catalysts Via VLS process

Hong Jin Fan, Peter Werner, and Margit Zacharias* *Small* **2006**, 2, 700.

Patterned Nanowire Arrays using Nanoparticle Array As catalysts Via VLS process

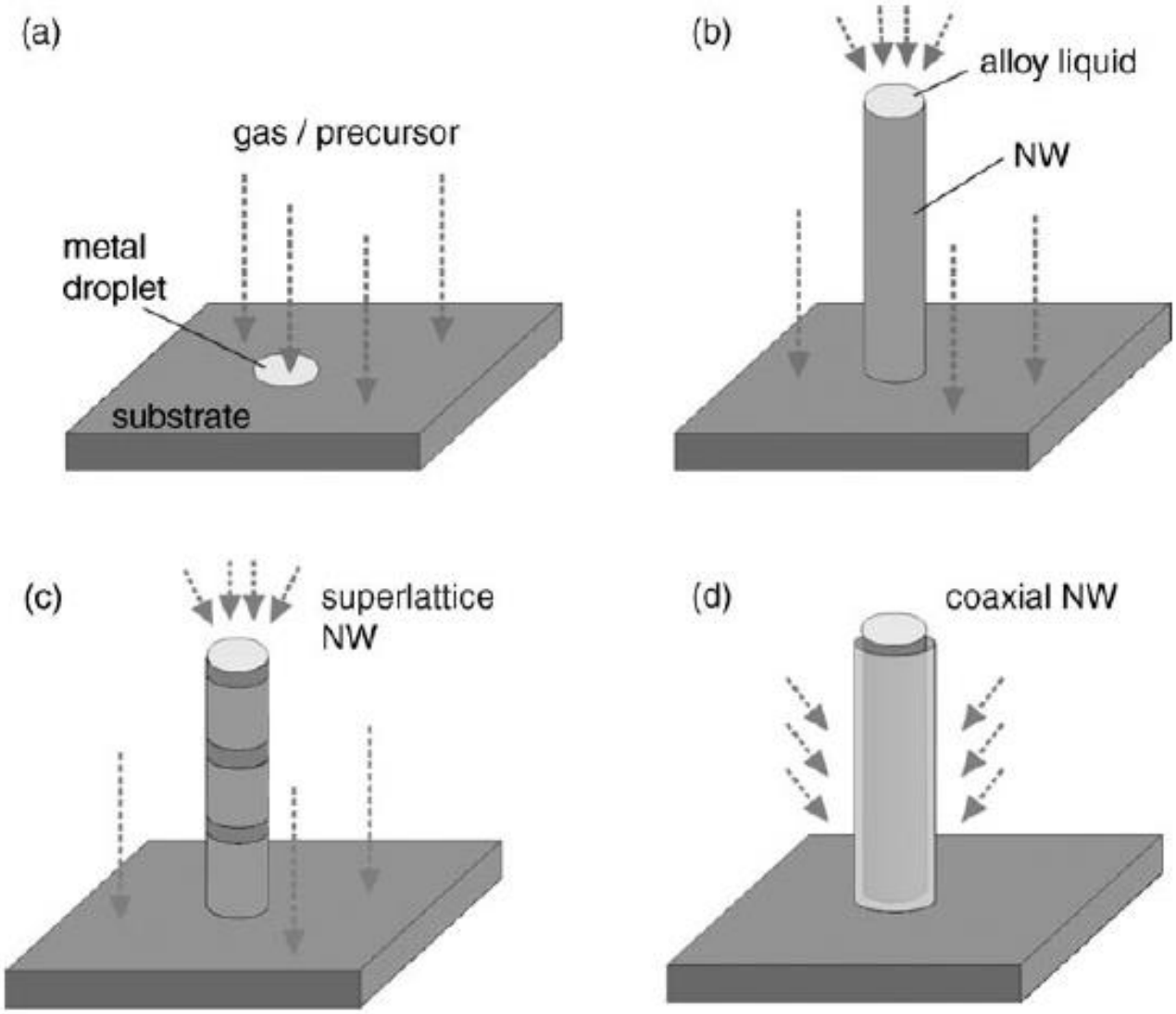

Table 1. Different semiconductor/metal combinations and growth methods for nanowires.

NW material	Source	Metal catalyst	Growth process[a]	Ref.
Si	$SiCl_4$	Au	CVD	[14, 15]
Si	$SiCl_4$	Au, Ag, Cu, Pt	CVD	[4]
Si, Ge	SiH_4, GeH_4	Au	CVD	[16]
Si	SiH_4	Au	CVD	[17]
Si, Ge		Fe, Si/Fe, Ge/Fe	PLD	[8]
Si	Si_2H_6	Au	CBE	[18]
GaAs	GaAs/Au	Au	PLD	[19]
InP	InP/Au	Au	PLD	[19]
CdSe	CdSe/Au	Au	PLD	[19]
Si	Si	Ga	microwave plasma	[20]
GaAs	Et_3Ga, Bu_3As	Au	CBE	[21]
ZnO	ZnO, C	Au	evaporation	[9]
Si	Si	Au	MBE	[12]
Si	SiO	Au	evaporation	[22]
Si	silyl radicals	Ga	microwave plasma etching	[23]
Si	SiH_4 or SiH_2Cl_2	Ti	CVD	[24]
GaAs/GaP	GaAs/GaP	Au	PLD	[25]
GaAs/InAs	Me_3Ga, Bu_3As, Me_3In	Au	CBE	[26]
Si/SiGe	$SiCl_4$	Au	Si: CVD; Ge: PLD	[27]

[a] PLD: pulsed laser deposition; CBE: chemical beam epitaxy.

ZnO nanowires using Au Nanoparticle catalysts

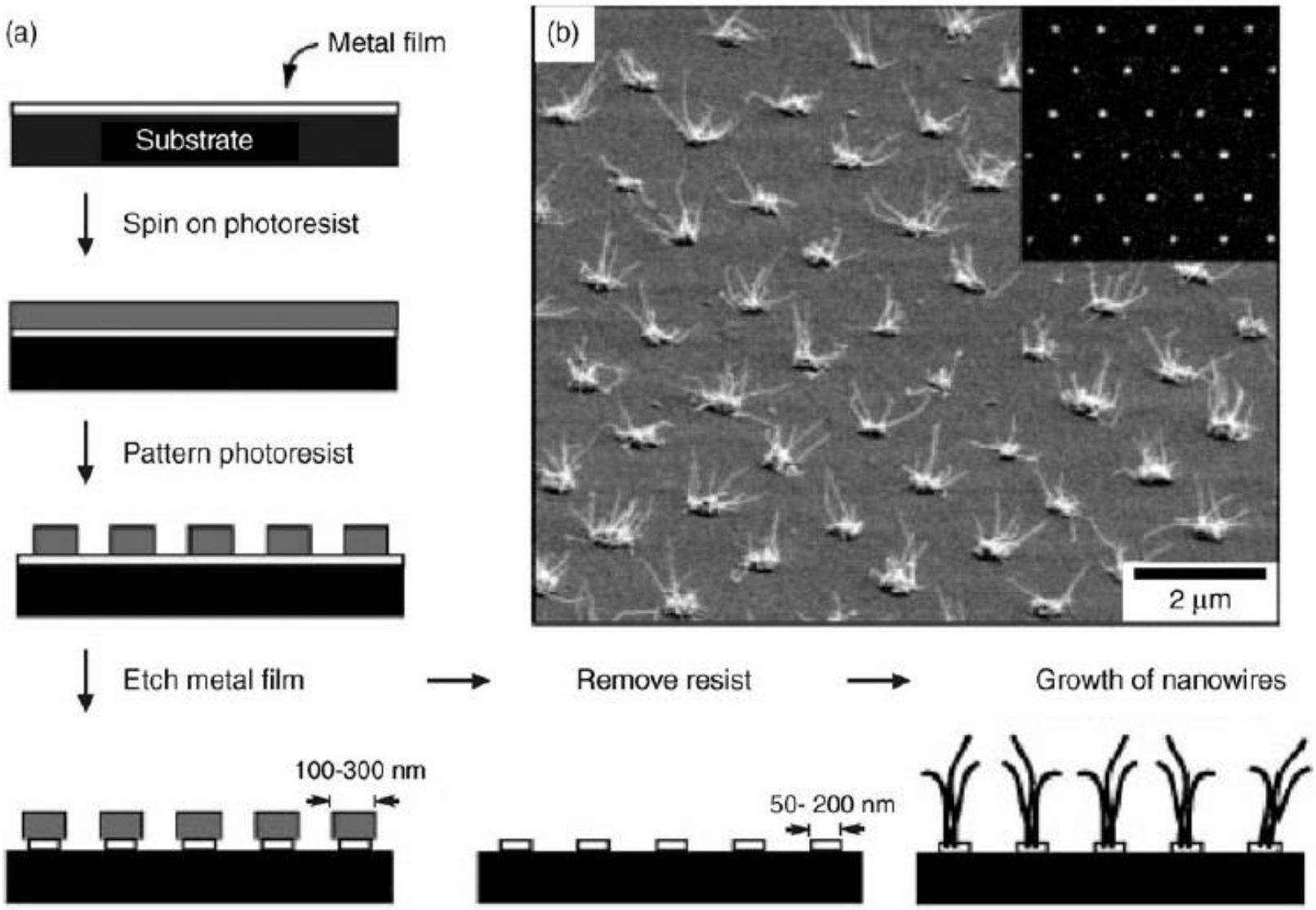

E. C. Greyson, Y. Babayan, T.W. Odom, *Adv. Mater*. **2004**, 16, 1348.

Si nanowires using Au Nanoparticle catalysts

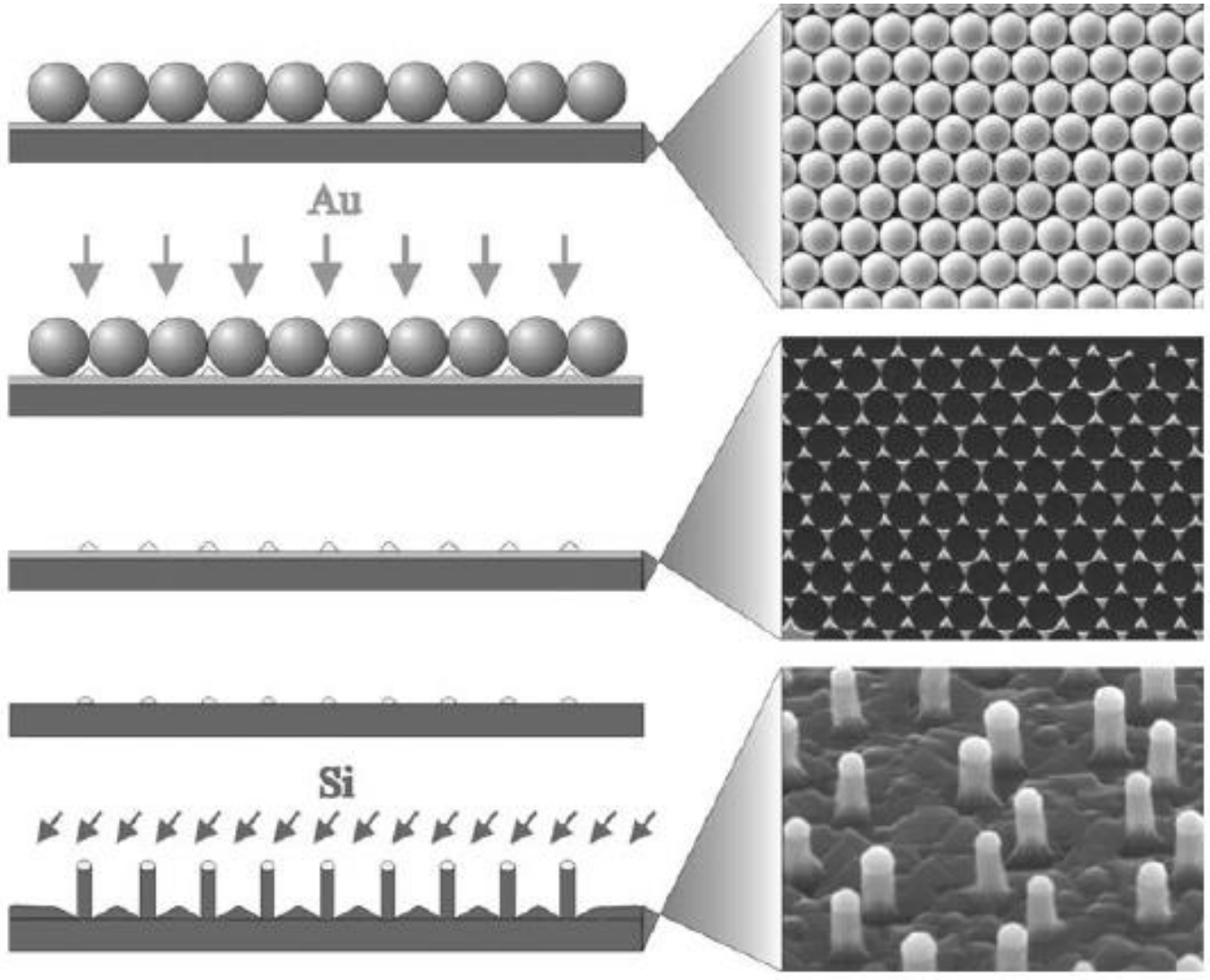

B. Fuhrmann, H. S. Leipner, H.-R. Hcche, L. Schubert, P. Werner, U. Gösele, *Nano Lett*. **2005**, 5, 2524.

InP nanowire arrays using Au nanoparticle arrays Fabricated using Nanoimprint Lithography

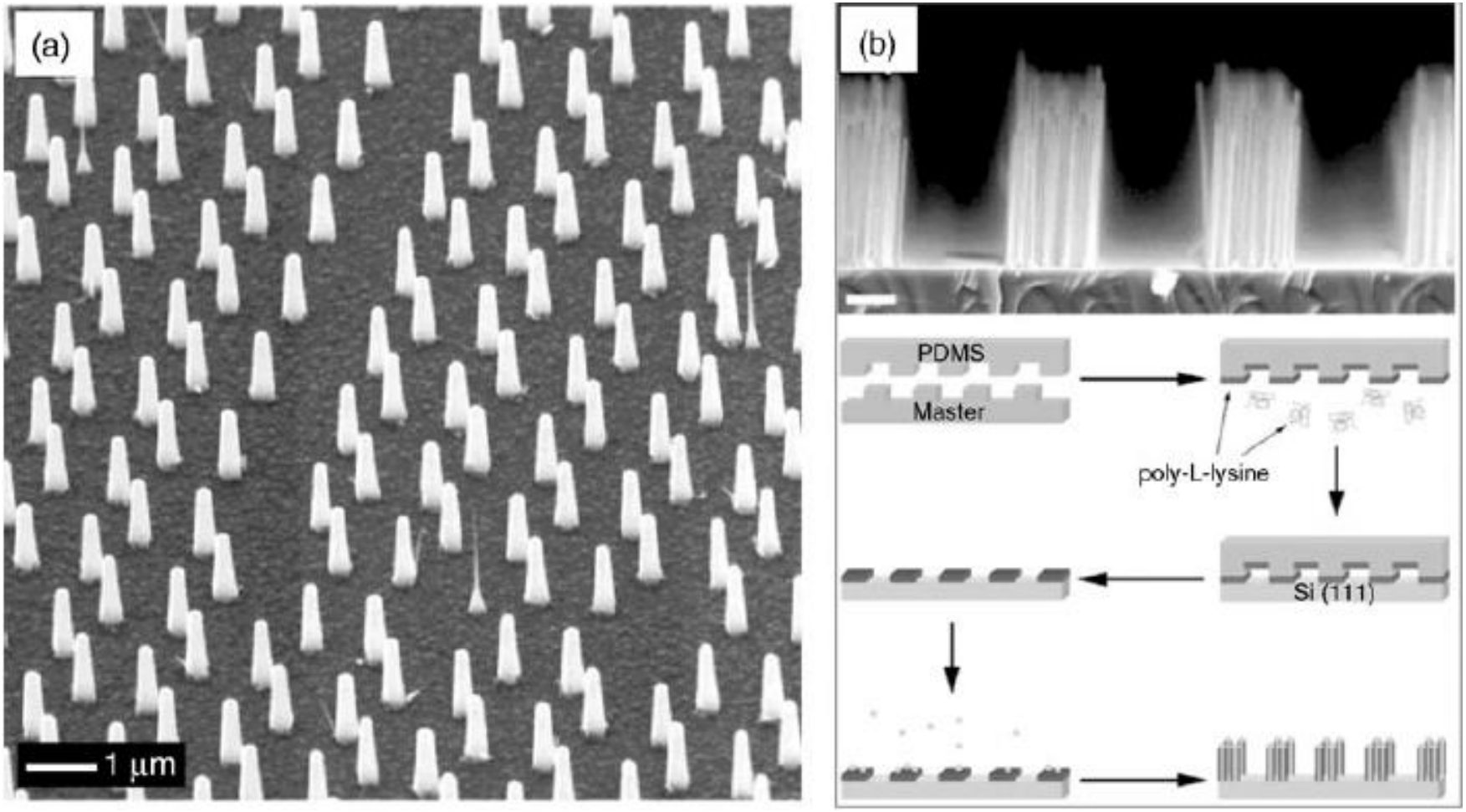

P.Yang, *Nano Lett*. **2005**, 5, 457.

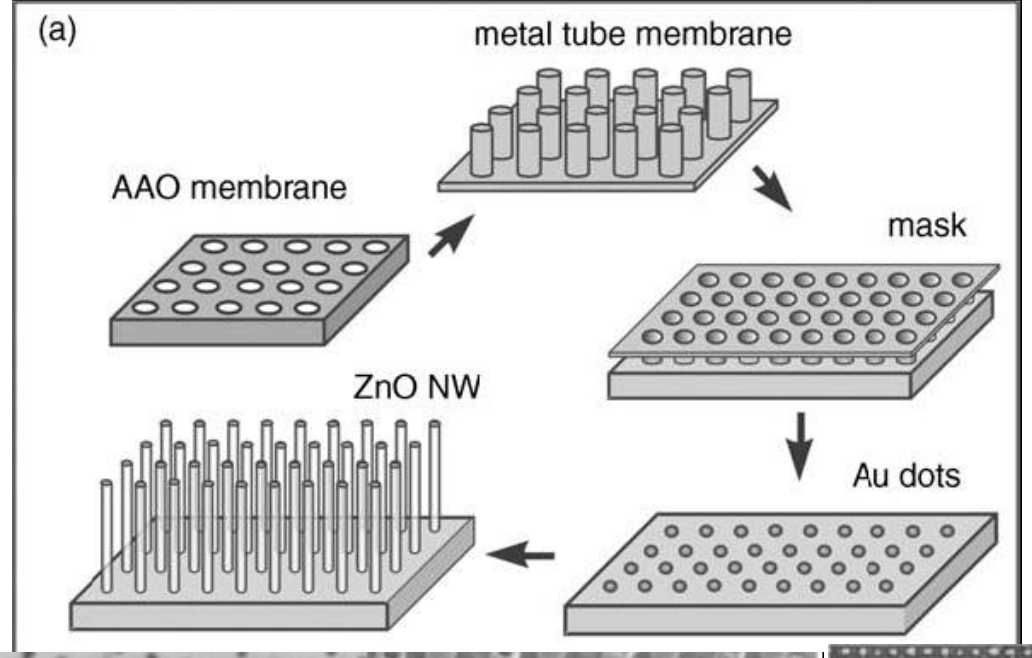

Zacharias, *Nanotechnology* **2005**, 16, 913.

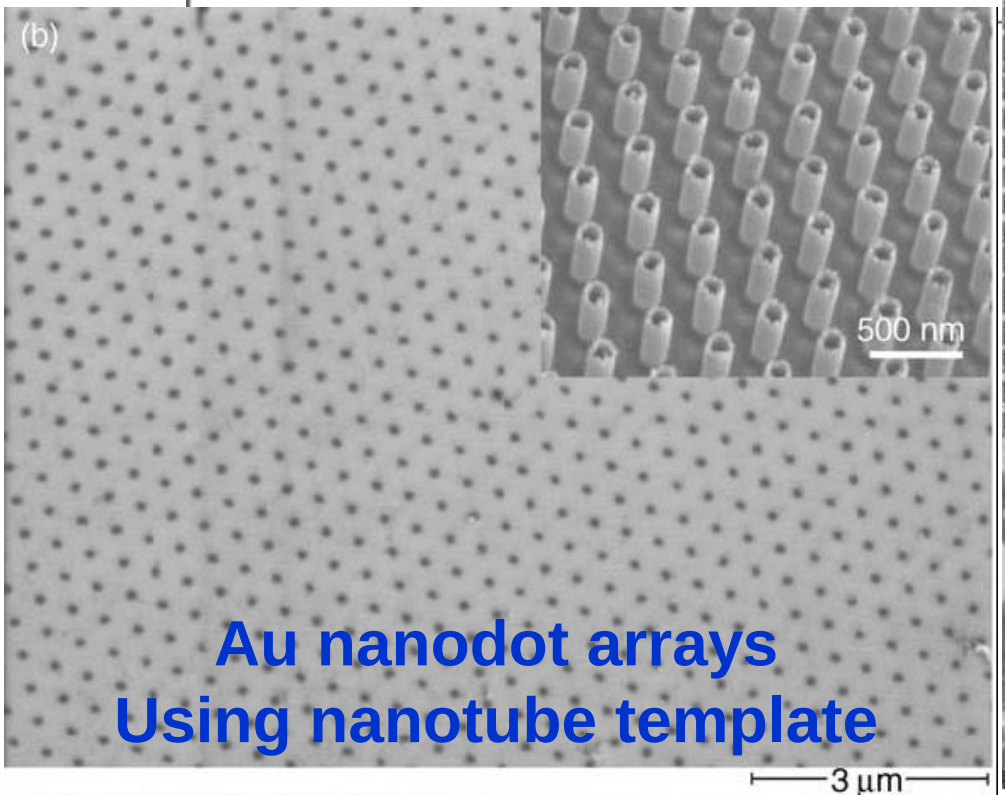

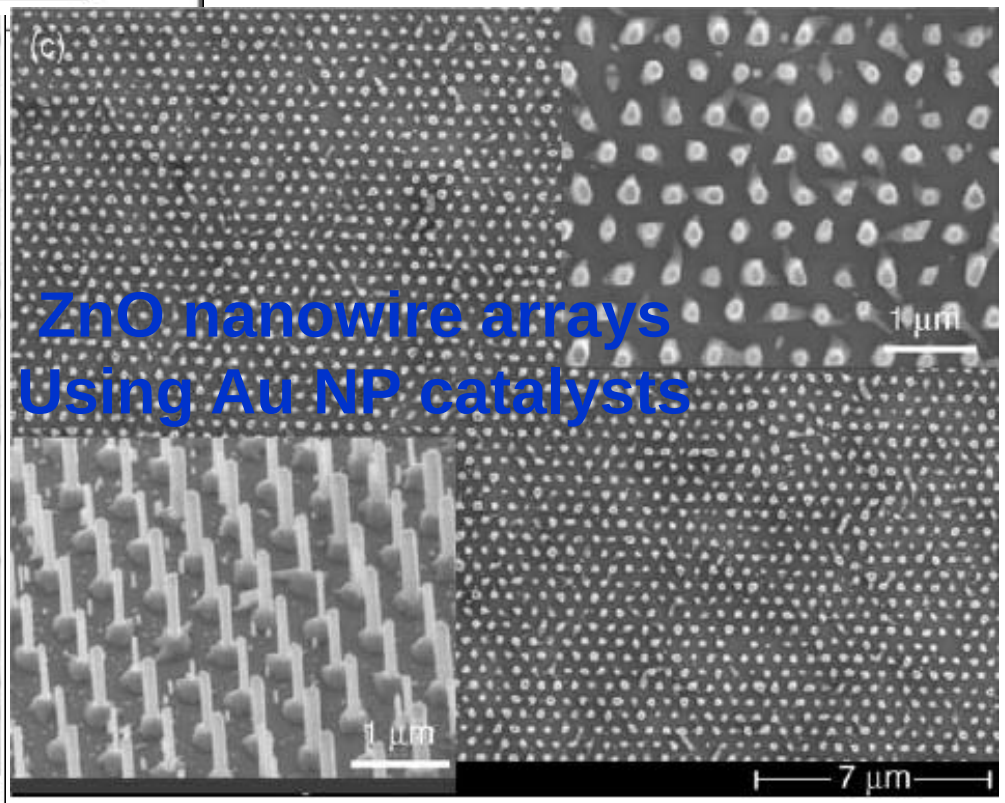

Field emitter using Aligned CNT or Si nanowires

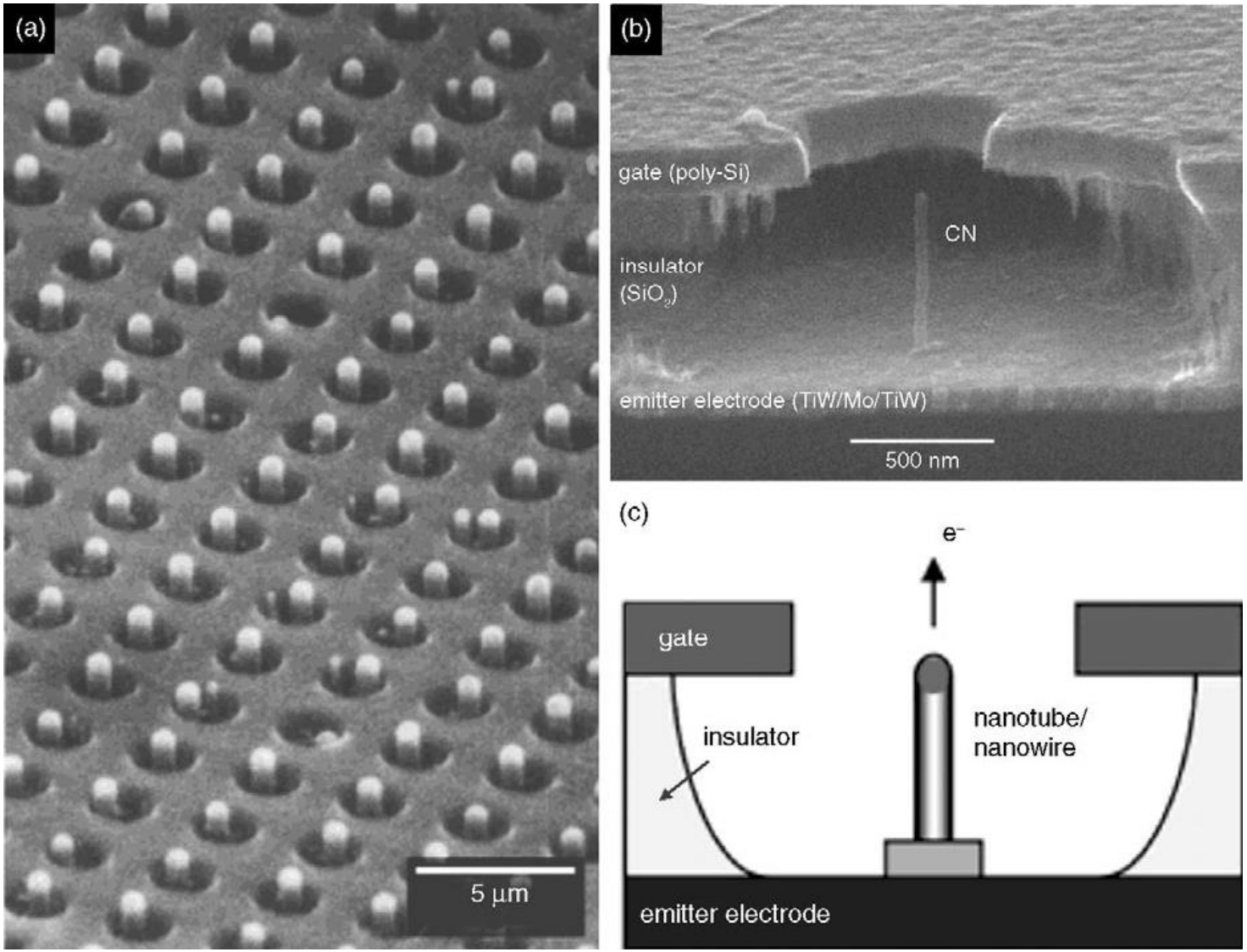

High aspect ratio of NWs, electrons can be easily extracted out from NW tips by an electric field

L. Gangloff, et. al., *Nano Lett.* **2004**, 4, 1575.

Part III.

Using Templates with 1D morphologies to Direct formation of 1D nanostructures

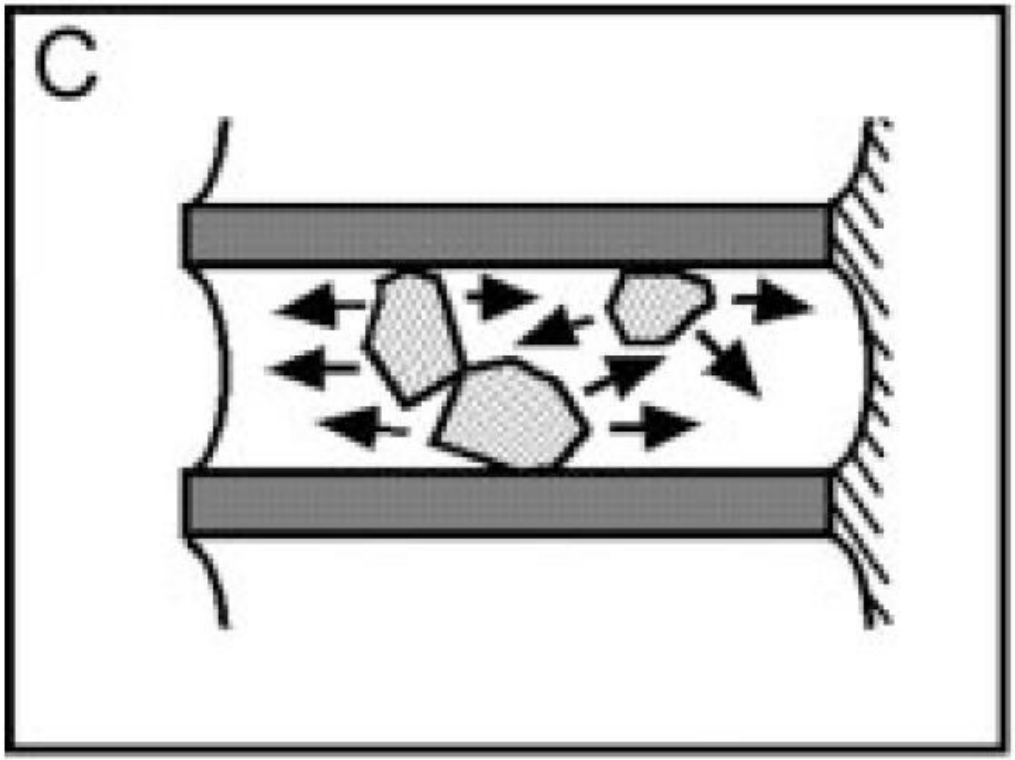

Template approaches to get nanowires

- Track etched Polymer (polycarbonate) membranes
- Anodic alumina membranes
- Mesoporous silicas (will be discussed later, if time allows)
- Zeolites

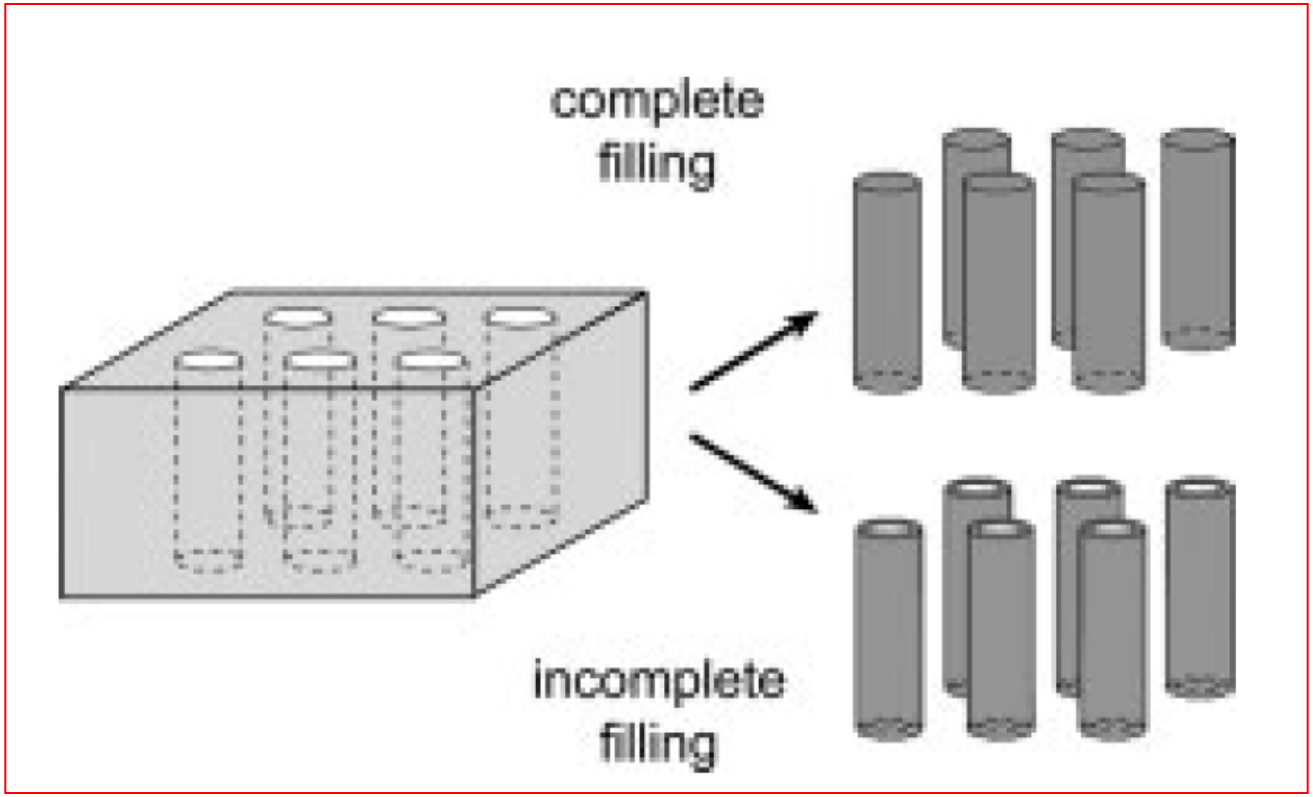

Highly ordered nanochannel-array architecture in anodic alumina

Hideki Masuda, Appl. Phys. Lett. 1997, **71, 2770.**

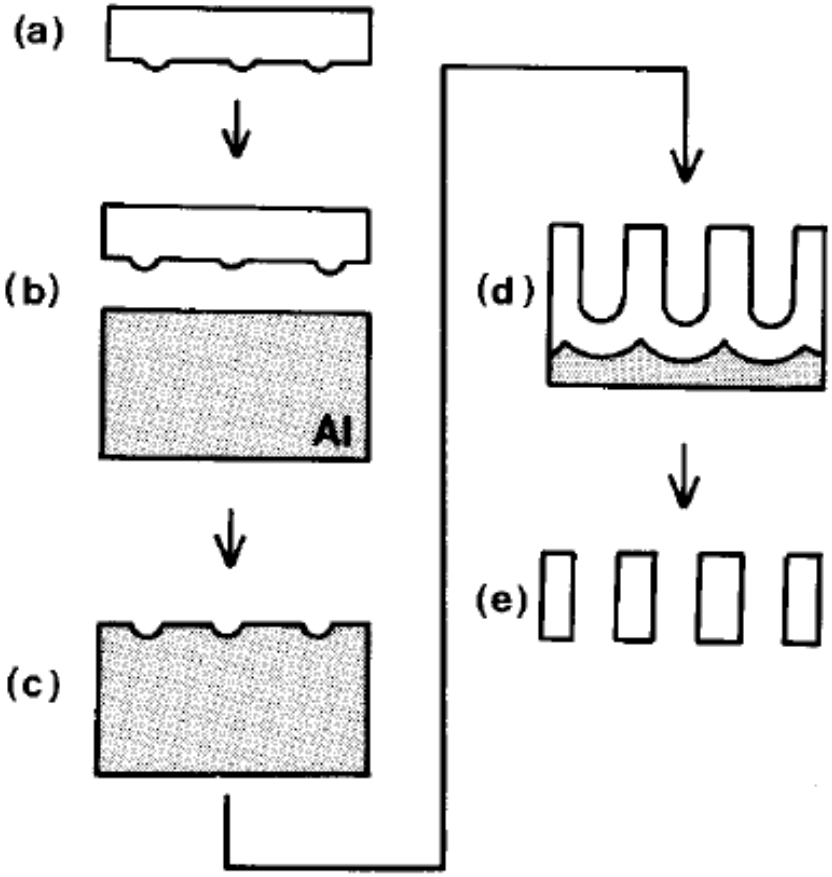

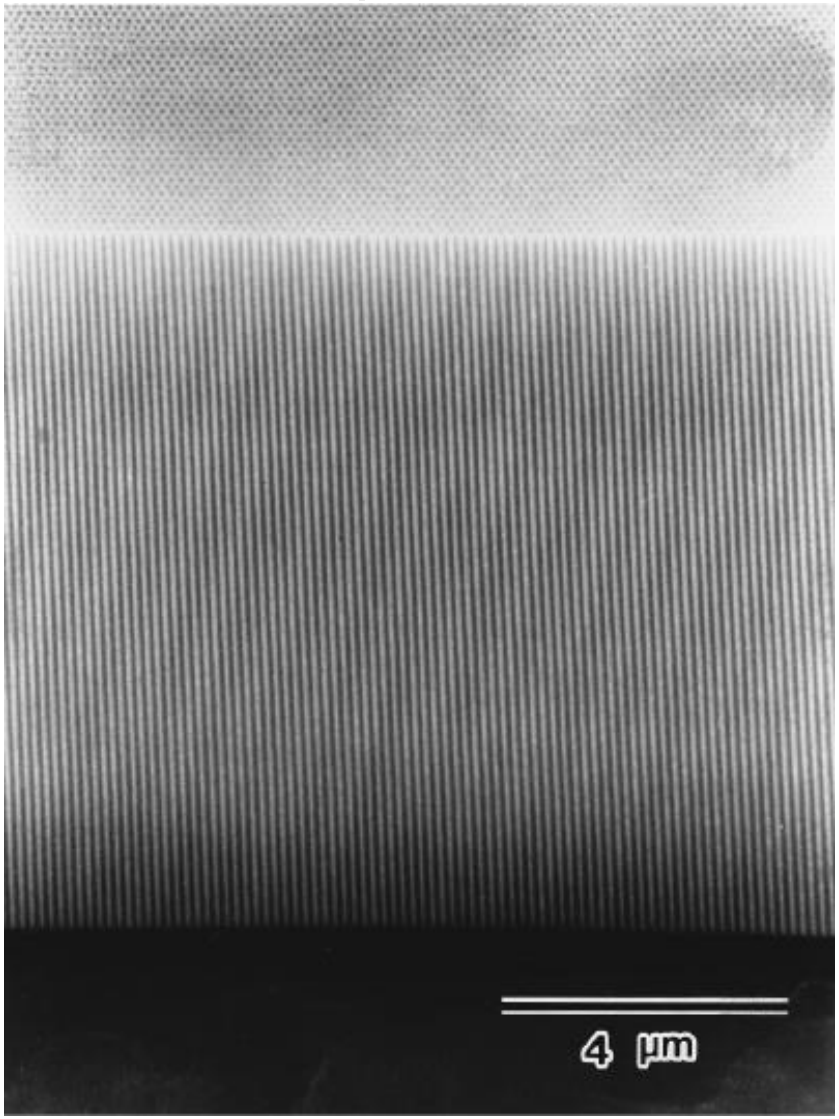

Anodic porous alumina: typical self-ordered nanochannel material formed by anodization of Al in an appropriate acid solution

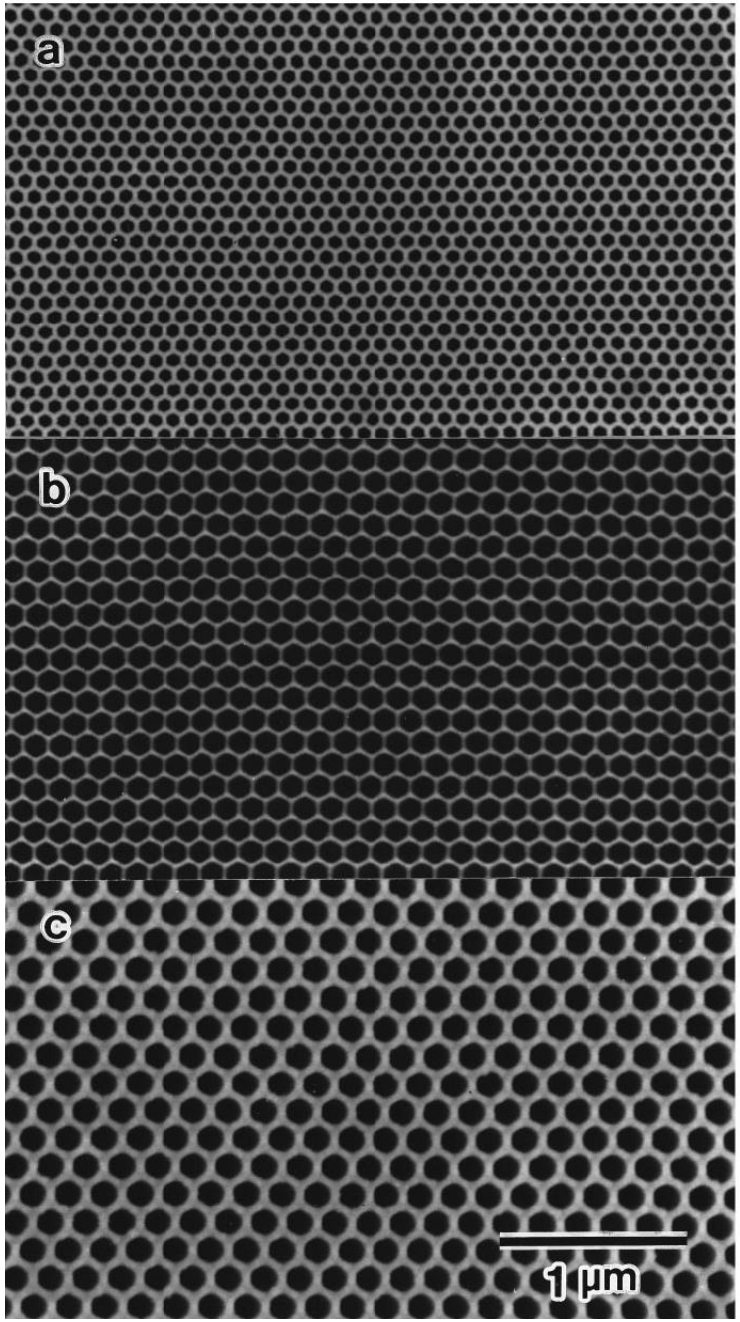
a
b
c
1 µm

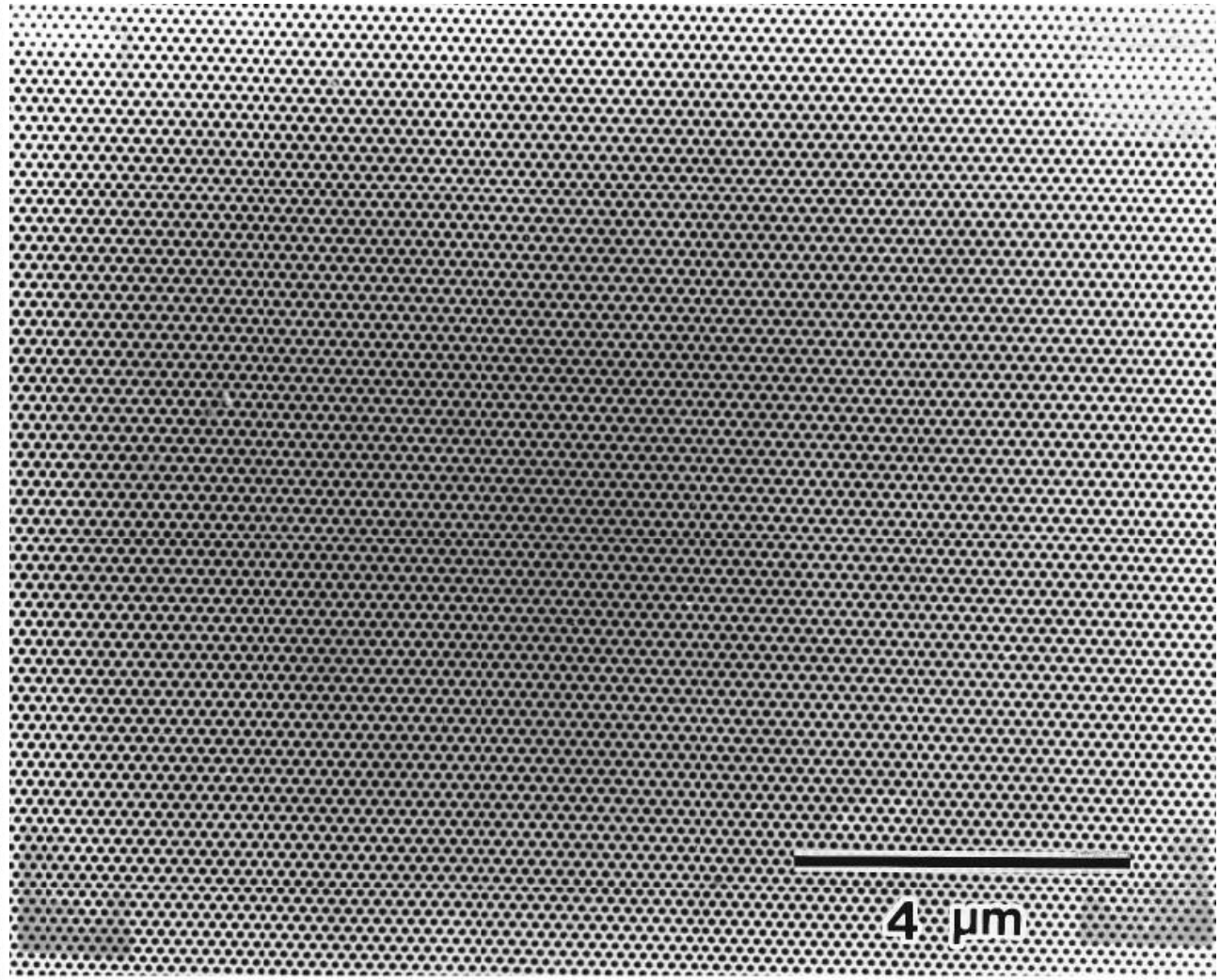
4 µm

Ordered Metal Nanohole Arrays Made by a Two-Step Replication of Honeycomb Structures of Anodic Alumina

Hideki Masuda 1 and Kenji Fukuda 1

Science 1995, 268, 1466.

- A highly ordered metal nanohole array (platinum and gold) was fabricated by a two-step replication of honeycomb structure of anodic porous alumina.
- Preparation of the negative porous structure of porous alumina followed by the formation of the positive structure with metal resulted in a honeycomb metallic structure.
- The metal hole array of the film has a uniform, closely packed honeycomb structure approximately 70 nanometers in diameter and from 1 to 3 micrometers thick.

Template approach

5 nm Metal depositon

PMMA formation

Nanotube array formation

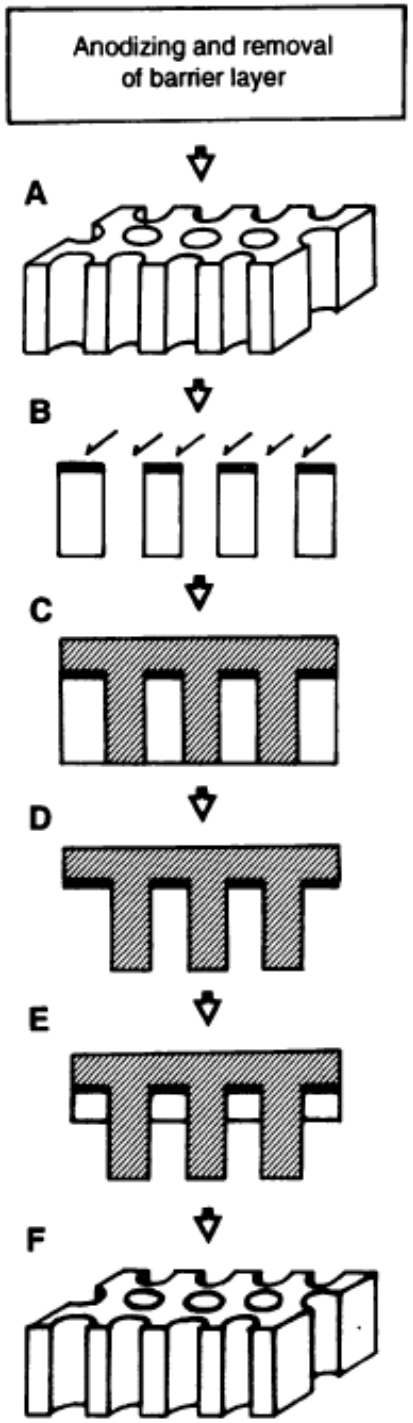

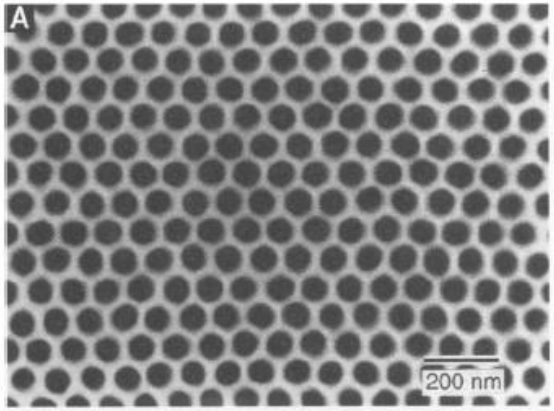

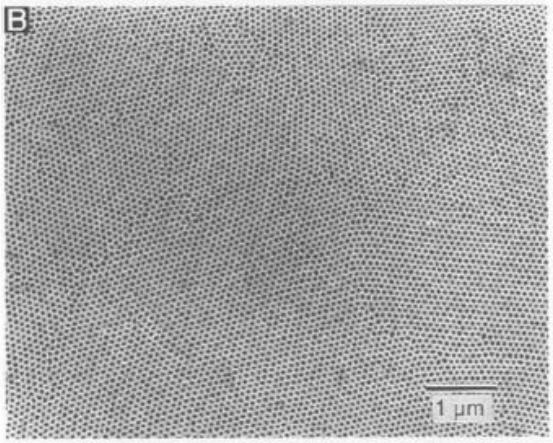

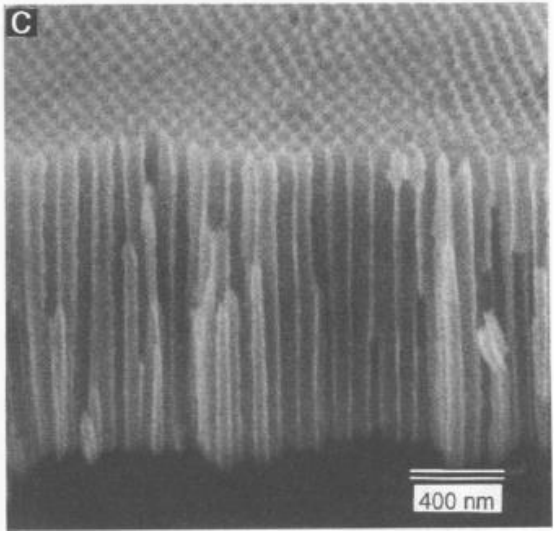

Multisegmented One-Dimensional Nanorods Prepared by Hard-Template Synthetic Methods

Chad A. Mirkin* *Angew. Chem. Int. Ed.* **2006**, 45, 4655.

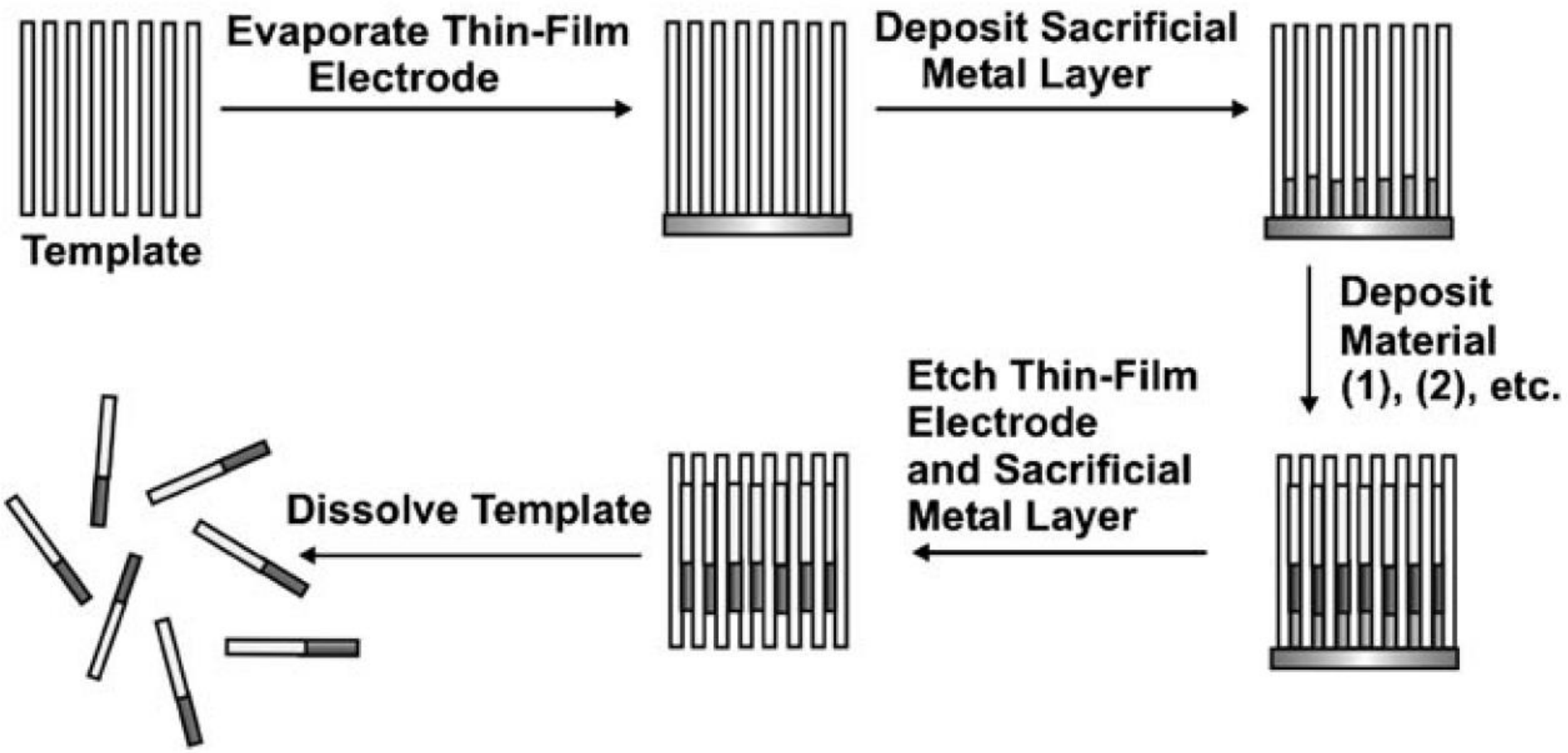

Template-Grown Metal Nanowires

Timothy R. Kline, Mingliang Tian,* Jinguo Wang,* Ayusman Sen,*
Moses W. H. Chan,* and Thomas E. Mallouk* *Inorg. Chem.* **2006**, 19, 7555.

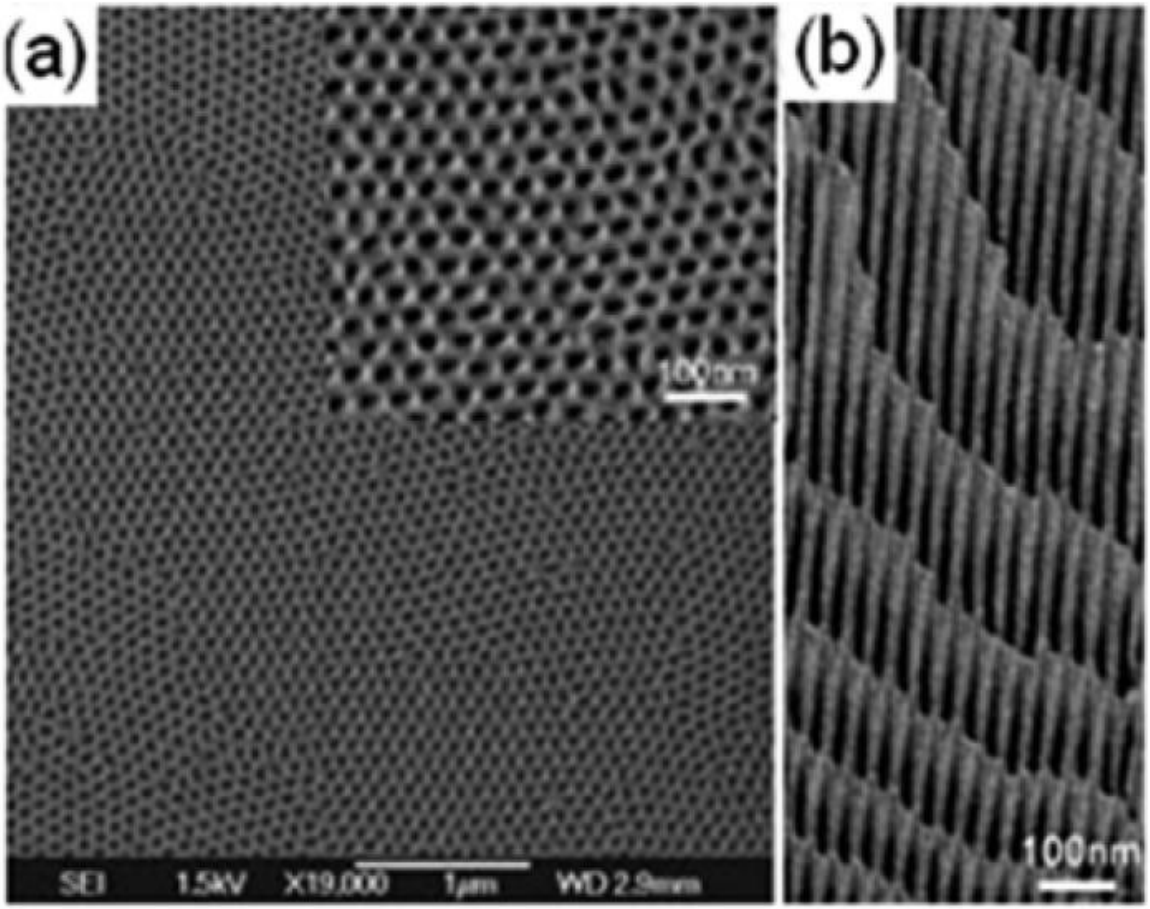

Anodic aluminum oxide (AAO) templates

Au-Pt-Au nanorods

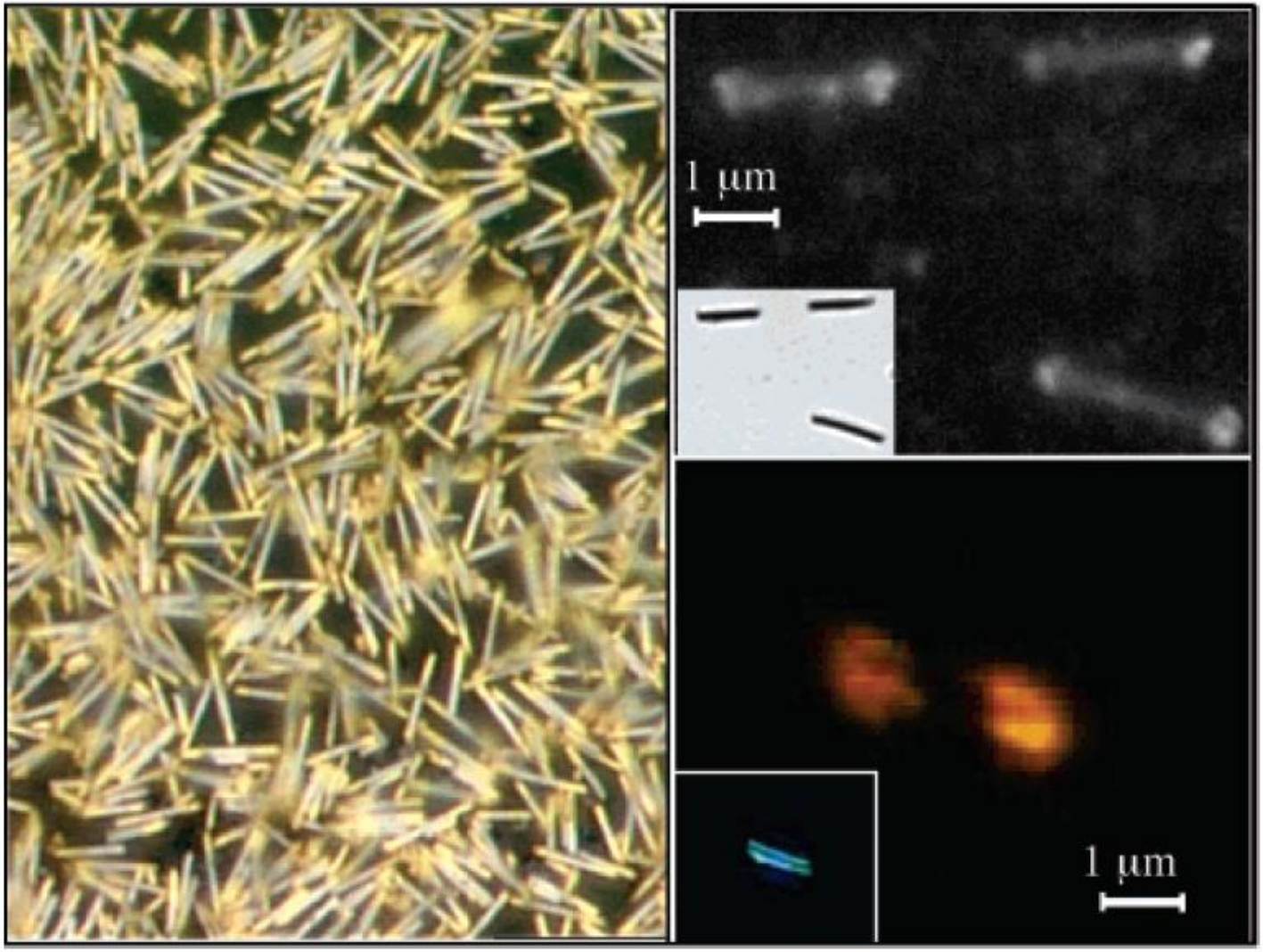

Au–Ppy–Cd–Au nanorods

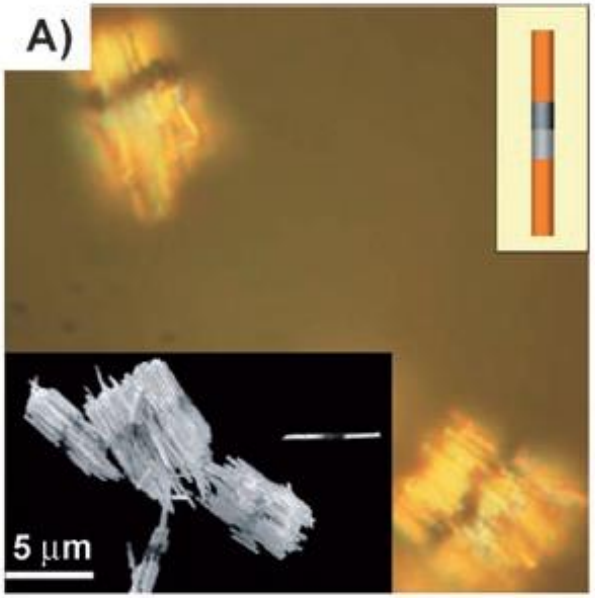

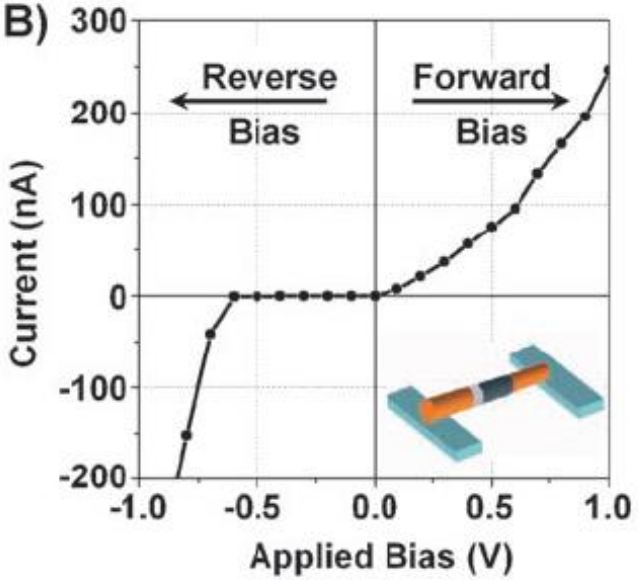

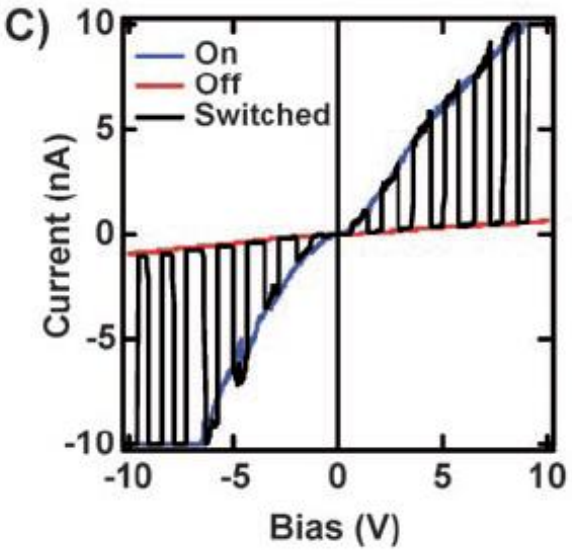

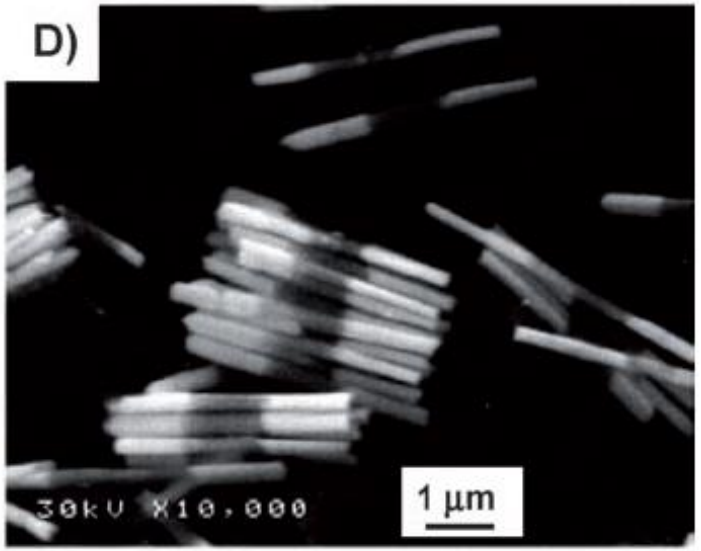

Au–CdSe–Au nanorods

Keywords:
molecular electronics · nanostructures · nanotechnology · template synthesis

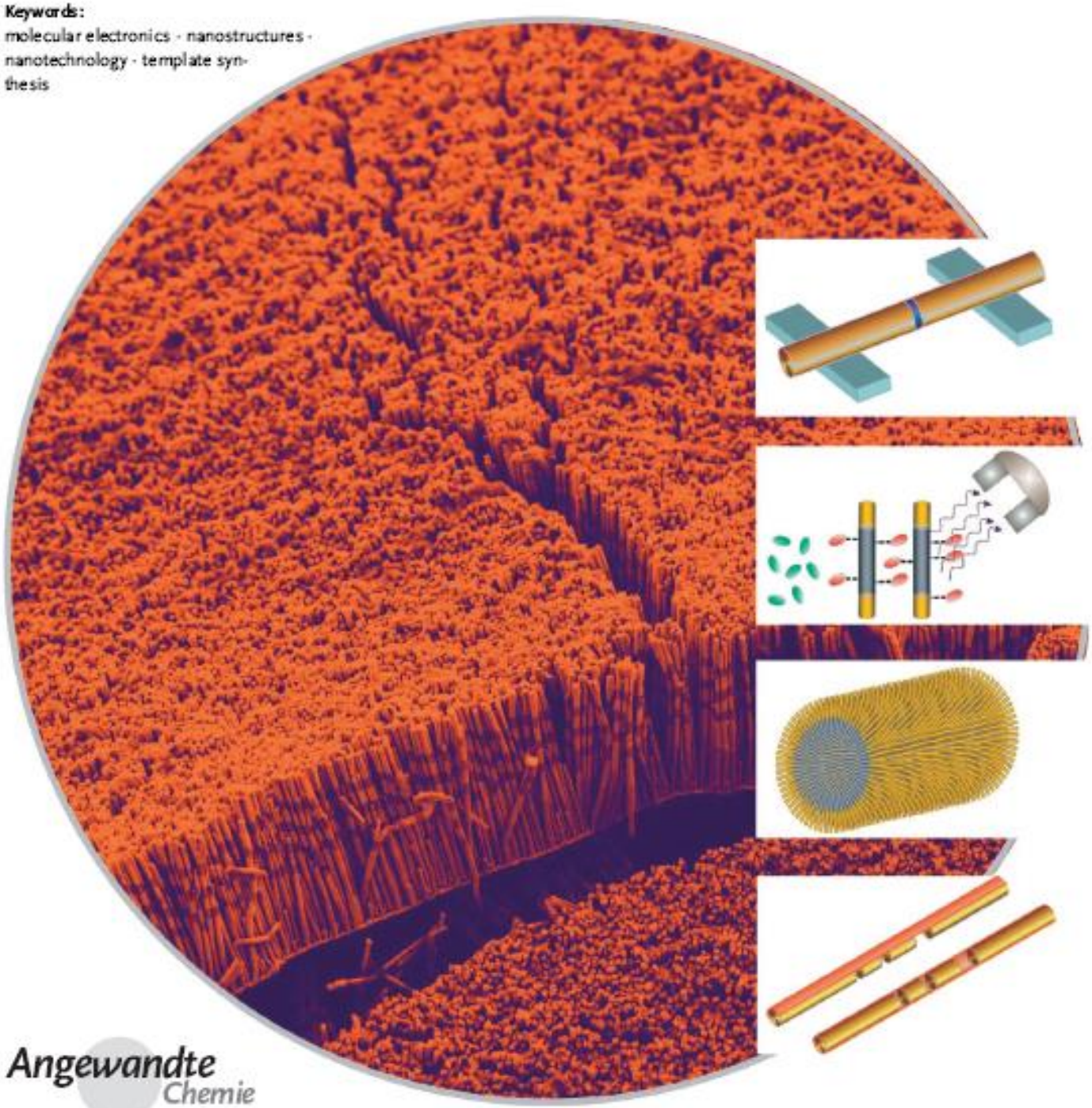

Angewandte Chemie

Ultrahigh-Density Nanowire Lattices and Circuits

James R. Heath (UCLA, now at CALTECH)

Science **2003**, *300*, 112.

- General method for producing ultrahigh-density arrays of aligned metal and semiconductor nanowires
- The technique is based on translating thin film growth thickness control into planar wire arrays.
- superlattice nanowire pattern transfer (SNAP)

Process diagram to create small pitch wires

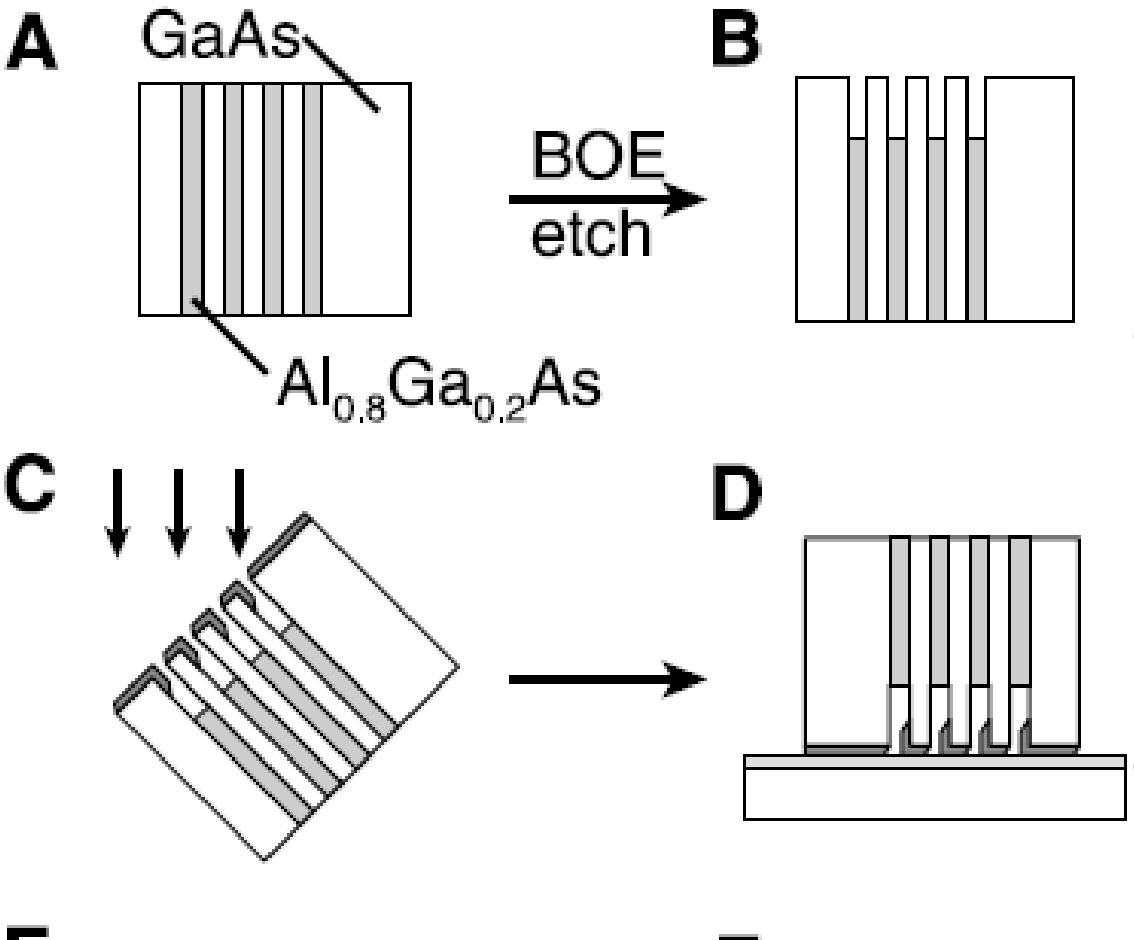

(A) The GaAs/AlGaAs Superlattice by MBE, (**B**) after selectively etching the AlGaAs, (**C**) Metal deposition while tilted at 36°, (**D**) contact of superlattice onto adhesive layer on Si (**E**) release of metal wires by etching GaAs oxide, (**F**) after optional O2 plasma to remove adhesive layer.

• Nanowires were fabricated with diameters and pitches (center-to-center distances) as small as 8 nanometers and 16 nanometers, respectively.

• The nanowires have high aspect ratios (up to 10^6), and the process can be carried out multiple times to produce simple circuits of crossed nanowires with a nanowire junction density in excess of 10^{11} per cm^2.

• The nanowires can also be used in nanomechanical devices; a high-frequency nano-mechanical resonator is demonstrated.

Aligned Pt nanowire arrays produced using the SNAP process

(**A**) 100 μm section of an array of 60 nanowires. (**B**) 40 Pt wires 10 nm in diameter at a pitch of 60 nm, and 20 Pt wires 10 nm in diameter at a pitch of 30 nm. (**C**) The highest density nanowire array fabricated, consisting of 20 Pt nanowires 8 nm in diameter at a pitch of 16 nm.

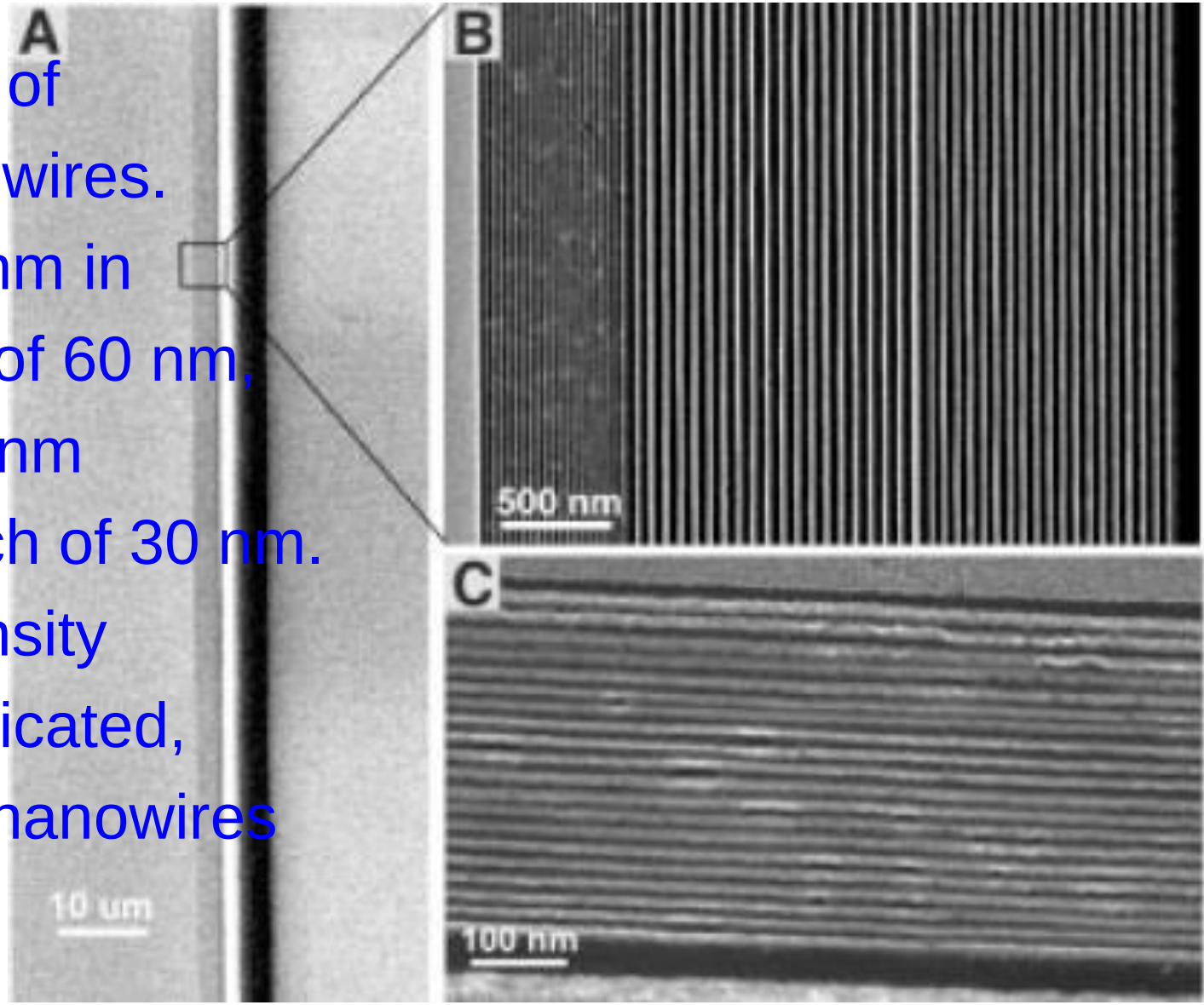

High-frequency nanomechanical resonator fabricated by the SNAP process

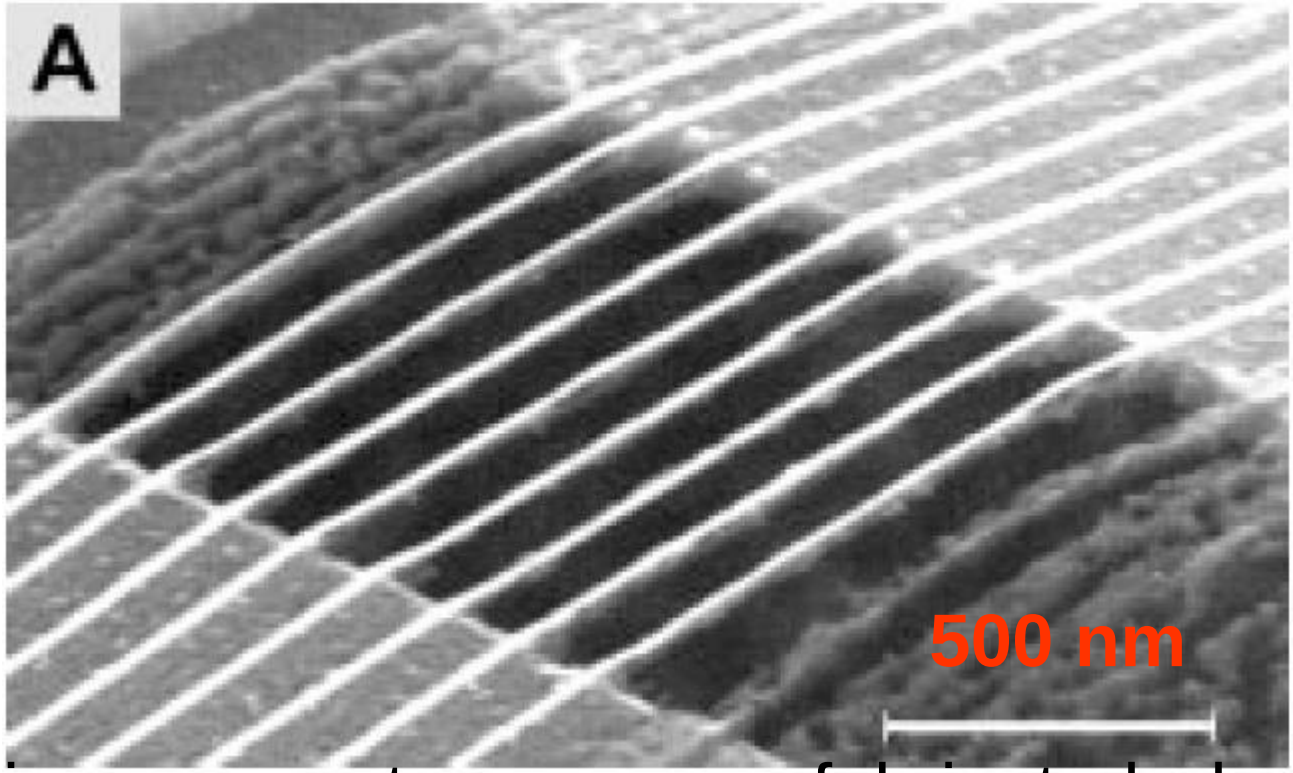

Pt nanowire resonators were fabricated by selectively undercutting the supporting substrate, thus suspending them over a trench. SNAP technique to deposit 20-nm Pt wires at 150-nm pitch onto a bare Si wafer; the epoxy was removed by O2 RIE plasma.

Few hundred Pt nanowire crossbar circuits fabricated by repeating the SNAP process.

The crossbars are fabricated from Pt nanowires with pitches ranging from 20 to 80 nm. The central crossbar has a junction density of 5×10^{10} cm^{-2}, and the two crossbars to the lower left and right of this central one are at a junction density of 10^{11} cm^{-2}.

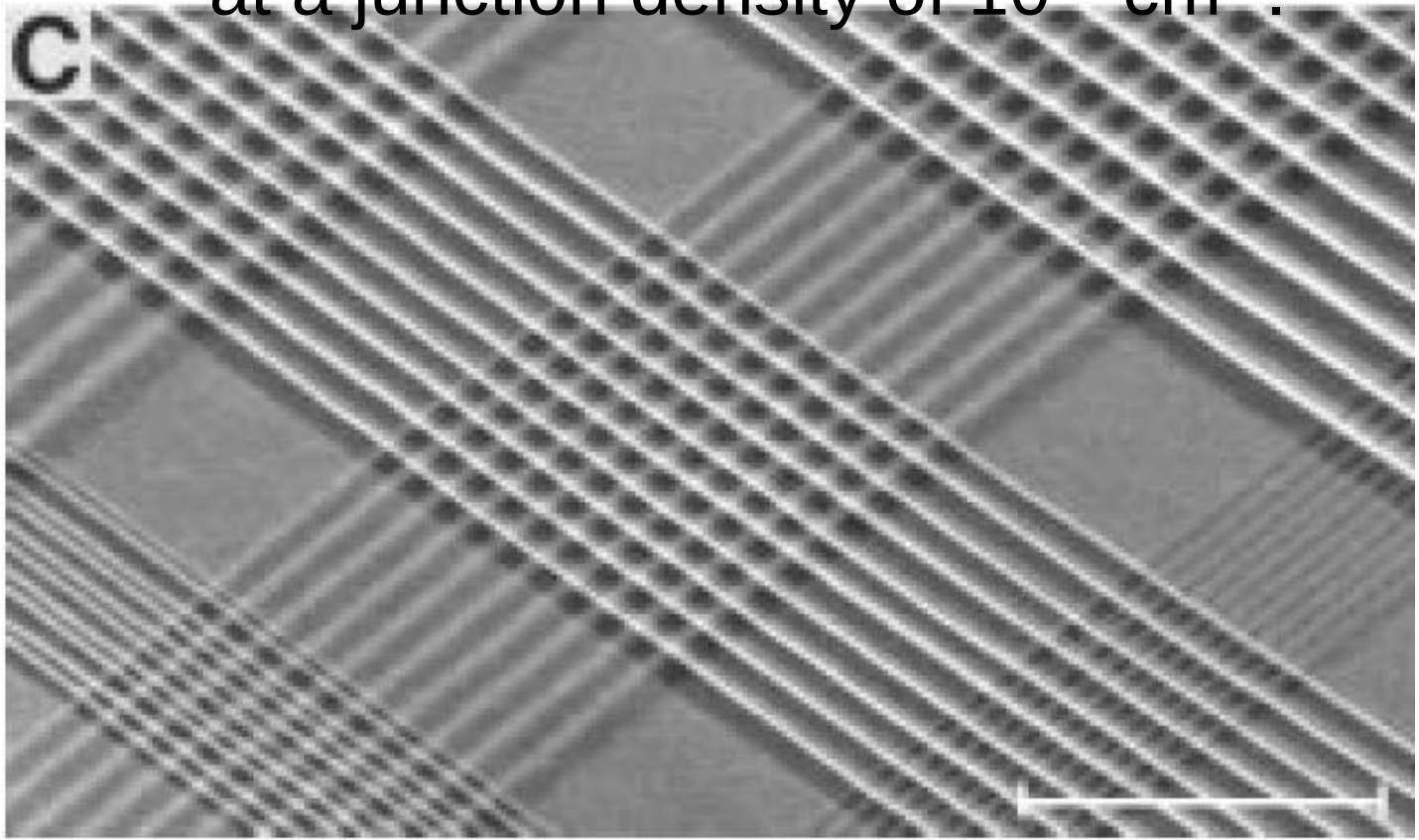

500 nm

Ultrahigh-density Nanowire arrays grown In self-assembled diblock copolymer templates

Science **2000**, 290, 2126 by Tom Russell at U. Mass Amherst

- Removal of soluble block after forming self-assembled diblock copolymer structures to get hexagonally packed pores
- Electrodeposition of Co to get Co nanowire arrays with densities > 1.9 X 10^{11} wires/cm^2
- Highly anisotropic magnetic ordering: enhanced coercivity

- Polystyrene-polymethylmethacrylate block copolymer

14 nm diameter PMMA cylinders hexagonally packed in PS matrix

- Spin cast onto conducting substrate
- Poling
- UV exposure removes PMMA block & polymerize PS block
- Formation of 14 nm pores
- Electrodeposition of Co to get nanowire array

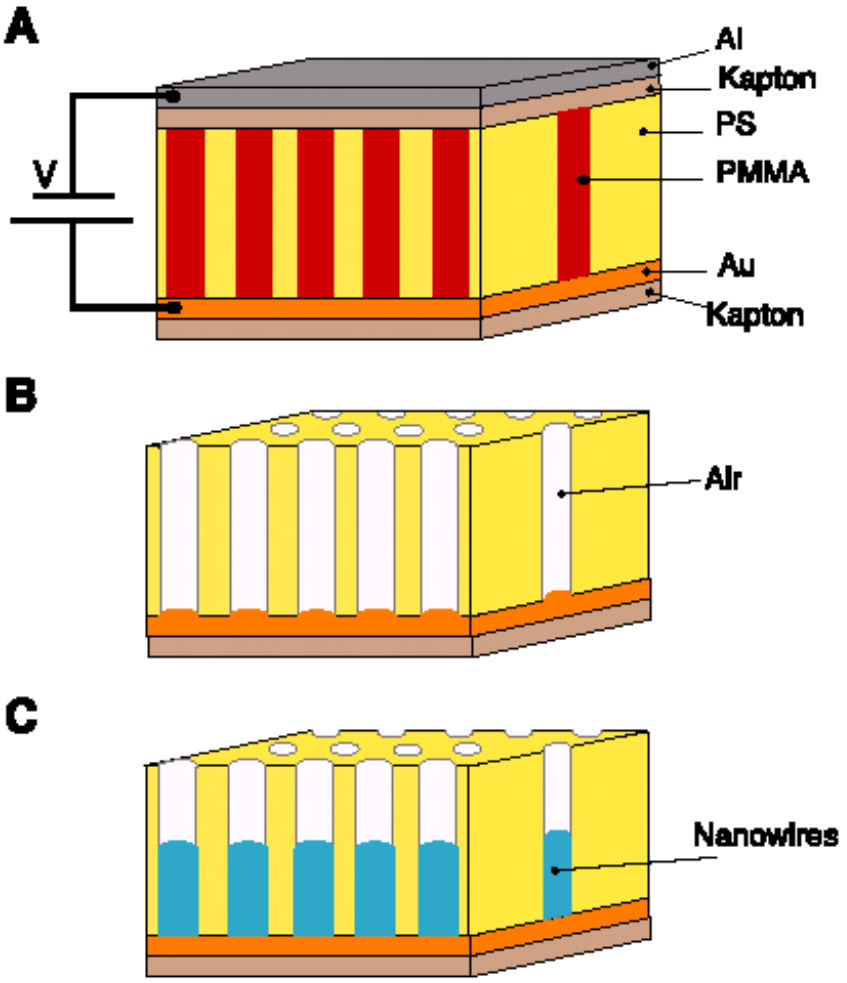

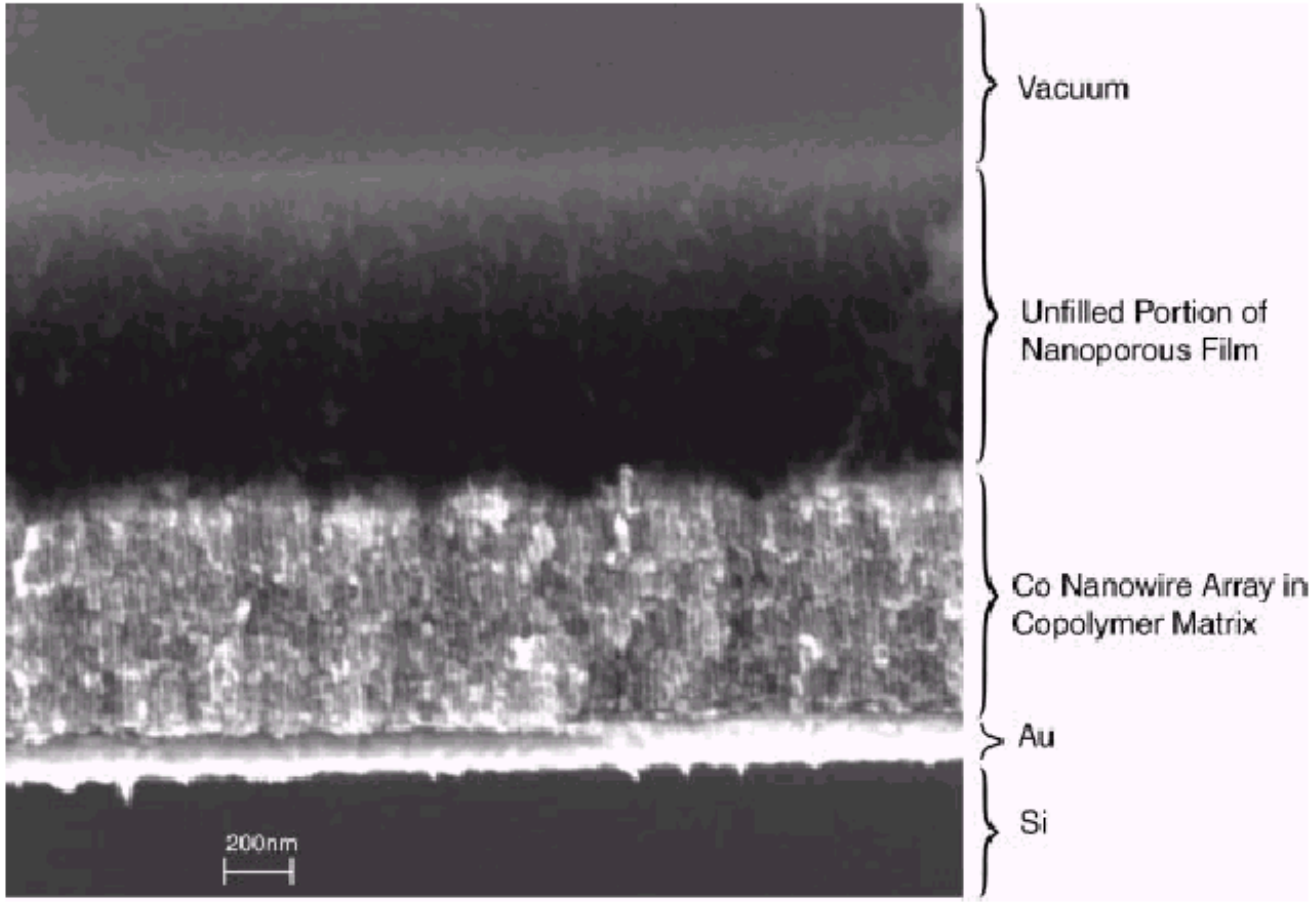
Vacuum
Unfilled Portion of
Nanoporous Film
Co Nanowire Array in
Copolymer Matrix
Au
Si
200nm

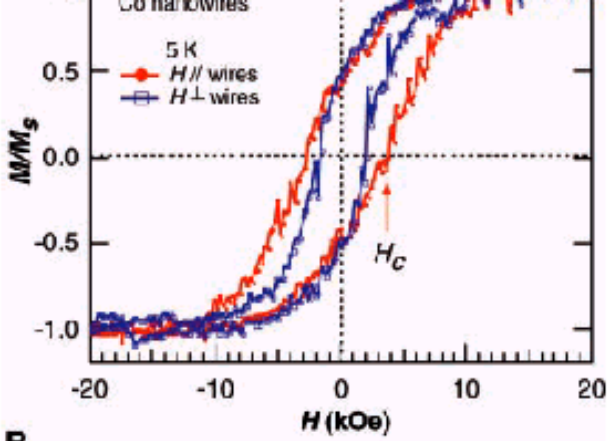

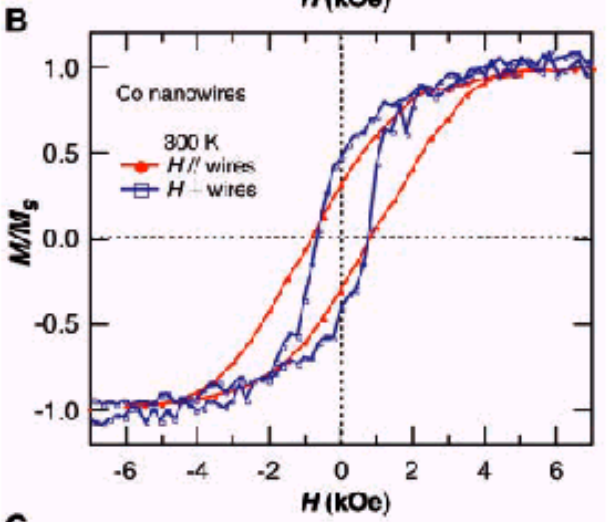

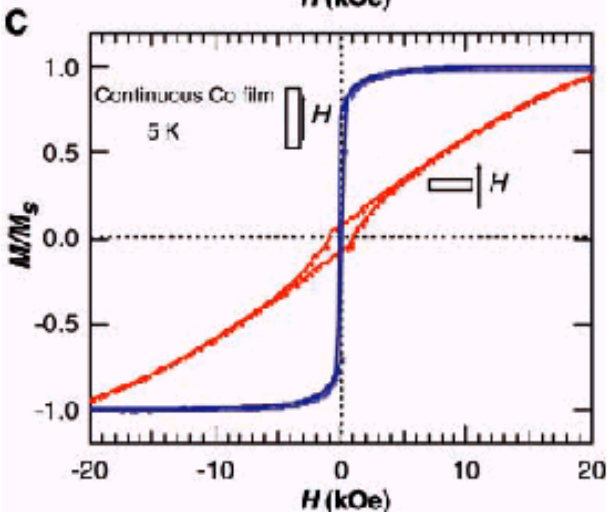

- Higher coercivity for nanwires Compared to regular thin film
- Higher coercivity parallel to the wire direction

Macroscopic 10-Terabit–per–Square-Inch Arrays from Block Copolymers with Lateral Order, Soojin Park1,*, Dong Hyun Lee1, Ji Xu1, Bokyung Kim1, Sung Woo Hong1, Unyong Jeong2, Ting Xu3,† and Thomas P. Russell1,† *Science* **2009**, 323, 1030.

Ordered arrays of cylindrical microdomains 3 nanometers in diameter, with areal densities in excess of 10 terabits per square inch.

Fig. 1. Schematic illustration of the strategy used for generating BCP cylindrical microdomains on highly oriented crystalline facets on a single-crystal surface.

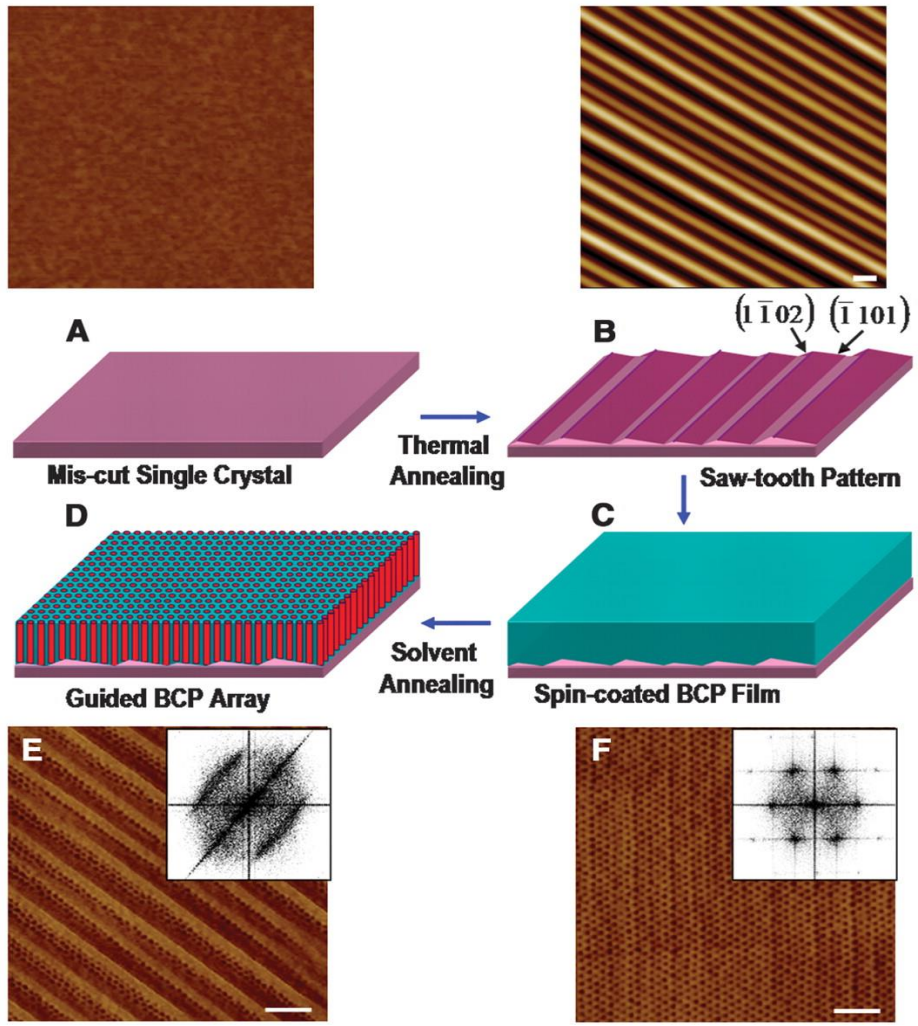

S Park et al. Science 2009;323:1030-1033

Fig. 2. AFM height images of sawtooth patterns and phase images of solvent-annealed PS-b-PEO thin films.

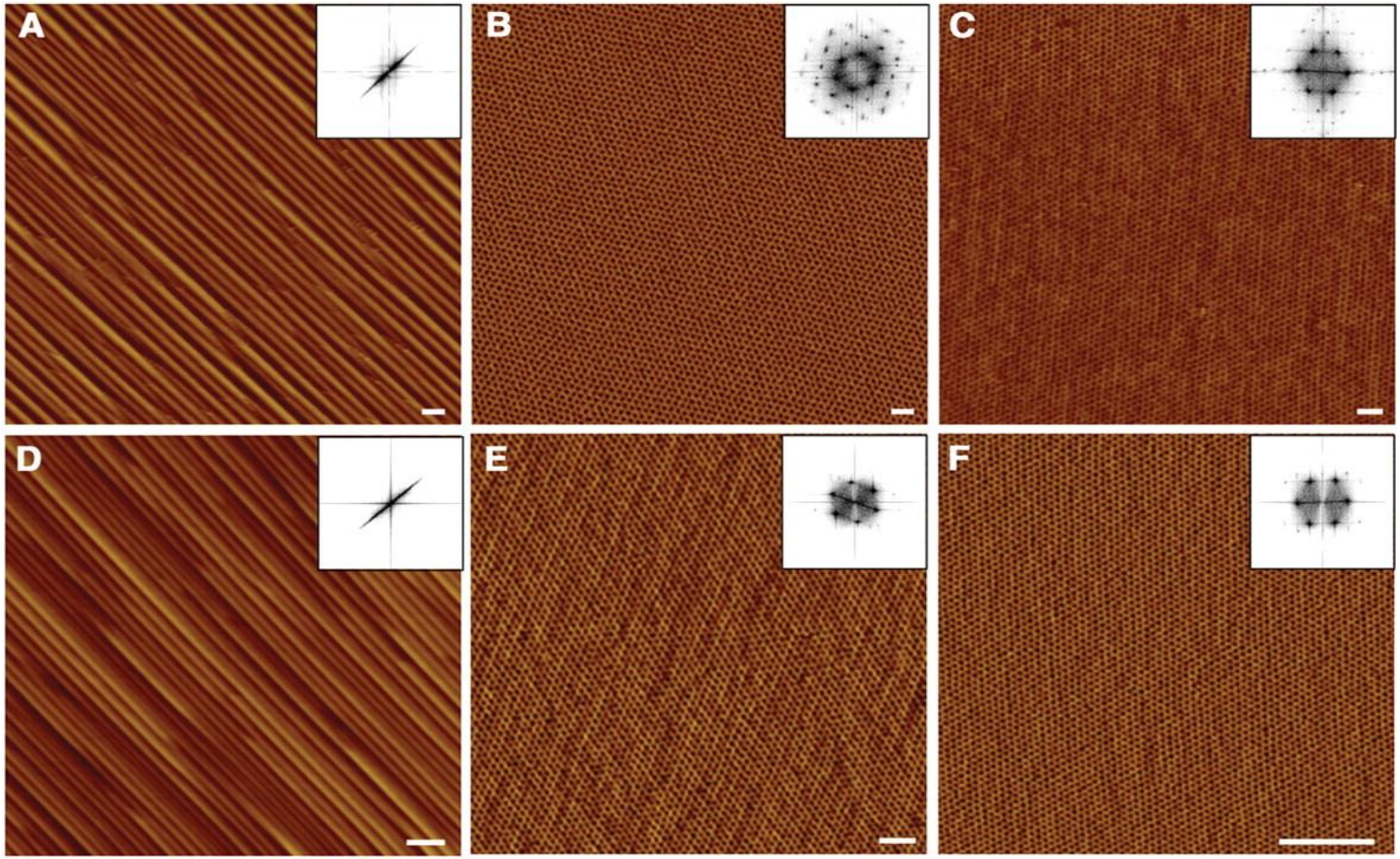

S Park et al. Science 2009;323:1030-1033

Part IV.

Oriented Attachment of Spherical Nanocrystals

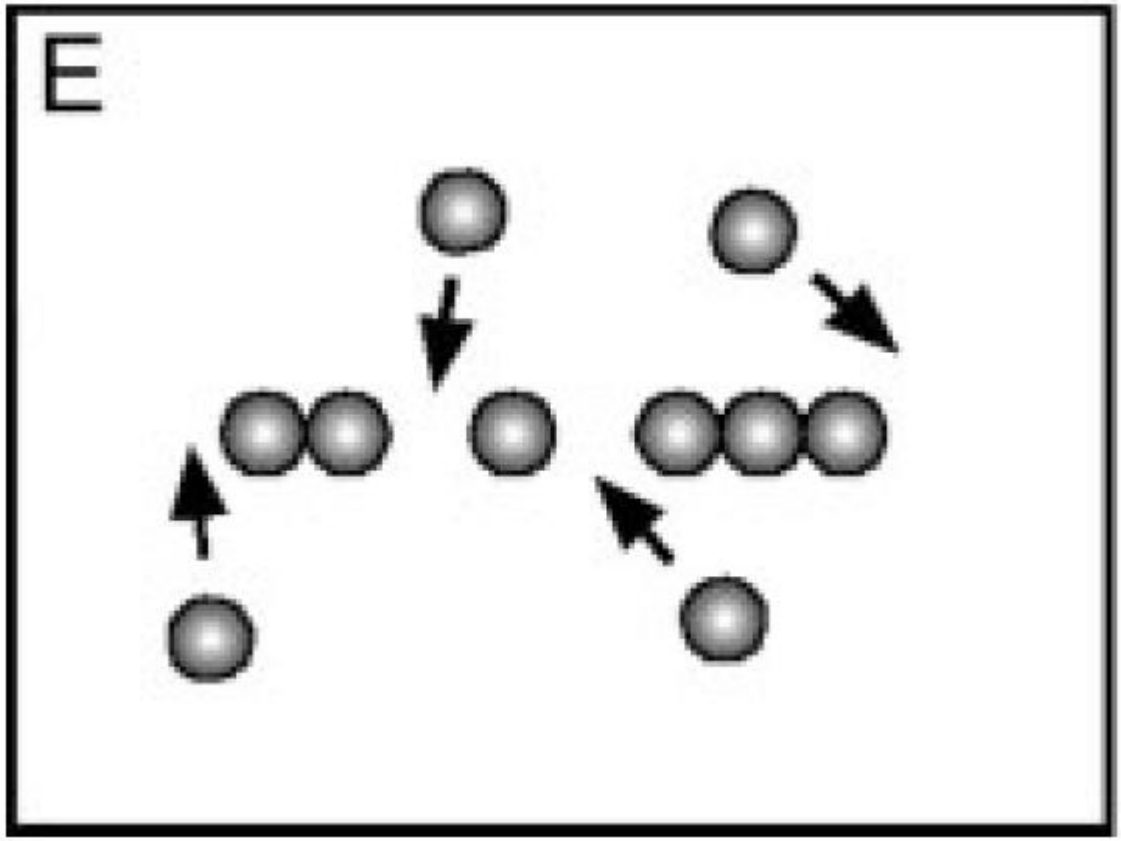

Synthesis of Uniform Iron Nanorods by Oriented Growth of Nanospheres

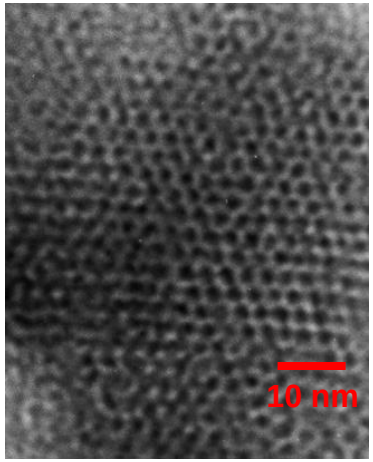

Oriented Attachment

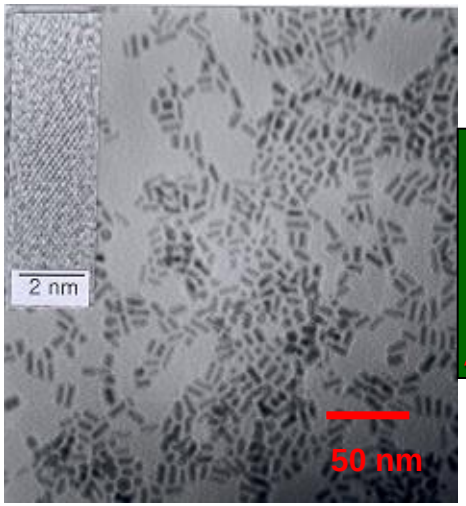

Further Oriented Attachment

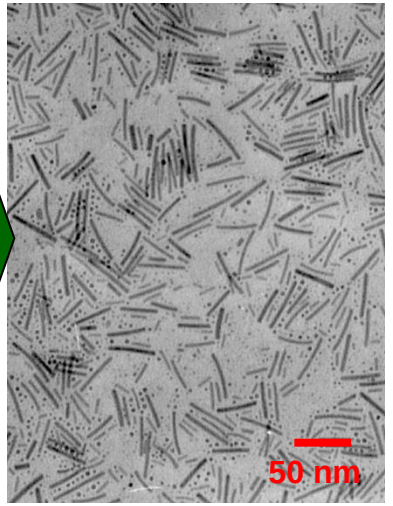

2 nm Fe Nanospheres

2 nm × 11 nm Fe Nanorods

2 nm × 36 nm Fe Nanorods

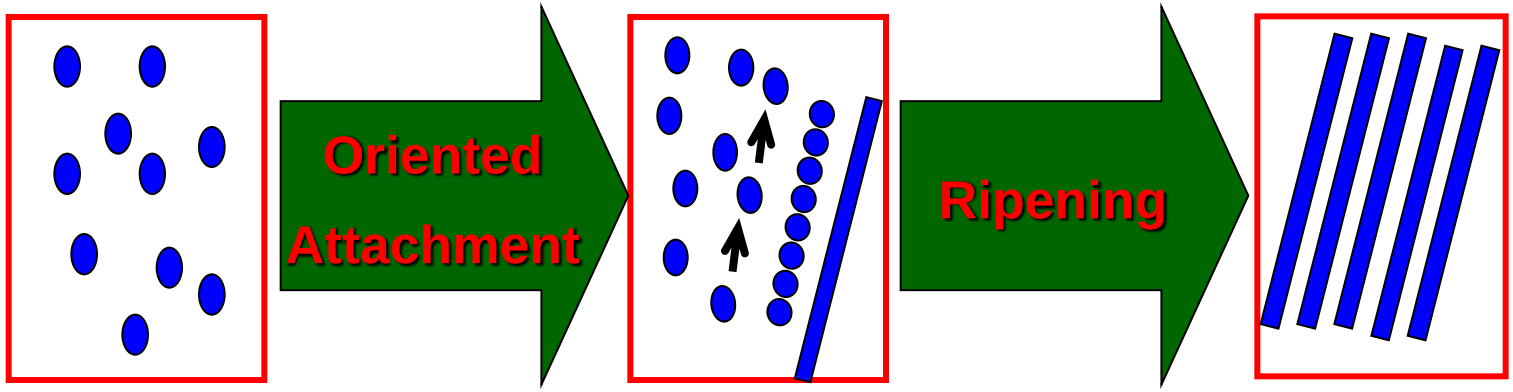

S.-J. Park, S. Kim, S. Lee, Z. G. Khim, K. Char, T. Hyeon *J. Am. Chem. Soc*. **2000**, 122, 8581.

Oriented attachment of nanospheres to get Nanorods (wires)

Spontaneous Organization of Single CdTe Nanoparticles into Luminescent Nanowires,

Nicholas A. Kotov, (OK S. U., Now at U. Michigan)

Science 2002, 297, 237.

One-Dimensional Assemblies of Nanoparticles: Preparation, Properties, and Promise, Nick Kotov, *Adv. Mater*. **2005**, 17, 951.

- Nanoparticles of CdTe were found to spontaneously reorganize into crystalline nanowires upon controlled removal of the protective shell of organic stabilizer.
- Electric dipole-dipole interaction between NPs
- CdTe colloids redissolved in pure water at pH 9.0 was allowed to age at room temperature for several days.

Spontaneous organization of single CdTe nanoparticles into luminescent nanowires, Author(s): Tang, ZY (Tang, ZY); Kotov, NA (Kotov, NA); Giersig, M (Giersig, M)
Source: SCIENCE Volume: 297 Issue: 5579 Pages: 237-240 DOI: 10.1126/science.1072086 Published: JUL 12 2002
Times Cited: 1248 (from Web of Science)

Author(s): Park, SJ (Park, SJ); Kim, S (Kim, S); Lee, S (Lee, S); Khim, ZG (Khim, ZG); Char, K (Char, K); Hyeon, T (Hyeon, T)
Source: JOURNAL OF THE AMERICAN CHEMICAL SOCIETY Volume: 122 Issue: 35 Pages: 8581-8582 DOI: 10.1021/ja001628c Published: SEP 6 2000
Times Cited: 410 (from Web of Science)

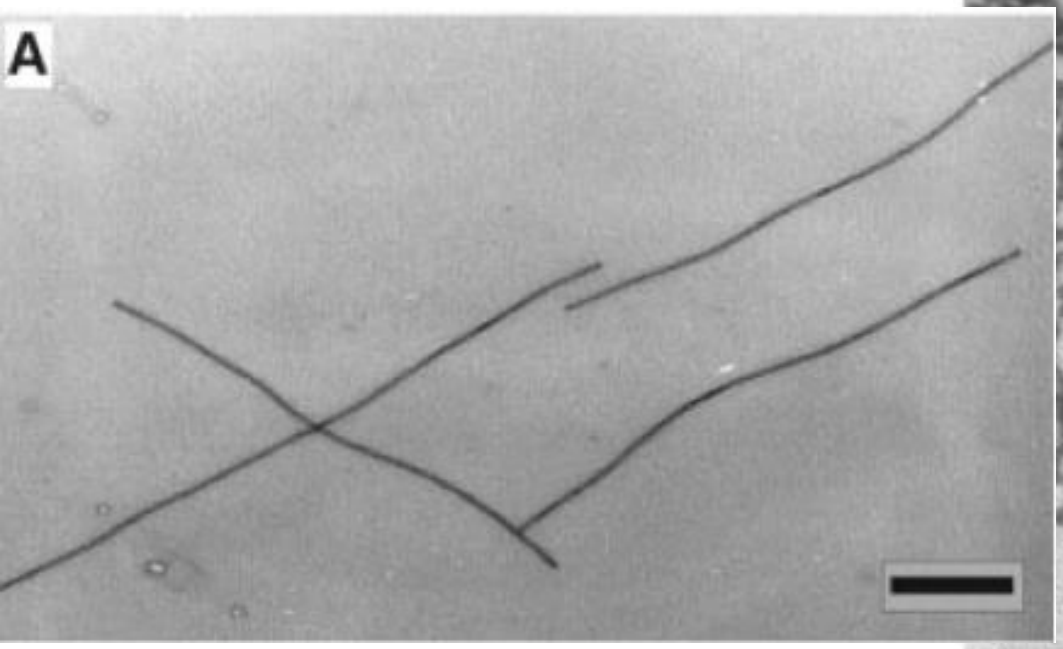
A

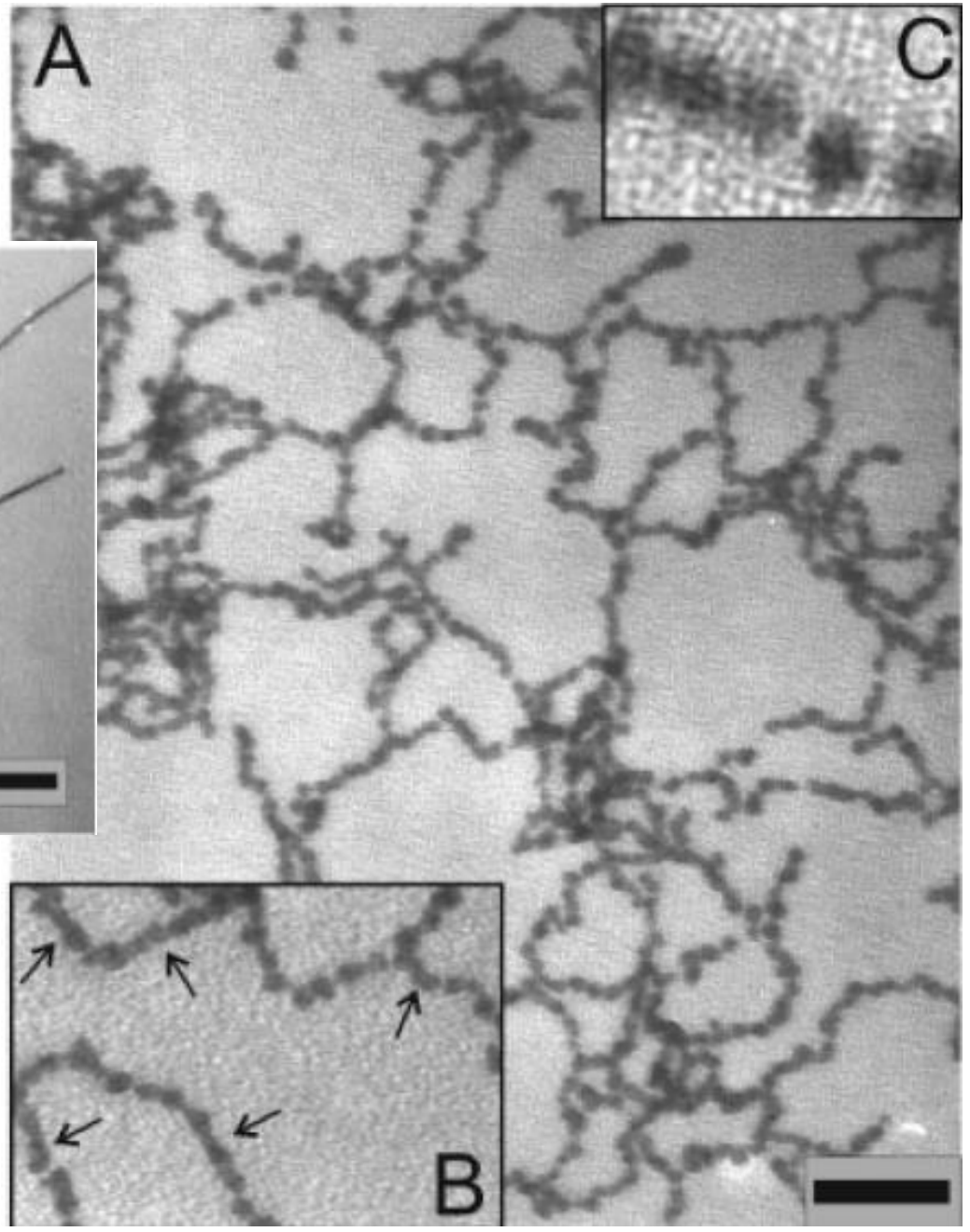
A
C
B

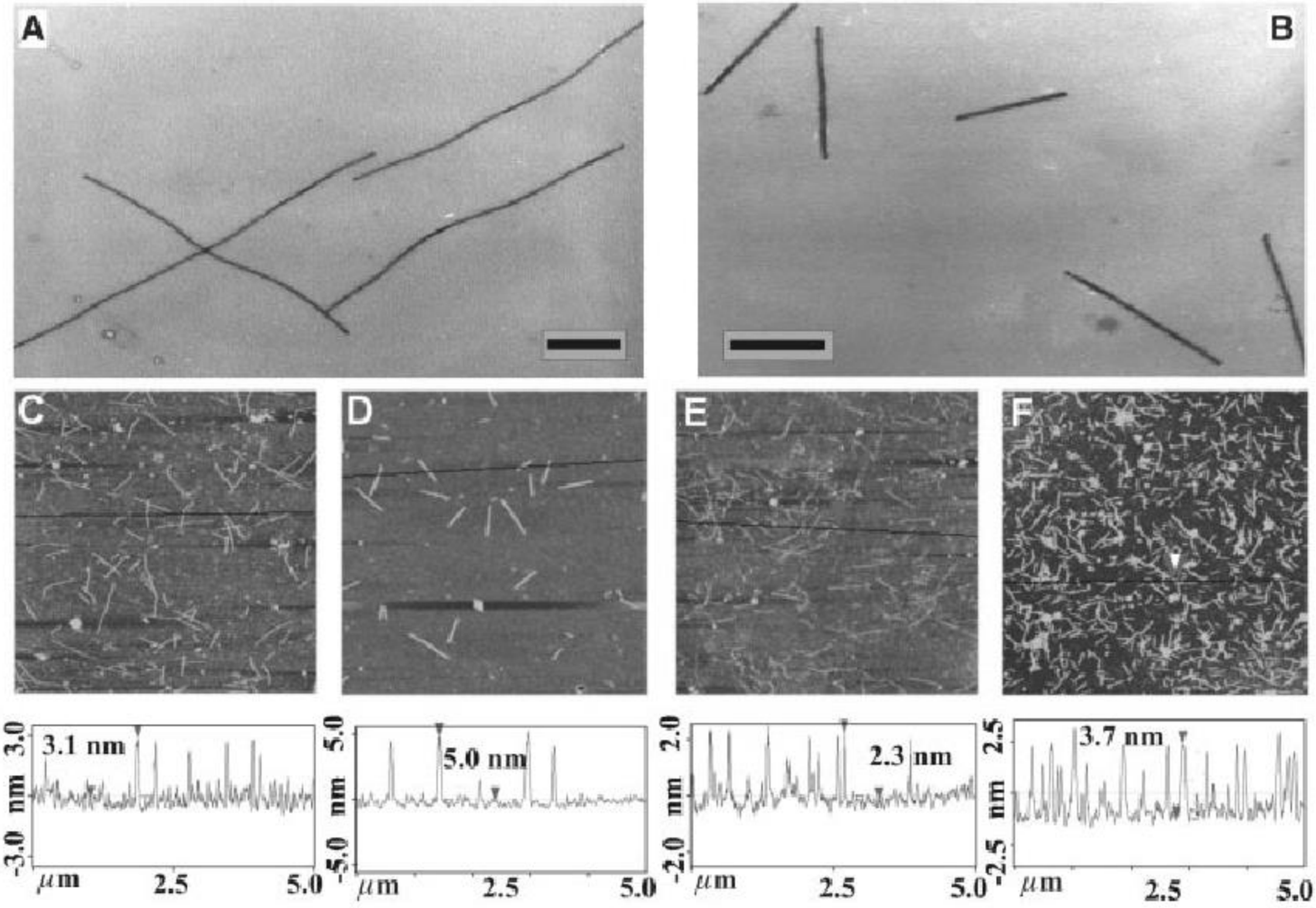
A
B
C
D
E
F
3.1 nm
3.0
nm
-3.0
μm
2.5
5.0
5.0 nm
5.0
nm
-5.0
μm
2.5
5.0
2.3 nm
2.0
nm
-2.0
μm
2.5
5.0
3.7 nm
2.5
nm
-2.5
μm
2.5
5.0

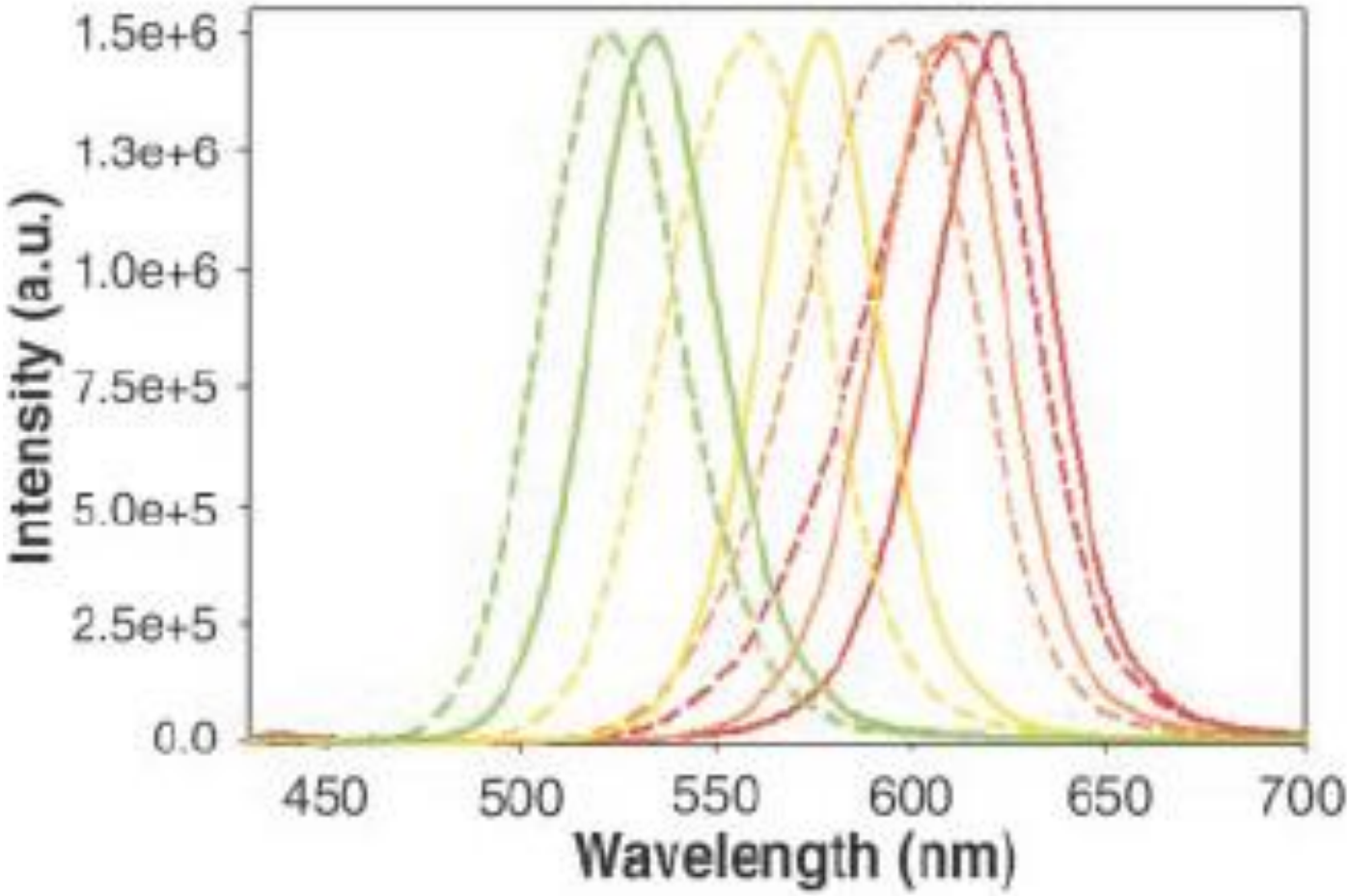
1.5e+6
1.3e+6
1.0e+6
7.5e+5
5.0e+5
2.5e+5
0.0
Intensity (a.u.)
450
500
550
600
650
700
Wavelength (nm)

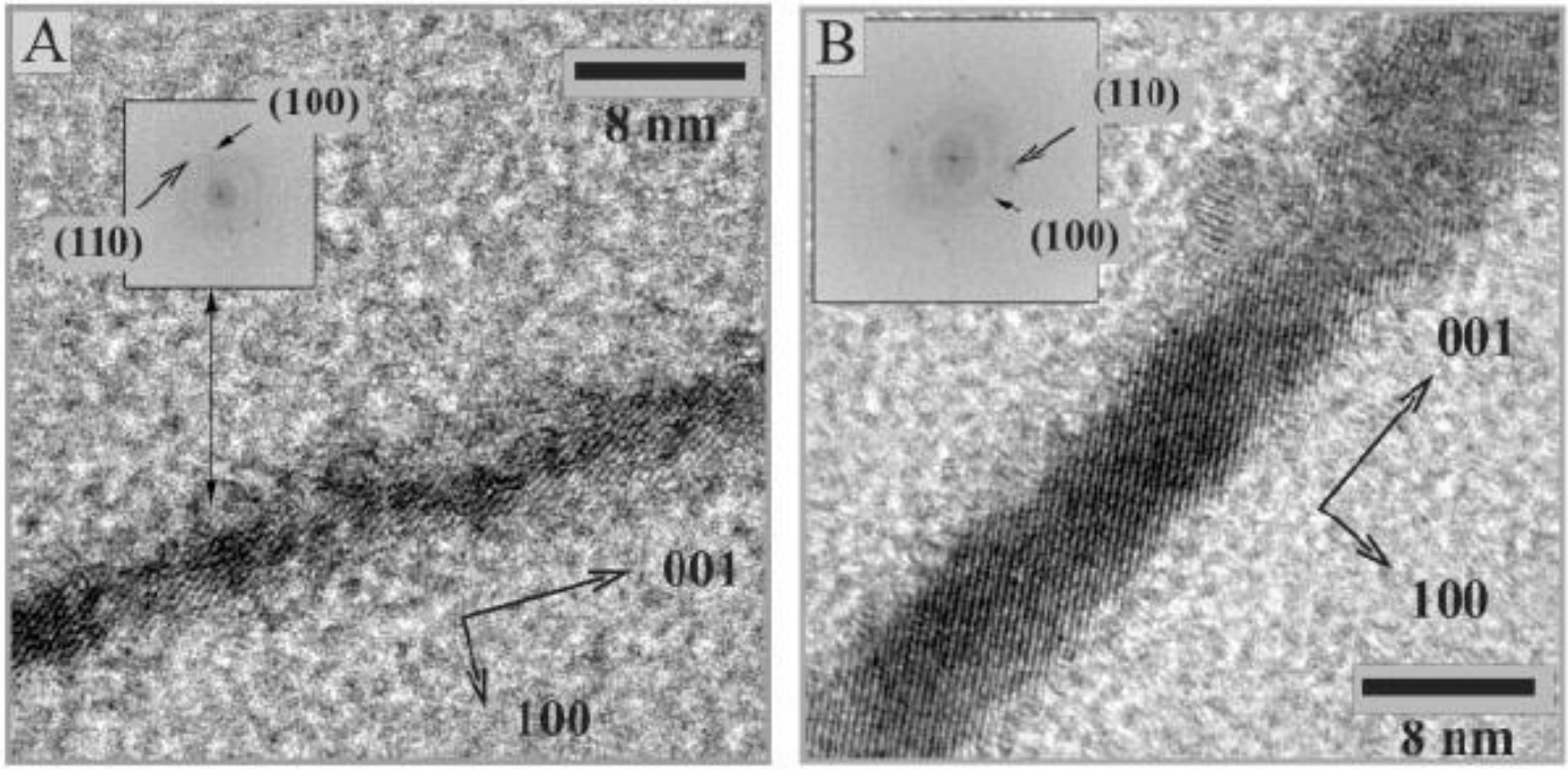
A
(100)
(110)
8 nm
001
100
B
(110)
(100)
001
100
8 nm

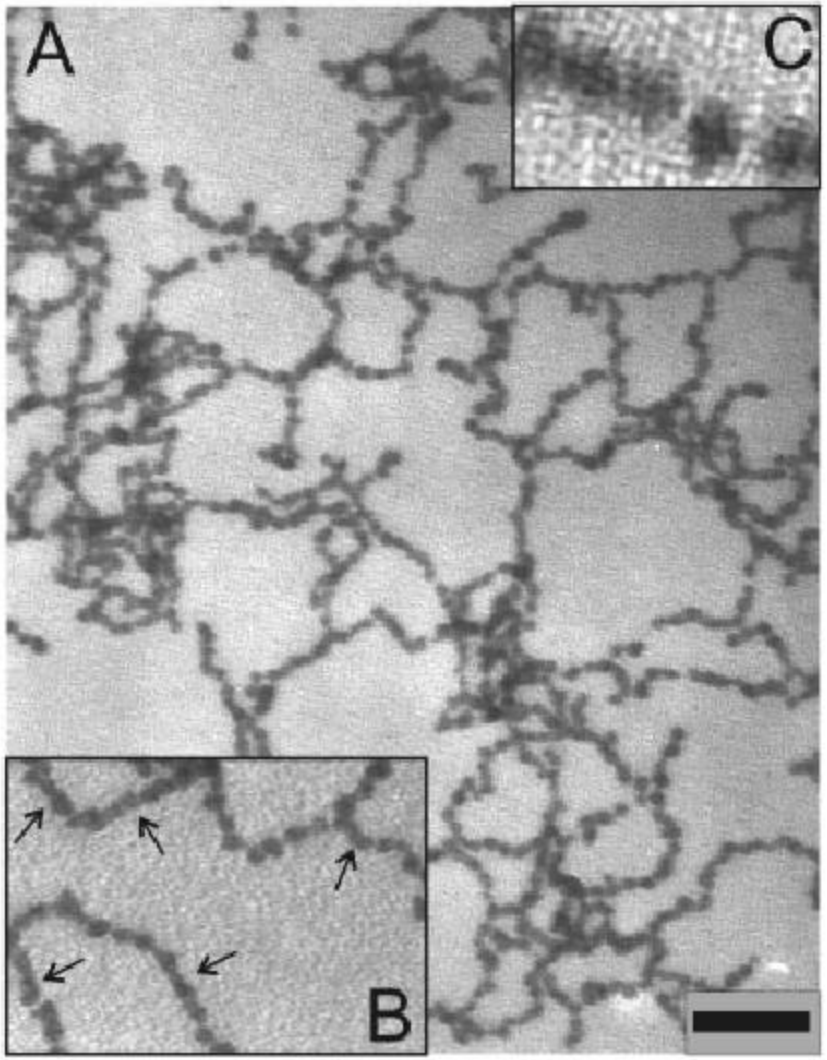

The intermediate step in the nanowire formation was found to be pearl-necklace aggregates. Strong dipole-dipole interaction is believed to be the driving force of nanoparticle self-organization. The linear aggregates subsequently recrystallized into nanowires whose diameter was determined by the diameter of the nanoparticles.

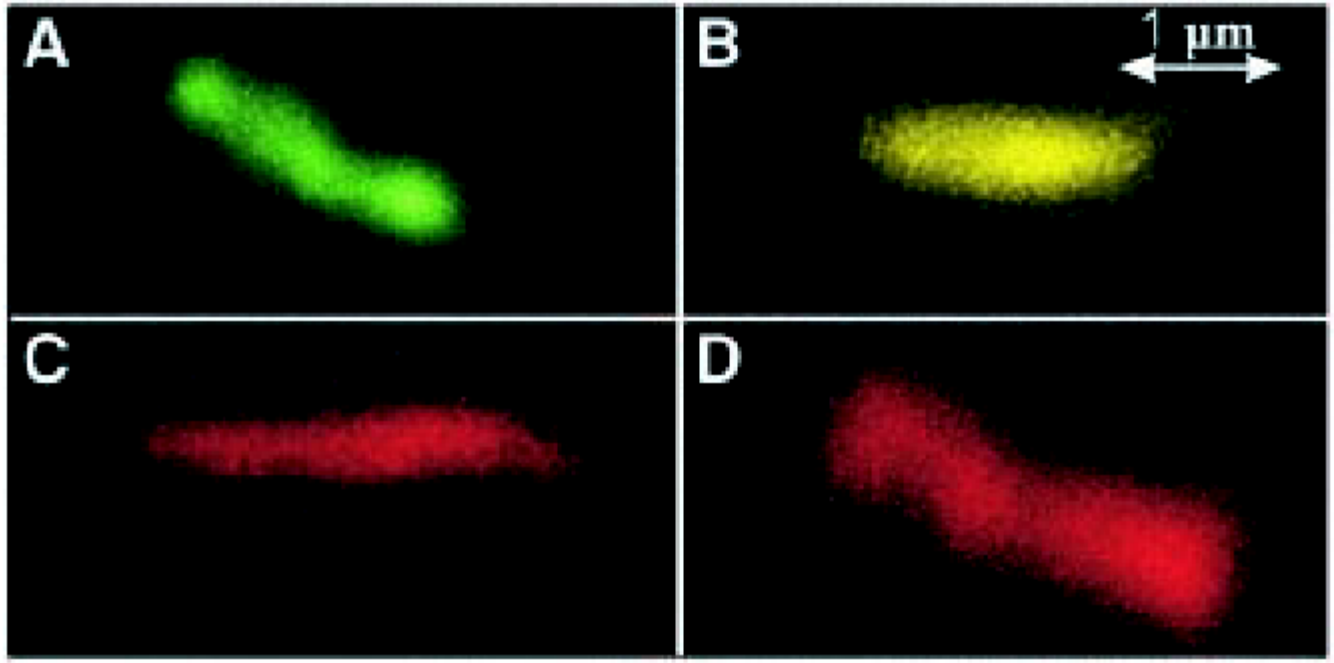

Fig. 5. Confocal microscopy images of individual nanowires with $d_{TEM} = 2.5$ (**A**), 3.5 (**B**), 4.2 (**C**), 5.6 nm (**D**) emitting in the green, yellow, orange, and red part of the spectrum, respectively.

The produced nanowires have high aspect ratio,uniformity, and optical activity. These findings demonstrate the collective behavior of nanoparticles as well as a convenient, simple technique for production of one-dimensional semiconductor colloids suitable for subsequent processing into quantum-confined superstructures, materials, and devices.

Synthesis of

Quantum-sized Cubic ZnS Nanorods

via Oriented Attachment Mechanism

J. H. Yu *et al*., *J. Am. Chem. Soc*. **2005**, 127, 5662.

5nm ZnS Nanocrystals (HDA)

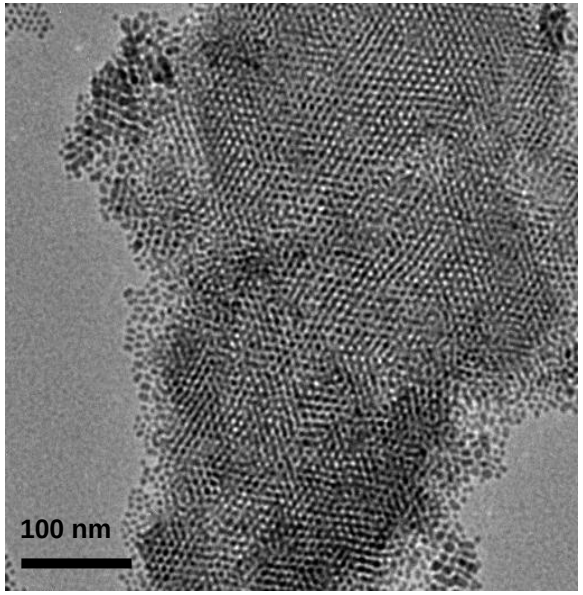

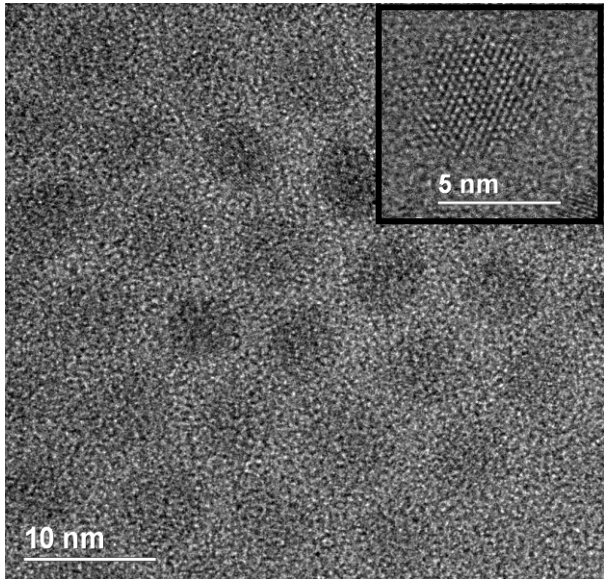

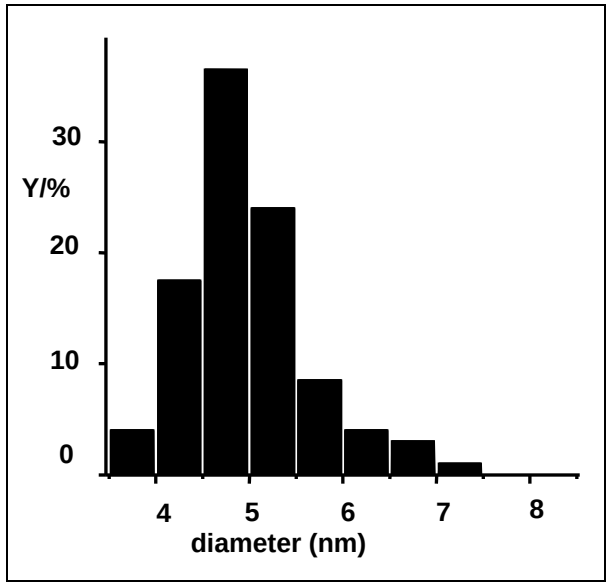

Monodisperse 5nm cubic spherical nanocrystal synthesized.

Proof of Oriented Attachment (2)

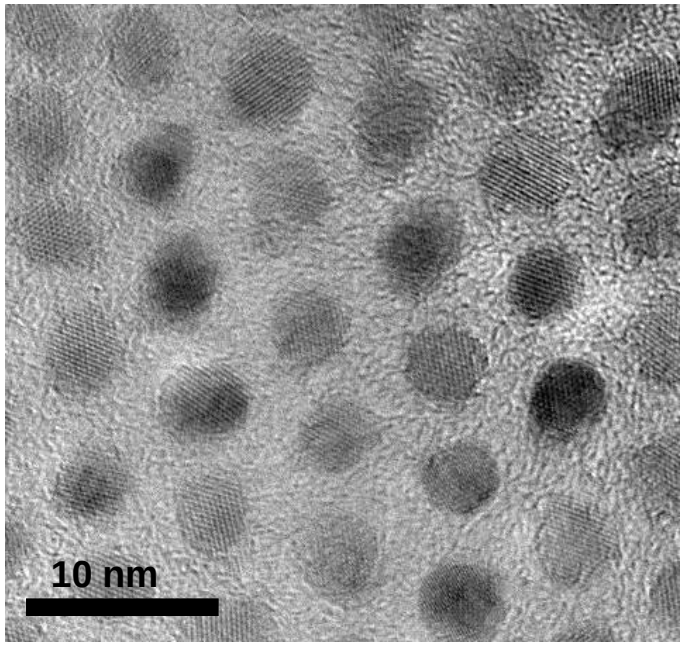

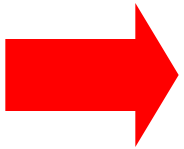

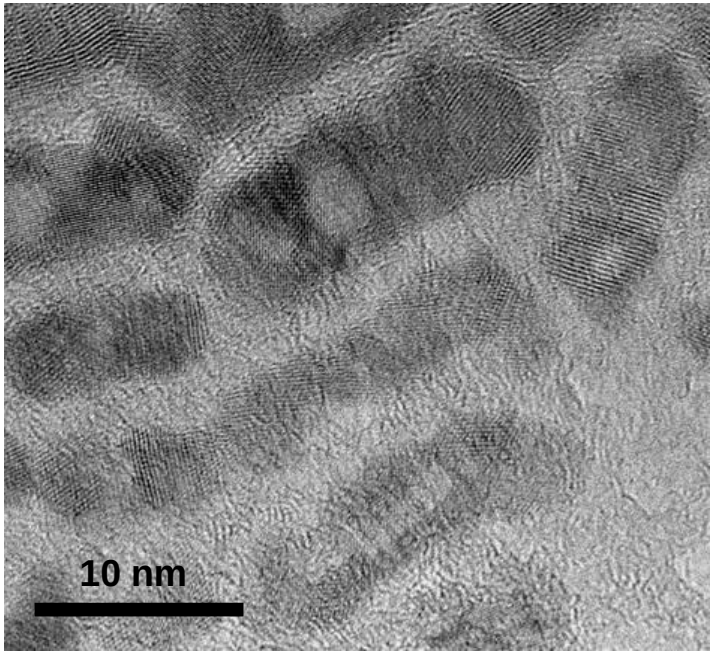

5nm nanoparticle with HDA

Nanorod formation by aging in oleylamine at 60 ^{o}C

Penn, R. L.; Banfield, J. F. ***Science*** **1998,** ***281,*** **969 and Weller, H.** ***Angew. Chem. Int. Ed.*** **2002,** ***41,*** **1188. .**

Part V.

Kinetic Control by Capping of Specific Crystal Faces using Appropriate Surfactants

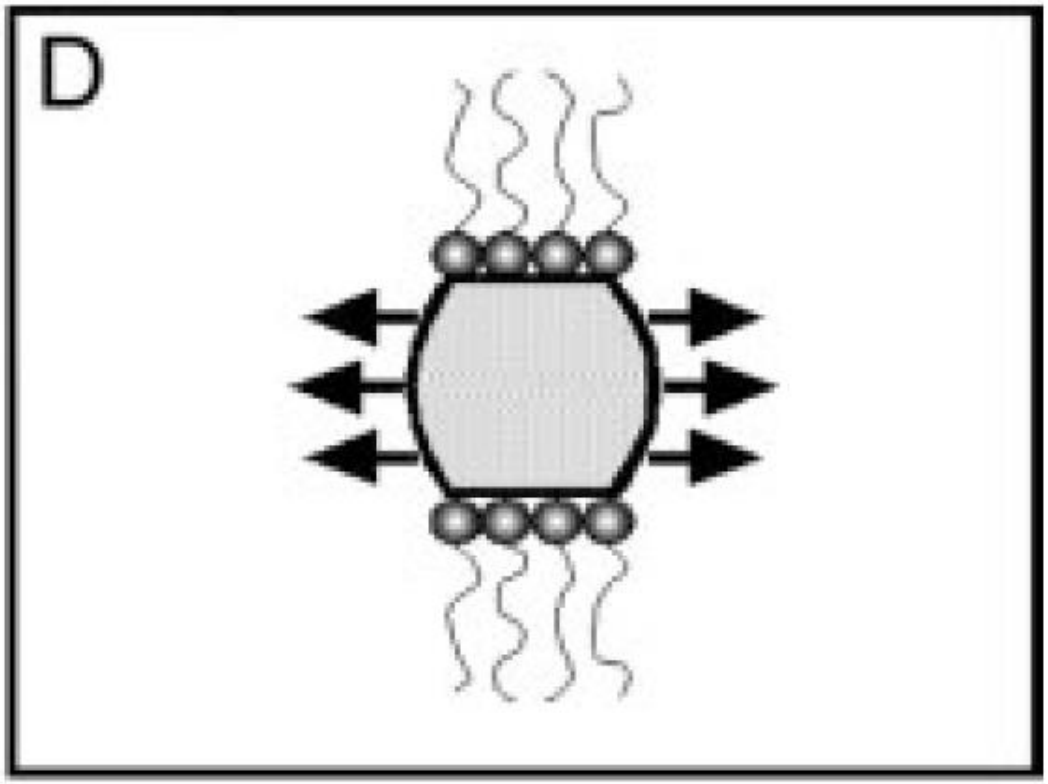

Synthesis of Soluble and Processable Rod-, Arrow-, Teardrop-, Tetrapod-shaped CdSe Nanocrystals

JACS 2000, 122, 12700 by Alivisatos

The most influential factors for Shape control

- Ratio of surfactants
- Injection volume
- Time-dependent monomer concentration

Oriented Growth of Spherical Nanoparticles

Previous work in Nature 2000, 404, 59.

Electrochemical Synthesis of Au Nanorods in the presence of Surfactants

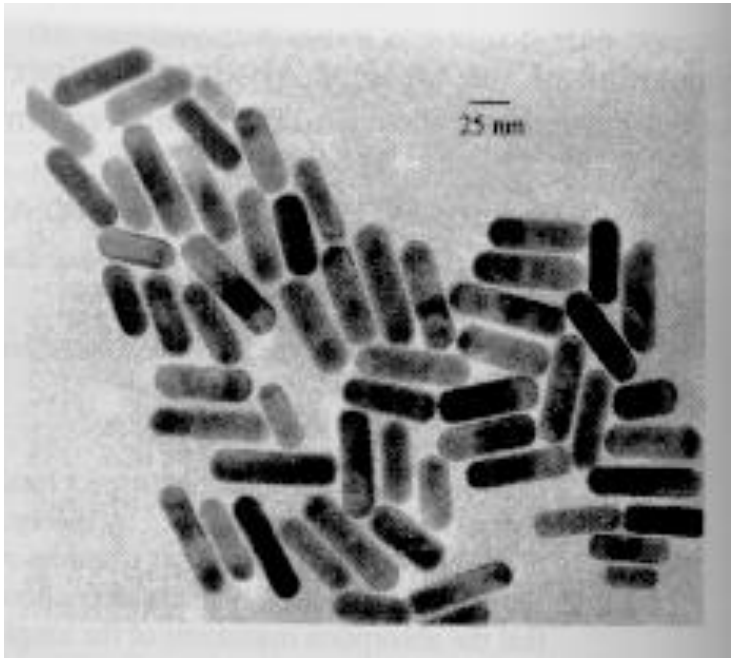

El-Sayed, *J. Phys. Chem*. **1999**, 103, 3073.

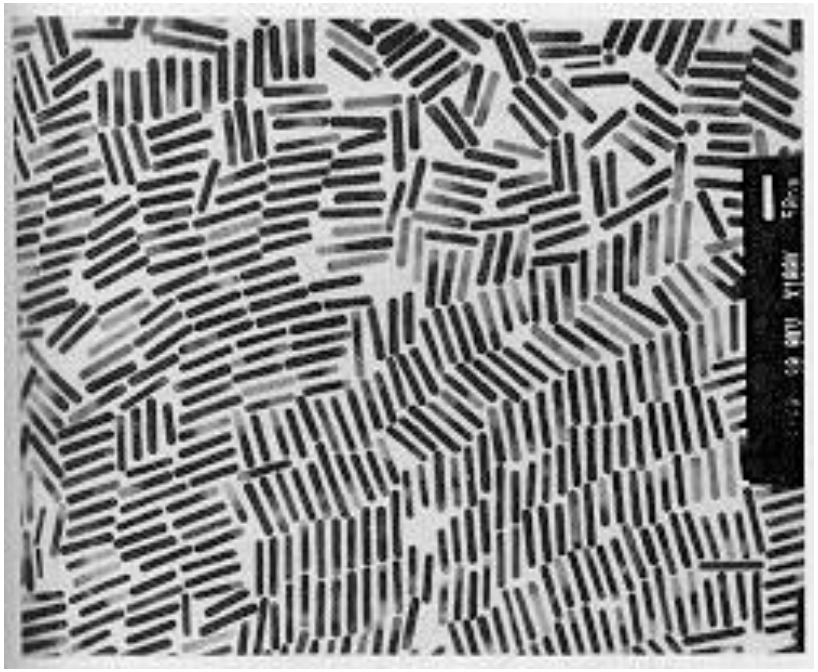

Wang, *Langmuir* **1999**, 15, 701.

Gold nanorods were prepared by an electrochemical method

- Gold electrode as the sacrificial anode
  Platinum electrode as the cathode.
- The electrolyte consists of a mixture of hexadecyltrimethylammonium bromide (CTAB) as the cationic surfactant and tetraoctylammonium bromide as the cosurfactant; the mixture is dissolved in water.
- The latter surfactant induces rod-shaped gold nanoparticle
- The ratio of the two surfactants determines the aspect ratio (the ratio of length to width) of the nanorod.

El-Sayed, *J. Phys. Chem. B* **2000,** *104,* 8635.

Controlling the aspect ratios of nanorods

Catherine J. Murphy* and Nikhil R. Jana

Adv. Mater. **2002**, 14, 80.

Shape matters !

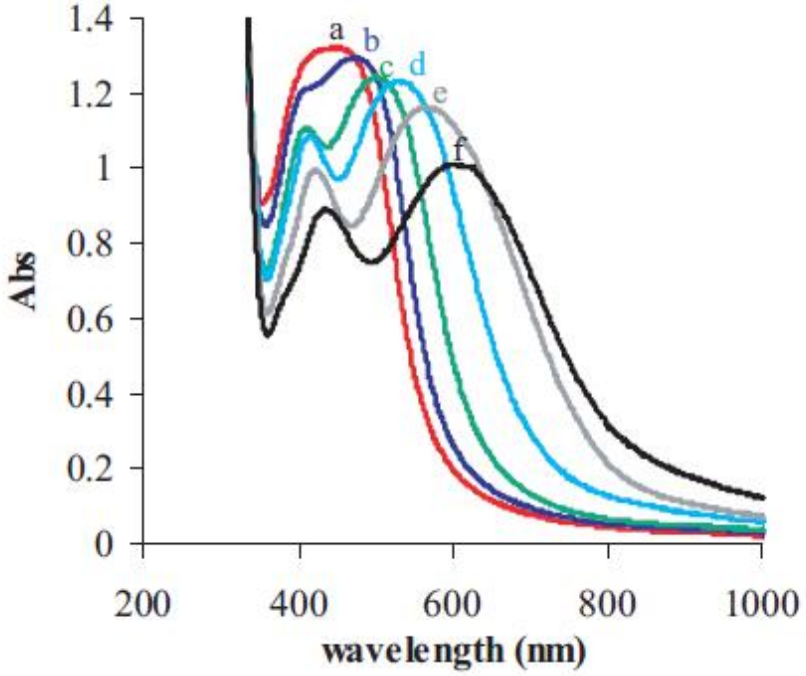

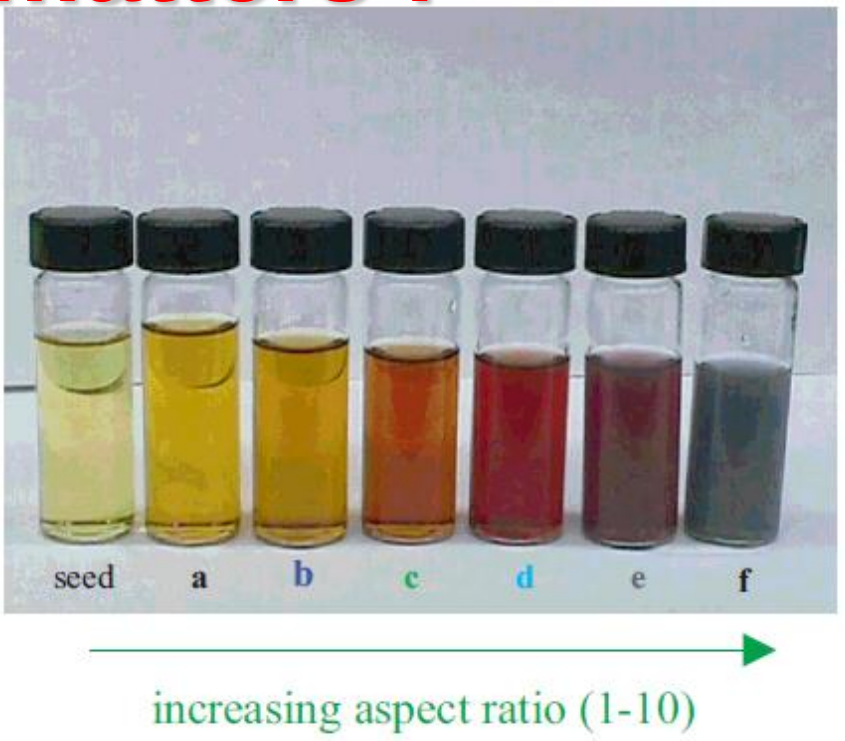

Aqueous solutions of silver nanoparticles show a beautiful variation in visible color depending on the aspect ratio of suspended nanoparticles

Seed-mediated growth for gold and silver nanorods

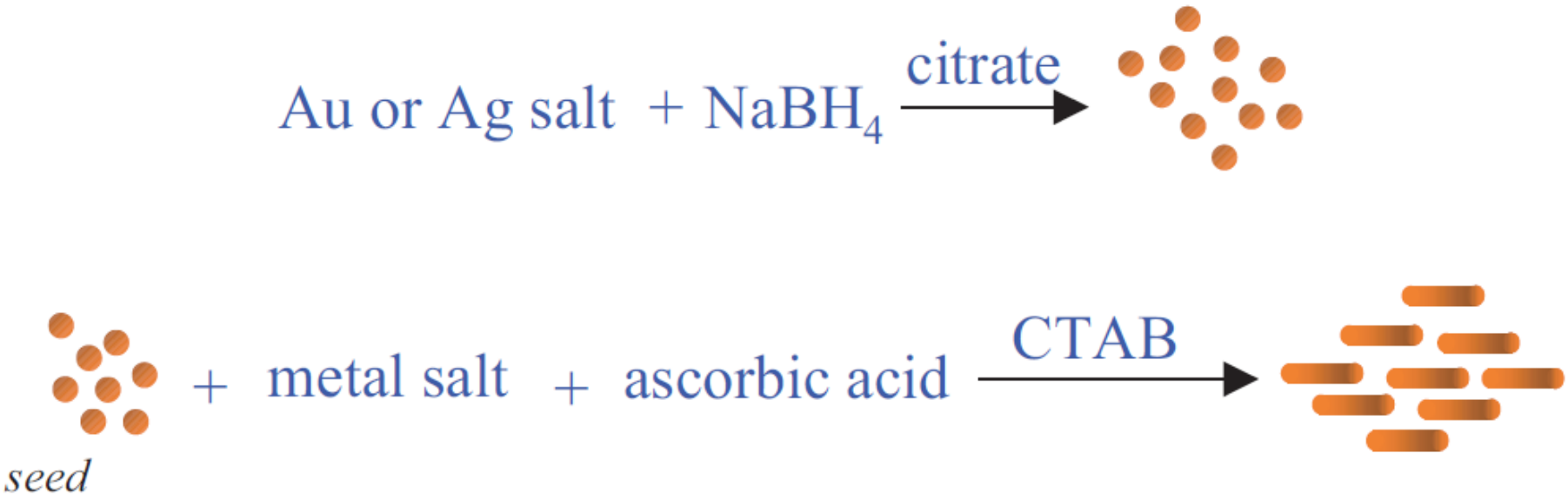

N. R. Jana, L. Gearheart, C. J. Murphy, *Chem. Commun*. **2001**, 617.

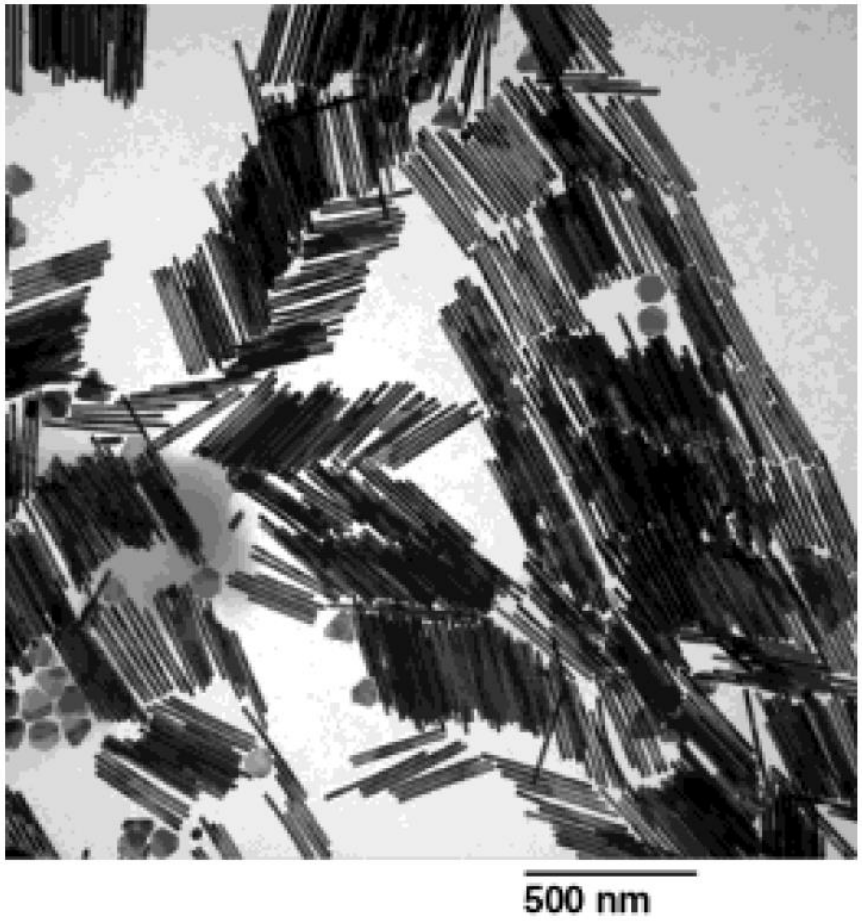

Gold nanorods with aspect ratio 18

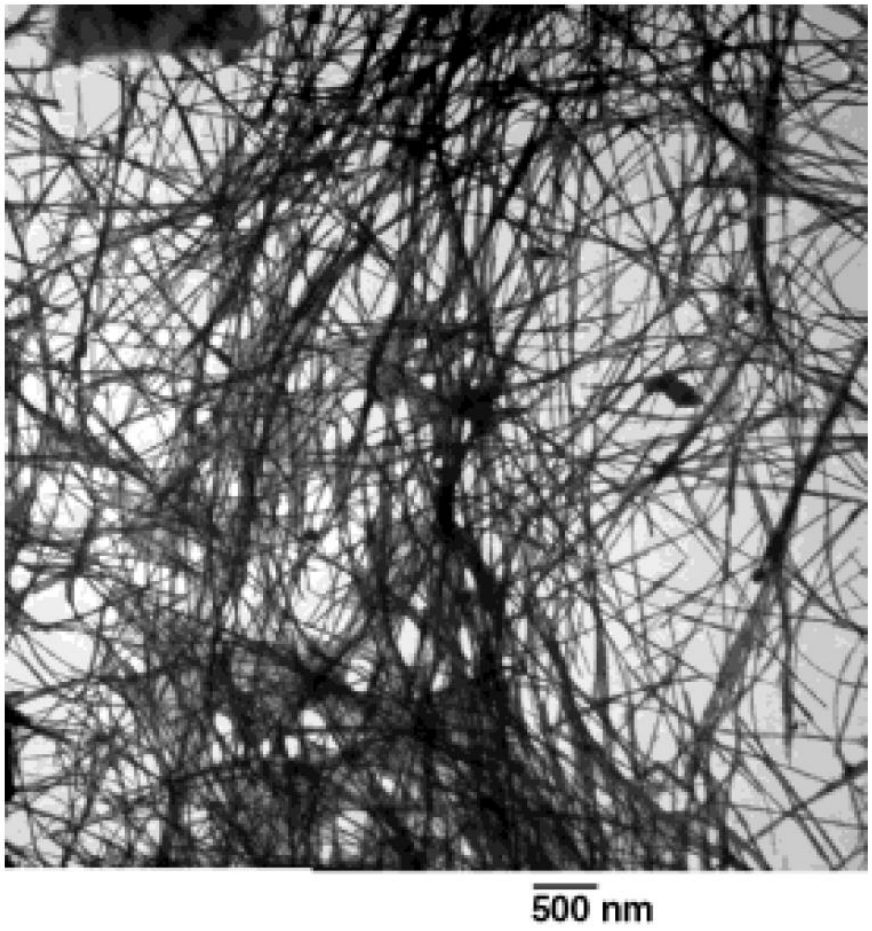

Silver nanowires with aspect ratio ~100

Colloidal Synthesis of CdSe Nanorods

Injection of Me_2Cd + Se in TOP into Hot impure TOPO

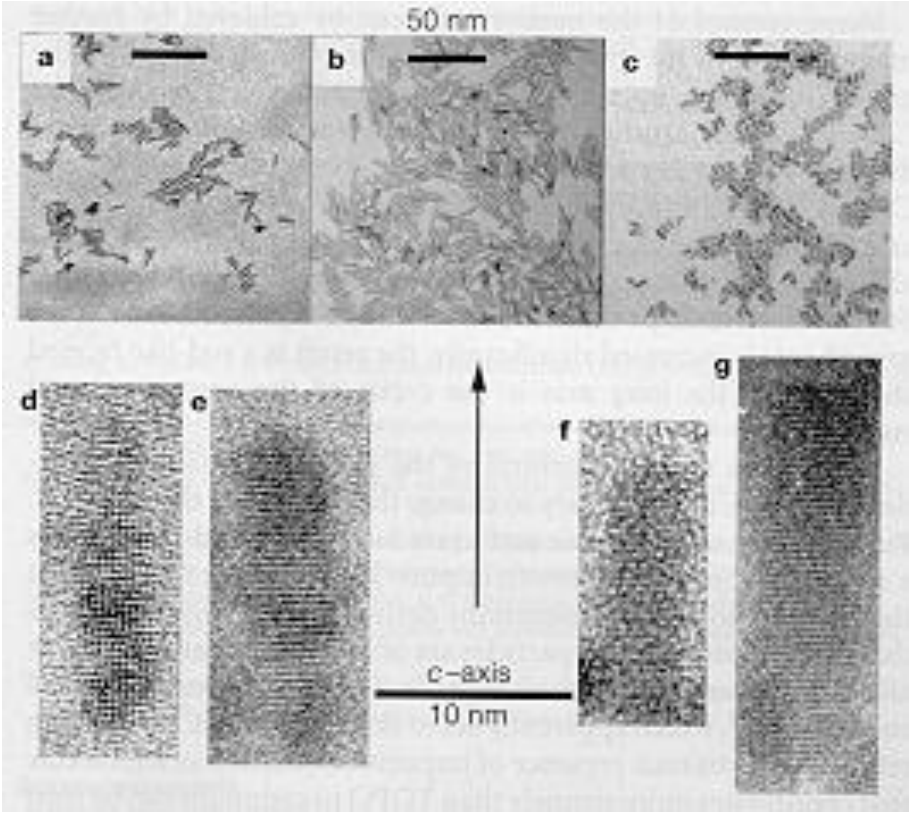

Alivisatos, *Nature* **2000**, 404, 59.

The selective adsorption of organic surfactants onto particular crystallographic facets is employed as a means of controlling the shape.

The concept of selective adsorption is to use an organic molecule to inhibit the growth of a particular crystallographic direction.

- At low monomer concentration, Ostwald ripening occurs, and favor the formation of a spherical particles.
- At high monomer concentration, relative differences between the growth rates of different faces can lead to anisotropic shapes.
- The relative growth rates of the different faces can be controlled by suitable variation of the ratio of trioctylphosphine oxide and hexylphosphonic acid.

Three parameters for shape & size control

- Ratio of surfactants (HPA/TOPO)
- Volume of initial injection
- Time dependence of the monomer concentration

With no HPA or < 10% HPA
: Nano-Spheres

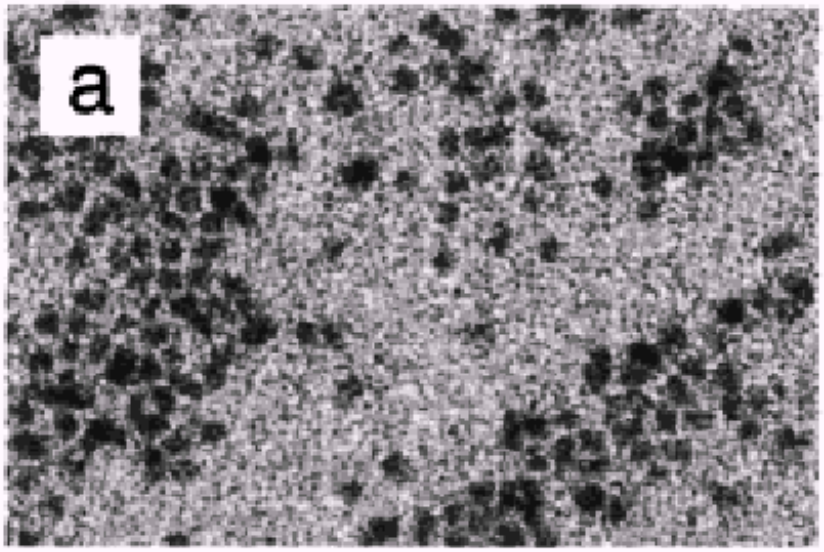

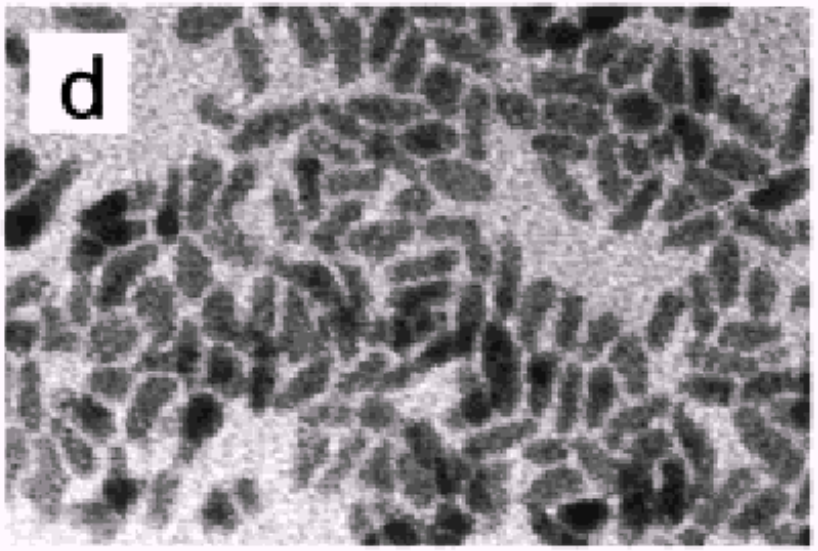

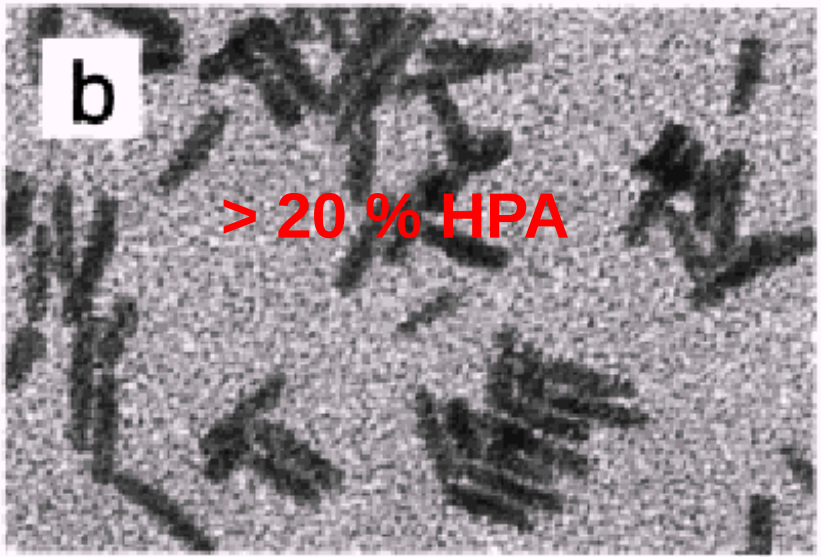

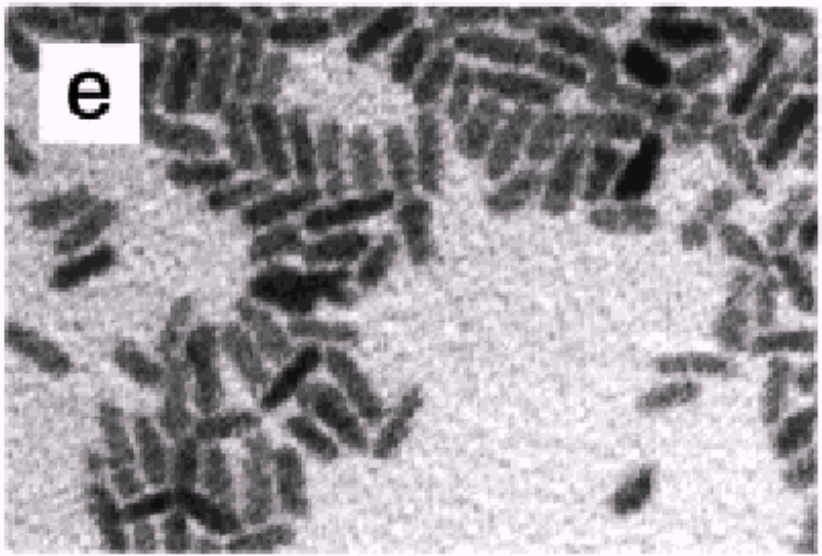

HPA concn (mol %)	injection vol (mL)	length (nm)	aspect ratio (c:a)
8	2.0	5.1 ± 0.8	1:1
20	2.0	21.8 ± 4.2	5:1
60	2.0	21.7 ± 2.0	varies
20	1.0	13.0 ± 2.1	2:1
20	1.5	16.4 ± 1.1	2.7:1
20	2.0	21.8 ± 4.2	5:1

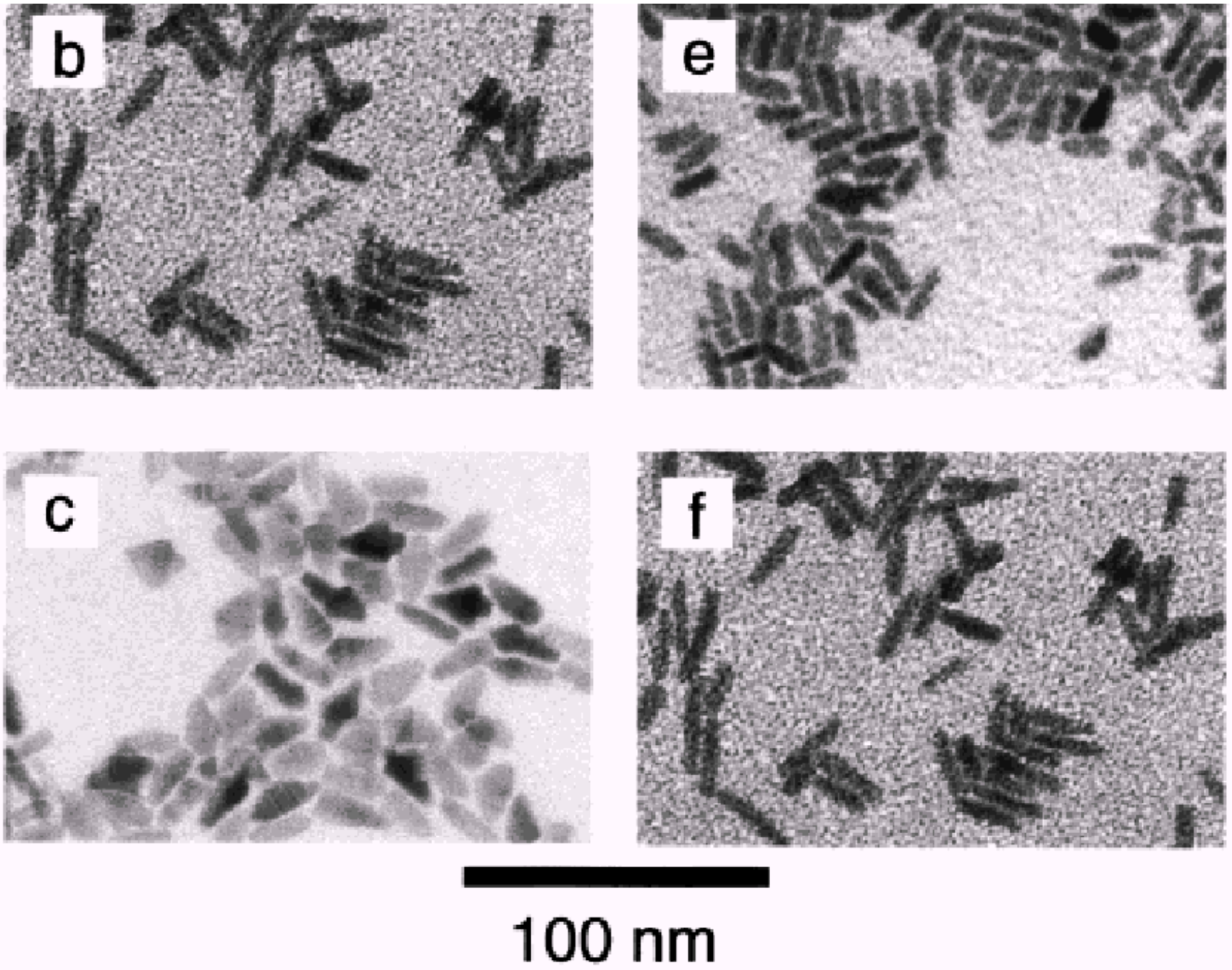
b
e
c
f
100 nm

Arrow-shaped CdSe nanoparticles for 60% HPA

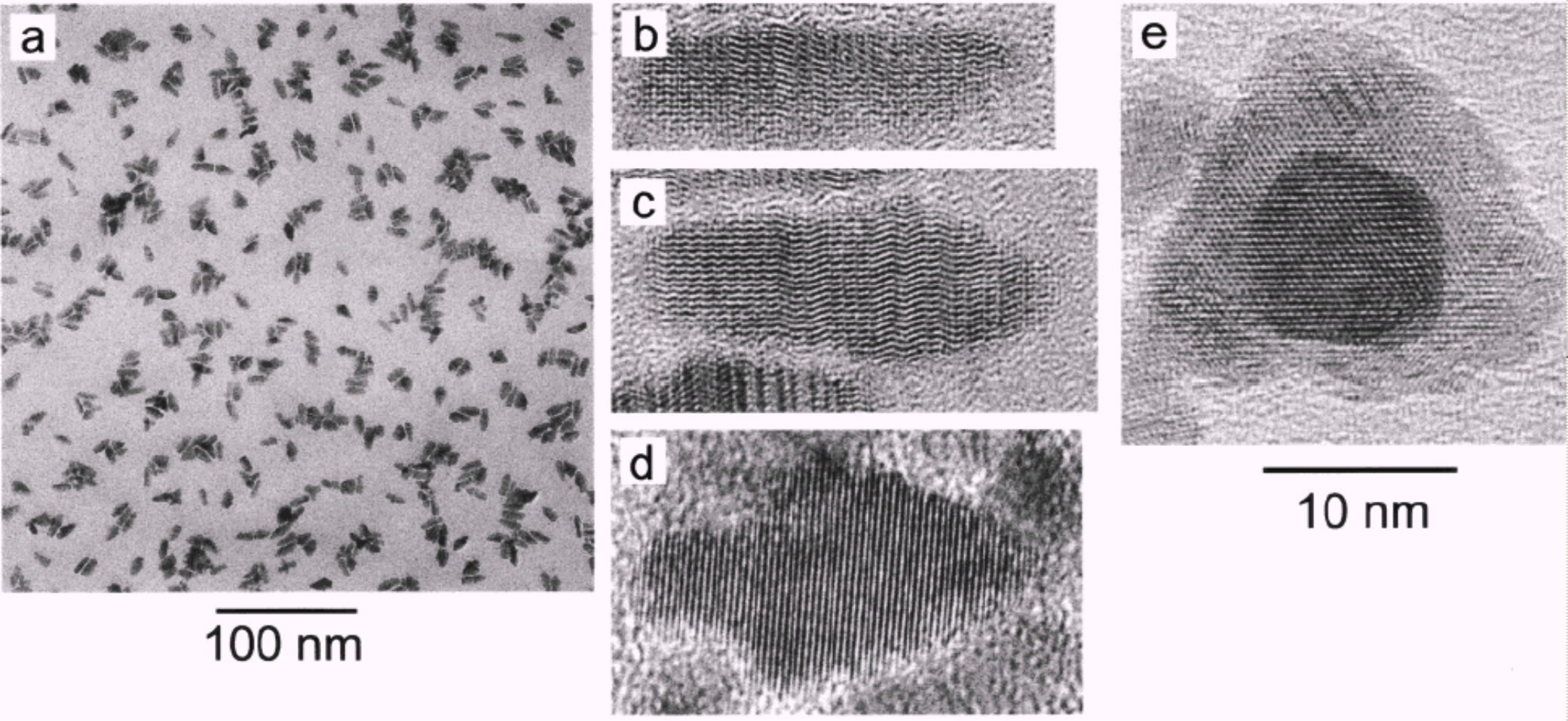

igure 2. TEMs of a typical 60% HPA concentration sample, showing (a) arrow-shaped nanocrystals. HRTEM images show the stages of gro om (b) pencil- to (c) arrow- to (d) pine tree-shaped nanocrystals. (e) A pine tree-shaped nanocrystal is also shown looking down the [0 rection (or long axis). HRTEM characterization shows that each shape of nanocrystal is predominately wurtzite and that the angled facets of rows are the (101) faces.

Extended Nanorods from multiple injection of monomers

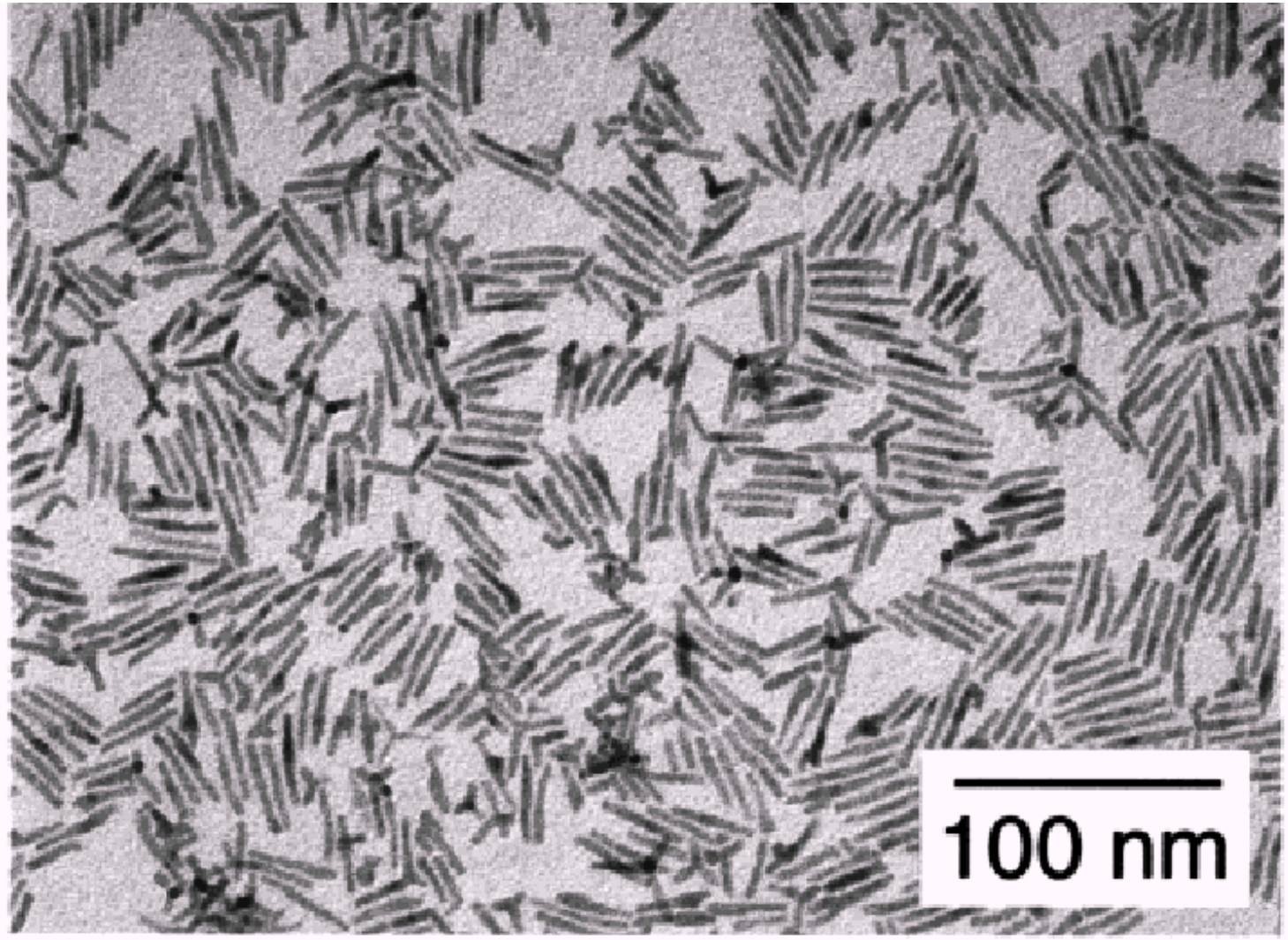

Figure 3. TEM of a typical multiple injection extended rod synthesis. The average length is 34.5 ± 4.4 nm with an aspect ratio of 10:1. The

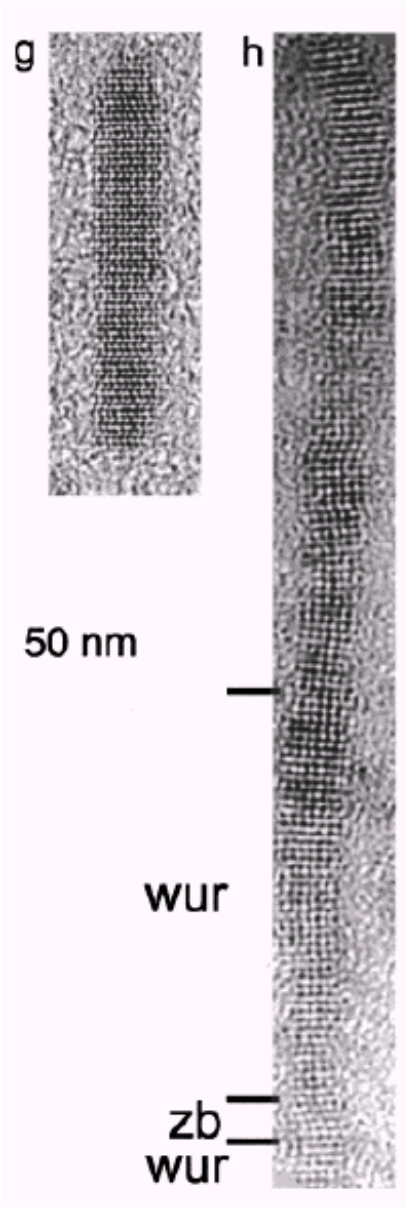

Crystal growth along c-axis of wurtzite structure

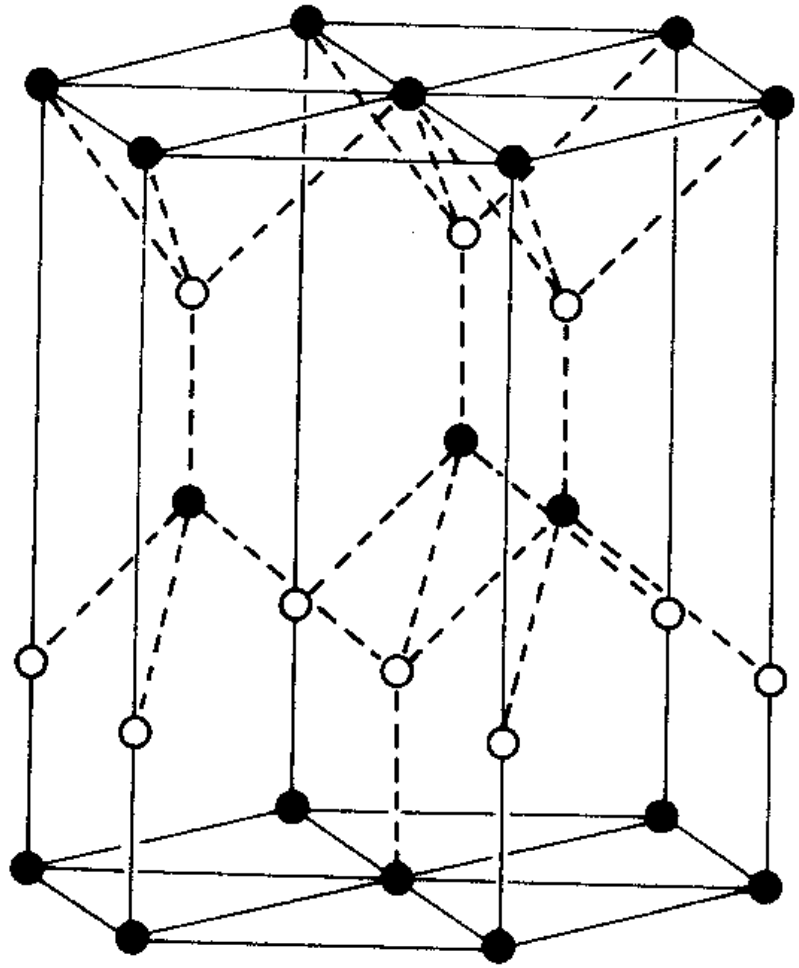

Based on hcp structure

Thermodynamics vs. Kinetics

- At slow growth rate, crystals tend to grow to spheres
- At high growth rate, rods from in unidirectional growth of one face
- Large injection volume or very high monomer concentration favors rod growth→ the difference in growth rates between the unique *c*-axis of the wurtzite crystal and the other axes is accentuated, and rods are obtained.
- HPA increase the growth rate of (001) face of CdSe relative to other faces.

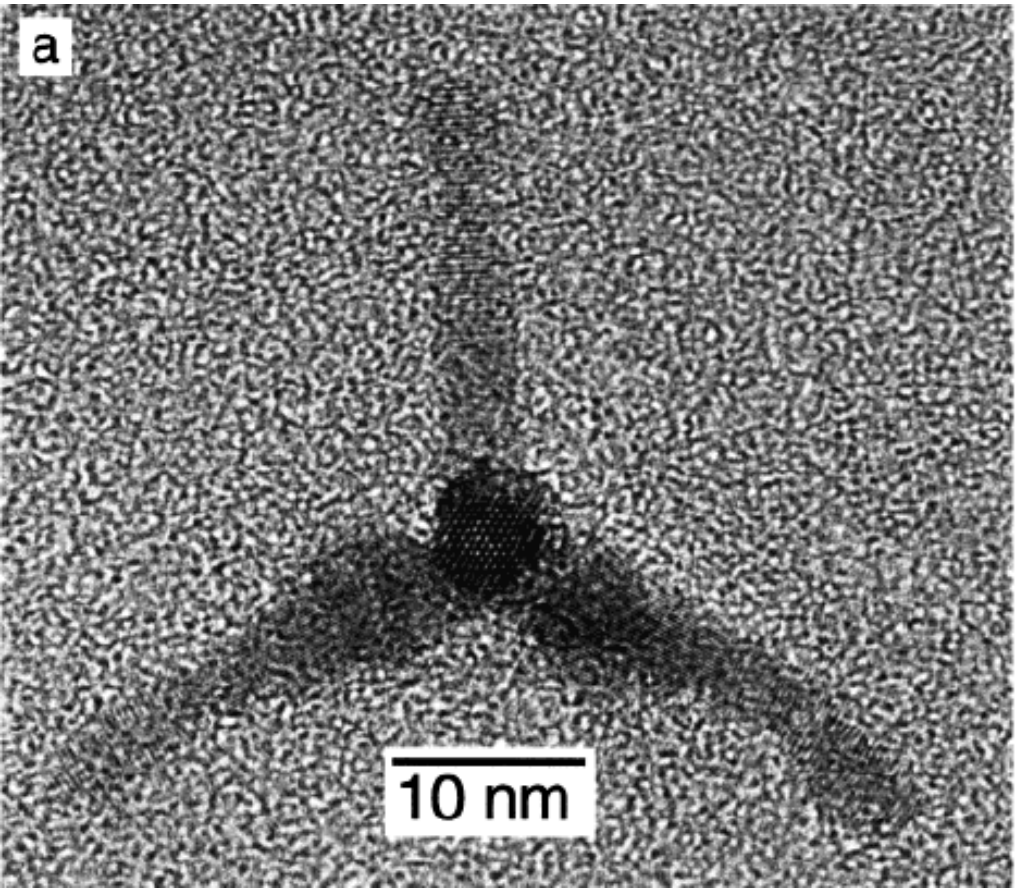

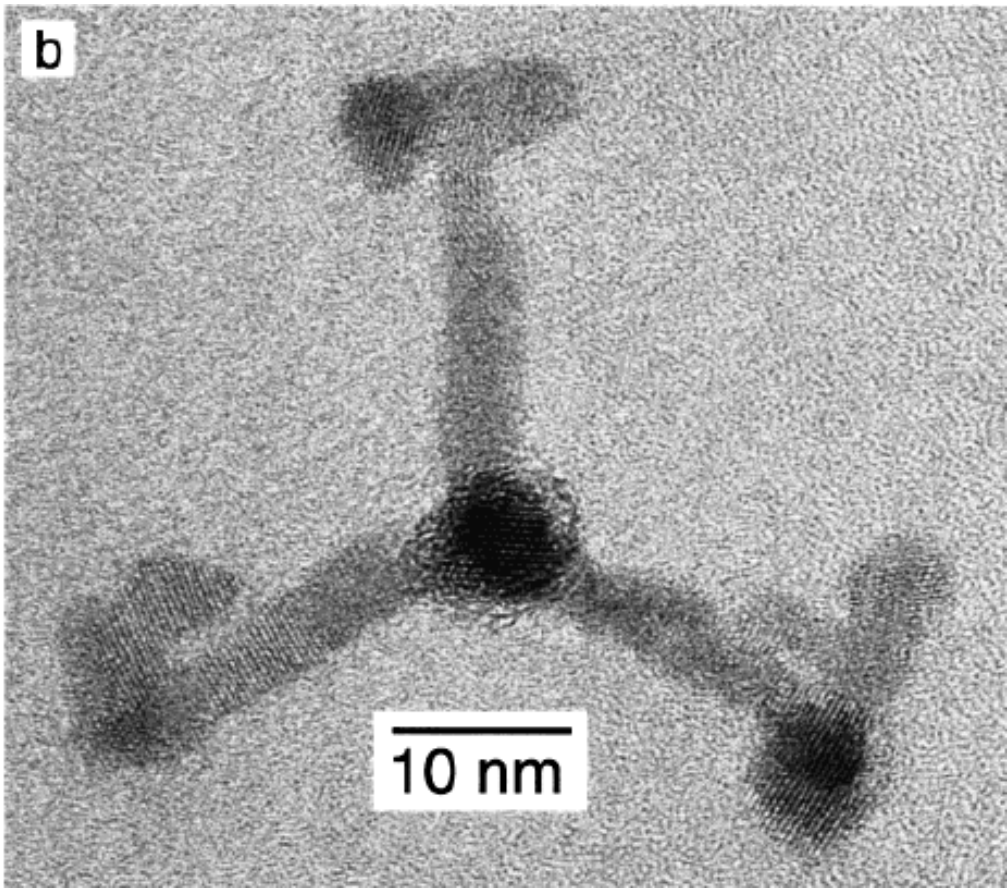

Tetrahedral zinc blende core with four wurtzite arms.

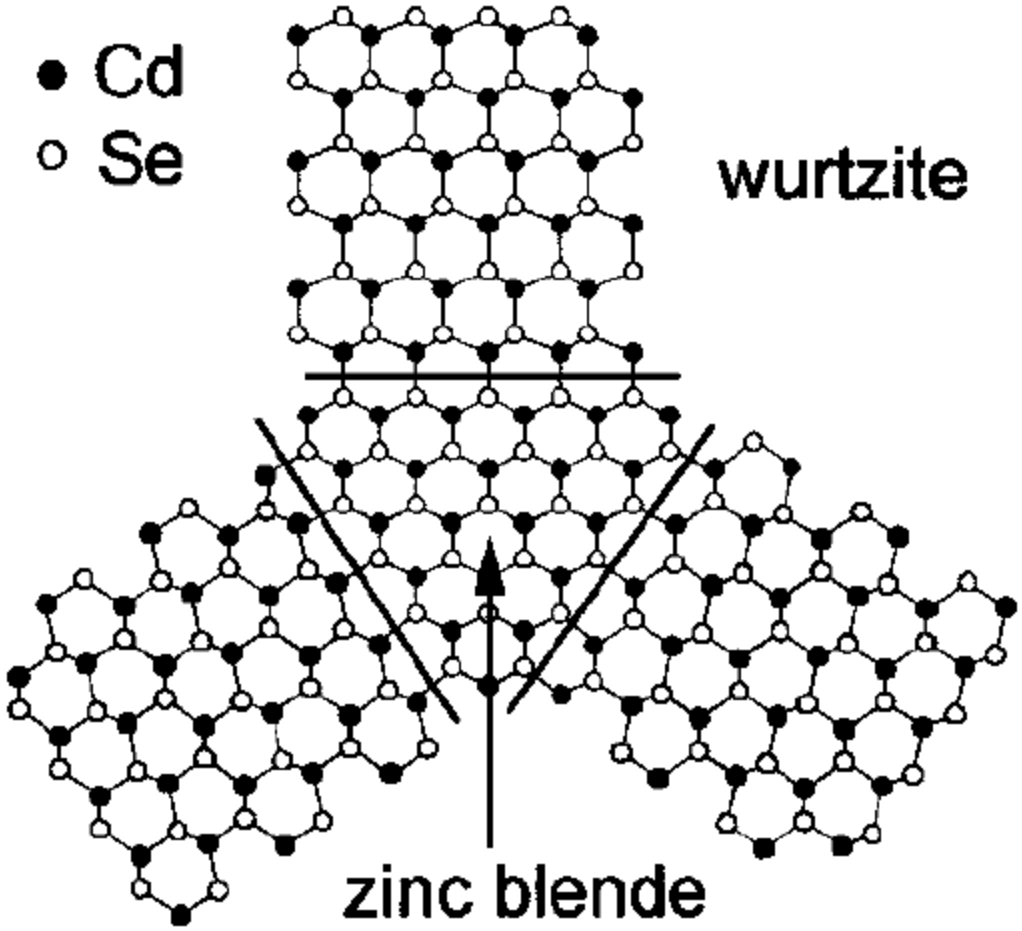

Figure 9. Two-dimensional representation showing the structure of a tetrapod. The nuclei is the zinc blende structure, with wurtzite arms growing out of each of the four (111) equivalent faces. Three are shown,

Applications

of Quantum Nanorods

and Nanowires

Highly ordered nanowire arrays on plastic substrates for ultrasensitive flexible chemical sensors

James R. Heath (CALTECH) *Nature Mater.* **2007**, 6, 384.

- Integrating high-performance semiconductors on flexible plastics

→ Important for chemical and biological sensing

- Semiconducting nanowires (and nanotubes) are particularly sensitive chemical sensors because of their high surface-to-volume ratios.
- The nanowires are excellent field-effect transistors, and, as sensors, exhibit parts-per-billion sensitivity to NO2, a hazardous pollutant.
- We also use SiO2 surface chemistries to construct a 'nano-electronic nose' library, which can distinguish acetone and hexane vapours via distributed responses.
- The excellent sensing performance coupled with bendable plastic

→ portable, wearable & implantable sensors.

Highly Ordered Nanowire Arrays on Plastic Substrates

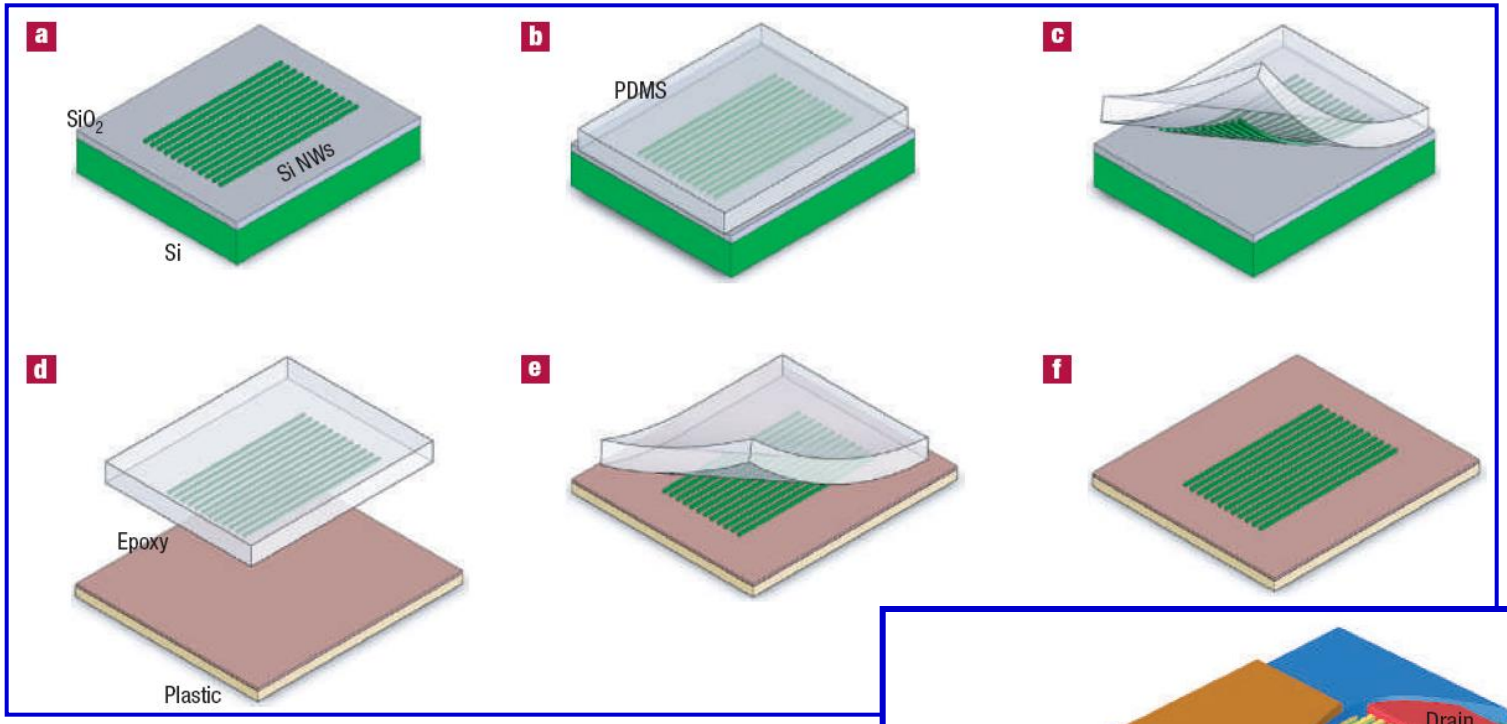

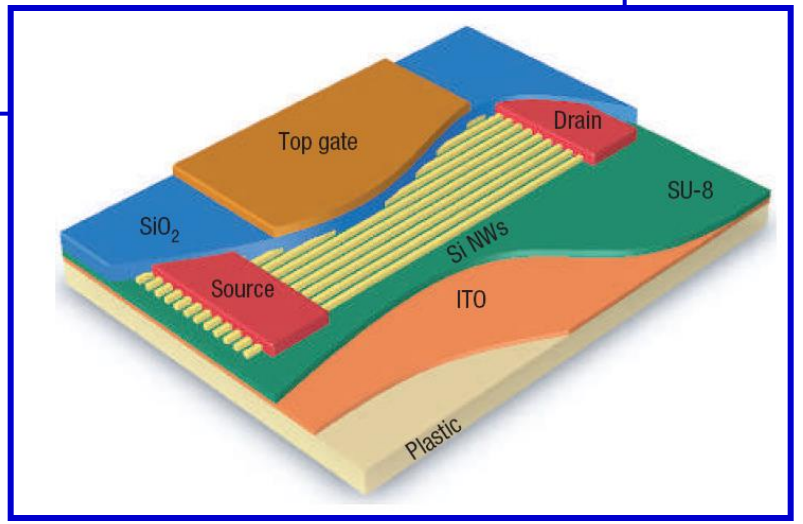

Superlattice nanowire pattern transfer (SNAP) approach

James R. Heath (CALTECH) *Nature Mater.* **2007**, 6, 384.

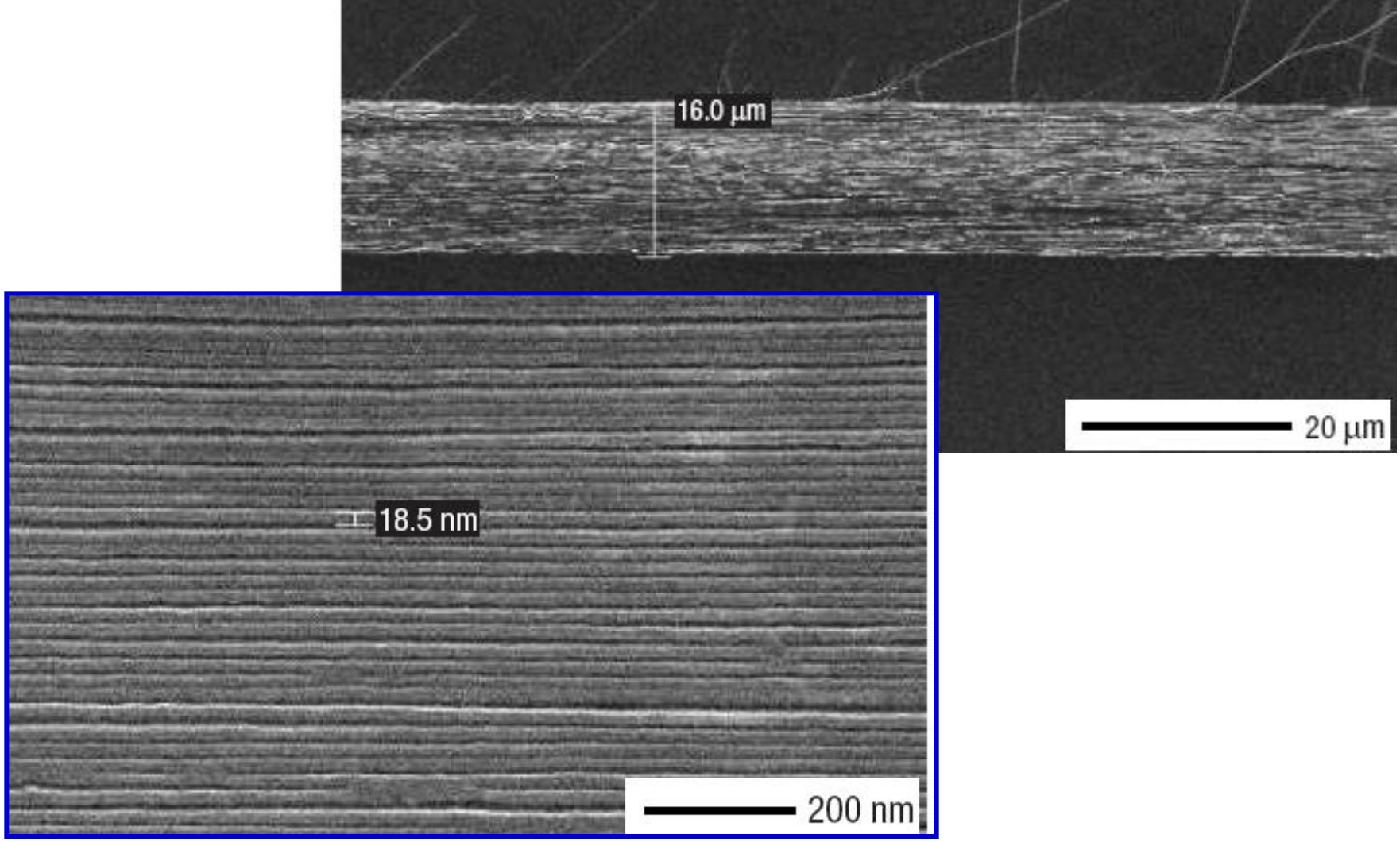

- Si NW of diameters of ~18 nm
- Total width of the NW array is about 16 µm.
- 390–400NWs transferred; average pitch of the NW array is ~ 41 nm

Ultrasensitive detection with nanowire-on-plastic gas sensors

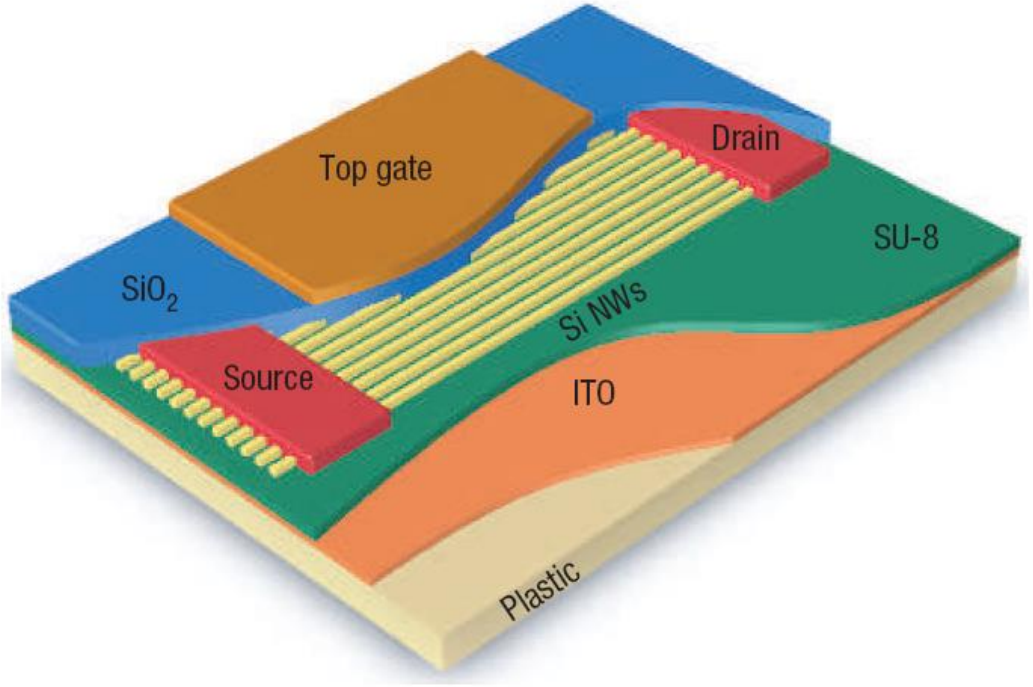

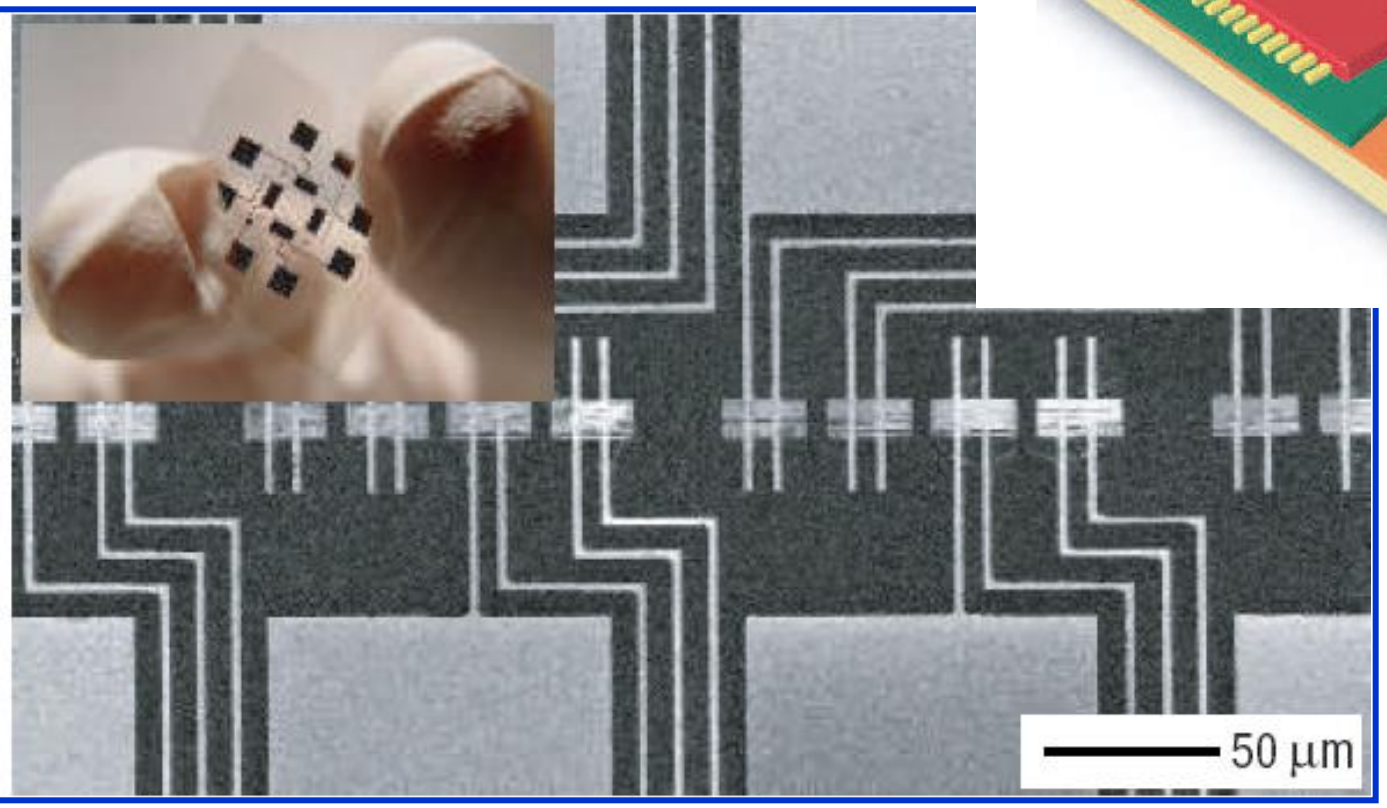

Electrical response of a nanowire sensor

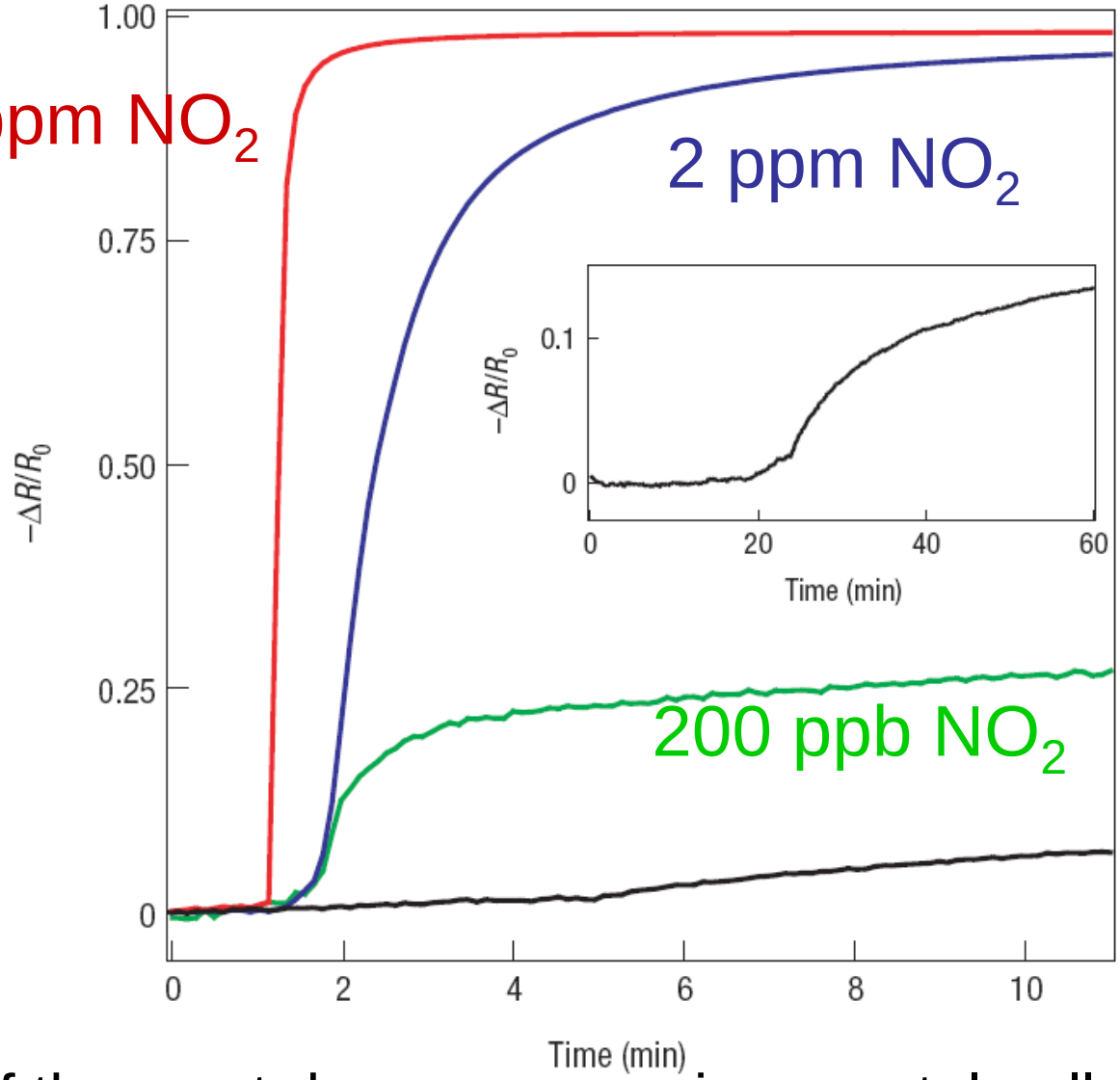

NO_2 is one of the most dangerous environmental pollutants, primarily produced from internal-combustion-engine emissions. National air quality standard of NO_2 exposure of < 53 ppb

Room temperature UV Nanowire Nanolaser

Science **2001**, 292, 1897 by Pedong Yang at UC-Berkeley

1 - 3.5 nm thick Au layer as catalyst

ZnO nanowire arrays with diameter of 20 ~ 150 nm

And length up to 10 micrometers

385 nm lasing with < 0.3 nm linewidth

Synthesis details: *Adv Mater* **2001**, 13, 113.

1 - 3.5 nm thick Au layer as catalyst ZnO nanowire arrays with diameter of 20 ~ 150 nm, length up to 10 μm

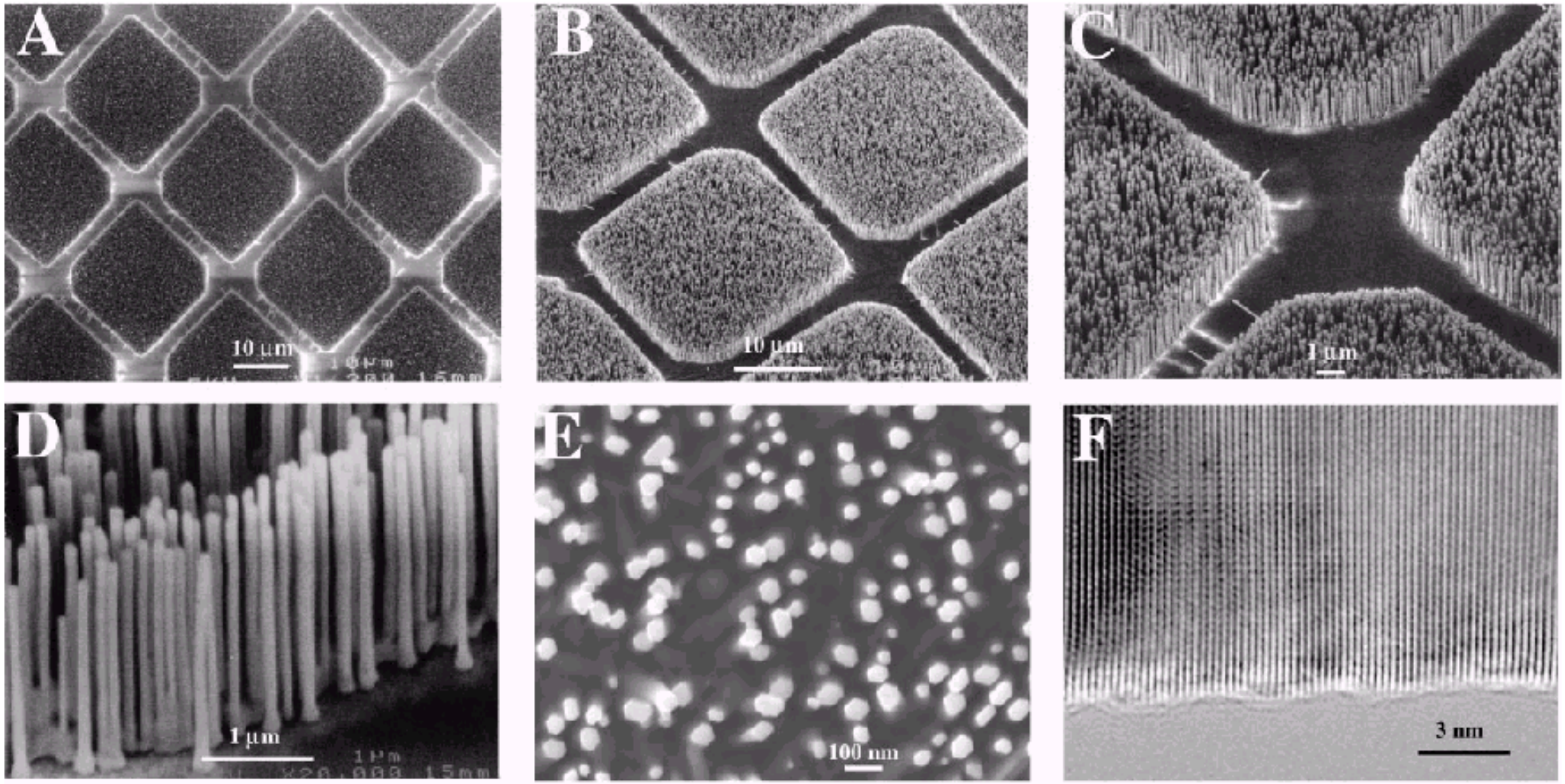

Fig. 1. (**A** through **E**) SEM images of ZnO nanowire arrays grown on sapphire substrates. A top view of the well-faceted hexagonal nanowire tips is shown in (E). (**F**) High-resolution TEM image of an individual ZnO nanowire showing its <0001> growth direction. For the nanowire growth, clean (110) sapphire substrates were coated with a 10 to 35 Å thick layer of Au, with or without using TEM grids as shadow masks (micro contact printing of thiols on Au followed by selective etching has also been used to create the Au pattern). An equal amount of ZnO powder and graphite powder were ground and transferred to an alumina boat. The Au-coated sapphire substrates were typically placed 0.5 to 2.5 cm from the center of the boat. The starting materials and the substrates were then heated up to 880° to 905°C in an Ar flow. Zn vapor is generated by carbothermal reduction of ZnO and transported to the substrates where ZnO nanowires grow. The growth generally took place within 2 to 10 min (*15*).

385 nm lasing with < 0.3 nm linewidth

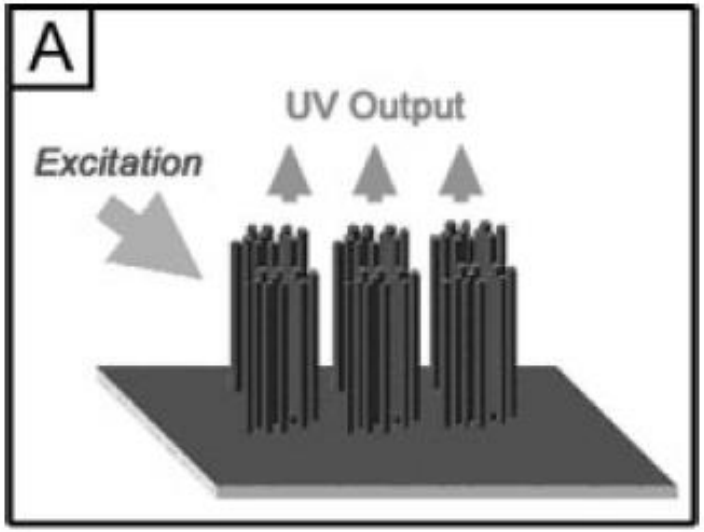

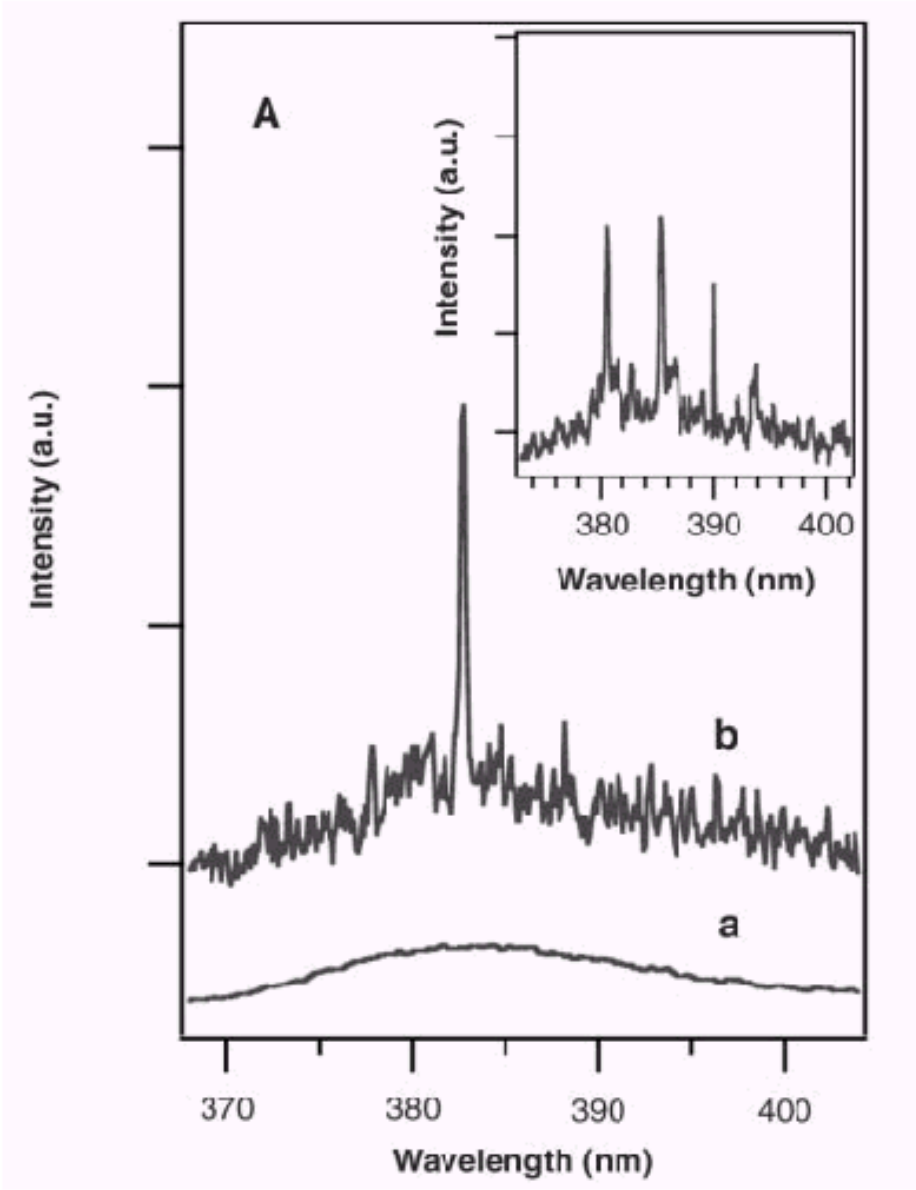

Applications

of Semiconductor Nanowires

To Biosensing

Nanowire –Based Nanoelectronic Devices in the Life Sciences, Fernando Patolsky, Brian P. Timko, G. Zheng, and Charles M. Lieber, MRS Bulletin, 2007, 32, 142.

• Interface between nanosystems and biosystems: bringing together biology, chemistry, physics, biotechnology, medicine, and many areas of engineering.

• Combination of these diverse areas of research promises to yield revolutionary advances in healthcare, medicine, and the life sciences.

• Creation of new and powerful tools that enable direct, sensitive, and rapid analysis of biological and chemical species.

• Devices based on nanowires have emerged as one of the most powerful and general platforms for ultrasensitive, direct electrical detection of biological and chemical species.

• Nanowire nanosensors for ultrasensitive detection of proteins and individual virus particles as well as recording, stimulation, and Inhibition of neuronal signals in nanowire–neuron hybrid structures.

Nanowire Field - Effect Sensors

- Underlying detection using semiconductor nanowires is their configuration as field-effect transistors (FETs), which exhibit a conductivity change in response to variations in the electric field or potential at the surface of the device.
- In a standard FET, the conductance of the semiconductor between the source and drain is modulated between on and off states by a third gate electrode capacitively coupled through a thin dielectric layer to the semiconductor.
- Binding of a protein with net negative charge to the surface of a p - type FET will lead to an accumulation of positive hole carriers and an increase in device conductance.
- Binding event will lead to a much greater change in device conductance for the nanowire versus a planar FET.

Nanowire Field - Effect Sensors

- Nanowire-based sensing devices can be configured from high-performance FETs by linking specific receptor groups to the surface of the nanowire.
- Specific binding to the receptor will lead to an increase or decrease in the device conductance depending on the net charge of the biomolecule and the semiconductor type
- Real time monitoring possible

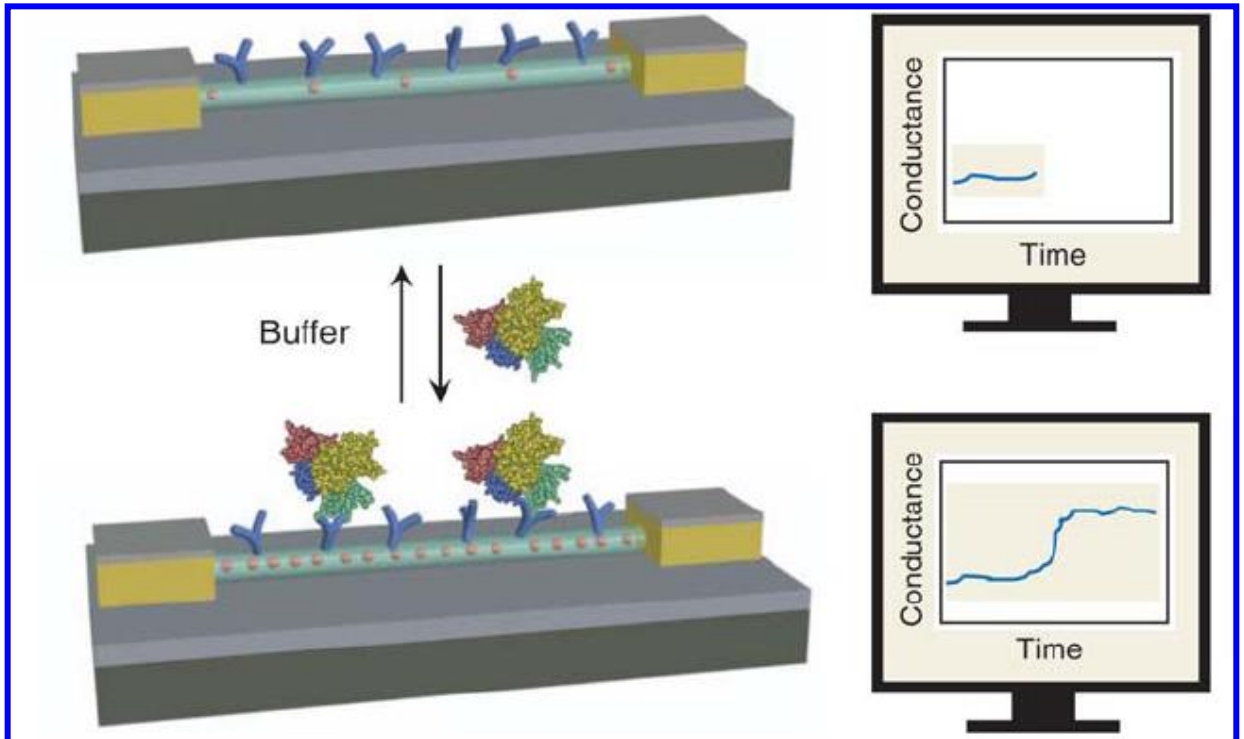

Multiplexed electrical detection of cancer markers with nanowire sensor arrays

Charles M Lieber, *Nat. Biotechnol.* **23** (2005) 1294.

- Highly sensitive, label-free, multiplexed electrical detection of cancer markers using silicon-nanowire field-effect devices.
- Nanowires and surface receptors are incorporated into arrays.
- Protein markers were routinely detected at femtomolar concentrations with high selectivity, and simultaneous incorporation of control nanowires enabled discrimination against false positives.
- Nanowire arrays allowed highly selective & sensitive multiplexed detection of prostate specific antigen (PSA), PSA-*a*1-antichymotrypsin, carcinoembryonic antigen & mucin-1, including detection to at least 0.9 pg/ml in undiluted serum samples.

- Nucleic acid receptors enabled real-time assays of the binding, activity and small-molecule inhibition of telomerase using unamplified extracts from as few as ten tumor cells.
- The capability for multiplexed real-time monitoring of protein markers and telomerase activity with high sensitivity and selectivity in clinically relevant samples opens up substantial possibilities for diagnosis and treatment of cancer and other complex diseases.

Nanowires suspended in ethanol are deposited onto a substrate wafer.
Photolithography followed by metallization defines contacts to the nanowires.

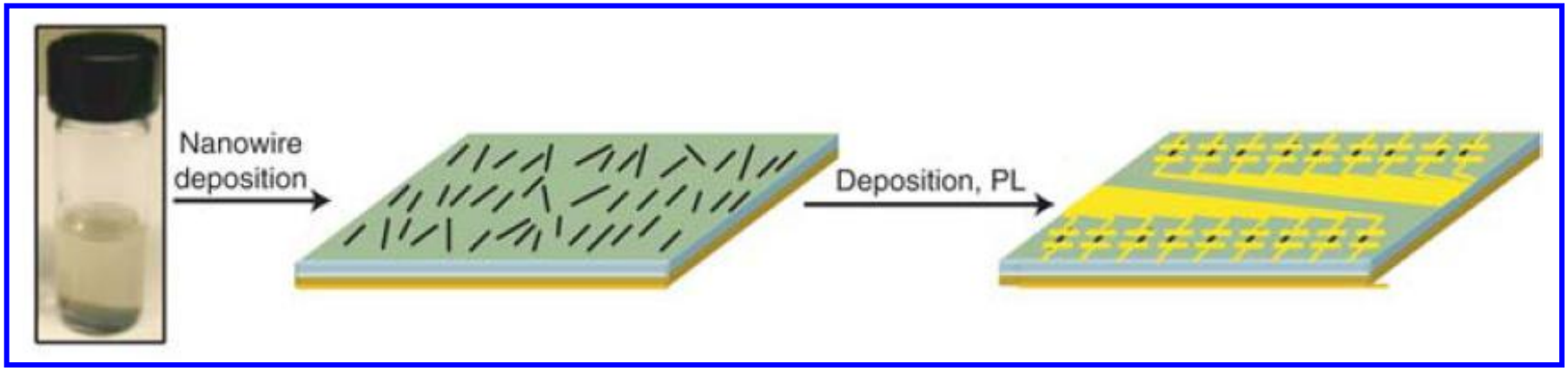

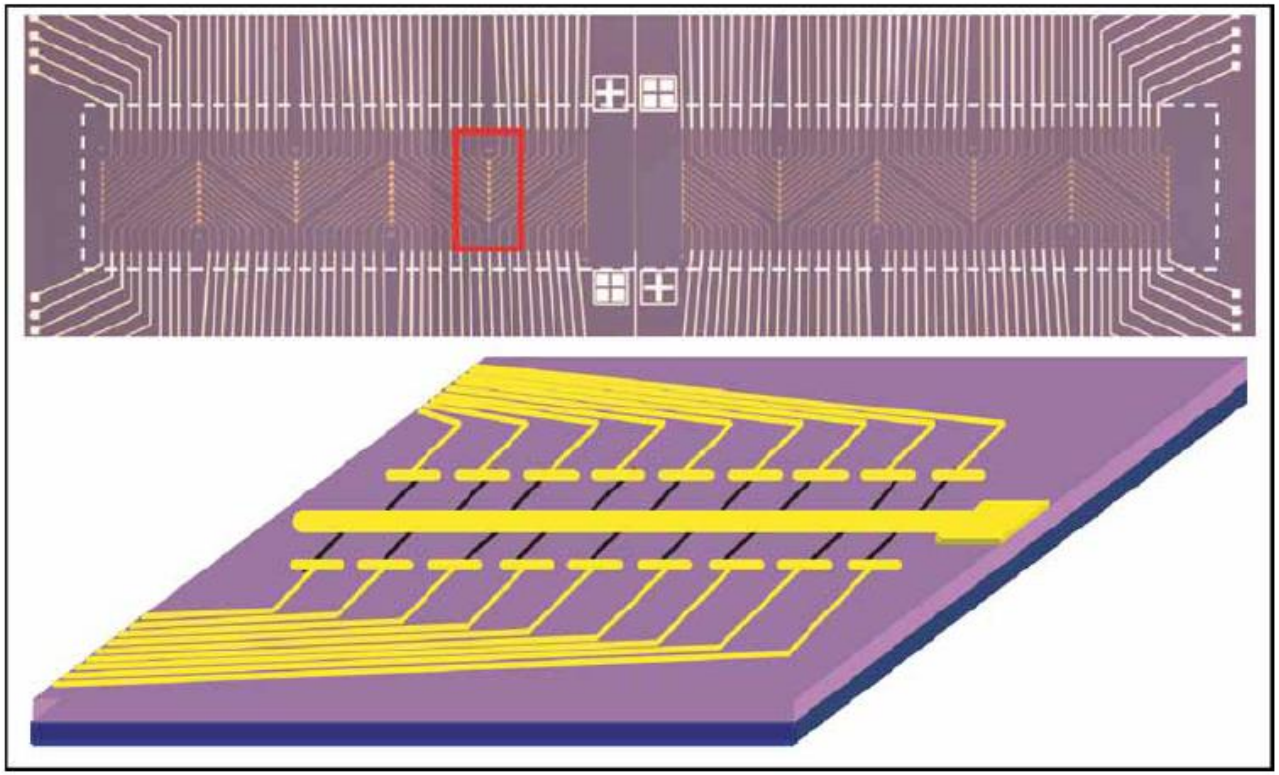

Two nanowire devices modified with different antibody receptors.

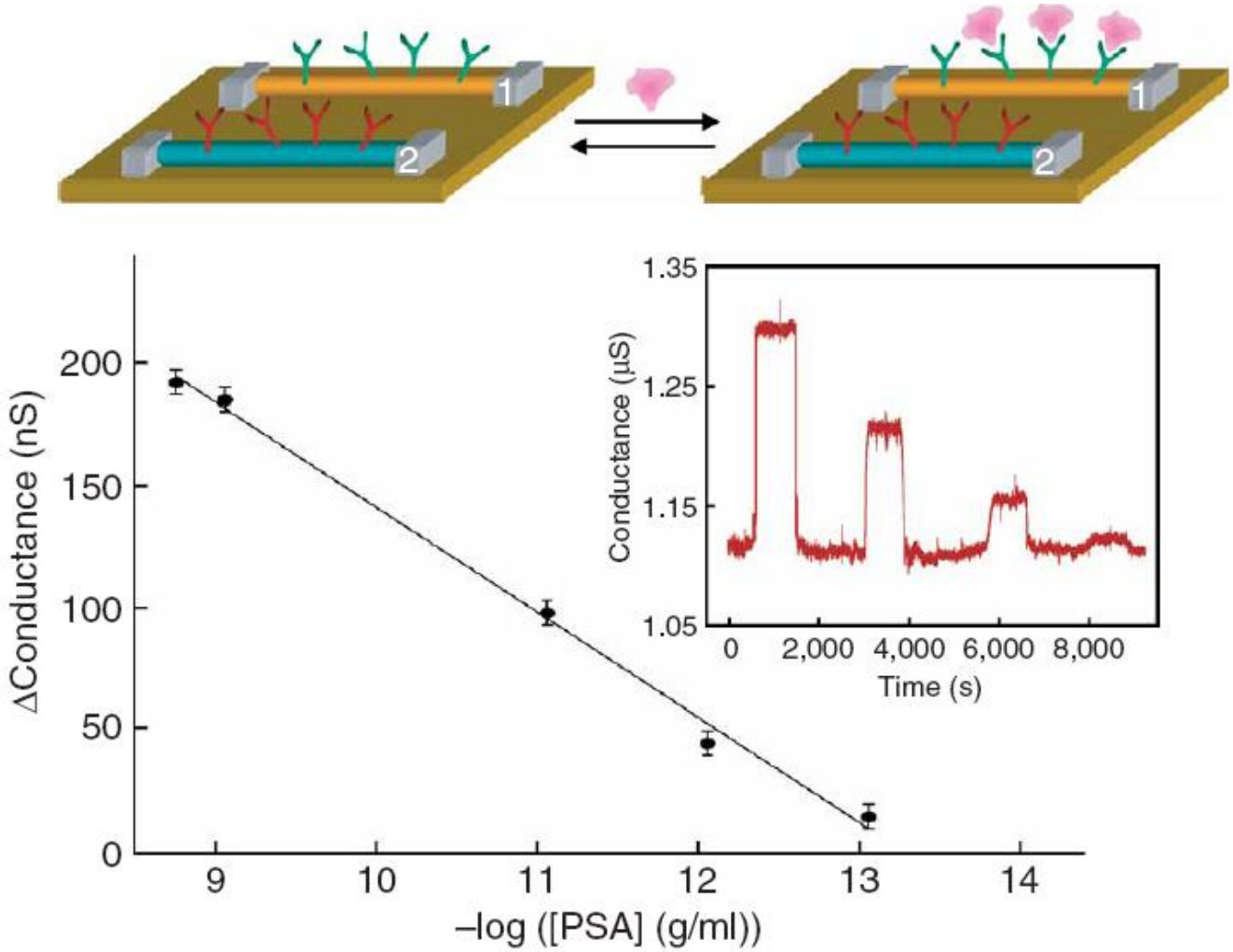

- Change in conductance versus concentration of PSA for a p-type silicon nanowire modified with PSA-Ab1 receptor.
- Inset: Conductance-versus-time data recorded after alternate delivery of PSA and pure buffer solutions;

Multiplexed detection with nanowire arrays

(a) Complementary sensing of PSA using p-type (NW1) and n-type (NW2) silicon-nanowire devices in the same array.
(b) Conductance-versus-time data recorded simultaneously from two p-type silicon-nanowire devices in an array, where NW1 was functionalized with PSA Ab1, & NW2 with ethanolamine.

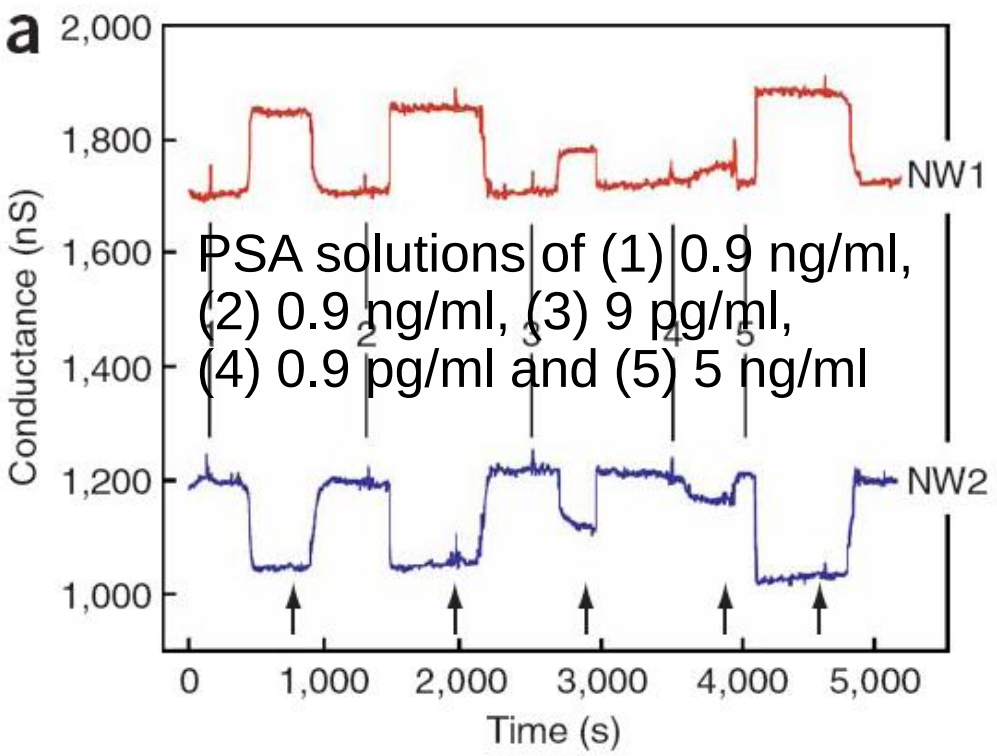

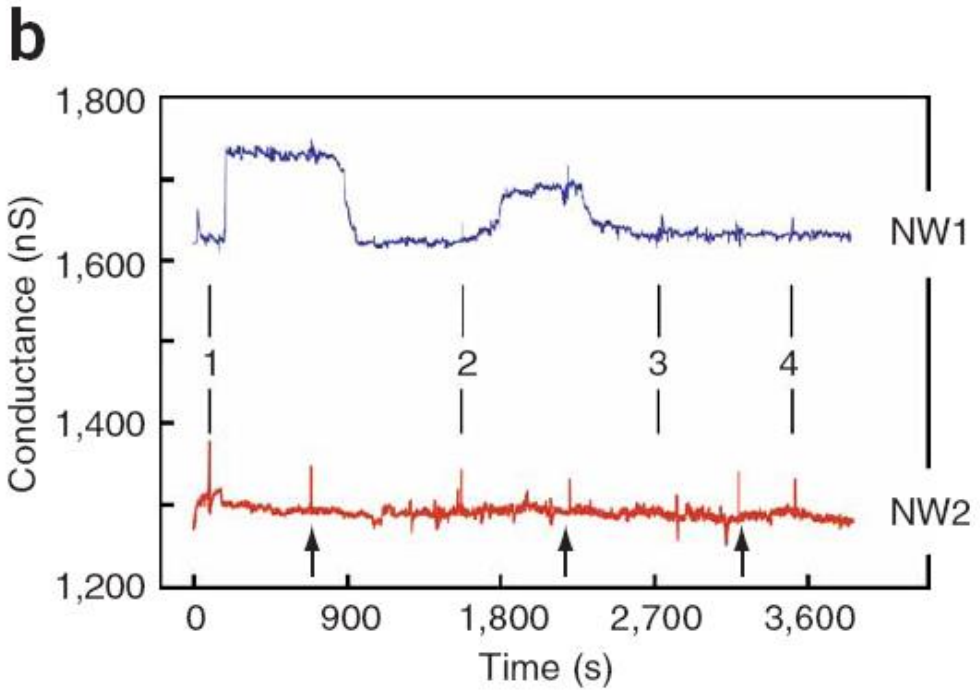

Multiplexed detection of cancer marker proteins

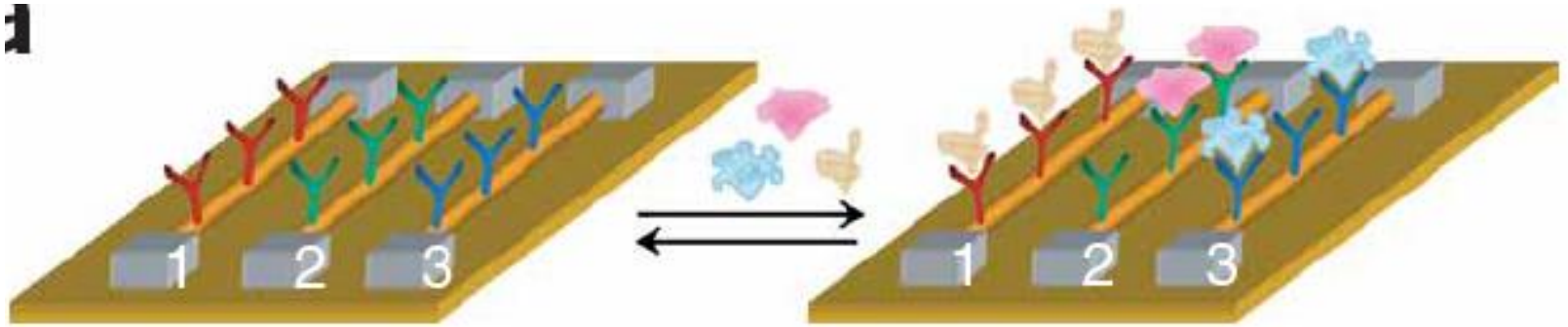

Devices 1, 2 and 3 are fabricated from p-type Si nanowires, and then differentiated with distinct mAb receptors specific to three different cancer markers: PSA, CEA and mucin-1.

Conductance versus-time data recorded for the simultaneous detection of PSA, CEA and mucin-1 on p-type silicon-nanowire array in which NW1, NW2 and NW3 were functionalized with mAbs for PSA, CEA and mucin-1, respectively.

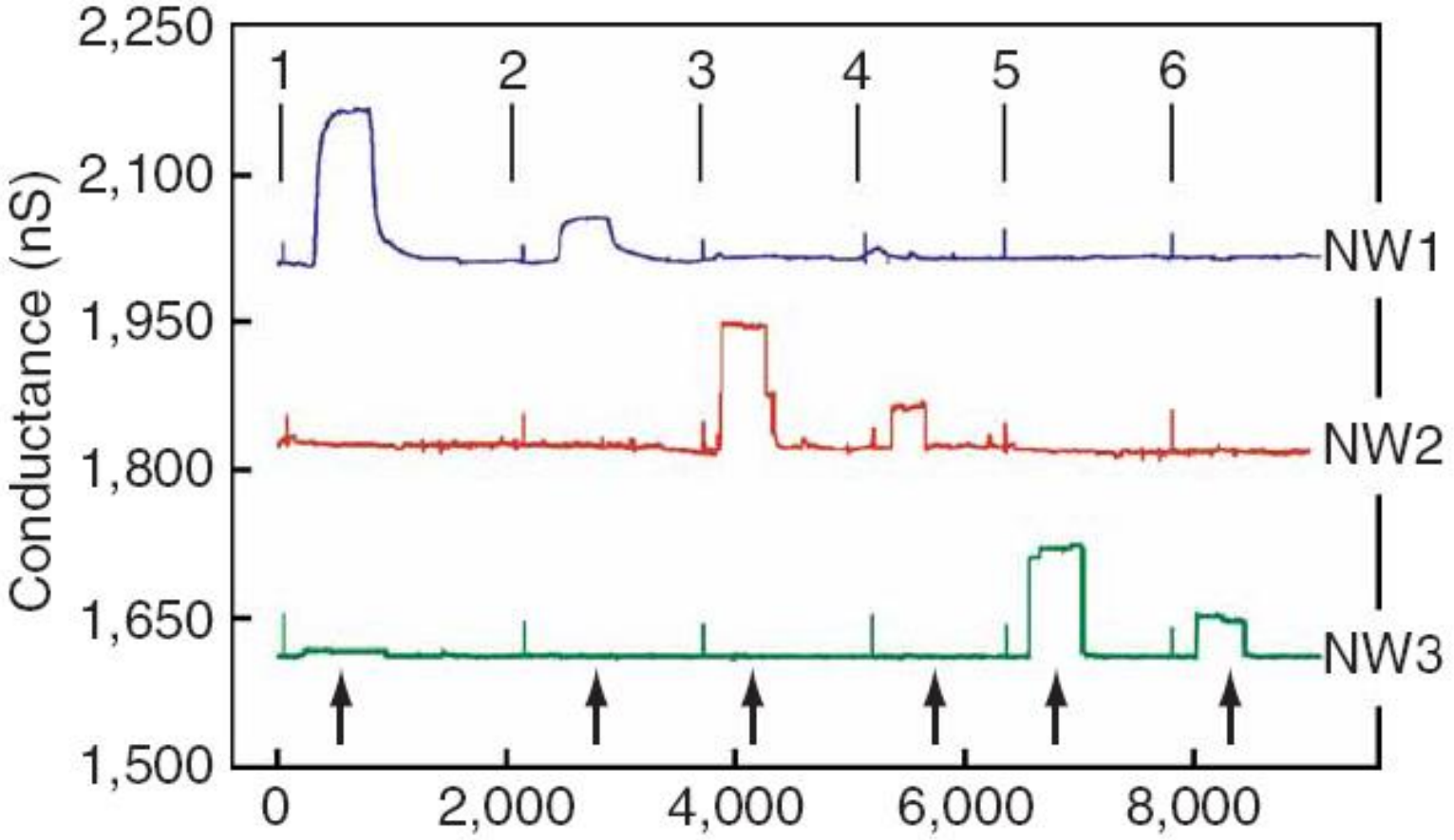

(1) 0.9 ng/ml PSA, (2) 1.4 pg/ml PSA, (3) 0.2 ng/ml CEA, (4) 2 pg/ml CEA, (5) 0.5 ng/ml mucin-1, (6) 5 pg/ml mucin-1.

Nanowire-Cell Interface

(a) penetrate cell membranes while leaving the cellular structures and functions intact.
(b) high surface to volume ratio ensures proper cell−nanowire interaction for chemical/bio/electrical Sensing and payload delivery.

Nanowire FET Based Neuron Physiology

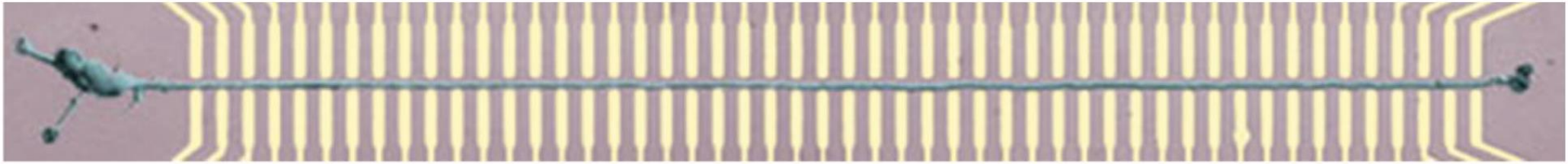

Optical image of a neuron (green) with an axon crossing an array of 50 nanowire FET devices (yellow) with 10 μm pitch. Signal propagation along the axon can be monitored in real time..

C. M. Lieber, *Science* **2006**, *313*, 1100.

Vertical Nanowire Arrays for Cell Culture&Payload Delivery

c) SEM of a mouse embryonic stem cell growing on vertical silicon nanowires. d) SEM image of a vertical nanowire electrode array (VNEA) pad constituent of nine Si nanowires (blue) with metal coated tips (white) (left; scale bar, 1 μm), and a rat cortical cell (yellow) on a VNEA pad (blue-scale bar,2.5μm), showing nanowires interfacing with the cellular membrane (inset; scale bar, 2.5 μm). Intracellularly record and stimulate neuronal activity in rat cortical neurons and can map multiple individual synaptic connections.

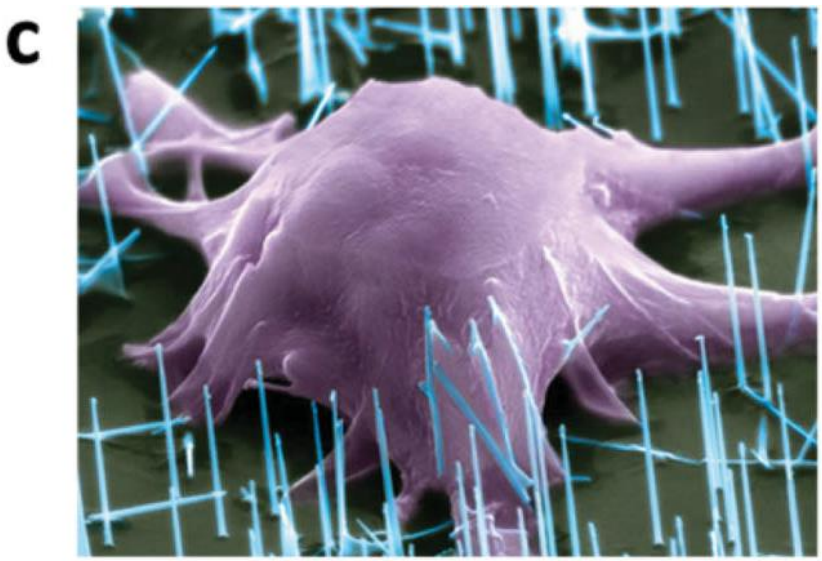

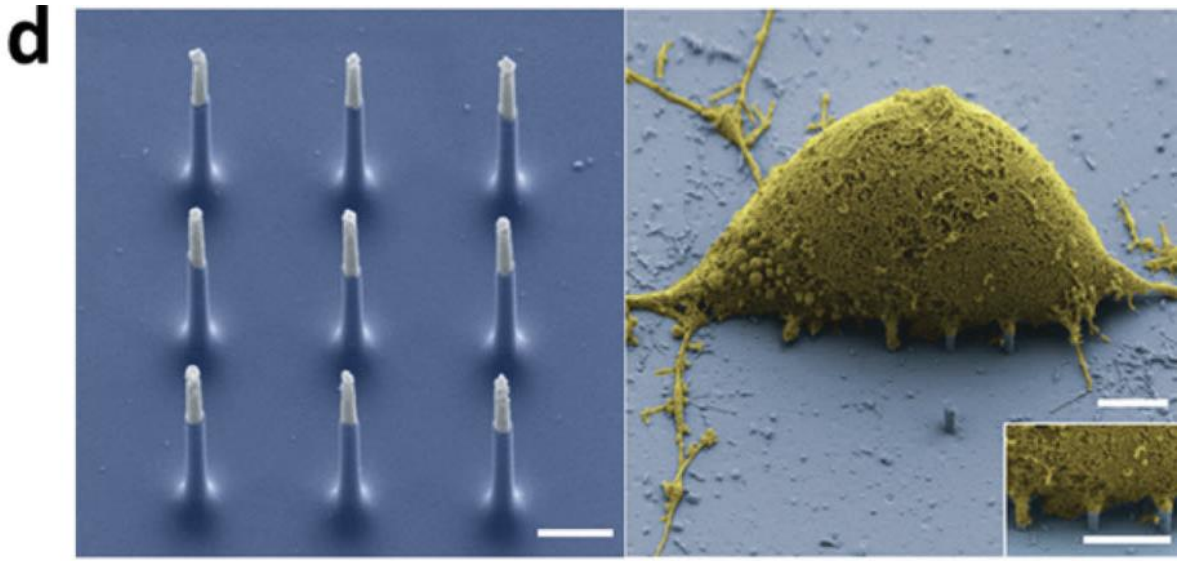

c) P. D. Yang , *J. Am. Chem. Soc.* **2007** , *129* , 7228; d) H. Park , *Nat. Nanotechnol.* **2012** , *7* , 180

Nanowire-Based Single Cell Endoscopy

Schematics of nanowire endoscope for highly localized subcellular illumination (left) and microscope images showing the dark field (second left) of a living Hela Cell and QD fluorescence images comparing focused laser (second right) and endoscope (right) excitations of two adjacent quantum dot clusters in the cell. The endoscope can selectively excite one of the clusters, showing the capability of high-resolution imaging.

Can guide visible light into intracellular compartments of a living mammalian cell, and can also detect optical signals from subcellular regions with high spatial resolution. Furthermore, we show that through light-activated mechanisms the endoscope can deliver payloads into cells with spatial and temporal specificity.

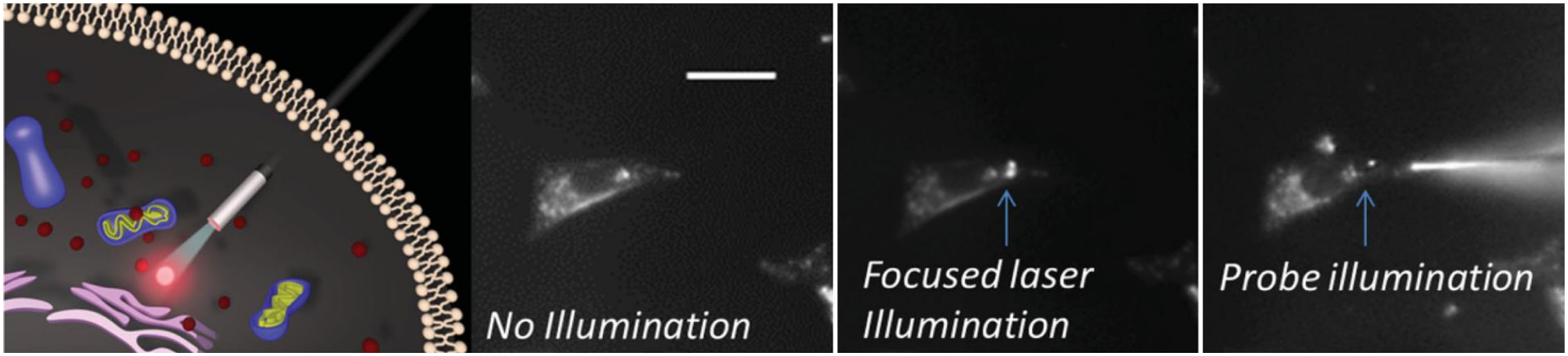

P. D. Yang , *Nat. Nanotechnol.* **2012** , *7* , 191

Colloidal Synthesis of Quantum-sized Two-Dimensional Semiconductor Nanocrystals

Jae Sung Son, Jung Ho Yu, Soon Gu Kwon, Jihwa Lee, Jin Joo,* and Taeghwan Hyeon,* “Colloidal Synthesis of Ultrathin Two-dimensional Semiconductor Nanocrystals,” *Adv. Mater*. **2011**, 23, 3214-3219.

Jiwoong Yang, Jae Sung Son, Jung Ho Yu, Jin Joo,* and Taeghwan Hyeon,* “Advances in the Colloidal Synthesis of Two-Dimensional Semiconductor Nanoribbons,” *Chem. Mater.* **2013**, *25*, 1190-1198.

Shape dependent properties of Semiconductor NCs

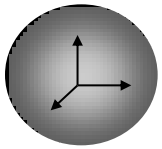

0-D structure (Dot)
3-D confinement

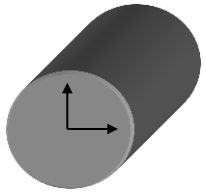

1-D structure (Wire or Rod)
2-D confinement

2-D structure (Ribbon)
1-D confinement

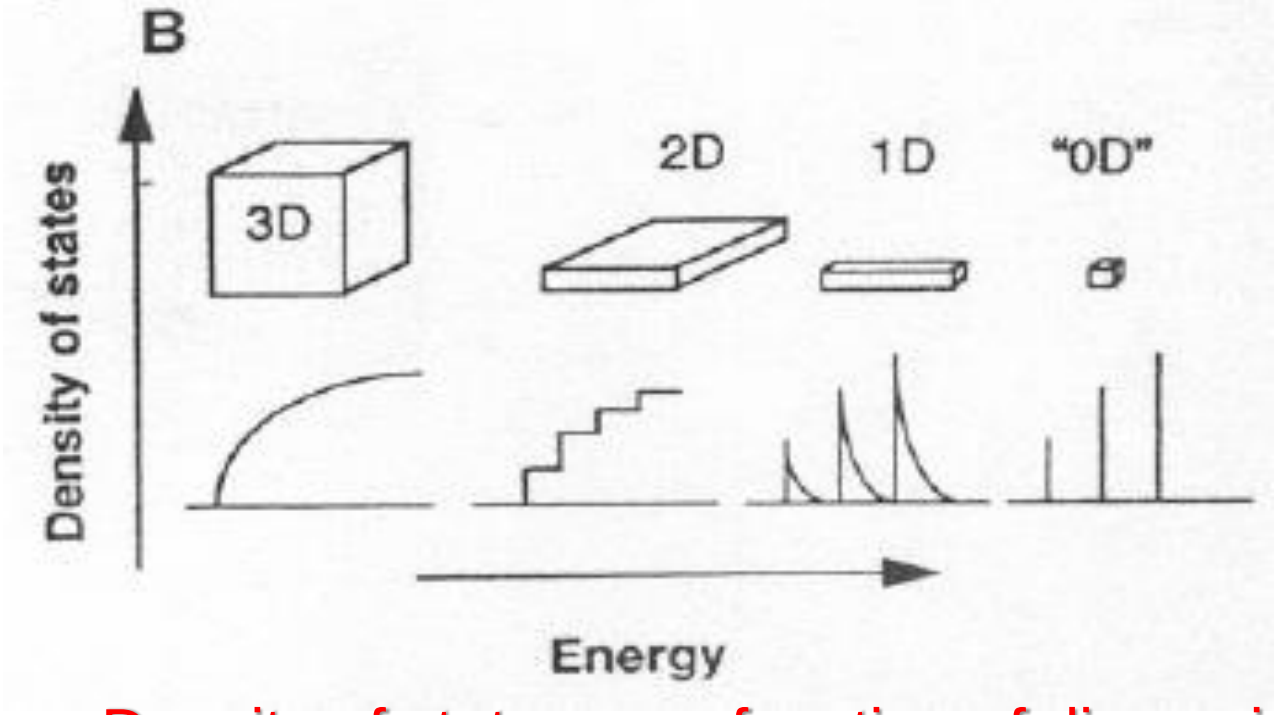

Density of states as a function of dimension

A. P. Alivisatos, Science, **1996**, *271*, 933.

Synthesis of Monodisperse Spherical CdSe Nanocrystals

MIT

5.1 nm CdSe

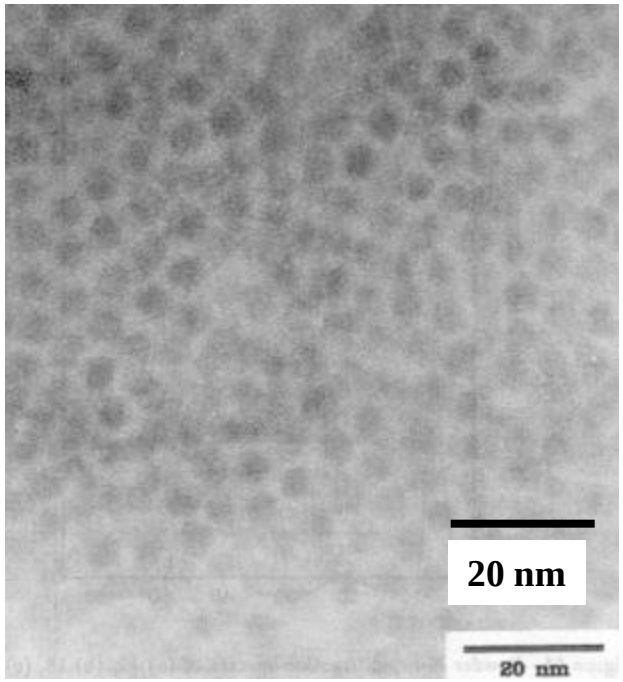

Murray, Norris and Bawendi,
J. Am. Chem. Soc. **1993**, 115, 8706

UC-Berkeley

8.5 nm CdSe

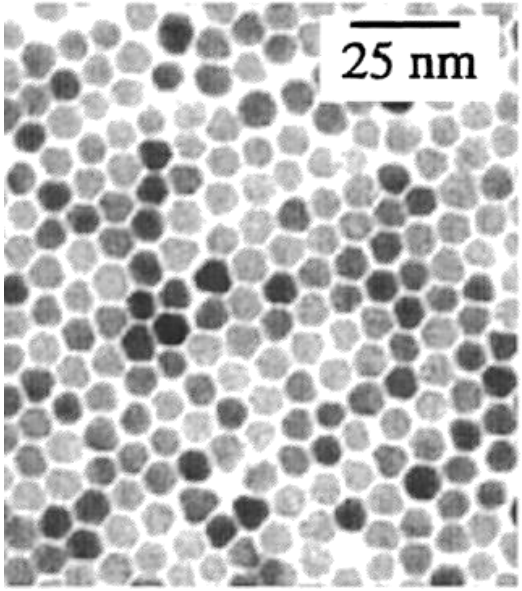

Peng and Alivisatos,
J. Am. Chem. Soc. **1998**, 120, 5343

Synthesis of 1-D CdSe Nanorods

Facile dimension control of nanocrystals in strong quantum confined regime.

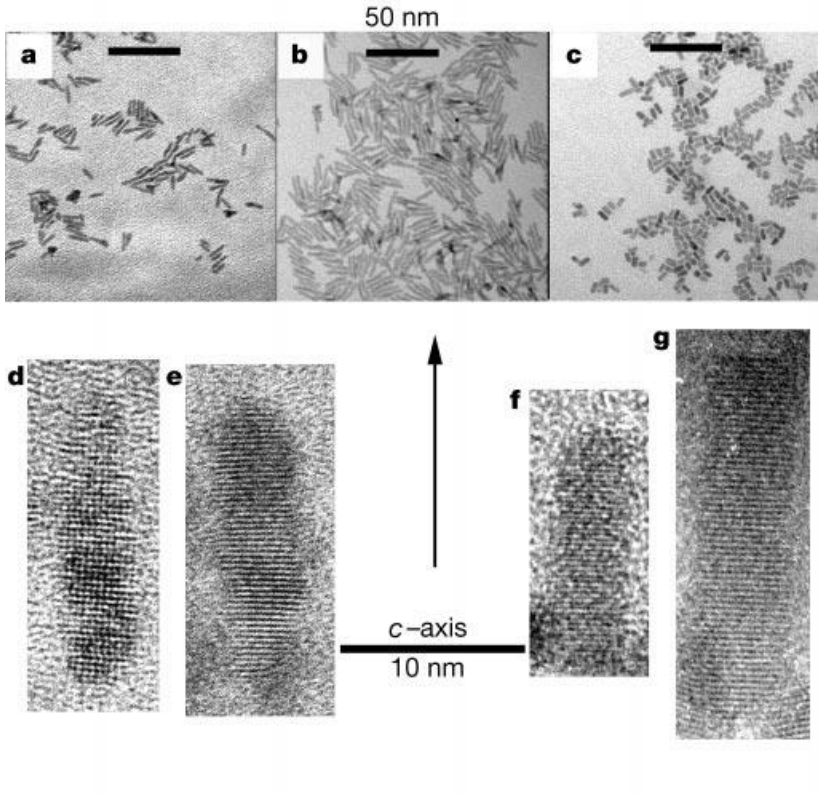

X. Peng *et al*., *Nature* **2000**, *404*, 59.

Fe nanorods from oriented attachment of Nanospheres

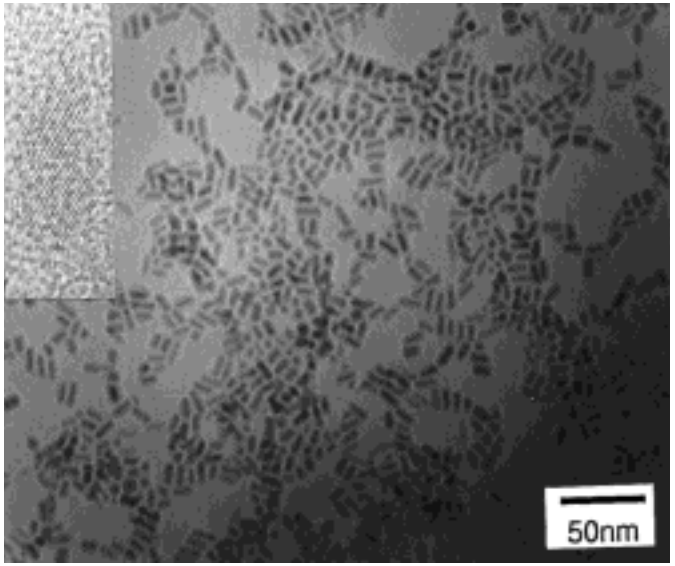

S.-J. Park, ----, T. Hyeon,
J. Am. Chem. Soc. **2000**, 122, 8581

Chemical synthesis of 2-D quantum well is more challenging!

2-Dimensional Semiconductor Quantum Well

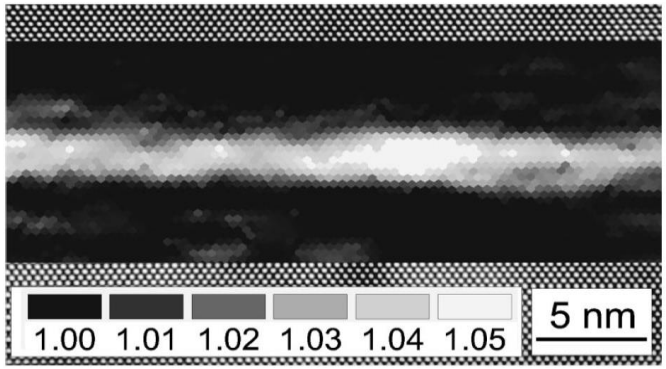

W. Langbein, *et al. Phys. Rev. B*, **1999**, *16*, 8773.

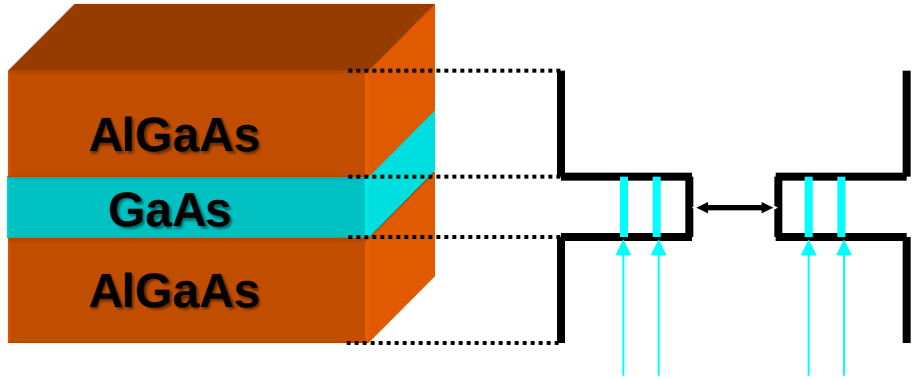

Quantized energy level

Various applications

Laser diode

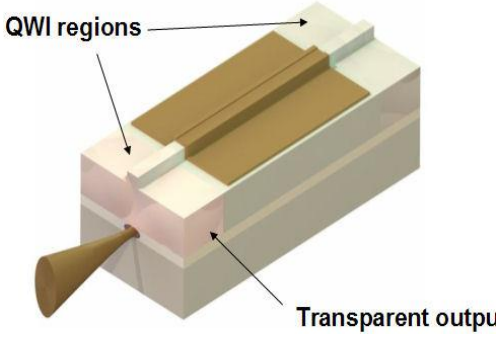

HEMT

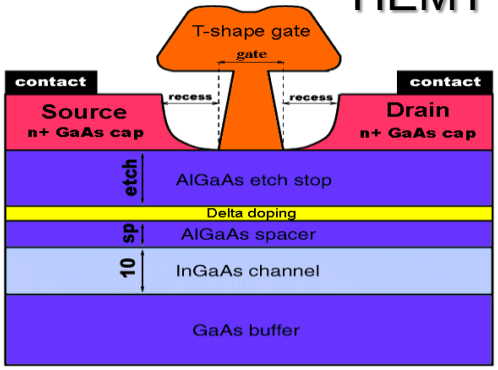

IR Photodetector

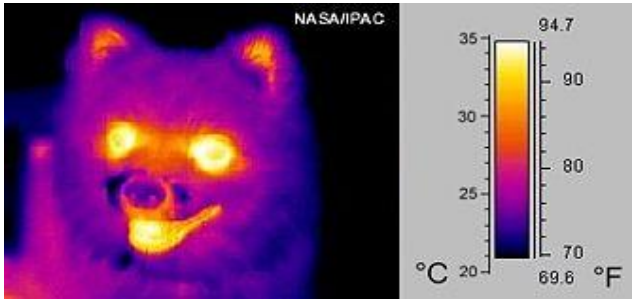

High-quality quantum well is very important for Various Applications

One of the biggest challenges in shape-controlled synthesis is fabrication of free-standing Colloidal Quantum-sized 2-dimensional nanosheets!!!

Ultrathin 1.4 nm thick CdSe nanoribbons

Exhibiting Ultranarrow photoluminescence

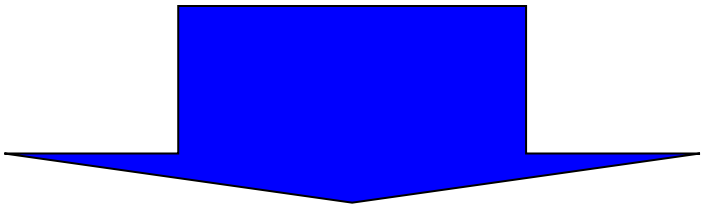

The First Free-standing

Colloidal Quantum Well Nanostructures

J. Joo, ----, T. Hyeon, *J. Am. Chem. Soc.* **2006**, 128, 5632.

Very challenging to synthesize 2-D CdSe Nanosheets Because very tiny surface energy difference between planes

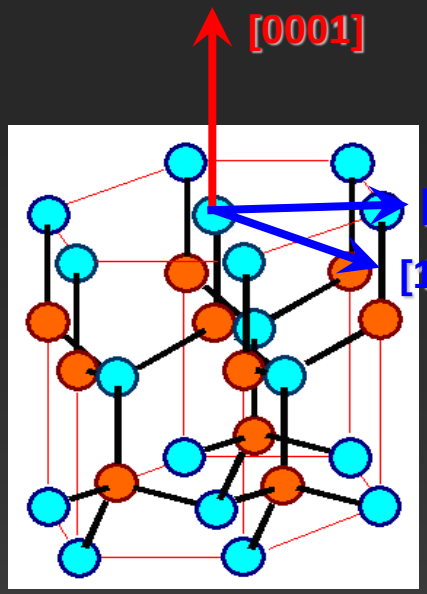

Hexagonal Wurtzite structure

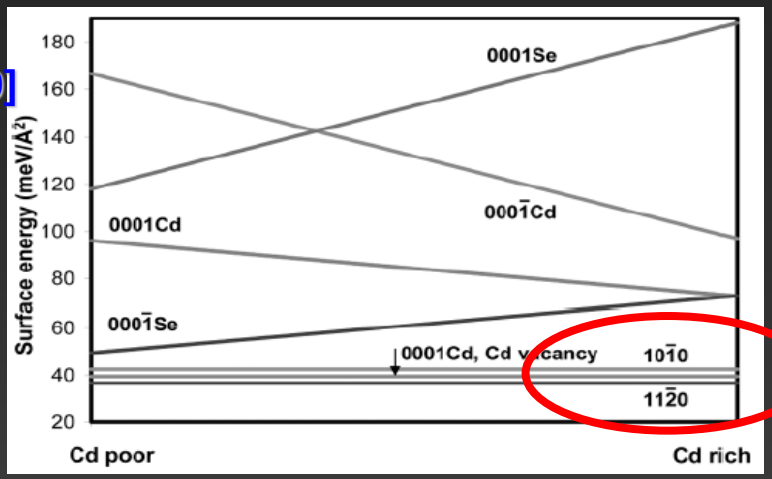

Alivisatos, A. P. *J. Phys. Chem. B* 2005, *109*, 6183.

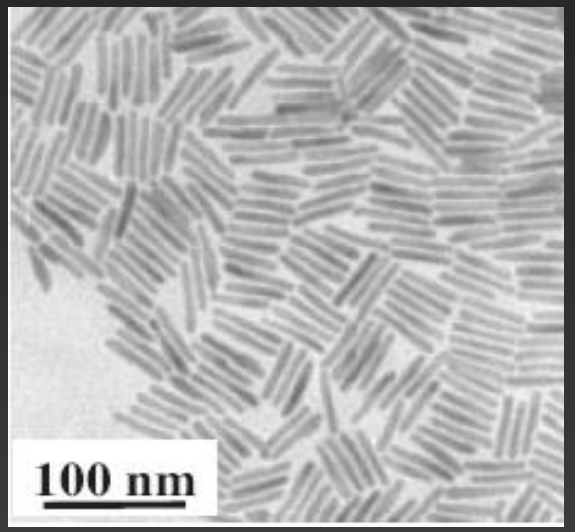

Peng, X. *Adv. Mater.* 2003, *15*, 459.

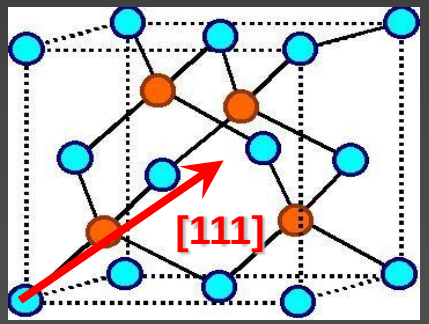

Cubic zincblende structure

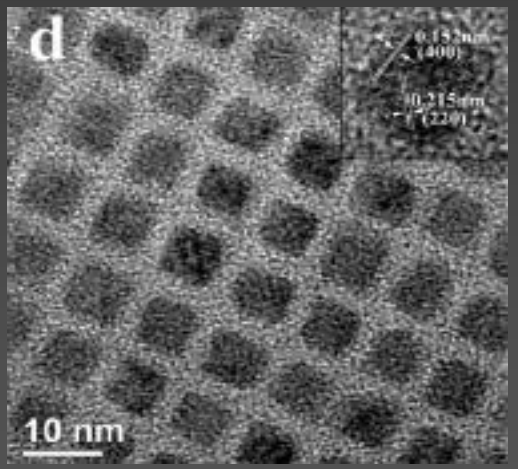

Liu, L., *et al. J. Am. Chem. Soc.* 2009, *131*, 16423.

Uniform 1.4 nm thick CdSe Nanoribbons

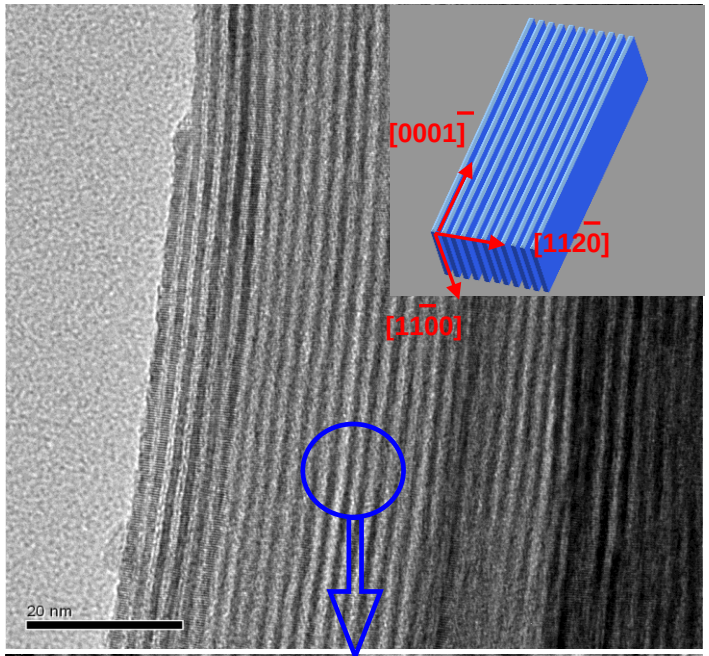

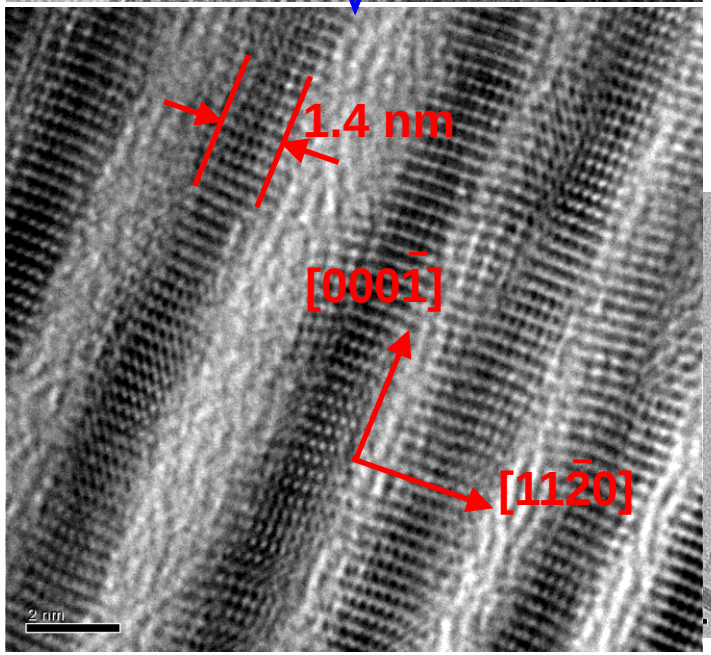

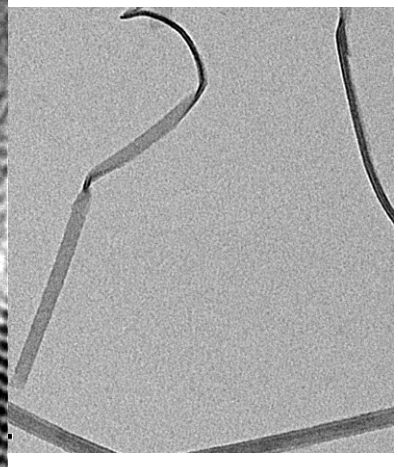

- Low temp (70ºC) synthesis
- Highly-reactive acid-base reaction

Cd^{2+} and $[R_2N\text{-}C(O)\text{-}Se]^-$

- Uniform 1.4 nm thick

J. Joo, ----, T. Hyeon,
J. Am. Chem. Soc. **2006**, 128, 5632.

The Sharpest UV-Vis and Blue Photoluminescence Approaching Linewidth of a Single QD

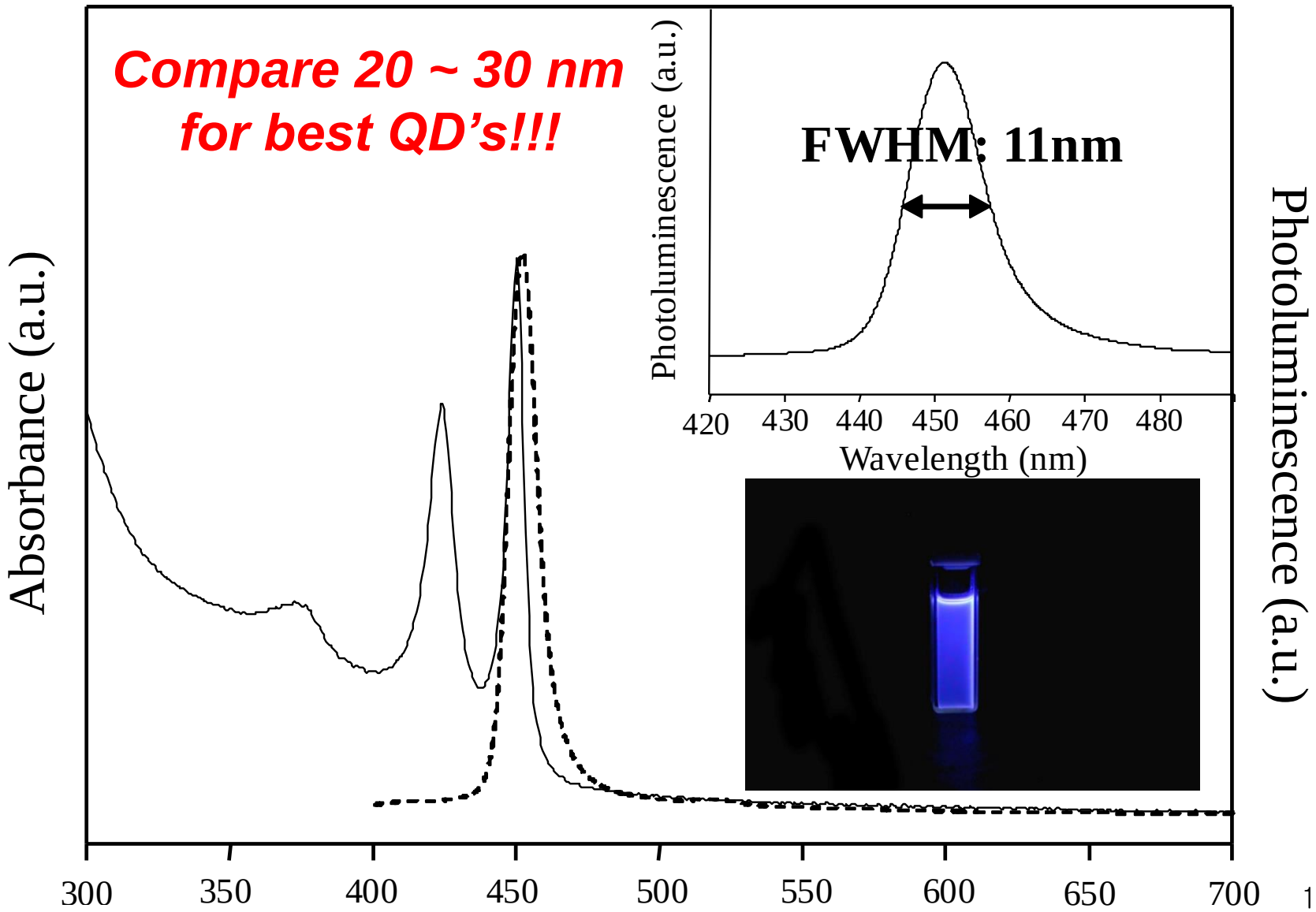

J. Joo, ----, T. Hyeon, *J. Am. Chem. Soc.* **2006**, 128, 5632.

Large-Scale Soft Colloidal Template Synthesis of 1.4 nm Thick CdSe Nanosheets

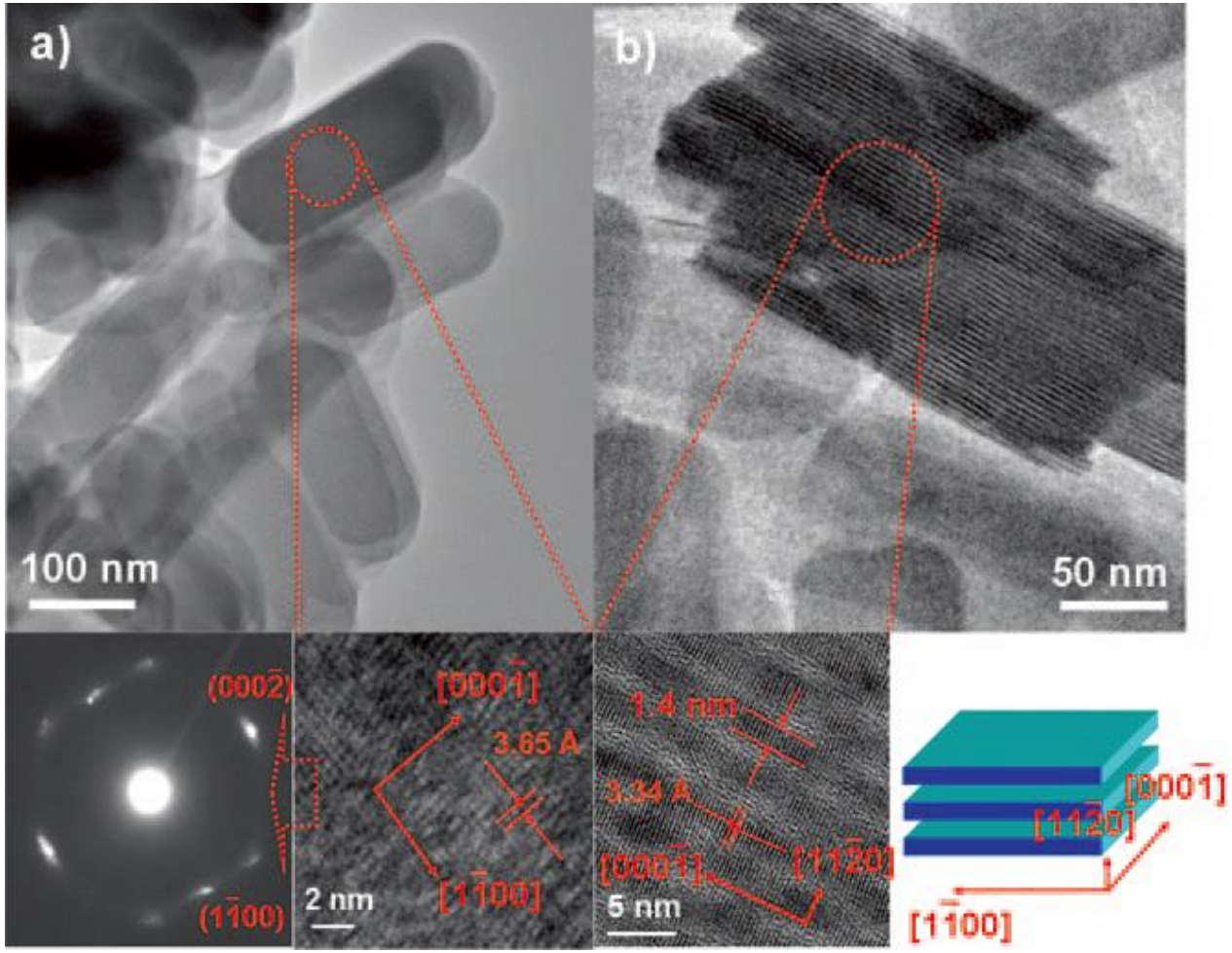

Uniform 1.4 nm thickness

> 30 nm wide

~ 100 nm long

Wurtzite structure

multi-gram synthesis

J. S. Son, ---, T. Hyeon, *Angew. Chem. Int. Ed.* **2009**, 48, 6861.

Precursor ($CdCl_2(OA)_2$) forms 2D lamellar assemblies, which act as "soft template"

2-D lamellar structured CdSe nanosheet

$CdCl_2$+ Octylamine → $CdCl_2(OA)_2$ 2-D template → Selenization → 

Strong Van der Waals attraction

2-D single-layered CdSe nanosheet

$CdCl_2$+ Octylamine / Oleylamine → $CdCl_2(OA, OLA)_2$ 2-D template → Selenization Sonication → 

Weak Van der Waals attraction

J. S. Son, ---, T. Hyeon, *Angew. Chem. Int. Ed.* **2009**, 48, 6861.

2-D Lamellar-structured CdSe Nanosheets

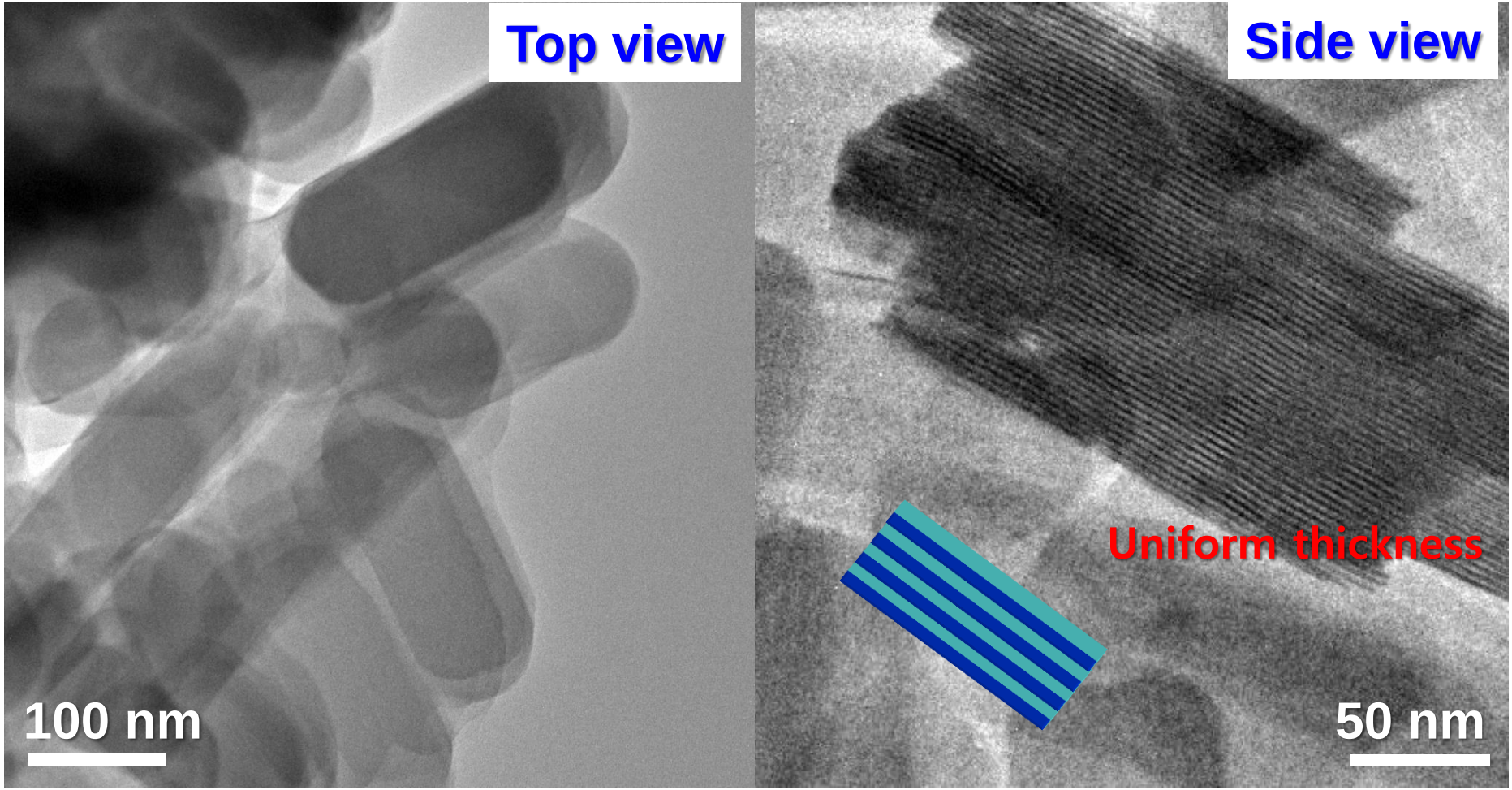

1.4 nm x 50~100 nm (width) x 200 ~ 300 nm (length)

2-D Single-layered CdSe Nanosheet

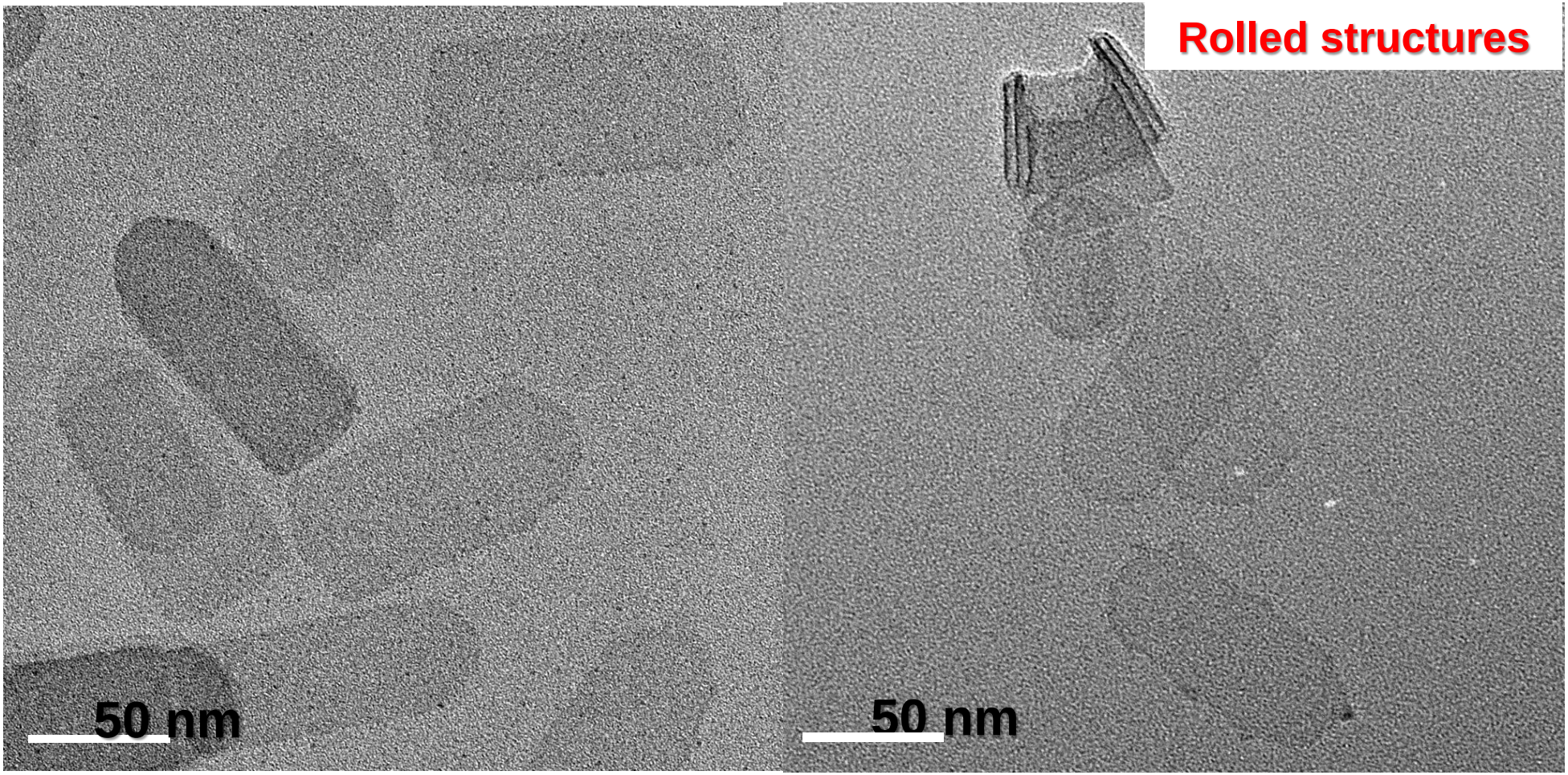

1.4 nm x 50~100 nm (width) x 100 ~ 200 nm (length)

Ultrathin Thickness of 1.4 nm: AFM

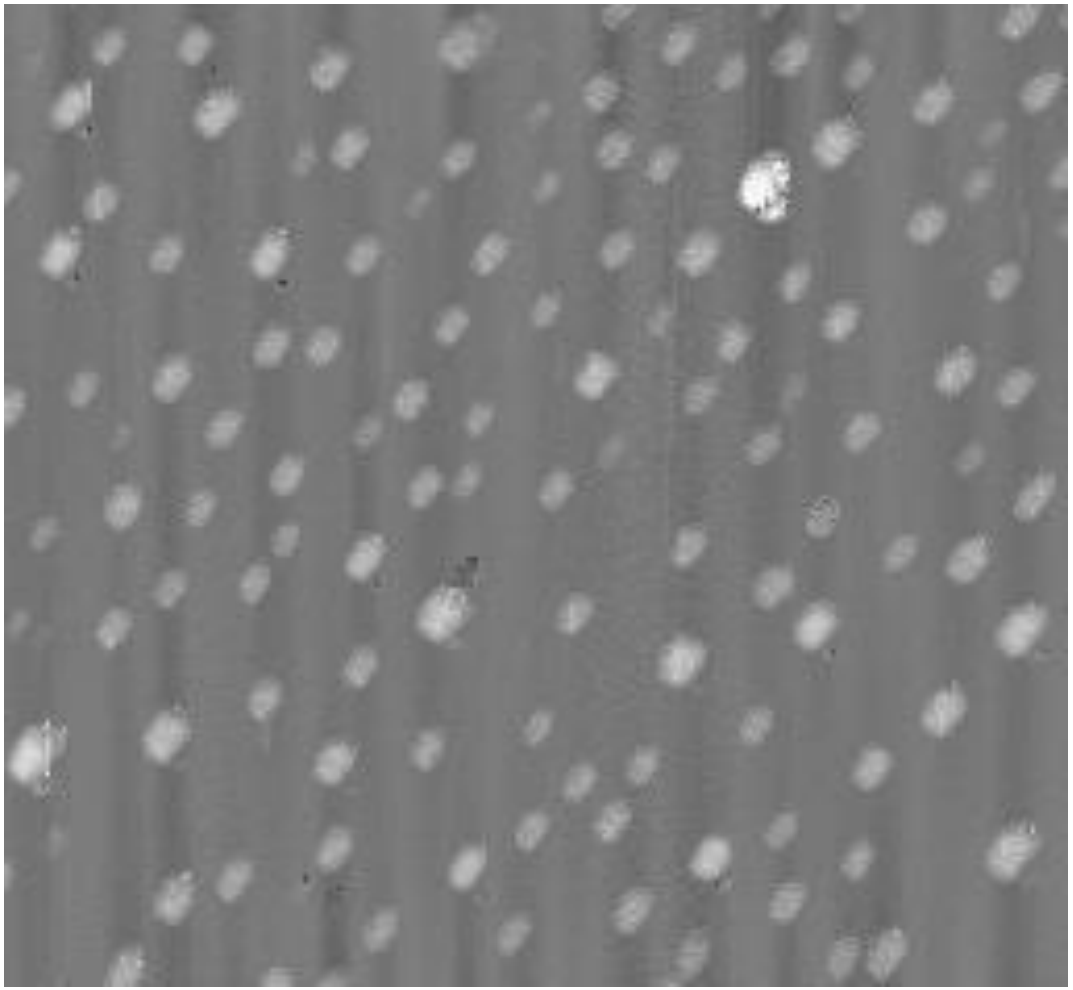

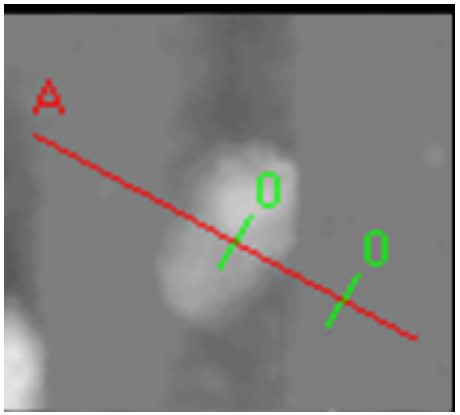

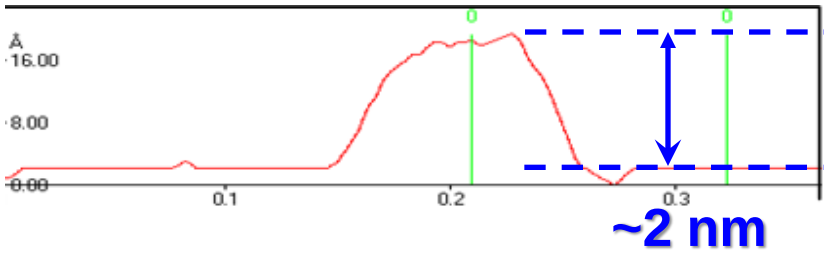

Thickness including organic layer

Hexagonal Wurtzite Crystal Structure: HRTEM

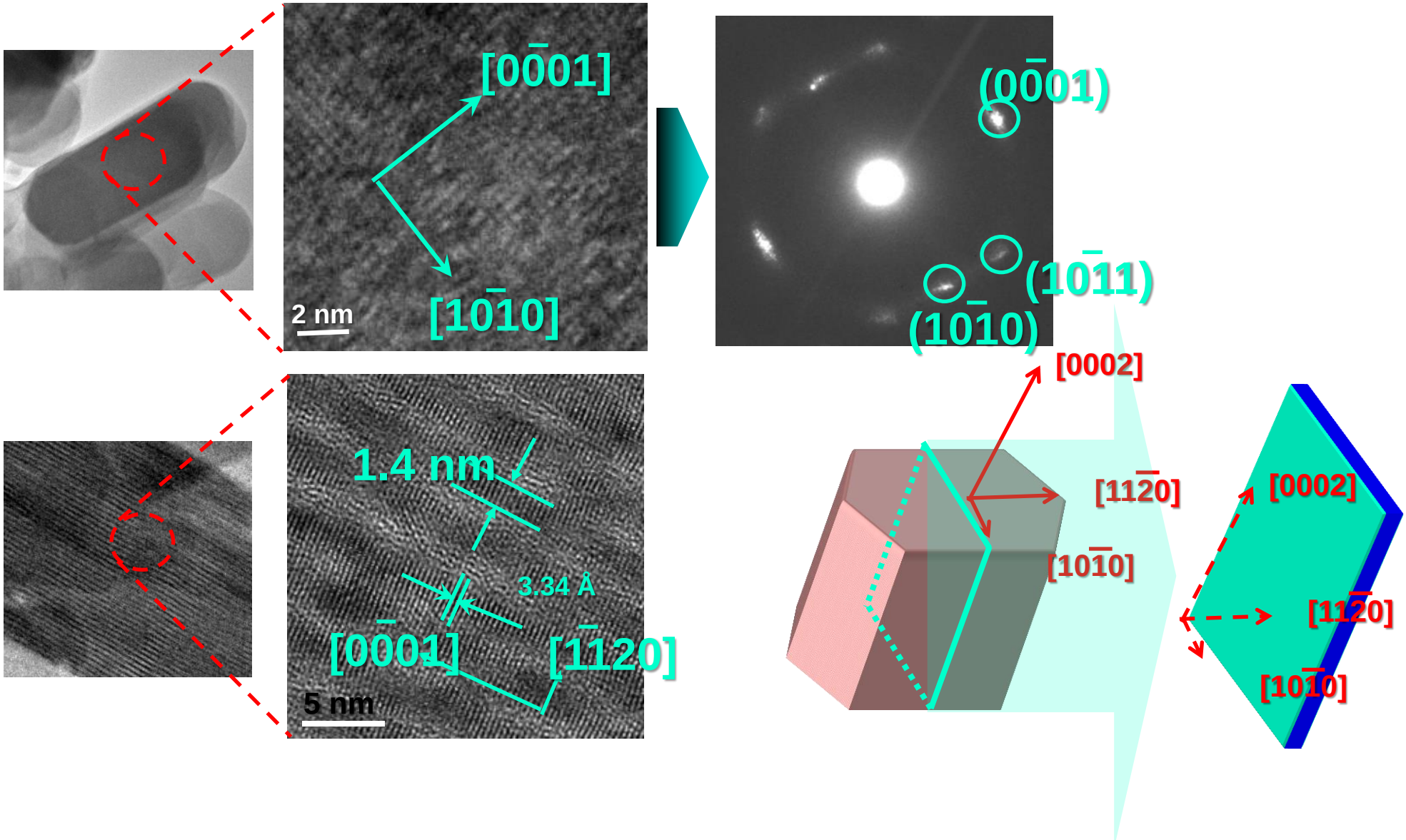

Structural Simulation of CdSe Nanosheet by DFT

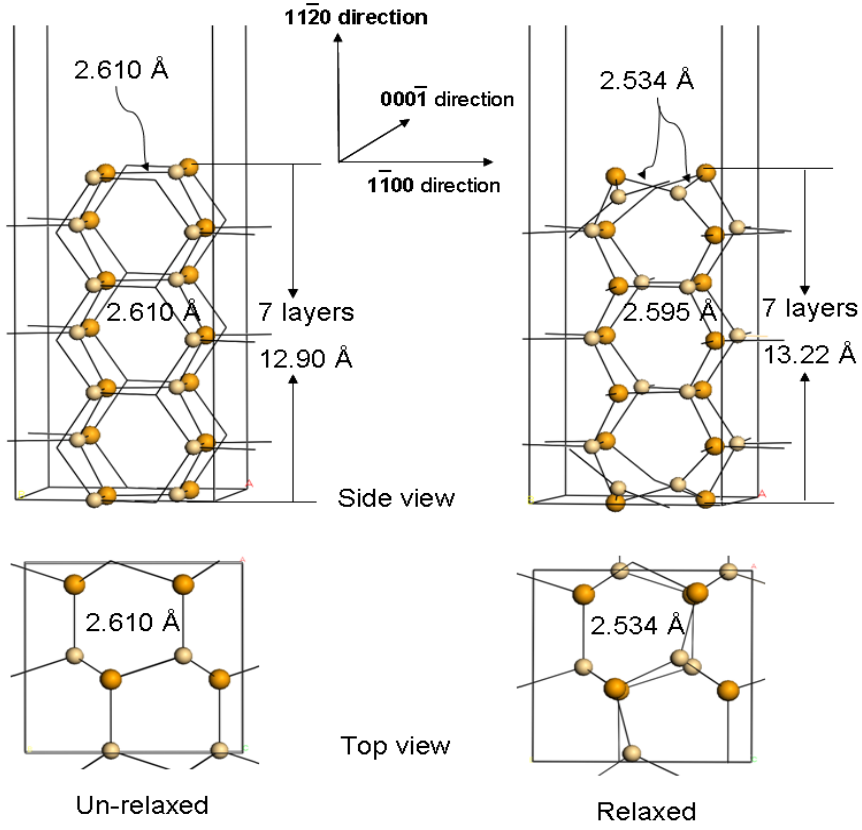

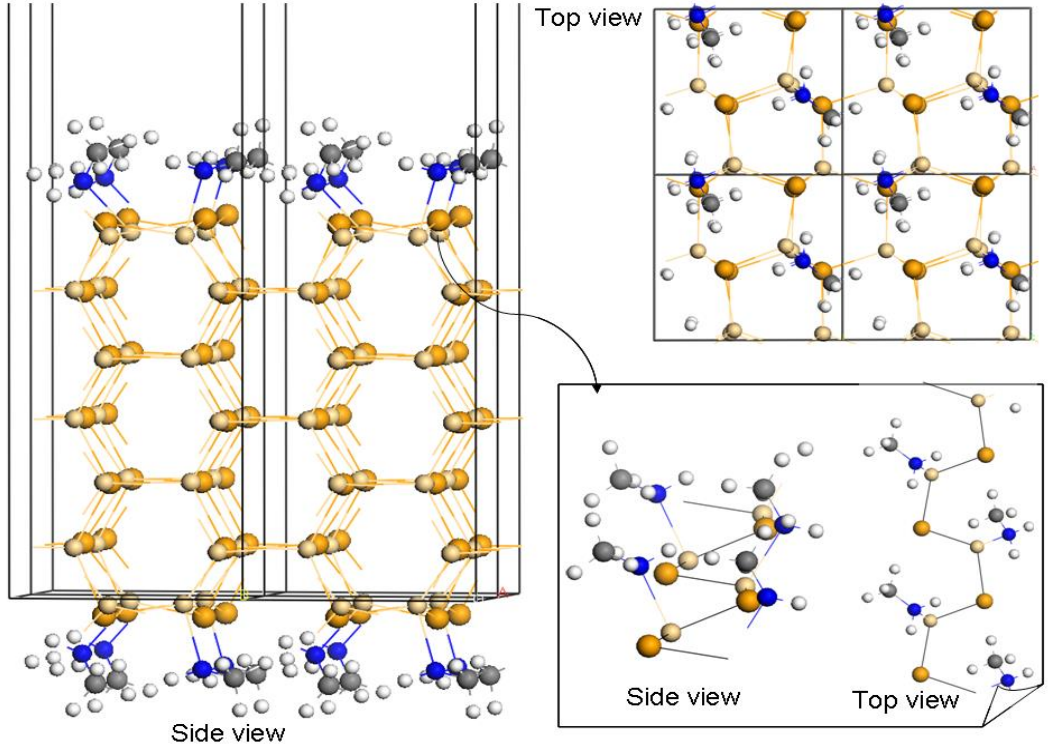

Without surfactants

→ Large relaxation

With methylamines

→ Small relaxation

Ultrathin thickness of 7 atomic layers; Amine stabilizing effect

Optical Properties

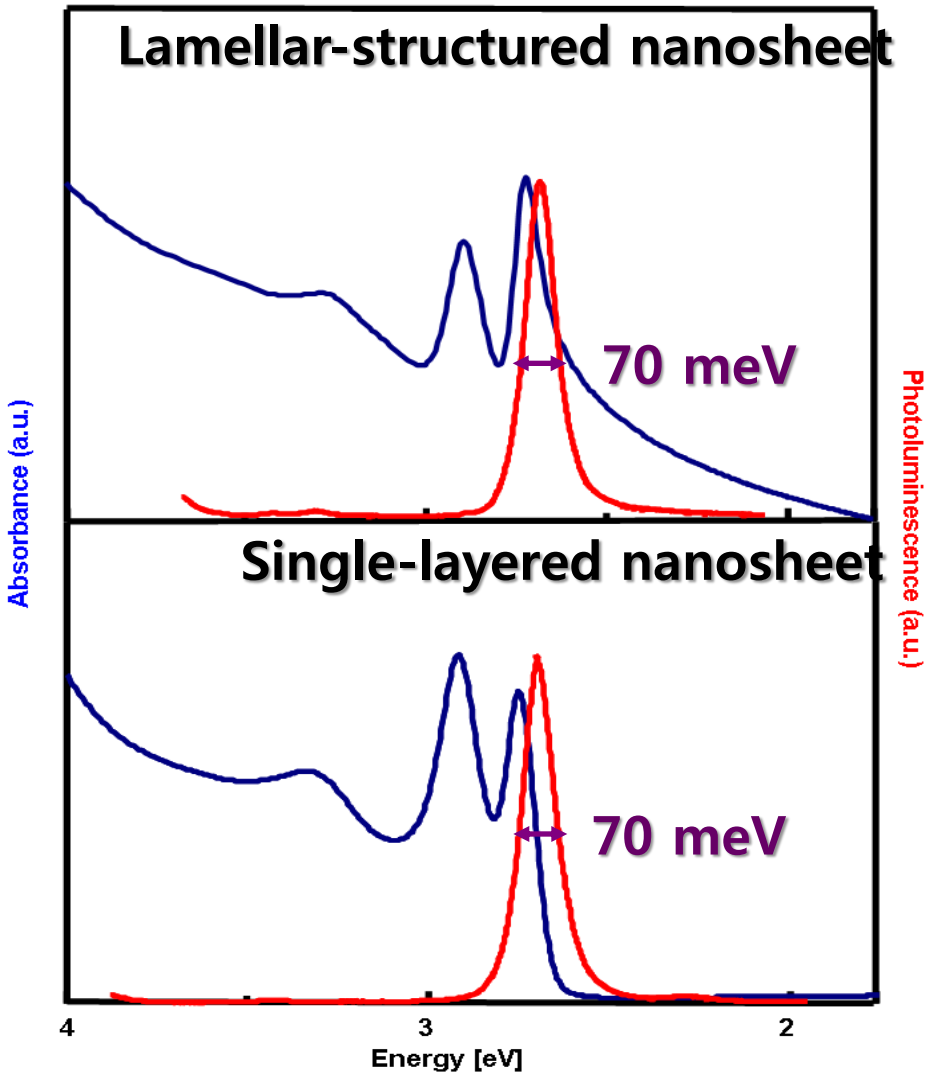

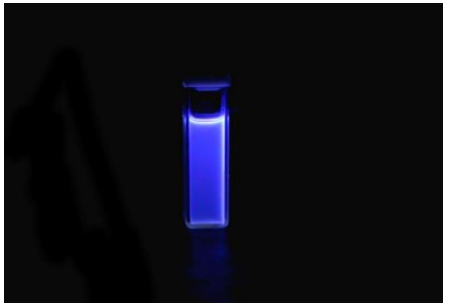

The Blue Photoluminescence Approaching homogeneously broadening limit of a single Q.D.
- Extremely uniform thickness

Polydisperse lateral dimension
→ 1-D confinement along the thickness direction

2-D Quantum Well

Large Scale Synthesis

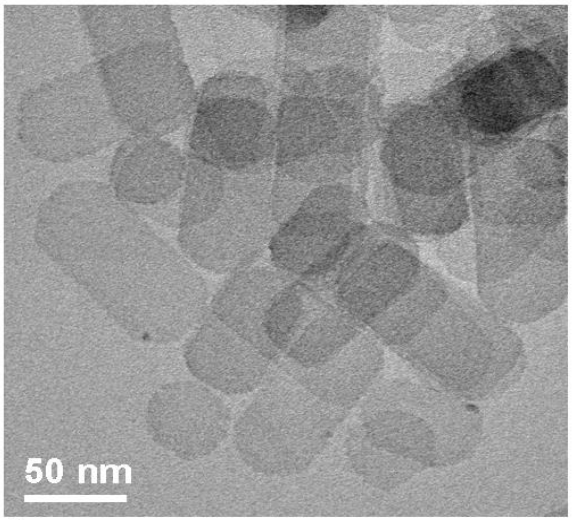

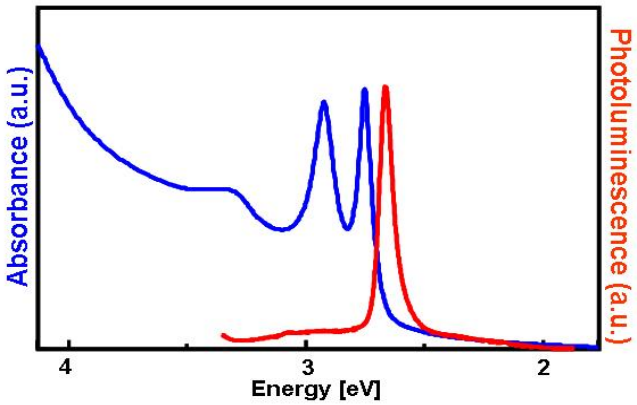

Gram scale

CdSe Quantum belts with wurtzite structure

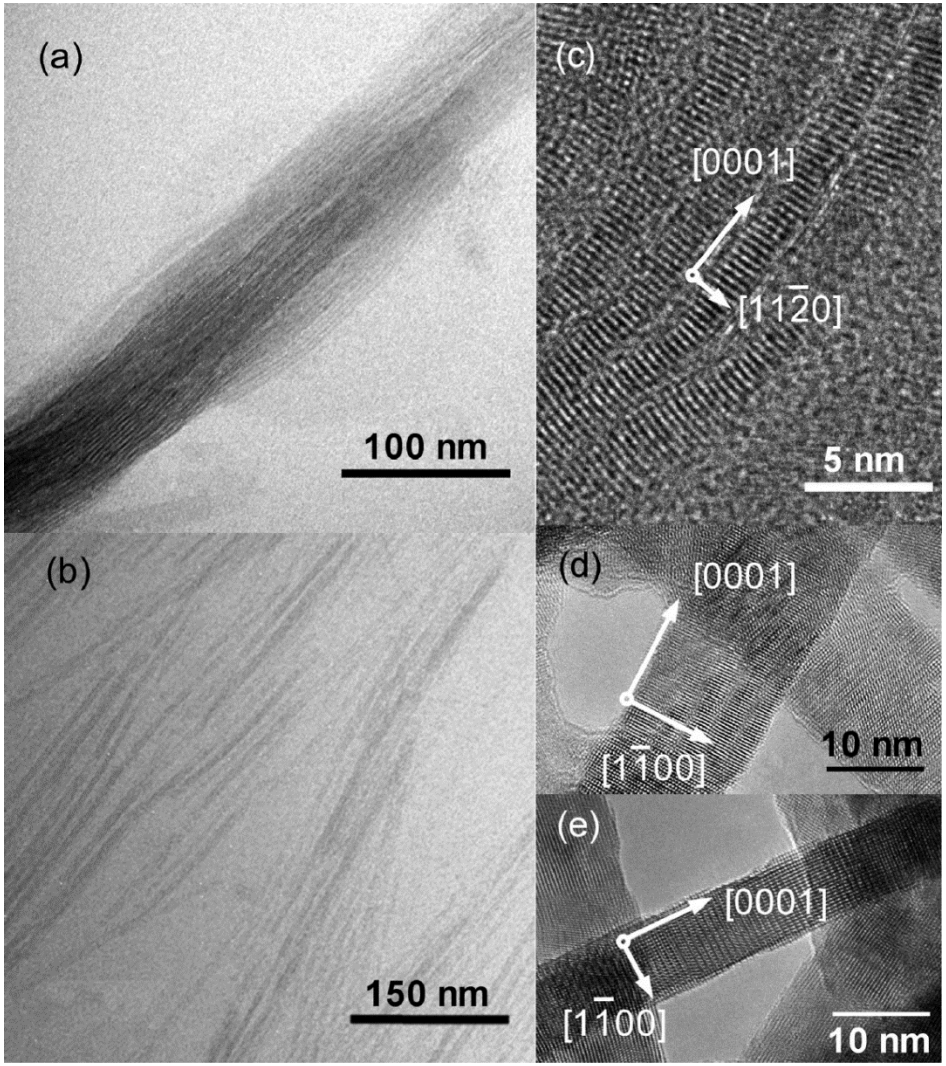

Length of 0.5-1.5 μm and thickness of 1.5-2.0 nm

Y.-H. Liu, ---, W. E. Buhro, *Nano Lett.* **2010**, 10, 352.

CdSe Quantum belts with wurtzite structure

Photoluminescence (PL) efficiencies of ~30%

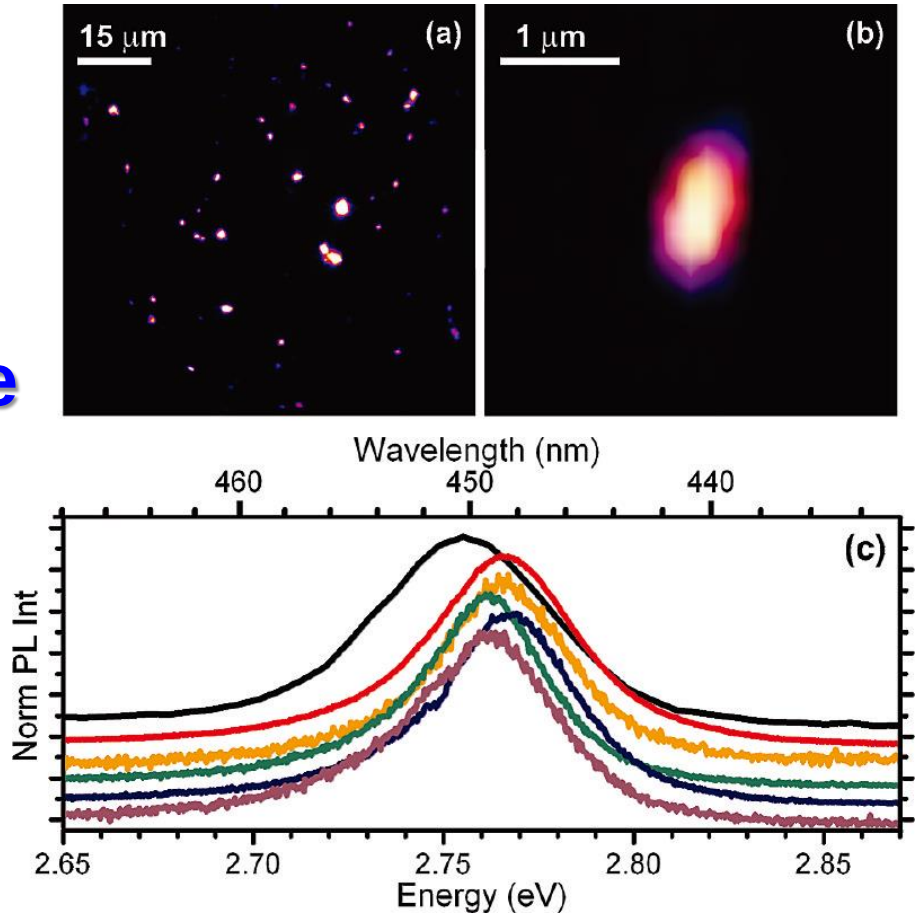

Each QBs showed similar PL.

Y.-H. Liu, ---, W. E. Buhro, *Nano Lett.* **2010**, 10, 352.

2D Colloidal CdSe Platelets with Thicknesses Controlled at the Atomic Level

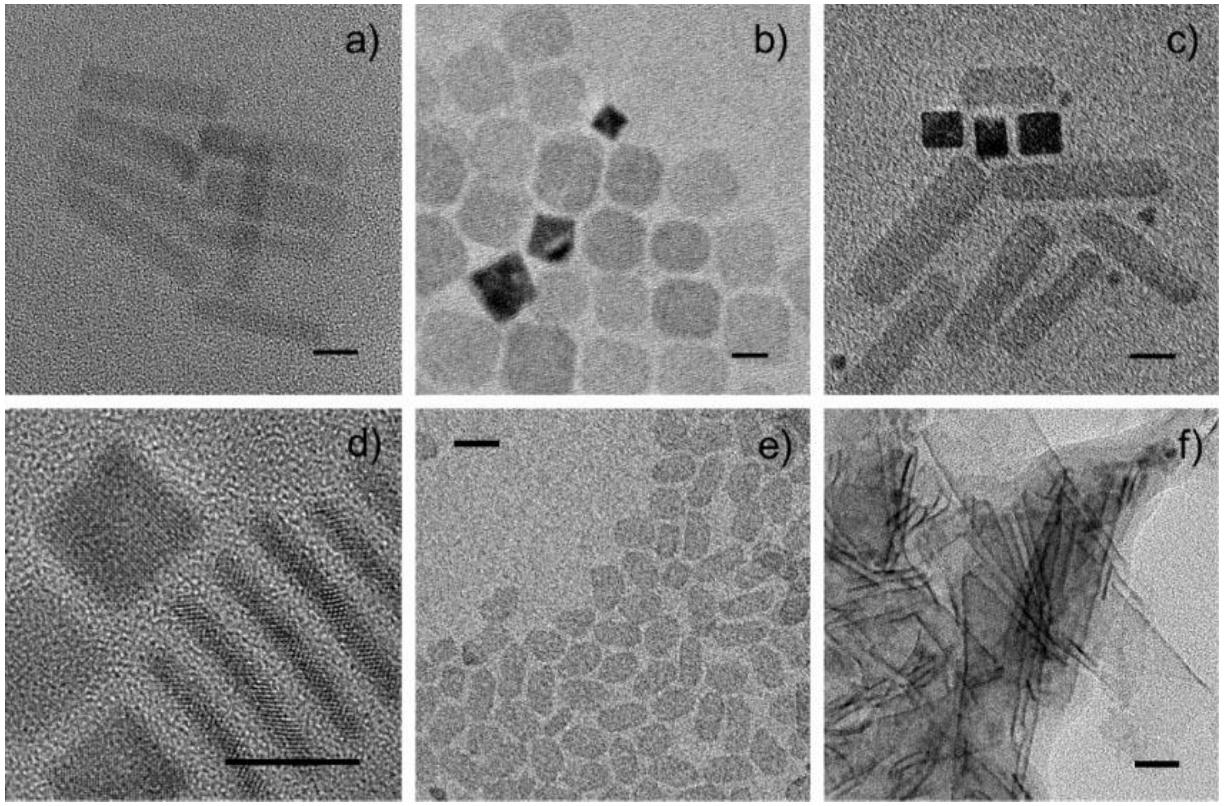

2D Nanoplatelets with zinc blende structure were reported.

S. Ithurria, B. Dubertret, *J. Am. Chem. Soc.* **2008**, 130, 16504.

2D Colloidal CdSe Platelets with Thicknesses Controlled at the Atomic Level

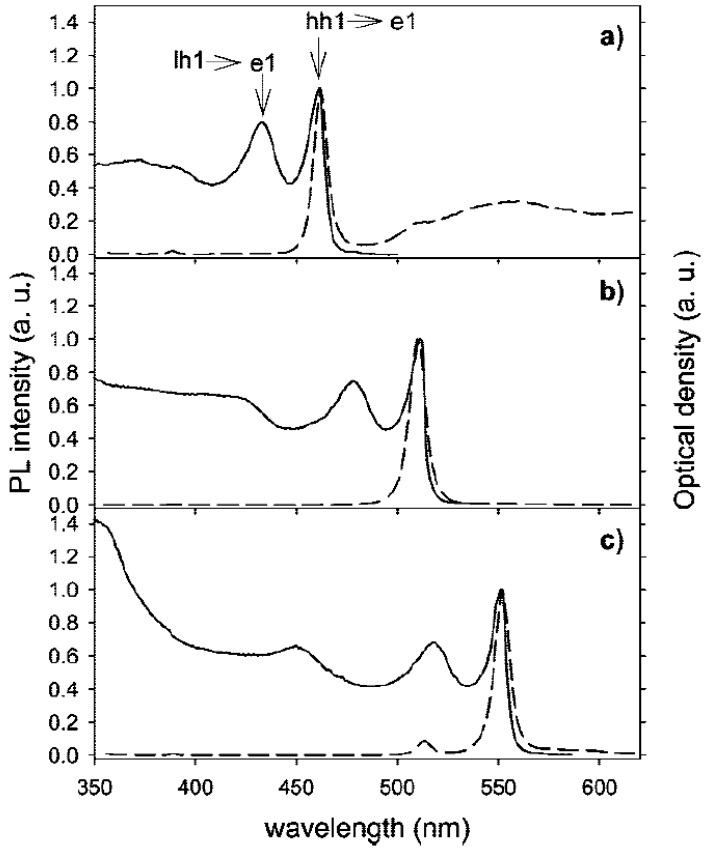

They show very sharp photoluminescence.

S. Ithurria, B. Dubertret, *J. Am. Chem. Soc.* **2008**, 130, 16504.

Continuous Transition from 3D to 1D Confinement Observed during the Formation of CdSe Nanoplatelets

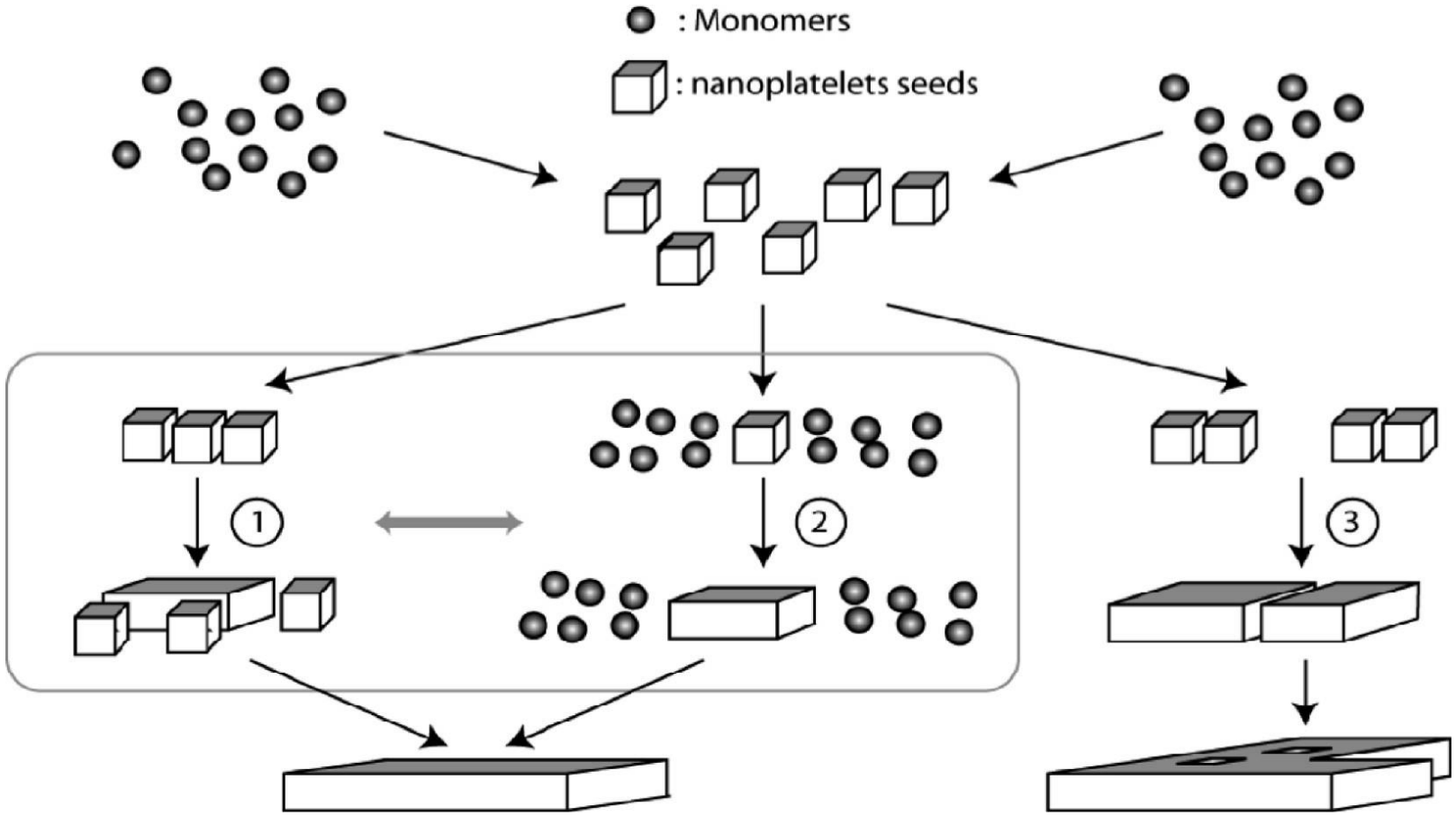

S. Ithurria, ----, B. Dubertret,, *J. Am. Chem. Soc.* **2011**, 133, 3070.

Continuous Transition from 3D to 1D Confinement Observed during Formation of CdSe Nanoplatelets

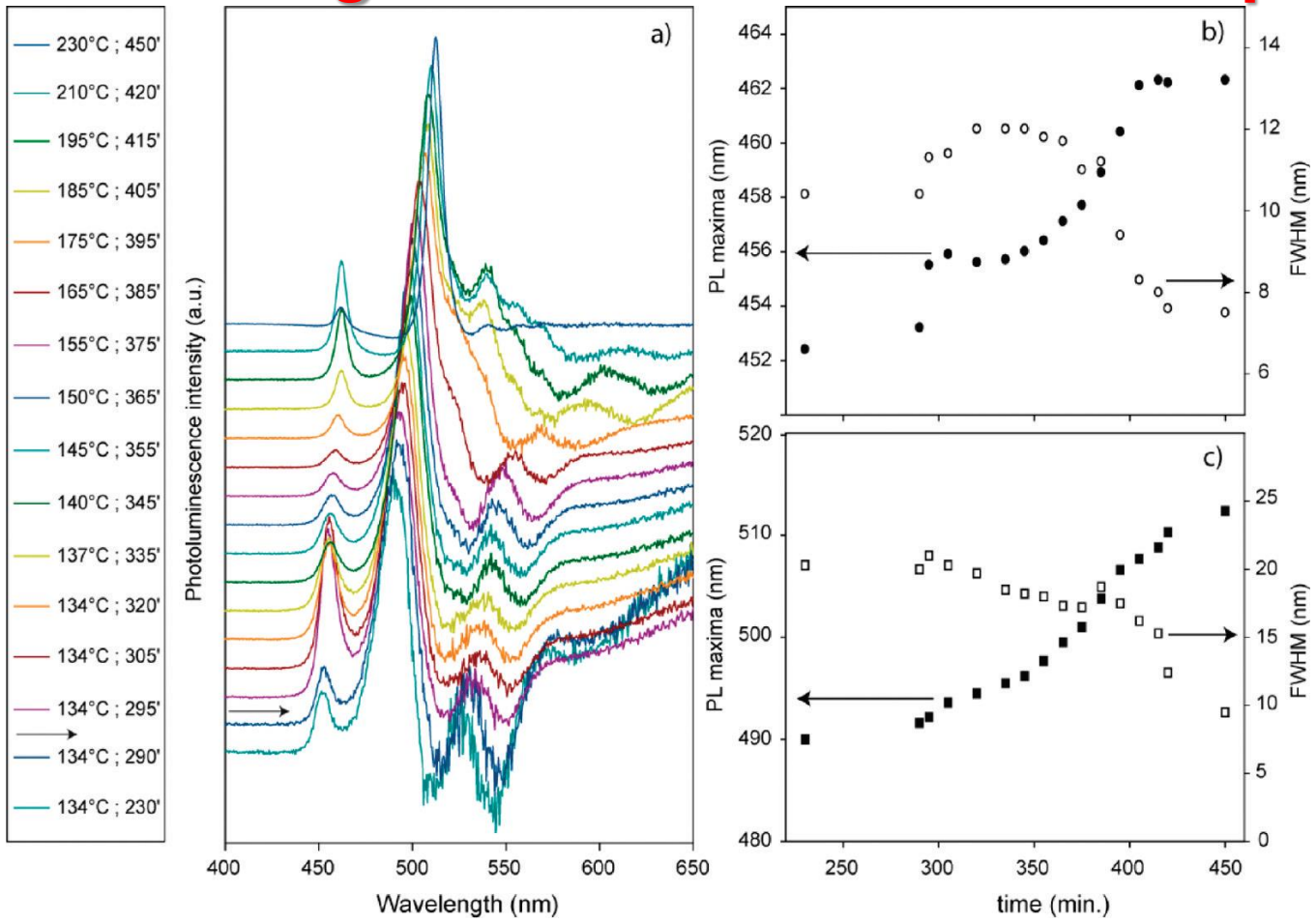

S. Ithurria, ----, B. Dubertret, *J. Am. Chem. Soc.* **2011**, 133, 3070.

Synthesis of Colloidal CdSe Quantum Disks with Zinc blende structure

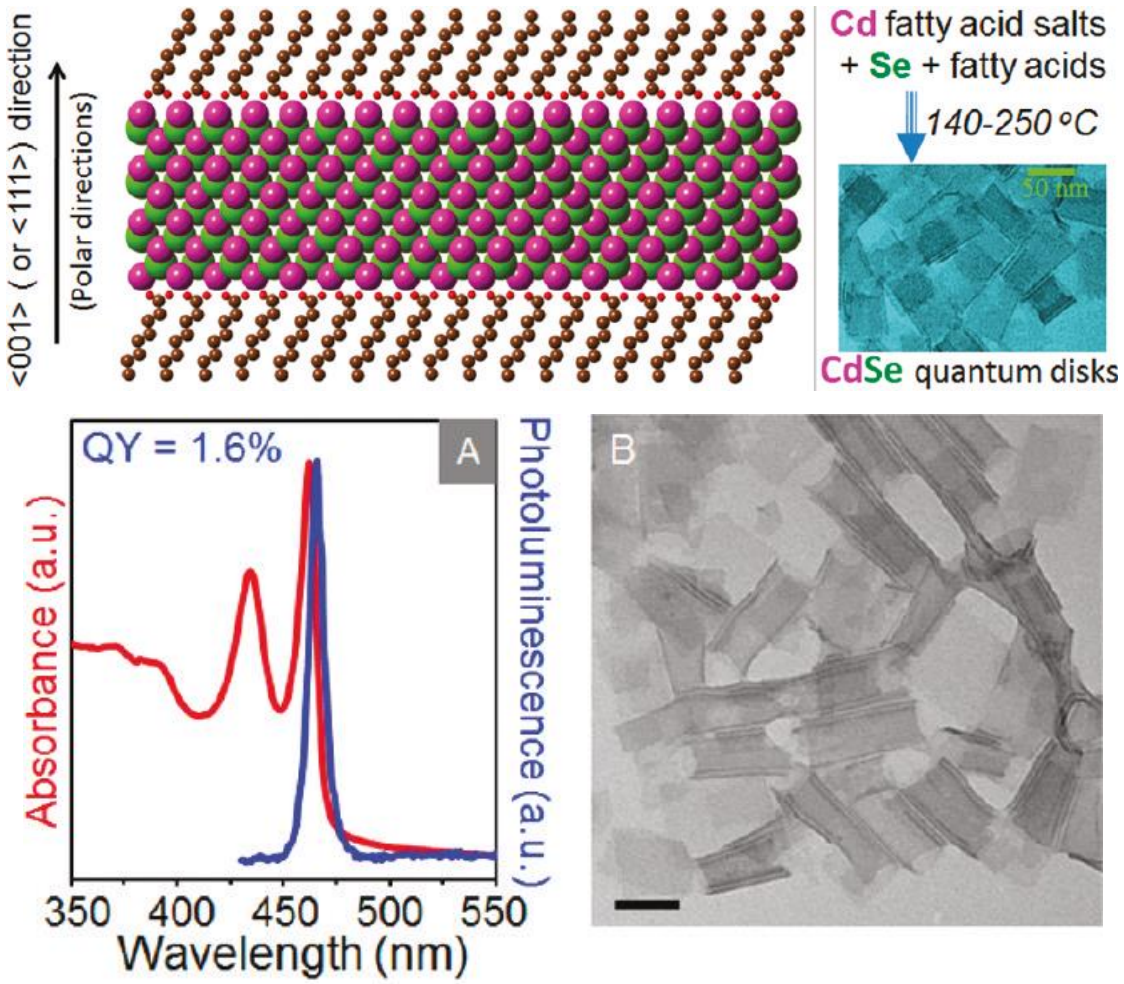

Z. Li and X. Peng, *J. Am. Chem. Soc.* **2011**, 133, 6578.

Synthesis of Colloidal CdSe Quantum Disks with Zinc blende structure

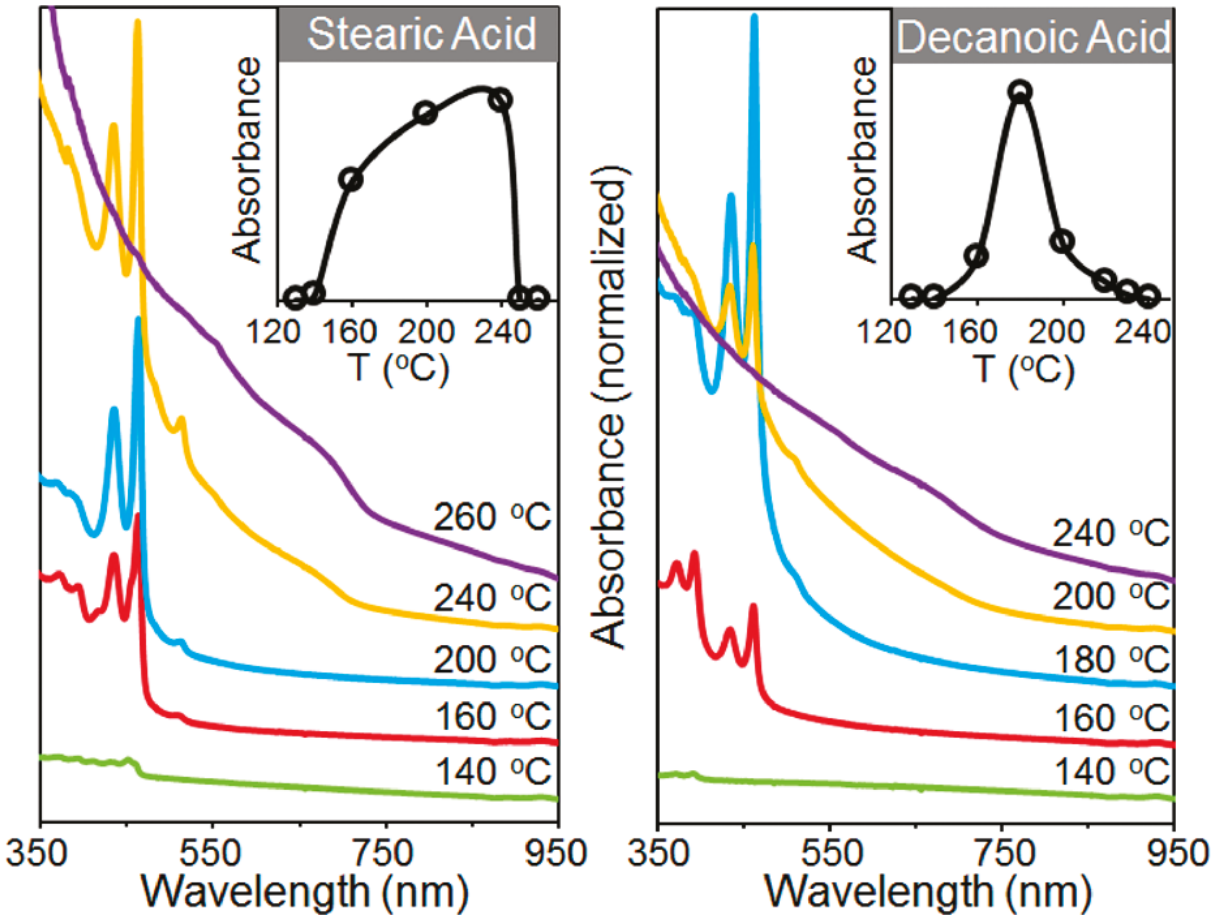

Soft template effect by acid ligand was suggested.

Z. Li and X. Peng, *J. Am. Chem. Soc.* **2011**, 133, 6578.

Summary of Optical property of 2D CdSe quantum Nanostructures

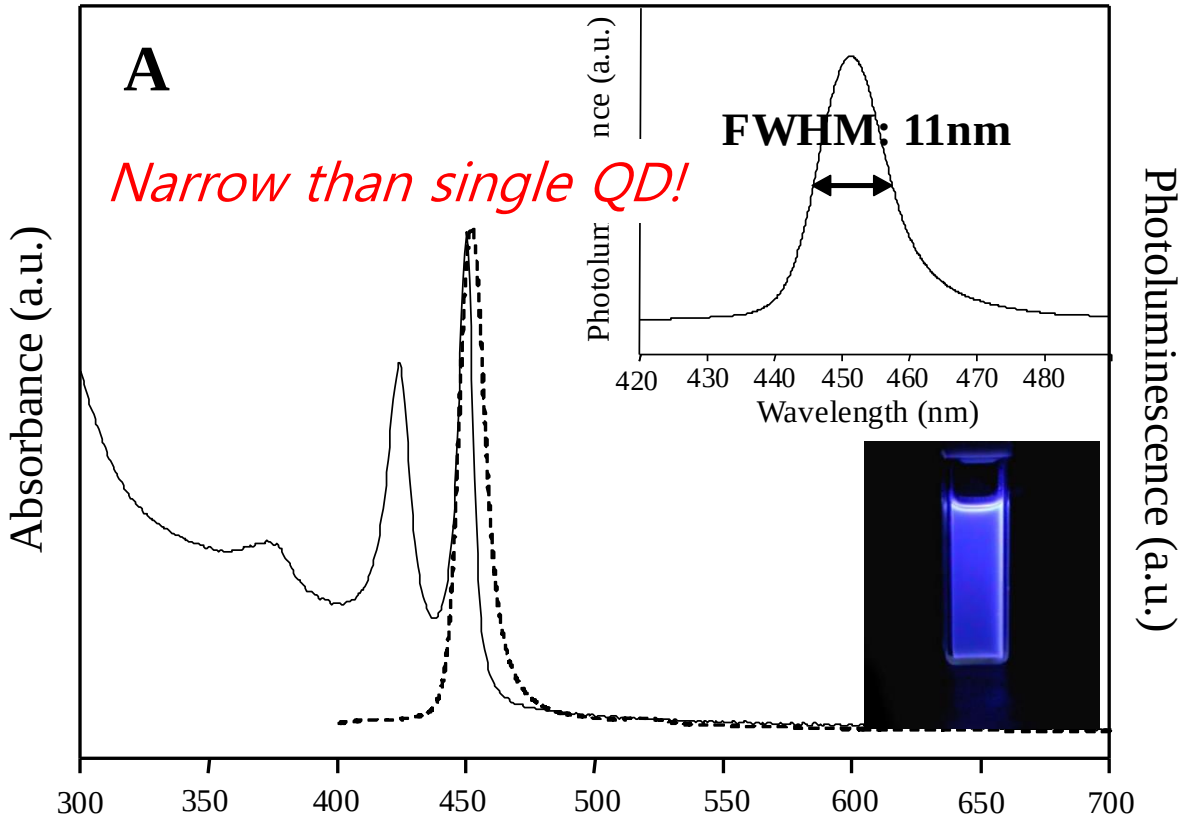

All of these 2D CdSe NCs shows very similar optical properties

→

Narrow band width, splitting of heavy-hole and light-hole subbands.

J. Joo, ----, T. Hyeon, *J. Am. Chem. Soc.* **2006**, 128, 5632.

Colloidal nanoplatelets with two-dimensional electronic structure

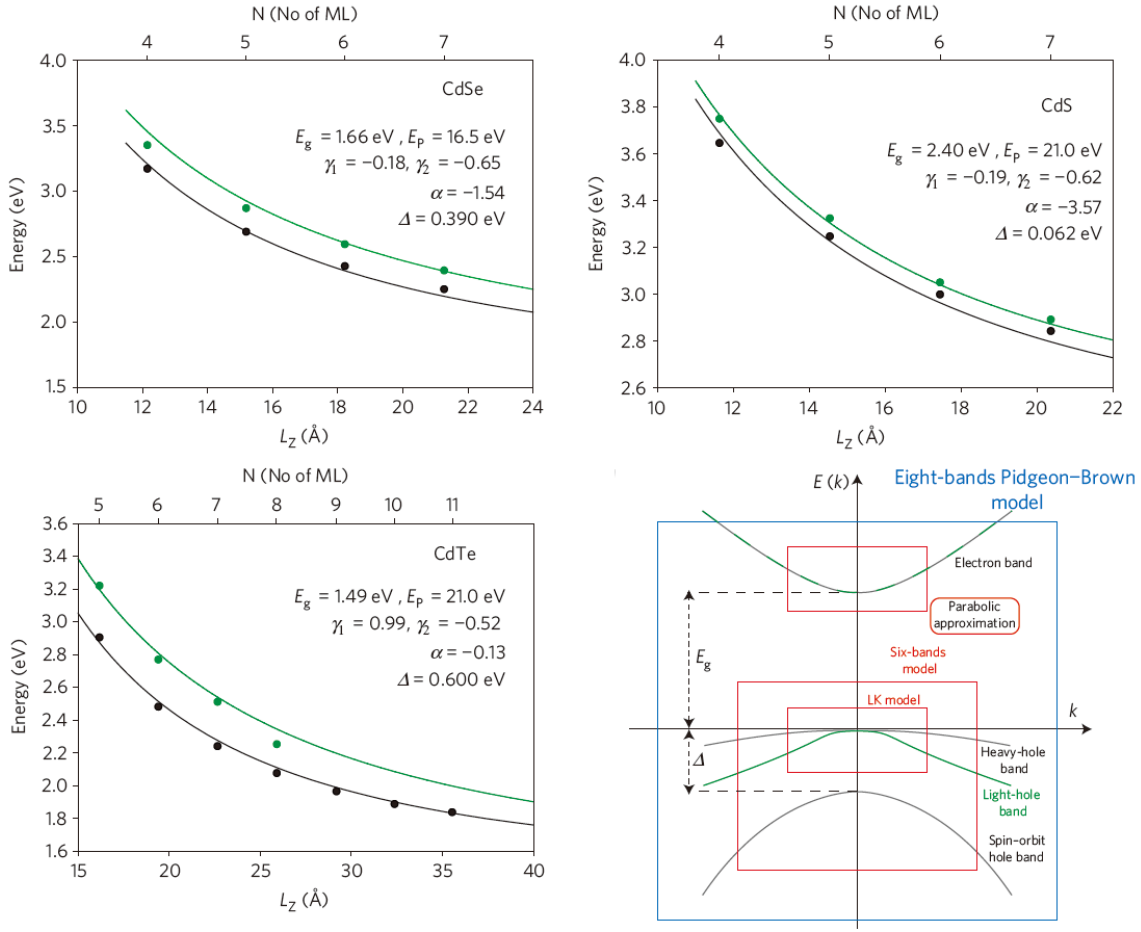

2D electronic structure was demonstrated.

S. Ithurria, ------, B. Dubertret, Al. L. Efros, *Nat. Mater.* **2011**, 10, 936.

Colloidal CdSe nanoplatelets with two-dimensional electronic structure

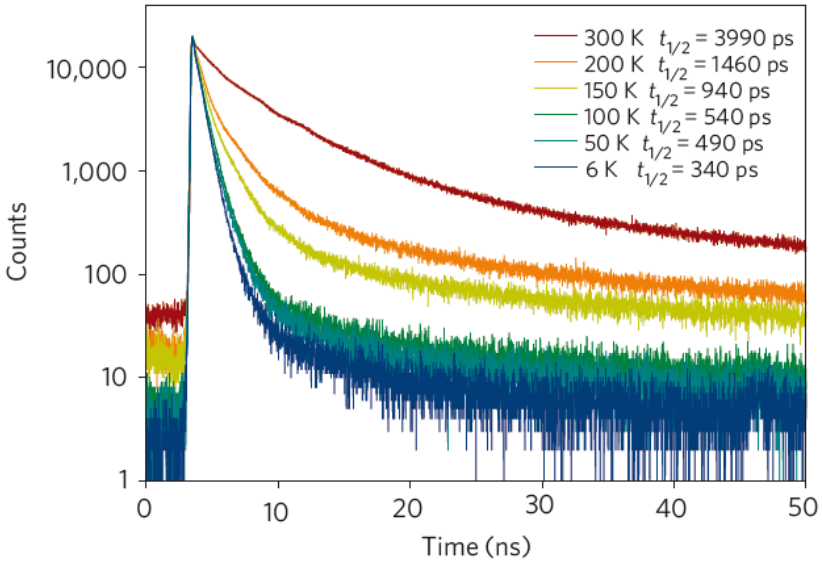

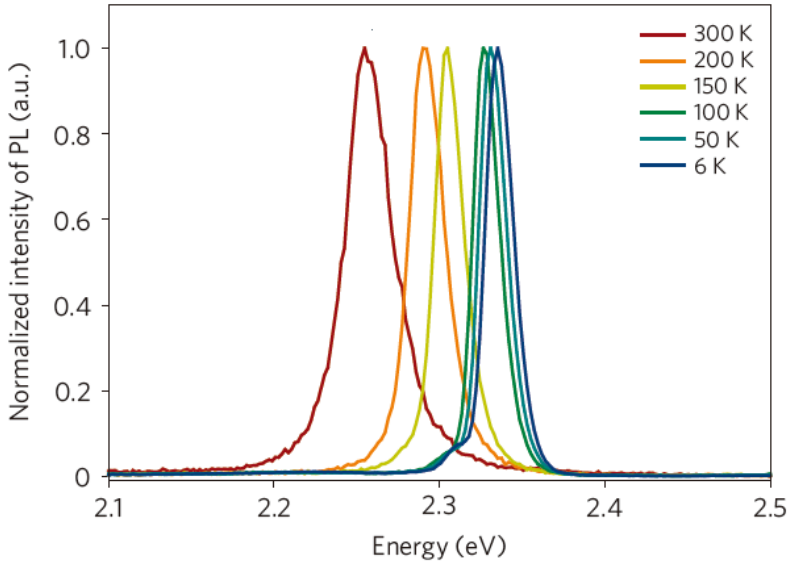

Fluorescence lifetime reaches to ~1 ns

➔ The fastest colloidal fluorescent emitters!

S. Ithurria, ------, B. Dubertret, Al. L. Efros, *Nat. Mater.* **2011**, 10, 936.

c-ALD using Self-Limiting Reactions at Nanocrystal Surface Coupled to Phase Transfer between Polar and Nonpolar Media

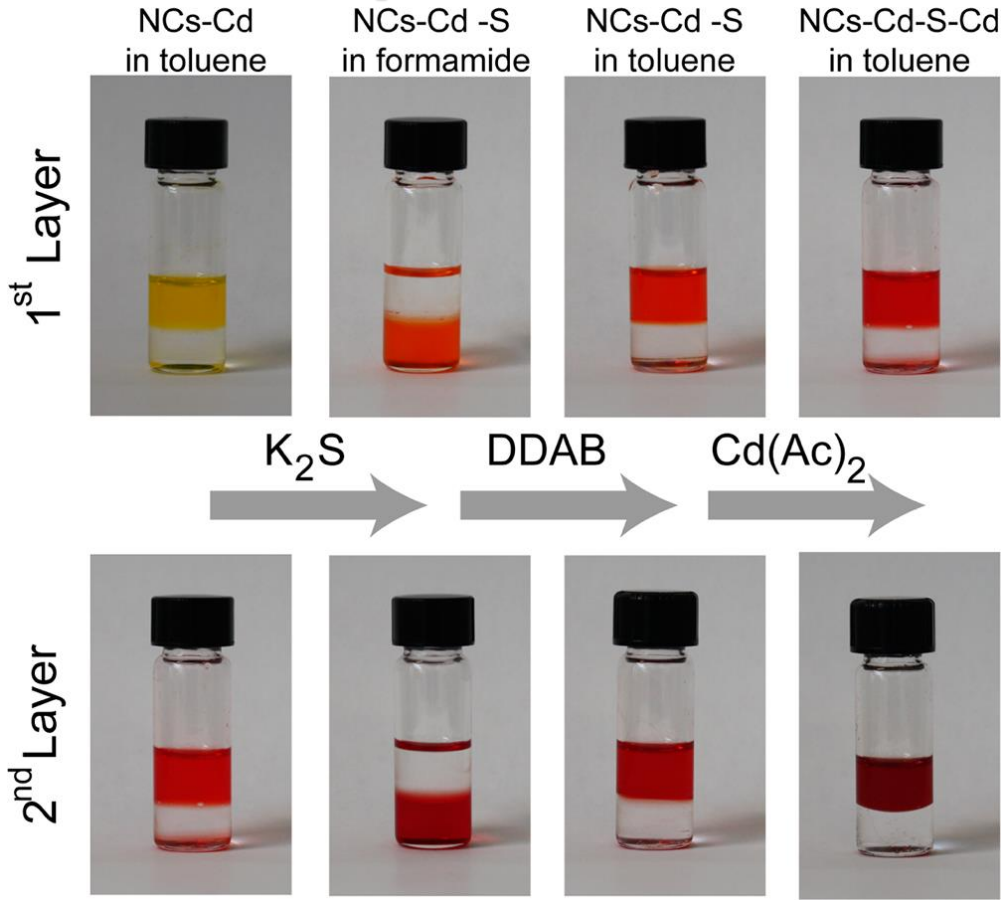

CdSe/CdS core/shell 2D NPLs was demonstrated.

S. Ithurria, D. V. Talapin, *J. Am. Chem. Soc.* **2012**, 134, 18585

Core/Shell Colloidal Semiconductor Nanoplatelets

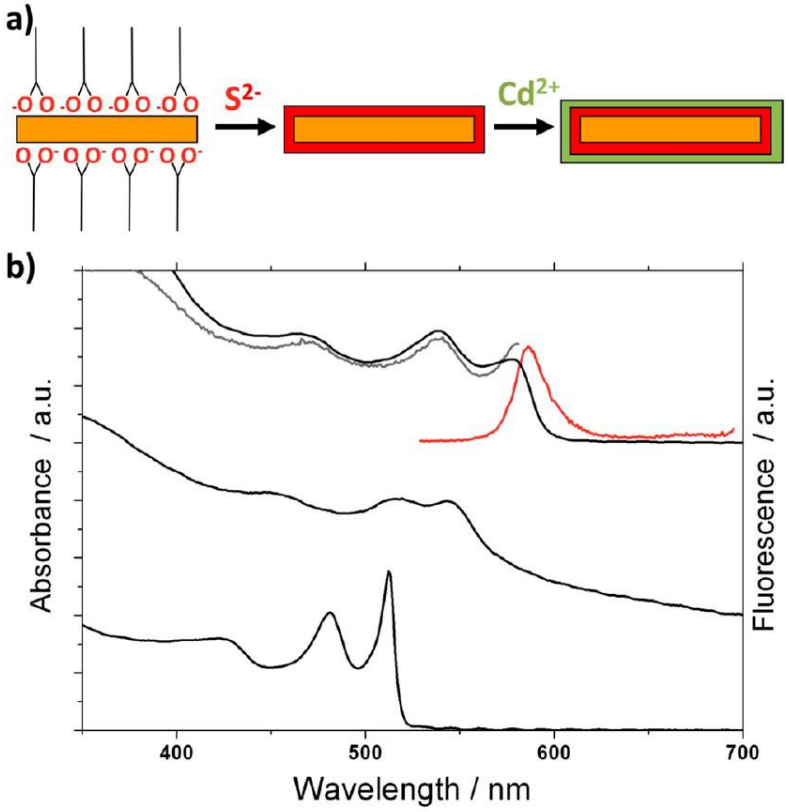

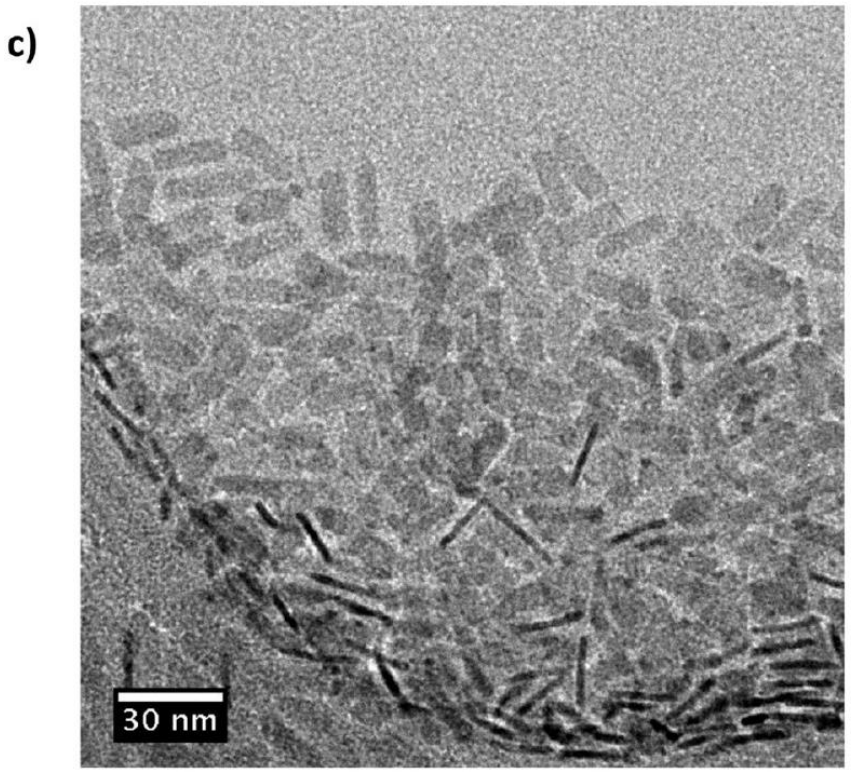

CdSe/CdS core/shell 2D NPLs was demonstrated.

B. Mahler, ----, B. Dubertret, *J. Am. Chem. Soc.* **2012**, 134, 18591.

Other 2D NCs – Wurtzite CdS Nanosheets

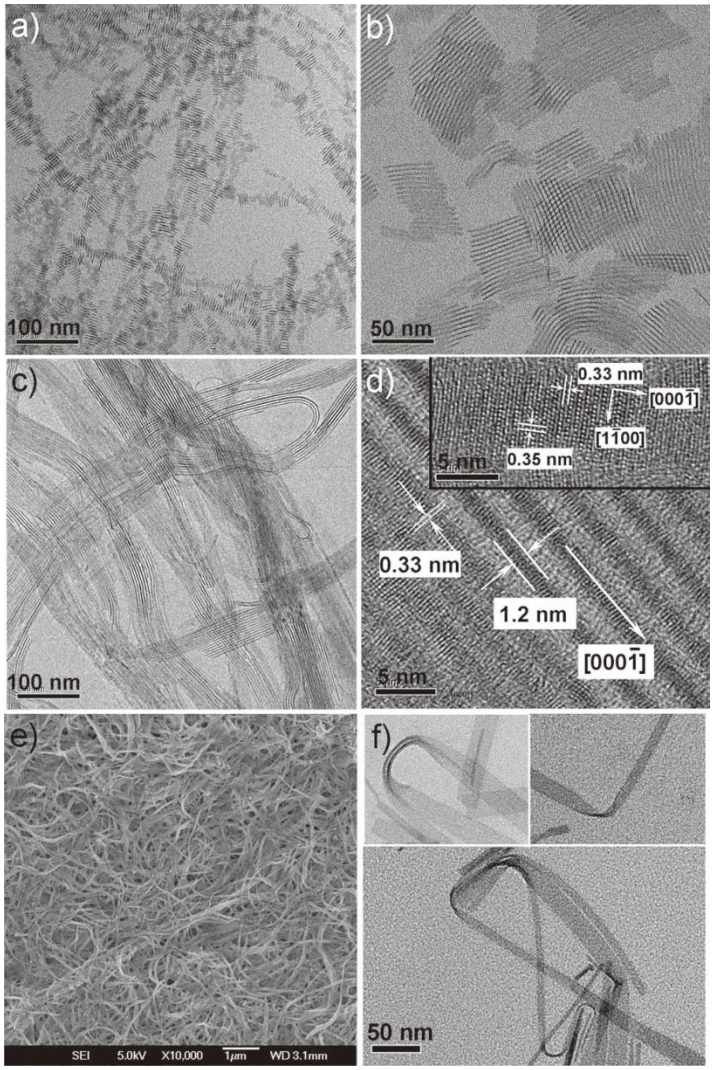

CdS Nanosheets and nanoribbons

J. S. Son, ---, T. Hyeon, *small* **2012**, 8, 2394.

Other 2D NCs – Wurtzite CdS Nanosheet

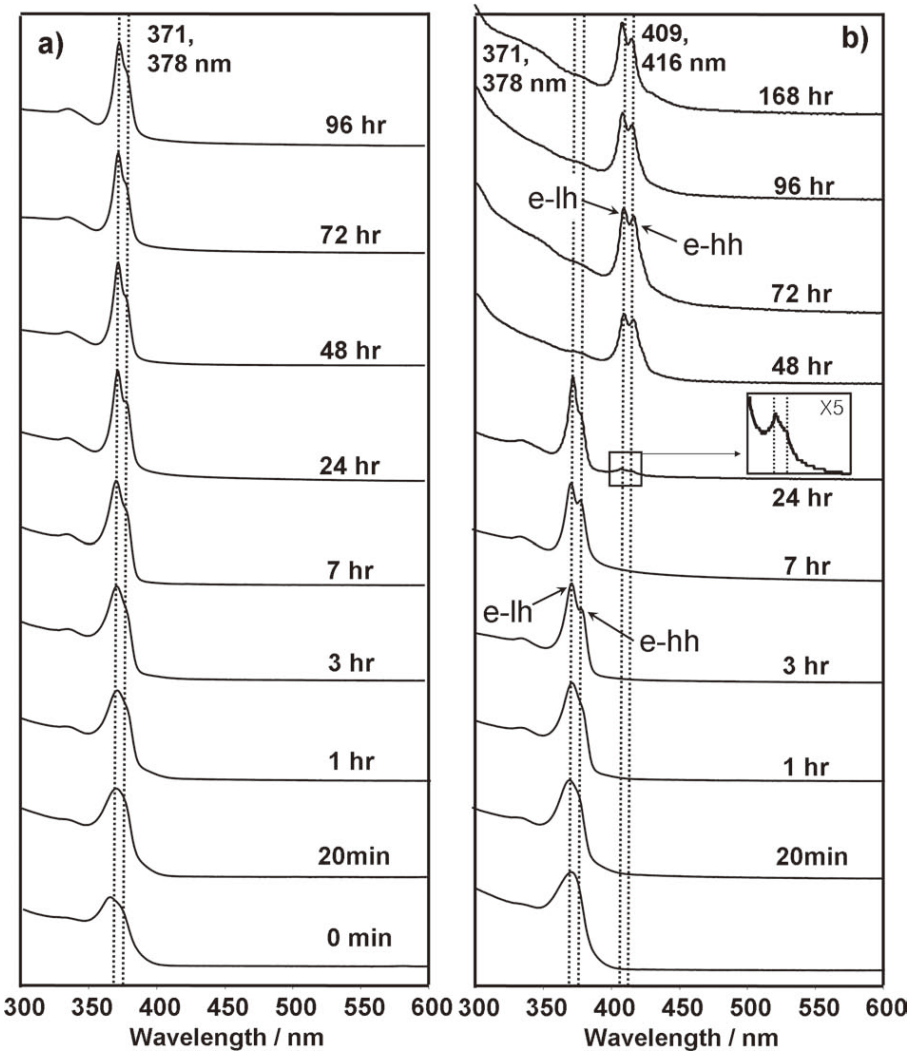

They show heavy hole and light hole splitting.

J. S. Son, ---, T. Hyeon, *small* **2012**, 8, 2394.

Other 2D NCs – Wurtzite CdTe Nanosheet

Lamellar-structured nanosheet

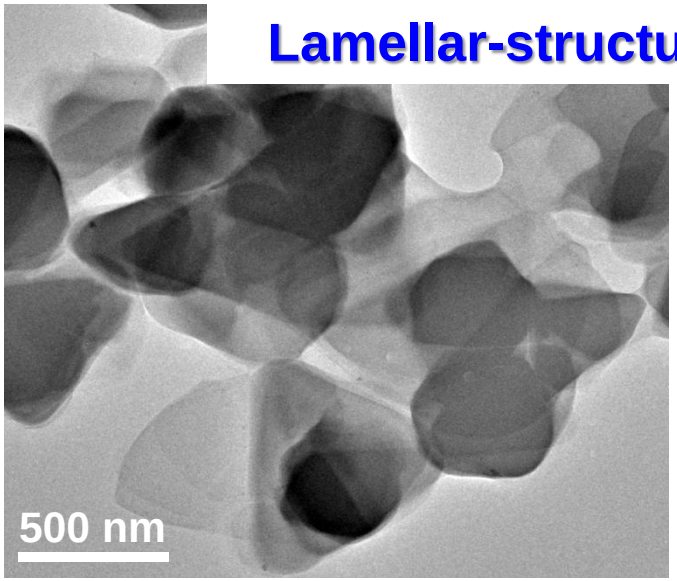

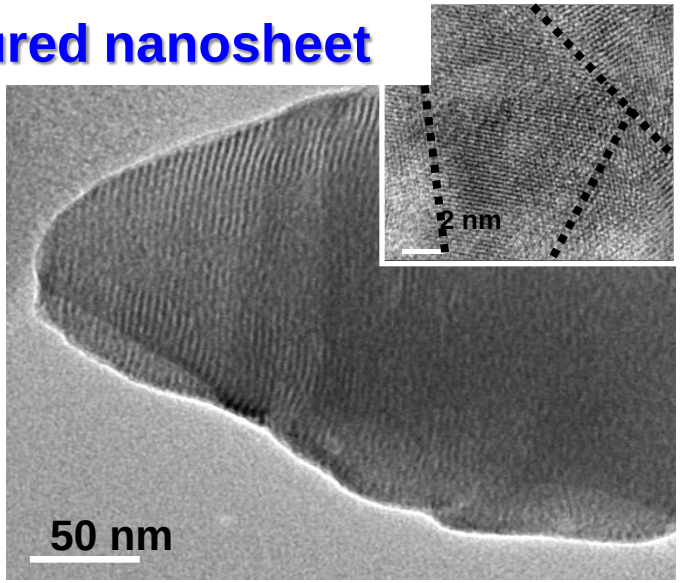

Single-layered nanosheet

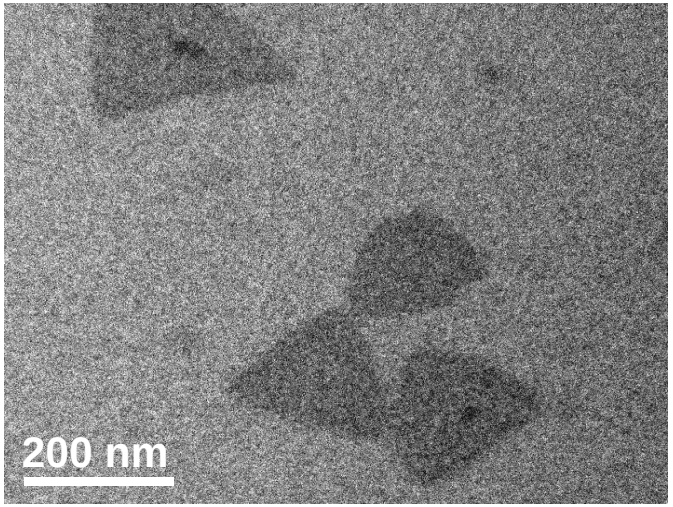

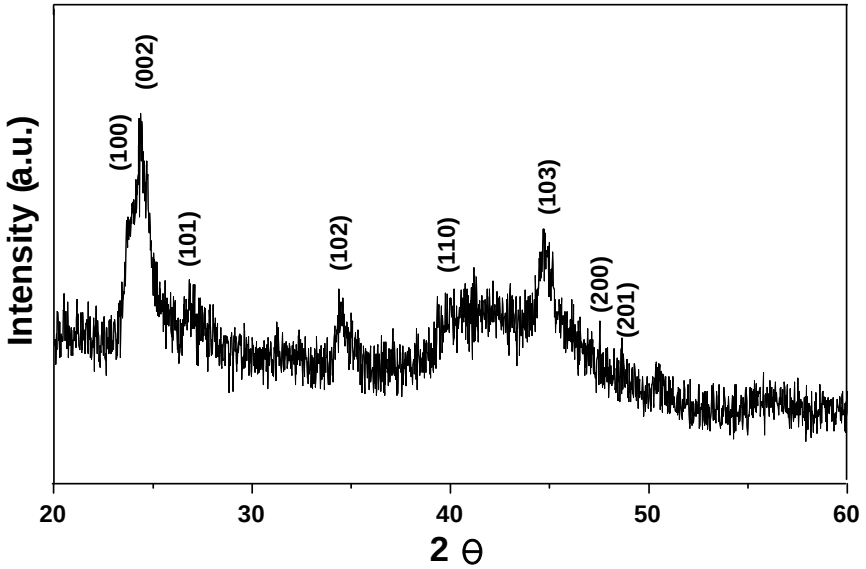

Other 2D NCs – PbS Nanosheet

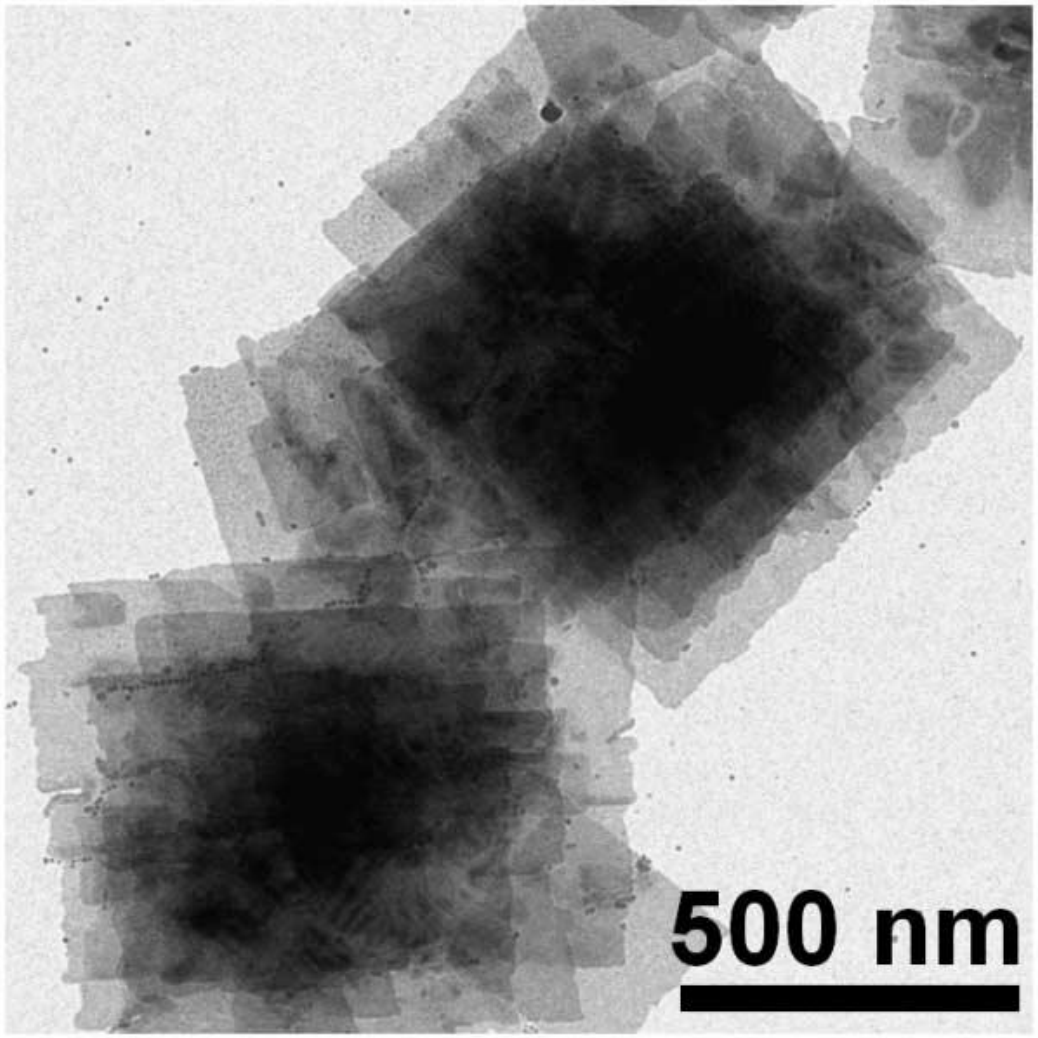

C. Schliehe, -----, H. Weller, *Science* **2010**, 329, 550.

Other 2D NCs – PbS Nanosheet

Oriented attachment of PbS QDs.

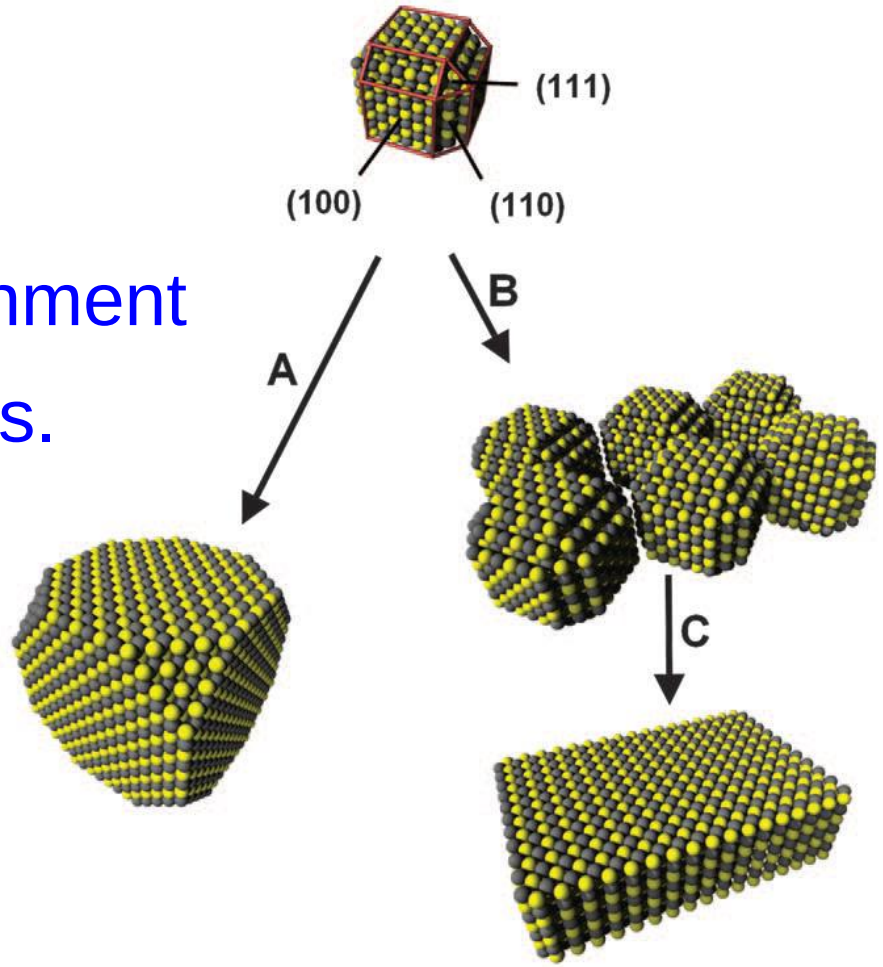

C. Schliehe, -----, H. Weller, *Science* **2010**, 329, 550.